NOTE TO USERS

This reproduction is the best copy available.

UMI®

UNIVERSITÉ DE MONTRÉAL

RHEOLOGY OF BAUXITE-BASED LOW-CEMENT SHOTCRETING CASTABLES

XIANXIN ZHOU

DÉPARTEMENT DE MATHÉMATIQUES ET DE GÉNIE INDUSTRIEL

ÉCOLE POLYTECHNIQUE DE MONTRÉAL

THÈSE PRÉSENTÉE EN VUE DE L'OBTENTION

DU DIPLÔME DE PHILOSOPHIAE DOCTOR (Ph.D.)

(GÉNIE MÉTALLURGIQUE)

AÔUT 2004

© Xianxin ZHOU, 2004

Library and Archives Canada

Published Heritage Branch

395 Wellington Street
Ottawa ON K1A 0N4
Canada

Bibliothèque et Archives Canada

Direction du Patrimoine de l'édition

395, rue Wellington
Ottawa ON K1A 0N4
Canada

Your file Votre référence
ISBN: 0-612-98188-6
Our file Notre référence
ISBN: 0-612-98188-6

NOTICE:
The author has granted a non-exclusive license allowing Library and Archives Canada to reproduce, publish, archive, preserve, conserve, communicate to the public by telecommunication or on the Internet, loan, distribute and sell theses worldwide, for commercial or non-commercial purposes, in microform, paper, electronic and/or any other formats.

The author retains copyright ownership and moral rights in this thesis. Neither the thesis nor substantial extracts from it may be printed or otherwise reproduced without the author's permission.

AVIS:
L'auteur a accordé une licence non exclusive permettant à la Bibliothèque et Archives Canada de reproduire, publier, archiver, sauvegarder, conserver, transmettre au public par télécommunication ou par l'Internet, prêter, distribuer et vendre des thèses partout dans le monde, à des fins commerciales ou autres, sur support microforme, papier, électronique et/ou autres formats.

L'auteur conserve la propriété du droit d'auteur et des droits moraux qui protège cette thèse. Ni la thèse ni des extraits substantiels de celle-ci ne doivent être imprimés ou autrement reproduits sans son autorisation.

In compliance with the Canadian Privacy Act some supporting forms may have been removed from this thesis.

While these forms may be included in the document page count, their removal does not represent any loss of content from the thesis.

Conformément à la loi canadienne sur la protection de la vie privée, quelques formulaires secondaires ont été enlevés de cette thèse.

Bien que ces formulaires aient inclus dans la pagination, il n'y aura aucun contenu manquant.

Canada

UNIVERSITÉ DE MONTRÉAL

ÉCOLE POLYTECHNIQUE DE MONTRÉAL

Cette thèse intitulée :

RHEOLOGY OF BAUXITE-BASED LOW-CEMENT SHOTCRETING CASTABLES

Présentée par : ZHOU Xianxin

En vue de l'obtention du diplôme de : Philosophiae Doctor

A été dûment acceptée par le jury d'examen constitué de:

M. ALLAIRE Claude, Ph.D., président

M. RIGAUD Michel, D.Sc.A., membre et directeur de recherche

M. CARREAU Pierre, Ph.D., membre

M. OPREA George, Ph.D., membre

ACKNOWLEDGEMENTS

First of all, I extend my heartiest gratitude to my supervisor, Prof. Michel Rigaud, Director of Ceramics and Industrial Refractories of École Polytechnique (CIREP) for his stimulating discussions, intellectual inspiration, outstanding expertise, enlightening guidance, constant advice and support throughout this work. The financial support he provided was well appreciated.

Words are inadequate to express my sincere thanks to Dr. N. S. Zhou, Director of High Temperature Materials Institute (HTMI), Henan University of Science and Technology, for his recommendation, constant support, guidance, help, parental care, for fully trusting me with this study program and arranging the shotcreting trials and sample testing. I will always be grateful for his support.

I am truly grateful to Mr. S. Q. Zhang, Chairman of Henan Gengsheng Refractories Co. for full understanding, trusting and supporting my study at CIREP, and the golden opportunity I have been given. Special thanks to my colleagues, G. P. Zhang, A. H. Zhou, D. T. Xu, R. J. Chen, H. W. Zhao et al. for carrying out the shotcreting trials and testing the samples at the company laboratory. I acknowledge the company for providing the raw materials, shotcreting equipment and also performing the trials for this project.

I take this opportunity to express my great appreciation to my colleague and good friend, Dr. K. Sankaranarayanane, for crucial and timely help, suggestion, discussion and support during the period of my thesis writing. Without his help, I could not do it better.

I would like to thank Prof. P. J. Carreau, Director of Applied Polymer Research Centre (CRASP), for permission to use Bohlin CVO 120 HR Rheometer and Mr. F. Cotton for his technical assistance for matrix rheology measurements.

I greatly appreciate the support and encouragement from Prof. Z. G. Li and my good friends, S. H. Zhang and T. H. Cui from Luoyang Institute of Refractories Research (LIRR). My appreciation also goes to Prof. N. Li, Wuhan University of Science and Technology (WUST), for his recommendation letter and Prof. Y. W. Li for his encouragement and help.

I extend my gratitude to my colleague, Dr. H. Q. He and my friends Dr. Z. Q. Guo, RHI Refractories, and Dr. C. L. Feng, University of Toronto, for their helps and support. I wish to thank J. P. Bouchard and A. Carbonneau for their technical support. I appreciate T. Crisson and H. Rioux for their secretarial helps at CIREP. In no particular order, I am thankful to all my friendly colleagues, M. H. Zhang, J. G. Gao, Dr. E. Paransky, Dr. E. Divry, Dr. S. Palco, Dr. Pelletier, Dr. S. Afshar, Dr. N. Ntakaburiumvo, Dr. F. B. Ye, Mr. V. Kovac, V. Ébacher, Y. Douche, R. Megateli, K. Balamurugan at CIREP, for their friendship and creating a pleasant learning atmosphere.

Special thanks must go to my parents and sisters for their support, affection and sacrifices. I acknowledge a great debt I owe to them. Last, but not least, I express my heartfelt gratitude to my beloved wife for her love, patience, understanding, support and encouragement to overcome difficulties. I could not imagine these years without her. I owed also a great deal to my young daughter for neglecting her during my overtime work.

I ever thank God for giving me life, health, confidence, perseverance and intelligence, and for putting so many wonderful people, T. & J. Law, L. & A. Lim, A. & J. Chan, T. & C. Chan, A. and S. Chai, Y. Tang and Z. Q. Hua et al. in MCAC, S. L. Yang, C. H. Liu, Y. C. Liu, X. J. Li, C. H. Li, H. Q. Jiang, B. Yun, Y. N. Jiang, X. H. Zhou, S. X. Yu and so on, for their help and friendship along the way. Although it is impossible to list all the persons who have ever done any in favor of my Ph. D. work, directly or indirectly, mentally or materially, I bear them firmly in my mind forever.

RÉSUMÉ

Ce travail avait pour but de définir une composition de béton projetable, à base de bauxite, à basse teneur en ciment, en cherchant à quantifier le comportement rhéologique des pâtes fraîches, après mélange.

L'essentiel de la thèse a été de quantifier expérimentalement le comportement de bétons complets (avec de l'ordre de 85% de charges solides) et de bétons partiels (partie matrice seulement : 60% de charges solides) à l'aide de deux équipements, un rhéomètre pour les bétons complets, un viscosimètre pour les bétons partiels.

Au total 170 compositions différentes ont été testées pour cerner l'influence de sept paramètres : la distribution granulométrique (5), la nature (3) et la quantité de dispersant (0 à 0.2%), la nature (2) et la quantité de ciment alumineux (0 à 6%), la nature (2) et la quantité de microsilice (0 à 7 %), la nature (5) et la quantité de fines d'alumine (0 à 10%), la quantité d'eau de gâchage (5 à 8%), le temps de travail jusqu'à la prise (jusqu'à 275 minutes).

Outre les limites d'écoulement et les viscosités apparentes sur toutes les compositions considérées, d'autres mesures ont été effectuées pour compléter la panoplie de résultats : la coulabilité sur table vibrante, les propriétés physiques des bétons, densité, porosité apparente, variation linéaire au séchage, et la résistance en flexion (3 pts) après séchage. Sur les bétons partiels, des mesures de conductibilité ionique et de pH, et des mesures de profil thermique, lors de la prise, sur des bétons complets, ont été effectuées en vue de cerner les différences entre ces 2 types de mélanges. Des observations macroscopiques ont aussi permis d'apprécier les finis de surface des échantillons. Des calculs sur les distances inter-particules (IPS) et sur l'épaisseur maximale de la barbotine entre les agrégats (MPT) ont été effectués pour

interpréter les résultats. Le travail a été complété, à la toute fin, par des essais de projection en grandeur nature.

Au total, il a été possible de mettre en relief l'utilité des mesures rhéologiques pour définir à priori un domaine ou une boîte de pompabilité de ces bétons. C'est là la contribution la plus importante de cette thèse. Il a été, en outre, démontré quantitativement l'incidence des paramètres cités précédemment sur la résistance à l'écoulement et sur la viscosité apparente de ceux-ci (bétons complets et bétons partiels).

Il ressort que les caractéristiques du béton haute alumine, à base d'agrégats de bauxite, à basse teneur en ciment, devraient être les suivantes : distribution granulométrique avec un coefficient d'Andreasen de 0.26, un diamètre maximal de bauxite de 5mm, 4% de ciment CA-14, 0.12% de dispersant SHMP, 5% de microsilice (Elkem 971 U), 9% de fines de bauxite, 7% d'eau. Les essais, en fin de thèse, de pompage-projection, ont été concluants et ont permis de valider la démarche de définir une composition adéquate de bétons à partir de la mesure de son comportement rhéologique.

ABSTRACT

Continuous research efforts on castable technology since two decades have lead to the transformation of placement mode from vibrating to self-flow to pumping and shotcreting. Shotcreting (an installation process of self-flow castables by combining pumping and shooting), as a high efficient installation technique, has demanded castable composition with specific characteristics in terms of rheology. Though, the understanding on self-low castable technology is appreciable, the state-of-art on shotcreting has not yet been revealed and the literature on this area is scarce. This demands an in-depth research on this particular subject.

The goal of the current investigation is to develop a predictive method of shotcreting castable with good pumpability and self-flowability through rheological approach and to validate the approach through shotcreting trial. A bauxite-based low-cement self-flow castable has been chosen for this purpose.

Basically, three test methods have been adopted to fulfill the stated purpose: flow table test, viscometer and a new rheometer. A rheometer has been used to measure the rheological behavior of chosen castables. Through this, two rheological constants are obtained which are used to predict the pumpability of chosen system. This approach has overcome the drawback of measuring rheology of fine matrix portion only to predict the castable behaviors. Fine matrix rheology has also been evaluated using viscometer for comparison purpose. The relationship between viscometer and rheometer measurement are analysed. To support the results of rheometer and viscometer, conductivity measurement on fine matrix portion, exothermic profile measurement on castable mix, mechanical and physical properties measurements after drying and the appearance of castable green bodies are also carried out.

The whole work is divided into four stages. In stage I, all raw materials used in this work, including bauxites, cements, microsilicas, reactive aluminas, have been characterized for chemical composition and particle size distribution. In stage II, the influence of different variables such as particle size distribution, dispersant, cement, microsilica, reactive alumina, water addition and aging time on the rheology of low-cement castables has been studied. The influences of these variables have been understood through the responses such as flow resistance, torque viscosity, self-flowability, mechanical and physical properties of castable. In stage III, the rheology of the fine matrix portion of the chosen castables has been carried out by a viscometer. The variables are the same with those matrix slurries in order to measure the castable rheology using a rheometer. The rheology of fine matrix slurries is characterized through plastic yield stress and plastic viscosity calculation of chosen matrixes. A "pumping box" has been designed using the two important rheological constant: flow resistance and torque viscosity derived from rheometer results. In stage IV, with the optimized castable composition through this work has been pumped and shotcreted in the field to validate the present approach.

Totally, more than 30 experiments have been carried out to characterize particle size distribution and chemical composition of the raw materials. About 80 experiments have been done on castables, in terms of rheology, self-flowability, water demand, mechanical and physical properties and sample appearance. Sixty experiments have been done on matrix slurries, in terms of rheology, conductivity and exothermic profile. Three trials have been done to characterize the castables, in terms of self-flowability, mechanical and physical properties.

Based on this work, it has been found that the chosen seven variables such as particle size distribution, dispersant, cement, microsilica, fine fillers, water addition and aging time strongly influence the rheological behaviors of castable and fine matrix. The results of the influence of these variables are briefly outlined below with an emphasis on the

fact that all the tested castables are Bingham fluids in nature and thixotropic when analyzed as a function of time.

The particle size distribution has got direct relation with rheological behavior of chosen castable. A castable with more fine particles in the matrix may not be a good pumpable castable. Castable with optimal particle size distribution depicts good rheological behavior. Through this work, it has been found that the castable with Andreasen modulus (q) value of 0.26 is rheologically superior. More fine particles in the matrix leads to high viscosity and flow resistance. On the other hand, the castable with less fine matrix has shown segregation. The results also reveal the fact that the maximum particle size (D_{max}) of the pumpable castable must be kept below 8 mm and 5 mm is optimal. When D_{max} of the castables exceeds this limit, they are prone to segregation even with optimal q value of 0.26. The fine matrix evaluation also shows the increase of plastic viscosity with decreasing q value while maintaining the plastic yield stress value at similar levels.

A castable designed with optimal particle size distribution may not be pumpable and/or shootable if the dispersant package is not properly chosen. The excess amounts of dispersants not only degrade the castable self-flowability but also the rheological characteristics under given conditions. The type of dispersants (FS-20, SHMP and Darvan 811D) chosen in the current study have proven this fact. The rheology of chosen castable is found to be strongly affected by the type and amount of dispersants. An optimally designed bauxite-based low-cement castable is found to be not self-flowing with FS-20, while SHMP and Darvan 811D have shown different rheological behaviors with different amounts. The flow resistance is found to increase with SHMP and decrease with increasing Darvan 811D. Torque viscosity is almost unaffected by dispersants. Similar observation has also been made with fine matrix rheology. The plastic viscosity remains similar with varying amount of dispersant while the plastic

yield stress keep on changing. With the results, the castable with 0.12 wt% SHMP is found to be rheologically superior under given conditions.

The chemistry and mineralogical phase composition of the chosen cement are found to be influencing the rheological behavior of both castable and fine matrix. The addition of cement CA-14 addition from 0 to 6 wt% is found to influence the torque viscosity of chosen castable. The flow resistance on the other hand remains similar. The change of cement type from CA-14 to CA-25R has shortened the working time of castable due to the presence of $C_{12}A_7$ inside CA-25R.

In the current investigation, it has been shown that not only the amount, but the source of microsilica also affects the rheology of castables mix. With 3 wt% Microsiclia-1 (Elkem Microsilica 971 U), the castable is neither self-flowing nor amenable for rheology measurement. Increasing microsilica drastically reduces both torque viscosity and flow resistance. Added with 5 wt%, the castable shows optimal rheological behaviors. When microsilica is increased to 7 wt%, segregation has been observed due to drastic reduction of both flow resistance and torque viscosity. Change of source of microsilica from 971U to another one has degraded the castable rheologically. The viscometer has given different results to the rheometer. The reason for the observed results is explained through interparticle separation distance (IPS) and maximum paste thickness (MPT) calculation of the chosen mix.

The role of fine fillers has given important and interesting results in the current study. With the given particle size distribution, dispersant and cement, the change of ultrafine bauxite particles (Bautixter-3) in the matrix has drastically influenced rheological properties. This behavior is correlated with the amount of fine particle less than 10 microns in the castables. Change of ultra-fine bauxite by reactive alumina, has been found to decrease the rheological constants with stickiness and segregation in the castables. The plastic viscosity has shown similar trend with torque viscosity while the

yield stress shows different trend than the flow resistance. This clearly dictates the fact that fine matrix rheology may not be similar to castable rheology.

The role of water addition is a well-known factor to affect flowability in self-flow castables. In this study, it has been found that the rheological constants drastically decrease when the water addition is increased. The same trends are observed with fine matrix rheology. This fact is understood through the calculation of IPS of fine matrix and MPT of castable mix, respectively. The water addition has shown linear relationship with torque viscosity, flow resistance, plastic viscosity and yield stress. When water addition exceeds 7 wt%, the castable has shown segregation. This is due to too much reduction in flow resistance and torque viscosity values of castable.

The change of rheology of castable with aging time has been studied in detail. The self-flowability measurement with time has shown 275 min as flow decay time and this could not dictate anything on rheological constant variations of the chosen castable. The mix has shown three distinct zones of rheological evolution, which are referred as homogenization, saturation and setting effect state when tested for rheology. Similar trend has also been observed with fine matrix rheology, but with different time scale. The results are well explained with conductivity of fine matrix slurry and exothermic profile of the castable mix.

A pumping box has been designed using the rheological parameters (flow resistance and torque viscosity) of all the castable mixes. With this pumping box, the boundaries of segregation and blockage zone with optimal rheological values have been defined. The field trials have been conducted successfully using this assessment. Based on above discussions, the general conclusions are drawn as follows:

1) The current study has obtained a new way to test the rheology of self-flow castables. The IBB rheometer is used to measure the rheology of castable to

overcome the drawbacks of measurements of only matrix portion. As a result, it has been found that two rheological parameters, flow resistance (G) and torque viscosity (H) could be used to describe the rheological properties of castable.

2) With the calculated values of flow resistance G and torque viscosity H, a "PUMPING BOX" has been designed which predicts the minimum and maximum values of G (1 ~ 2.5 Nm) and H (6 ~10 Nm.s) for trouble-free pumping of castable.

3) An optimized composition with q value of 0.26 and D_{max} of 5 mm, 0.12 wt% dispersant SHMP, 4 wt% cement CA-14, 5 wt% Microsilica-1 (Elkem 971 U), 9 wt % Bauxite-3 and 7 wt% water has shown overall desirable rheological properties and pumpability.

4) The optimal composition castable has been successfully pumped and shotcreted and this proves that the prediction of pumpability by the rheological approach is valid and the test method is meaningful.

CONDENSÉ

Suite aux efforts de recherche soutenus dans le domaine des bétons réfractaires, les techniques d'installation ont évolué très substantiellement, des bétons vibrés, aux bétons auto coulants, aux bétons pompables et finalement projetables. Cette dernière technique d'installation a requis un ajustement des compositions pour satisfaire des comportements rhéologiques particuliers. Toutefois, les critères concernant la rhéologie de ces bétons sont encore non-définis dans la littérature. La définition de tels critères a donc servi d'amorce à ce présent travail.

Le but de cette thèse a été de développer une méthode de mesure pour prédire la pompabilité et le degré d'auto-écoulement des bétons projetables, qui soit validée par essais de gunitage. Un béton de bauxite, à basse teneur en ciment a été sélectionné à cette fin.

Essentiellement, trois techniques ont été mises en œuvre pour atteindre notre but : des essais sur table vibrante et des mesures de viscosimètre et de rhéométrie. L'aspect original tourne autour de l'utilisation d'un rhéomètre, particulièrement adapté pour les bétons (modèle IBB).

A l'aide de cet instrument, il a été possible de calculer deux «constantes» qui ont permis de fixer des limites de pompabilité, sur des compositions complètes, à 85% de charges solides.

La rhéologie des bétons partiels, ne considérant que les fines constituant la matrice, avec 65% de charges solides, a aussi été suivi à l'aide d'un viscosimètre classique (modèle Bohlin). Les résultats obtenus, à partir du viscosimètre et du rhéomètre, ont été analysés et comparés.

Pour compléter ces études, des mesures de conductivité et de profils thermiques (dus à l'exothermicité de la prise des bétons) ainsi que des mesures concernant les propriétés physiques et mécaniques des meilleurs bétons ont été effectuées.

L'ensemble du travail s'est déroulé en quatre parties. Initialement, toutes les matières premières utilisées, bauxites, ciments, microsilices, alumines réactives, ont été dûment caractérisées en terme de distribution granulométrique et analyse chimique. Dans la deuxième partie, le comportement rhéologique des bétons et leurs caractéristiques physiques et mécaniques ont été mesurés en faisant varier la distribution granulométrique, la nature des dispersants utilisés et leurs quantités utilisées, la nature et la proportion de la phase cémenteuse, de la microsilice (deux types) de l'alumine réactives (deux types) des fines de bauxite (3 types), la quantité de l'eau de gâchage et le temps de mixage. Dans la troisième partie, le même genre d'étude a été effectué mais cette fois sur la matrice des bétons à l'aide d'un viscosimètre plutôt qu'un rhéomètre. Les paramètres rhéologiques ont permis de définir les termes de résistance à l'écoulement, de viscosité apparente et d'auto-écoulement, alors qu'a l'aide du viscosimètre, les paramètres dits d'écoulement plastique et de viscosité plastique ont été déduits. A l'aide des mesures, il a été possible de définir un domaine de pompabilité des bétons dérivé des mesures de rhéomètre. Dans la quatrième et dernière partie, une composition dite optimale,a été manipulée dans une machine à gunitage humide, pour valider à l'échelle semi-industrielle les résultats accumulés et la notion de domaine de pompabilité.

Au total, plus de 30 essais ont été effectués, pour bien caractériser l'influence de la distribution granulométrique et la nature chimique des matières premières. Puis 80 autres essais ont été effectués sur des bétons (composition complète) pour définir leurs caractéristiques rhéologiques en contrôlant leur degré d'auto-écoulement en fonction de la quantité d'eau de gâchage utilisée et des propriétés physiques et mécaniques obtenues, tout en tenant compte de l'apparence externe des échantillons obtenus. Enfin, 60 essais

ont été effectués sur des compositions partielles de bétons (matrice sans agrégats), ce qui a permis de corréler les mesures de viscosimètre à celles de conductivité et d'exothermicité durant la prise des bétons.

Suite à ce travail expérimental, totalisant 170 essais, il a été possible de bien cerner l'influence des 7 paramètres suivants : la distribution granulométrique, la nature et la quantité de dispersants, de ciments, de microsilice et d'additions de fines, la quantité d'eau et le temps de mélange jusqu'à la prise, sur les propriétés rhéologiques des bétons complets et des bétons partiels. Les principaux résultats sont résumés ci-après en soulignant que tous les mélanges testés sont des pâtes dits de type Bingham, et thixotropiques lorsqu'analysées en fonction du temps.

La distribution granulométrique est le premier paramètre à considérer pour obtenir un béton avec le comportement rhéologique escompté : coulable, pompable et projetable. Les résultats obtenus démontrent que, sur la classe des bétons bauxitiques traités, la valeur du module d'Andreasen, q, doit être de 0.26. Ceci définit alors la quantité de fines à utiliser. Avec plus de fines, la limite d'écoulement et la viscosité des bétons augmentent. Avec moins de fines, les bétons sont sujets à des effets de ségrégation, inadmissibles pour obtenir des propriétés physiques et mécaniques adéquates. En outre, le diamètre maximal des agrégats doit être compris entre 5 et 8mm, pour être pompé et projeté dans des tuyaux de 50 à 80 mm de diamètre. Pour des diamètres supérieurs à 8mm, avec q = 0.26, les bétons sont alors eux aussi sujets à ségrégation, durant l'écoulement. Dernier point d'intérêt, la proportion de fines dans les bétons partiels (matrice seulement) qui croît lorsque la valeur de q diminue, a une action directe sur la viscosité plastique qui croît alors que la limite d'écoulement plastique demeure peu affectée. Deuxième aspect, un béton avec une valeur de q = 0.26 ne sera pas nécessairement pumpable si les «bons» dispersants ne sont pas sélectionnés.

Les dispersants ont une influence directe sur l'auto-écoulement et les caractéristiques rhéologiques. Parmi les dispersants utilisés (FS-20, SHMP et Darvan 811D), non seulement la nature mais le pourcentage utilisé sont à considérer. Il n'a pas été possible d'obtenir un béton auto-coulant, avec une distribution granulométrique correspondant à q = 0.26, en utilisant le FS-20. Pour les 2 autres dispersants, la limite d'écoulement du béton croît lorsque la quantité de SHMP utilisée croît mais décroît avec des ajouts de Darvan 811D, alors que la viscosité «apparente», elle, n'est pas affectée. Les mêmes effets ont été enregistrés tant sur les bétons complets (matrice + agrégats) que sur les bétons partiels (matrice seulement). De l'ensemble de tous ces résultats, il ressort que c'est au niveau de 0.12% poids de SHMP que l'on obtient les meilleurs résultats (toujours avec q = 0.26).

Les compositions chimique et minéralogique des ciments utilisés, ont aussi une influence marquée sur la rhéologie des bétons (complets et partiels). La viscosité apparente croît régulièrement selon la proportion de ciment utilisé, entre 0 et 6% alors que la limite d'écoulement n'est pas influencée. En comparant les ciments commerciaux CA-14 et CA-25R, il s'avère que le temps de prise avec le CA-25R est grandement réduit, et cela à cause manifestement de la présence de plus de $C_{12}A_7$.

La nature et la proportion de microsilice utilisée ont aussi une grande influence. Avec 3% de microsilice (Elkem 971U), le béton (q = 0.26) n'est pas auto-coulable. Avec 7%, le béton est sujet à ségrégation, la limite d'écoulement et la viscosité dynamique décroissant de façon drastique. 5% est la quantité optimale à utiliser. Toutefois, le comportement sur les bétons complets et les bétons partiels ne sont pas en accord l'un avec l'autre. Ceci est interprété à partir de calculs sur la distance de séparation inter particulaire (IPS) et sur l'épaisseur maximale de la barbotine qui entoure les particules (MPT).

Le rôle des additifs fins, entre la microsilice et le ciment, a été illustré en faisant varier la proportion et la taille de 3 bauxites fines et de alumines réactives. La proportion de particules inférieures à 10 microns est très influente. La substitution des bauxites fines par de l'alumine réactive a permis, non seulement de distinguer l'effet bénéfique des alumines, mais a révélé cette fois, que le comportement rhéologique mesuré sur les bétons complets avec le rhéomètre ne concordaient pas avec celui des bétons partiels en utilisant un viscosimètre. Alors que l'incidence sur la viscosité mesurée varie de la même façon, la limite d'écoulement varie en sens inverse.

Le rôle de la quantité d'eau de gâchage a aussi été quantifié. La valeur des paramètres rhéologiques décroît drastiquement avec tout surplus d'eau, dans tous les cas. Comme précédemment, les calculs de IPS et MPT permettent d'interpréter ces résultats. Tout surplus d'eau, au delà de 7% entraîne irrémédiablement des effets de ségrégation, les valeurs de limite d'écoulement et de viscosité apparente étant alors très faibles.

Les mesures pour tenir compte de l'influence du temps de prise et du temps de malaxage, ont permis de dégager la certitude que les constantes rhéologiques mesurées entre 0 et 45mm ne sont pas fonction du temps de prise. Toutefois dans le temps, en poursuivant les mesures rhéologiques, sur les bétons complets, sur de plus longs intervalles (jusqu'à 185 minutes), il est possible de dégager 3 stades distincts : un d'homogénéisation du mélange, deux de stagnation puis trois de saturations et prise du ciment. Les mêmes 3 stades sont discernables sur les bétons partiels, mais l'échelle de temps n'est pas la même. Ces résultats ont été corrélés à des mesures de conductivité ionique et de pH et des mesures de profil thermique.

A la fin, un domaine ou une boîte de pompabilité a pu être déterminée en termes de valeurs minimale-maximale requises pour la limite d'écoulement et la viscosité apparente des bétons complets. Ces 4 limites ont été établies, à priori, en vue d'éviter tout phénomène de ségrégation ou de blocage ou de bouchage lors de la projection. Des

essais à l'échelle semi-industrielle ont été effectués, en suivant ces recommandations et ont été couronnés de succès.

A partir de l'ensemble de ces résultats, il est possible de conclure que :

1) l'utilisation du rhéomètre IBB est bien adaptée pour caractériser les bétons réfractaires et permet d'éviter les pièges qui découlent de mesures rhéologiques sur des bétons partiels seulement. Les deux caractéristiques que l'on peut calculer à partir des mesures : la limite d'écoulement (G) qui correspond au couple minimal à exercer sur les béton pour le cisailler (le mettre en mouvement) et la viscosité apparente (H) (proportionnelle à la viscosité dynamique), sont significatives pour décrire le comportement rhéologique de bétons coulables, pompables et projetables.

2) La boîte de pumpabilité, qui a été déterminée à partir des valeurs minimales et maximales de G (1 et 2.5 Nm), et de H (6 et 10 Nm.s), a permis de projeter, dès le premier essai, un mélange bauxitique, à basse teneur en ciment 4%, avec 7% d'eau.

3) La composition optimale d'un tel béton est établie avec un coefficient d'Andreasen, de distribution granulométrique de 0.26, diamètre maximal de l'agrégat de bauxite de 5mm, 0.12% de dispersant SHMP, 5% de microsilice (Elkem 971 U), avec 9% de fines de bauxite, ce qui en fait une composition économiquement attrayante (moins d'alumine plus de bauxite.

4) La notion de boîte de pumpabilité est la principale contribution de cette thèse. Elle permet de quantifier les paramètres rhéologiques requis pour mettre au point des bétons projetables – sans procéder par un cheminement d'essais et erreurs avec des installations grandeurs nature. Elle permet aussi de tester à priori tout mélange soumis et donc servir de critères de sélection.

TABLE OF CONTENTS

ACKNOWLEDGEMENTS.....iv

RÉSUMÉ.....vi

ABSTRACT.....viii

CONDENSÉ.....xiv

TABLE OF CONTENTS.....xx

LIST OF TABLES.....xxviii

LIST OF FIGURES.....xxxi

LIST OF SYMBOLS AND NOMENCLATURE.....xxxix

CHAPTER 1 – INTRODUCTION.....1

CHAPTER 2 - THEORETICAL BACKGROUND OF RHEOLOGY AND SHOTCRETING.....9

PART 1: RHEOLOGY.....9

2.1 Introduction.....9

2.2 Fundamentals of Rheology.....11

2.2.1 Definition of Rheological Terms.....11

2.2.2 Classification of Fluids.....15

2.3 Practical Rheology.....19

2.3.1 Particle Size Distribution (PSD).....19

2.3.2 Interparticle Separation Distance (IPS).....21

2.3.3 Solid Loading Index (SLI).....25

2.3.4 Paste Thickness Index (PTI) and Maximum Paste Thickness (MPT).....29

2.4 Application in Castables.....32

2.4.1 Classification of Castables by Rheology.....32

2.4.2 Rheology and Fluidity Test Methods used in Castables.....33

2.4.3 Rheological Behavior of Some Monolithic Refractories.....39

2.5 Conclusions.....44

PART 2: SHOTCRETING.....44

2.6 Introduction.....44

2.7 Advantages of Shotcreting.....47

2.8 Application of Shotcreting.....50

2.8.1 Steel Ladle.....50

2.8.2 Cement Plant (Pre-heater).....51

2.8.3 Torpedo Ladle.....51

2.8.4 Blast Furnace Trough.....52

2.9 Conclusions.....54

PART 3: DESIGN OF SHOTCRETING CASTABLES:

A RHEOLOGICAL APPROACH.....55

2.10 Introduction.....55

2.11 Design of Shotcreting Castables by Optimizing Particle Size Distribution.....56

2.12 Design of Shotcreting Castables by Optimizing Additives 62

CHAPTER 3 - EXPERIMENTAL PROCEDURE.....63

3.1 Experimental Program.....63

3.2 Raw Materials.....64

3.2.1 Bauxite.....64

3.2.2 Calcium Aluminate Cement.....66

3.2.3 Reactive Alumina.....67

3.2.4 Microsilica.....68

3.2.5 Dispersant 68

3.3 Compositions of Castables 69

3.4 Experimental Set-ups to Measure Rheology and Exothermic Profile 69

3.4.1 IBB Rheometer V1.0 for Castable Rheology.....69

3.4.2 CVO 120 High Resolution Rheometer for Matrix Rheology.....71

3.4.3 Testing Set-up for Exothermic Profile Measurements.....73
3.5 Sample preparation 74
3.6 Test Methods 74
3.6.1 Flowability, Flow Decay and Water Demand.....74
3.6.2 Mechanical and Physical Properties.....75
3.6.3 Castable Rheology.....75
3.6.4 Matrix Rheology.....75
3.6.5 Conductivity.....76
3.6.6 Exothermic Profile.....76
3.6.7 Bonding Water Measurements for Cement Hydration Process 76

CHAPTER 4 - PARTICLE SIZE DISTRIBUTION.....77
4.1 Introduction.....77
4.2 Compositions.....78
4.3 PSD of the Castables 78
4.4 Water Demand and Self-flowability 79
4.5 Castable Rheology 81
4.5.1 Torque vs. Speed.....81
4.5.2 Equivalent Apparent Viscosity.....84
4.5.3 Thixotropy.....84
4.5.4 Flow Resistance and Torque Viscosity.....86
4.6 Matrix Rheology 89
4.6.1 Shear Stress vs. Shear Rate.....89
4.6.2 Apparent Viscosity vs. Shear Rate.....91
4.6.3 Thixotropy.....92
4.6.4 Plastic Yield Stress and Plastic Viscosity.....93
4.7 The IPS of the Matrix Slurries and MPT of the Castables.....95
4.8 Mechanical and Physical Properties 95
4.9 Appearance of the Castable Samples.....96

4.10 Optimization of the Castables.....97
4.11 Conclusions.....98

CHAPTER 5 - DISPERSANT.....100
5.1 Introduction.....100
5.2 Compositions.....103
5.3 Water Demand and Self-flowability.....103
5.4 Castable Rheology.....106
5.4.1 Torque vs. Speed.....106
5.4.2 Equivalent Apparent Viscosity.....110
5.4.3 Thixotropy.....110
5.4.4 Flow Resistance and Torque Viscosity.....112
5.5 Matrix Rheology.....114
5.5.1 Shear Stress vs. Shear Rate.....114
5.5.2 Apparent Viscosity vs. Shear Rate.....115
5.5.3 Thixotropy.....116
5.5.4 Plastic Yield Stress and Plastic Viscosity.....117
5.6 Mechanical and Physical Properties.....117
5.7 Appearance of Castables Samples.....117
5.8 Dispersants and Rheology.....119
5.9 Optimization of Castables.....120
5.10 Conclusions.....121

CHAPTER 6 - CALCIUM ALUMINATE CEMENT.....123
6.1 Introduction.....123
6.2 Compositions.....125
6.3 The PSD of the Castables.....126
6.4 Water Demand and Self-flowability.....126
6.5 Castable Rheology.....128

6.5.1 Torque vs. Speed.....128
6.5.2 Equivalent Apparent Viscosity.....130
6.5.3 Thixotropy.....131
6.5.4 Bonding Water and Free Water.....132
6.5.5 Flow Resistance and Torque Viscosity.....133
6.6 Matrix Rheology 135
6.6.1 Shear Stress vs. Shear Rate.....135
6.6.2 Apparent Viscosity vs. Shear Rate.....136
6.6.3 Thixotropy.....137
6.6.4 Plastic Yield Stress and Plastic Viscosity.....138
6.7 IPS of Matrix Slurries and MPT of Castables.....138
6.8 Mechanical and Physical Properties 139
6.9 Appearance of Castables Samples.....141
6.10 Optimization of Castables.....141
6.11 Conclusions.....142

CHAPTER 7 - MICROSILICA.....143
7.1 Introduction.....143
7.2 Compositions.....145
7.3 The PSD of the Castables 146
7.4 Water Demand and Self-flowability 146
7.5 Castable Rheology 148
7.5.1 Torque vs. Speed.....148
7.5.2 Equivalent Apparent Viscosity.....150
7.5.3 Thixotropy.....151
7.5.4 Flow Resistance and Torque Viscosity.....152
7.6 Matrix Rheology 155
7.6.1 Shear Stress vs. Shear Rate.....155
7.6.2 Apparent Viscosity vs. Shear Rate.....156

7.6.3 Thixotropy.....157
7.6.4 Plastic Yield Stress and Plastic Viscosity.....157
7.7 The IPS of Matrix Slurries and MPT of Castables.....158
7.8 Mechanical and Physical Properties.....158
7.9 Appearance of Castables Samples.....158
7.10 Optimization of Castables.....160
7.11 Conclusions.....162

CHAPTER 8 – FINE FILLERS: REACTIVE ALUMINA.....163
8.1 Introduction.....163
8.2 Compositions.....166
8.3 PSD of the Castables.....166
8.4 Water Demand and Self-flowability.....168
8.5 Castable Rheology.....169
8.5.1 Torque vs. Speed.....169
8.5.2 Equivalent Apparent Viscosity.....172
8.5.3 Thixotropy.....173
8.5.4 Flow Resistance and Torque Viscosity.....174
8.6 Matrix Rheology.....177
8.6.1 Shear Stress vs. Shear Rate.....177
8.6.2 Apparent Viscosity vs. Shear Rate.....178
8.6.3 Thixotropy.....179
8.6.4 Plastic Yield Stress and Plastic Viscosity.....179
8.7 The IPS of Matrix Slurries and MPT of Castables.....180
8.8 Mechanical and Physical Properties.....180
8.9 Appearance of Castables Samples.....181
8.10 Structure of Matrix and Castable.....183
8.11 Optimization of Castables.....186
8.12 Conclusions.....187

CHAPTER 9 - WATER ADDITION.....188
9.1 Introduction.....188
9.2 Compositions.....189
9.3 Water Demand and Self-flowability 189
9.4 Castable Rheology 190
9.4.1 Torque vs. Speed.....190
9.4.2 Equivalent Apparent Viscosity.....192
9.4.3 Thixotropy.....193
9.4.4 Flow Resistance and Torque Viscosity.....194
9.5 Matrix Rheology.....196
9.5.1 Shear Stress vs. Shear Rate.....196
9.5.2 Apparent Viscosity vs. Shear Rate.....197
9.5.3 Thixotropy.....198
9.5.4 Plastic Yield Stress and Plastic Viscosity.....199
9.6 The IPS of Matrix Slurries and MPT of Castables 199
9.7 Discussions.....200
9.7.1 Solid Content.....200
9.7.2 Relationship between IPS and Rheology of the Matrix Slurries.....201
9.7.3 Relationship between MPT and Rheology of the Castable Mixes.....201
9.5.4 Relationship between Castable and Matrix Rheology.....202
9.5.5 Relationship between Self-flowability and Rheology.....203
9.5.6 Relationship between Self-flowability and IPS and MPT.....204
9.5.7 Summary.....205
9.8 Mechanical and Physical Properties 205
9.9 Appearance of Castables Samples.....205
9.10 Optimization of Castables.....207
9.11 Conclusions.....208

CHAPTER 10 – AGING TIME.....209

10.1 Introduction.....209
10.2 Compositions.....212
10.3 Flow Decay.....213
10.4 Castable Rheology 214
10.4.1 Torque vs. Speed.....214
10.4.2 Equivalent Apparent Viscosity.....218
10.4.3 Thixotropy.....218
10.4.4 Flow Resistance and Torque Viscosity.....219
10.5 Matrix Rheology 220
10.5.1 Shear Stress vs. Shear Rate.....220
10.5.2 Apparent Viscosity vs. Shear Rate.....222
10.5.3 Shear-thinning and Thixotropy.....223
10.5.4 Plastic Yield Stress and Plastic Viscosity.....224
10.6 Conductivity.....224
10.7 Exothermic Profile.....225
10.8 Discussion.....226
10.8.1 Relationship between Castable and Matrix Rheology.....226
10.8.2 Relationship between Castable Rheology and Conductivity.....228
10.8.3 Relationship between Matrix and Exothermic Profile 228
10.9 Mechanical and Physical Properties 229
10.10 Appearance of Castables Samples.....229
10.11 Conclusions.....230

CHAPTER 11 – SHOTCRETING TRIAL.....231

CHAPTER 12 – COMPREHENSIVE DISCUSSIONS, CONCLUSIONS AND RECOMMENDATIONS 236

REFERRENCES.....244

LIST OF TABLES

Table 2.1 Definition of some rheological terms.....12
Table 2.2 Workability in relation with rheological parameters.....40
Table 2.3 Refractory lining installation methods.....48
Table 2.4 Typical properties of the materials after installation for steel ladles.....48
Table 2.5 Dust concentration measurement in various gunning technique.....49
Table 2.6 Typical shotcreting material properties for steel ladles.....50
Table 2.7 Comparison between shotcreted and cast lining (25 tons steel ladle).....51
Table 2.8 Typical shotcreting material properties cement pre-heater.....51
Table 2.9 Typical shotcreting material properties for torpedo ladles.....52
Table 2.10 Typical shotcreting material properties for hot BF trough in Japan.....53
Table 2.11 Dependence of pumping on PSD.....57

Table 3.1 Chemical composition of Chinese bauxite.....65
Table 3.2 Particle size distribution of bauxite aggregates fractions.....65
Table 3.3 Chemical and mmineralogical composition of cements.....66
Table 3.4 Properties of reactive aluminas.....67
Table 3.5 Properties of microsilicas.....68
Table 3.6 Specification of dispersants.....69

Table 4.1 Details of the castable mixes to study the effect of PSDs.....78
Table 4.2 T_{max} for the 4 compositions at the impeller speed of 1.10 s^{-1} in 1st loop.....84
Table 4.3 G and H values for all the compositions.....87
Table 4.4 Solid content and τ_{max} of the matrix slurries at the shear rate of 400 s^{-1}.....90
Table 4.5 Plastic viscosity and yield stress of the four matrix slurries.....95
Table 4.6 IPS of the matrix slurries and MPT of the castables.....95
Table 4.7 CMOR and AP of all the compositions.....96
Table 5.1 Details of the castable mixes to study the effect of dispersants.....103

Table 5.2 T_{max} for the 4 compositions at the impeller speed of 1.10 s^{-1} at 0 min.....110
Table 5.3 G and H values for all the compositions.....112
Table 5.4 τ_{max} of the 7 compositions at the highest shear rate of 400 s^{-1}.....114
Table 5.5 Plastic viscosity and yield stress of the 7 matrix slurries.....117
Table 5.6 CMOR and AP of the compositions DS-1, 2 and 3.....117

Table 6.1 Effect of temperature on hydration-reaction products of a typical 70 % alumina CAC.....124
Table 6.2 Details of the castable mixes to study the effect of cements.....126
Table 6.3 T_{max} for the 5 compositions at the impeller speed of 1.10 s^{-1} at 0 min.....130
Table 6.4 G and H values for all the compositions.....133
Table 6.5 τ_{max} of the 5 matrix slurries at the highest shear rate of 400 s^{-1}.....136
Table 6.6 Plastic viscosity and yield stress of the 5 matrix slurries.....138
Table 6.7 IPS of the matrix slurries and MPT of the castables.....139
Table 6.8 CMOR and AP of the compositions DS-1, 2 and 3.....139

Table 7.1 Details of castable mixes to study the effect of microsilicas.....145
Table 7.2 T_{max} for the 3 compositions at the impeller speed of 1.10 s^{-1} at 0 min.....150
Table 7.3 G and H values for the 3 compositions.....152
Table 7.4 τ_{max} of the matrix slurries at the highest shear rate of 400 s^{-1}.....156
Table 7.5 Plastic viscosity and yield stress of all the matrix slurries.....158
Table 7.6 IPS of the matrix slurries and MPT of the castables.....158
Table 7.7 CMOR and AP of all the compositions.....158

Table 8.1 Details of castable mixes to study the effect of fine fillers.....166
Table 8.2 T_{max} for the 5 compositions at the impeller speed of 1.10 s^{-1} at 0 min.....172
Table 8.3 G and H values for the 5 compositions.....175
Table 8.4 τ_{max} of the matrix slurriesat the highest shear rate of 400 s^{-1}.....178
Table 8.5 Plastic viscosity and yield stress of all the matrix slurries.....180

Table 8.6 IPS of the matrix slurries and MPT of the castables.....180
Table 8.7 CMOR and AP of all the compositions.....181

Table 9.1 Details of castable mixes to study the effect of water additions.....189
Table 9.2 T_{max} for the 4 compositions at the impeller speed of 1.10 s^{-1} at 0 min.....192
Table 9.3 G and H values for the 3 compositions.....195
Table 9.4 τ_{max} of the compositions at the highest shear rate of 400 s^{-1}.....197
Table 9.5 Plastic viscosity and yield stress of all the matrix slurries.....199
Table 9.6 IPS of the matrix slurries and MPT of the castables.....199
Table 9.7 CMOR and AP of all the compositions.....205

Table 10.1 Details of castable mixes to study the effect of aging time.....213
Table 10.2 T_{max} at the impeller speed of 1.10 s^{-1} at different time.....215
Table 10.3 G and H values at different time from 0 to 185 min.....219
Table 10.4 τ_{max} at the highest shear rate of 400 s^{-1} at different time.....221
Table 10.5 Plastic viscosity and yield stress at different time.....224
Table 10.6 CMOR and AP at different time.....229

Table 11.1 Operating parameters of shotcreting machine.....232
Table 11.2 Physical and mechanical properties of pumped and shotcreted castables...235

Table 12.1 Optimized composition with different parameters.....239

LIST OF FIGURES

Figure 1.1 Factors Influencing rheology and workability of castables.....2

Figure 2.1 Diagrammatic representations of three simple rheological models.....13
Figure2.2 Viscous flow between two planes.....15
Figure 2.3 Flow patterns under low shear rate.....16
Figure 2.4 Two time-dependent rheologies showing dependent on shear rate.....17
Figure 2.5 Schematic response of a thixotropic material to two shear-rate histories.....18
Figure 2.6 Schematic flow curves of positive and negative thixotropic materials.....19
Figure2.7 CPFT as a function of D for four hypothetical body compositions, with different largest particle size, DL.....23
Figure 2.8 Percent porosity and volume surface area as a function of IPS at 90 volume % solids suspensions containing powder.....24
Figure 2.9 Relative viscosity versus amount of small particles for bimodal mixtures of spheres with a size ratio of 21 (large: small) 27
Figure 2.10 Relative viscosity versus the Mooney equation.....28
Figure 2.11 The concept of a lubricating layer.....29
Figure 2.12 Representation of the coaxial cylinders viscometer.....34
Figure 2.13 Slump test.....36
Figure 2.14 Table flow test.....37
Figure 2.15 V-funnel flow test.....38
Figure 2.16 Pipe flow test.....38
Figure 2.17 Interaction potentials between dispersed particles.....39
Figure 2.18 Adhesion of shotcreting mix.....43
Figure 2.19 Line diagram of Shotcreting process.....45
Figure 2.20 Structure of double piston pump.....47
Figure 2.21 Shotcreting a refractory castable in a rotary kiln (note lack of dusting) 49
Figure 2.22 Illustration of the evolution of castables over the last 30 years.....54

Figure 2.23 Influence of q value on pumping pressure and adhesive ratio.....58
Figure 2.24 Flow values as a function of fine particle (-200 mesh) content.....59
Figure 2.25 Rheological behavior of matrix A in comparison with matrix B.....60
Figure 2.26 Flow values of the low cement castables with matrix A and B.....61
Figure 2.27 Relation between grain size and pumping behaviour of material.....61

Figure 3.1 Experimental programs.....63
Figure 3.2 Particle size distributions three bauxite powders Bauxite-1, 2 and 3.....65
Figure 3.3 Particle size distribution of cements CA-14 and CA-25R.....66
Figure 3.4 Particle size distributions of A-1000SG and A-3000FL.....67
Figure 3.5 Photograph of IBB Rheometer V1.0.....69
Figure 3.6 Line diagram of bowl and impeller of IBB rheometer 70
Figure 3.7 Photograph of CVO 120 High Resolution rheometer.....71
Figure 3.8 Line diagram of the impeller of CVO 120 rheometer 73
Figure 3.9 Line diagram of the set-up for exothermic profile measurement.....73

Figure 4.1 PSD of the four compositions with different q value and D_{max} 79
Figure 4.2 Self-flowability vs. water addition.....80
Figure 4.3 Comparison of self-flowability of the castables at different time.....80
Figure 4.4 Torque vs. impeller speed for CM-1.....81
Figure 4.5 Torque vs. impeller speed for CM-2.....82
Figure 4.6 Torque vs. impeller speed for CM-3.....82
Figure 4.7 Torque vs. impeller speed for CM-4.....83
Figure 4.8 Equivalent apparent viscosity vs. impeller speed for CM-2 84
Figure 4.9 Equivalent apparent viscosity vs. time at high and low impeller speed.....85
Figure 4.10 Calculation methods of G and H for CM-2 at 0 min.....86
Figure 4.11 Flow resistance vs. PSD.....88
Figure 4.12 Torque viscosity vs. PSD.....89
Figure 4.13 Shear stress vs. shear rate for all the matrix slurries.....90

Figure 4.14 Apparent viscosity vs. shear rate for all the matrix slurries.....91
Figure 4.15 Thixotropy degree and loop's area for all the matrix slurries.....93
Figure 4.16 Plastic yield stress and viscosity for all the matrix slurries.....94
Figure 2.17 (a)-(h) Appearance of samples CM-1, 2, 3 and 4 at different time 97
Figure 4.18 Flow resistance vs. torque viscosity.....98

Figure 5.1 Self-flowability vs. water addition.....105
Figure 5.2 Comparison of self-flowability of the castables at different time.....154
Figure 5.3 Torque vs. impeller speed for DS-1.....106
Figure 5.4 Torque vs. impeller speed for DS-2.....106
Figure 5.5 Torque vs. impeller speed for DS-3.....107
Figure 5.6 Torque vs. impeller speed for DS-4.....108
Figure 5.7 Torque vs. impeller speed for DS-5.....108
Figure 5.8 Torque vs. impeller speed for DS-6.....109
Figure 5.9 Torque vs. impeller speed for DS-7.....109
Figure 5.10 Equivalent apparent viscosity vs. impeller speed for DS-1 110
Figure 5.11 Equivalent apparent viscosity vs. time at high and low impeller speed....111
Figure 5.12 Relationship between self-flowability and flow resistance.....112
Figure 5.13 Flow resistance vs. dispersants.....113
Figure 5.14 Torque viscosity vs. dispersants.....114
Figure 5.15 Shear stress vs. shear rate for all the matrix slurries.....115
Figure 5.16 Apparent viscosity vs. shear rate for all the matrix slurries.....116
Figure 5.17 Thixotropy degree and loop's area for all the matrix slurries.....116
Figure 5.18 (a)-(g) Appearance of samples DS-1, 2 and 3 at different time.....118
Figure 5.19 Flow resistance vs. torque viscosity.....121

Figure 6.1 PSD of the 5 compositions with different cements.....126
Figure 6.2 Self-flowability vs. water addition.....127
Figure 6.3 Comparison of self-flowability of the castables at different time.....127

Figure 6.4 Torque vs. impeller speed for CA-1.....128
Figure 6.5 Torque vs. impeller speed for CA-2.....128
Figure 6.6 Torque vs. impeller speed for CA-3.....129
Figure 6.7 Torque vs. impeller speed for CA-4.....129
Figure 6.8 Torque vs. impeller speed for CA-5.....130
Figure 6.9 Equivalent apparent viscosity vs. impeller speed for CA-4 131
Figure 6.10 Equivalent apparent viscosity vs. time at high and low impeller speed....132
Figure 6.11 Bonding water and free water content of castables CA-1, CA-2, CA-3 and CA-4, with different cement CA-14 addition.....133
Figure 6.12 Flow resistance vs. cements.....134
Figure 6.13 Torque viscosity vs. cements.....135
Figure 6.14 Shear stress vs. shear rate for all the matrix slurries.....136
Figure 6.15 Apparent viscosity vs. shear rate for all the matrix slurries.....137
Figure 6.16 Thixotropy degree and loop's area for all the matrix slurries.....138
Figure 6.17 CMOR of castables CA-1, CA-2, CA-3 and CA-4 at different time.....139
Figure 6.18 AP of castables CA-1, CA-2, CA-3 and CA-4 at different time.....140
Figure 6.19 (a)-(d) Appearance of samples CA-1 and 2 cast at different time.....141
Figure 6.20 Flow resistance vs. torque viscosity.....142

Figure 7.1 PSD of the 3 compositions with different amount of microsilicas.....146
Figure 7.2 Self-flowability vs. water addition.....147
Figure 7.3 Comparison of self-flowability of the castables at different time.....148
Figure 7.4 Torque vs. impeller speed for MS-2.....149
Figure 7.5 Torque vs. impeller speed for MS-3.....149
Figure 7.6 Torque vs. impeller speed for MS-4.....150
Figure 7.7 Equivalent apparent viscosity vs. impeller speed for MS-2.....151
Figure 7.8 Equivalent apparent viscosity vs. time at high and low impeller speed.....152
Figure 7.9 Flow resistance vs. microsilica.....154
Figure 7.10 Torque viscosity vs. microsilica.....154

Figure 7.11 Shear stress vs. shear rate for all the matrix slurries.....155
Figure 7.12 Apparent viscosity vs. shear rate for all the matrix slurries.....156
Figure 7.13 Thixotropy degree and loop's area for all the matrix slurries.....157
Figure 7.14 (a)-(n) Appearance of samples CA-1 and 2 cast at different time.....160
Figure 7.15 Flow resistance vs. torque viscosity.....161

Figure 8.1 Plug flow of a castable in hose.....165
Figure 8.2 Schematic show of the segregation of a castable in hose.....166
Figure 8.3 PSD of FM-1, 2 and 3 between 1 and 100 μm with different Bauxite-3.....167
Figure 8.4 PSD of FM-2, 4 and 5 between 0.1 and 10 μm with different fine fillers....167
Figure 8.5 Self-flowability vs. water addition.....168
Figure 8.6 Comparison of self-flowability of the castables at different time.....169
Figure 8.7 Torque vs. impeller speed for FM-1.....169
Figure 8.8 Torque vs. impeller speed for FM-2.....170
Figure 8.9 Torque vs. impeller speed for FM-3.....170
Figure 8.10 Torque vs. impeller speed for FM-4.....171
Figure 8.11 Torque vs. impeller speed for FM-5.....171
Figure 8.12 Equivalent apparent viscosity vs. impeller speed for FM-1.....172
Figure 8.13 Equivalent apparent viscosity vs. impeller speed for FM-5.....173
Figure 8.14 Equivalent apparent viscosity vs. time at the impeller speed of 1.10 s^{-1}...173
Figure 8.15 Comparison of the results obtained by the fast and normal speed tests.....174
Figure 8.16 Flow resistance vs. fine fillers.....176
Figure 8.17 Torque viscosity vs. fine fillers.....176
Figure 8.18 Shear stress vs. shear rate for all the matrix slurries.....177
Figure 8.19 Apparent viscosity vs. shear rate for all the matrix slurries.....178
Figure 8.20 Thixotropy degree and loop's area for all the matrix slurries.....179
Figure 8.21 (a)-(j) Appearance of all the samples cast at different time.....183
Figure 8.22 Flocs form and films envelope particles.....183
Figure 8.23 Flow curve and schematic model for structural breakdown.....184

Figure 8.24 The matrix paste surrounding the aggregates.....185
Figure 8.25 Flow resistance vs. torque viscosity.....186

Figure 9.1 Self-flowability vs. water addition.....190
Figure 9.2 Torque vs. impeller speed for WA-2.....191
Figure 9.3 Torque vs. impeller speed for WA-3.....191
Figure 9.4 Torque vs. impeller speed for WA-4.....192
Figure 9.5 Equivalent apparent viscosity vs. impeller speed for WA-3.....193
Figure 9.6 Equivalent apparent viscosity vs. time at high and low impeller speed.....193
Figure 9.7 Bonding water and free water of castables WA-1, 2, 3 and 4.....194
Figure 9.8 Flow resistance vs. water additions.....195
Figure 9.9 Torque viscosity vs. water additions.....196
Figure 9.10 Shear stress vs. shear rate for all the matrix slurries.....197
Figure 9.11 Apparent viscosity vs. shear rate for all the matrix slurries.....198
Figure 9.12 Thixotropy degree and loop's area for all the matrix slurries.....199
Figure 9.13 Relationship between water addition and IPS and MPT.....200
Figure 9.14 Solid content of the castables and matrix slurries.....201
Figure 9.15 Relationship between IPS and plastic yield stress and viscosity.....201
Figure 9.16 Relationship between MPT and flow resistance and torque viscosity.....202
Figure 9.17 Relationship between flow resistance of the castables and plastic yield stress of the matrix slurries.....202
Figure 9.18 Relationship between torque viscosity of the castables and plastic viscosity of the matrix slurries.....203
Figure 9.19 Relationship between self-flowability and flow resistance of the castables and plastic yield stress of the matrix slurries.....203
Figure 9.20 Relationship between self-flowability and torque viscosity of the castables and plastic viscosity of the matrix slurries.....204
Figure 9.21 Relationship between self-flowability and IPS of the matrix slurries and MPT of the castables.....204

Figure 9.22 (a)-(h) Appearance of samples WA-1, 2, 3 and 4 cast at different time....206
Figure 9.23 Flow resistance vs. torque viscosity.....207

Figure 10.1 Flow decay.....213
Figure 10.2 Torque vs. impeller speed for 0-185 min.....214
Figure 10.3 Torque vs. impeller speed for 0-45 min.....216
Figure 10.4 Torque vs. impeller speed for 50-95 min.....216
Figure 10.5 Torque vs. impeller speed for 100-145 min.....217
Figure 10.6 Torque vs. impeller speed for 150-185 min.....217
Figure 10.7 Equivalent apparent viscosity vs. impeller speed for 0-50 min.....218
Figure 10.8 Equivalent apparent viscosity vs. time at high and low impeller speed....219
Figure 10.9 Flow resistance at different testing time.....220
Figure 10.10 Shear stress vs. shear rate for the matrix slurry at the different time.....221
Figure 10.11 Apparent viscosity vs. shear rate of the matrix slurry at different time....222
Figure 10.12 Apparent viscosity of the matrix slurry at different constant shear.....223
Figure 10.13 Thixotropy degree and loop's area of the matrix slurry at different time.224
Figure 10.14 Fine matrix conductivity with the water/solid ratio of 2.5 at 20 °C.....225
Figure 10.15 Exothermic profile of the castable at 20 °C.....226
Figure 10.16 Flow resistance of the castable and plastic yield stress of the matrix slurry at different aging time.....227
Figure 10.17 Torque viscosity of the castable and plastic viscosity of the matrix slurry at different aging time.....228
Figure 10.18 (a)-(f) Appearance of samples cast after 0, 45 and 185 min of testing....230

Figure 11.1 Photograph of pumping and shotcreting equipment Allentown RP-10.....231
Figure 11.2 Pumping of the castable mix with 6.5 wt% water addition.....232
Figure 11.3 After pumping (1#: 6.0 wt%, 2#: 6.5 wt%, 3#:7.0 wt% water).....233
Figure 11.4 The castable mix with 6.0 wt% after shotcreting.....233
Figure 11.5 The castable mix with 6.5 wt% water is being shotcreted.....234

Figure 11.6 The castable mix with 7.0 wt% water is being shotcreted 234

Figure 12.1 Flow resistance vs. torque viscosity of all the castables.....237
Figure 12.2 "PUMPING BOX" for predicting the pumping of all the castables.....238

LIST OF SYMBOLS AND NOMENCLATURE

A.P.	Apparent porosity
B.D.	Bulk density
CCS	Cold crush strength
CMOR	Cold modulus of rupture
G	Flow resistance
H	Torque viscosity
IPS	Interparticle separation distance
LCC	Low cement castable
MPT	Maximum paste thickness
PLC	Permanent linear change
PSD	Particle size distribution
PTI	Paste thickness index
SLI	Solid loading index
T	Torque
ULCC	Ultra-low cement castable

CHAPTER 1 – INTRODUCTION

In the late 90s, a new installation method known as shotcreting (a term from concrete industry equivalent to "wet-spraying" or "wet-gunning" in castable technology) has been attracting more and more interests because of its simplicity in installation [1-3]. In this process, refractory ingredients (aggregates, fine powders, binder and dispersing agent) premixed with water are transported with the help of a pump to a nozzle where some accelerators are added and projected at high velocity onto a receiving surface.

In the case of a pumpable castable, only the wet mix is directly transported by a two-piston pump to the application field. It is possible to obtain similar properties of high strength and density with those of vibrated castables. The main advantages in this process are:

- No nozzle-man needed.
- No rebound thus saving raw materials.
- Dust and noise-free and hence friendly to the installation environment.
- High efficiency process (less labor and installation time).
- Installation of complicated or random thickness lining.
- Homogeneous installation and no lamination.

Compared to a normal self-flow castable, a pumpable castable not only needs to flow well in pipe, but also to maintain self-flowability after pumping. So, the following characteristics are required:

- ✓ Good self-flowability during the whole process.
- ✓ Stable flowability and no segregation leading to blockage.
- ✓ Optimum working time and no setting inside pipes.
- ✓ Easy cleaning-up.

Since castable refractories consist of aggregates, fine powders, dispersants and water, it can be considered as a crowded particulate suspension of aggregate-matrix-water system with high solid content. The study of the flow behaviour of such system is quite important to improve the workability of castables. For a good pumpable castable, the rheological properties are critical factors governing the installation quality during the whole pumping process. Meanwhile, interactions exist among ingredients in the castable because they are not independent of each other in their effects, and these make the suspension rheological behaviour more complicated and sensitive. Even a very small variation will bring some critical effects on the rheology of a castable. There are many factors influencing the rheological behaviour and then the workability of the castables as shown in Figure 1.1.

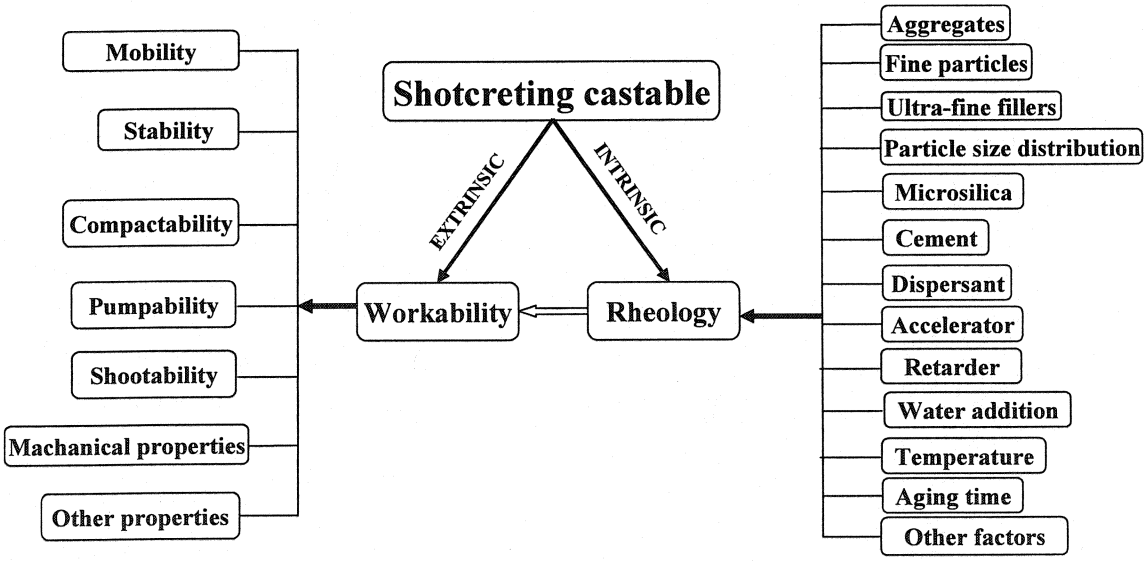


Figure 1.1 Factors Influencing rheology and workability of castables.

From Figure 1.1, it is understood that the study of the castable rheology is important to maximize the performance during installation. Unfortunately, most of the researchers worked only on the rheology of fine matrix part of castable and then attempted to correlate the behaviour of castable mix with fine matrix rheology [4-7]. In practice, it is found that when coarse aggregates are introduced into the matrix, there is a drastic

change in the rheological behaviour of the mix. This necessitates one to consider the study of the castable rheology rather than considering the rheology of the matrix.

The goal of this work is to design a shotcreting castable with good pumpability and to develop a new evaluation method to predict pumpability by a rheological approach.

To satisfy this purpose, the present work uses two kinds of rheometers to measure the rheological behaviour both the castable and the matrix portion and to predict the pumpability of the bauxite-based low-cement self-flow castables, through analyzing the influence of seven key factors on rheological properties, in the following order:

- ✓ Particle size distribution (PSD)
- ✓ Dispersant
- ✓ Cement
- ✓ Microsilica
- ✓ Fine fillers
- ✓ Water addition
- ✓ Aging time

So far low-cement castable technology is very matured and widely used. In this work, a bauxite-based low-cement castable system is considered. Therefore, the scope of this thesis includes the following steps:

1) To develop and evaluate a testing method to measure the rheological behavior of both the castable and the matrix;

2) To analyze the influence of the seven above-mentioned variables on the self-flowability, rheology of castables and matrix slurries, and the physical and mechanical properties of the green body.

3) To correlate the self-flowability, rheology between the castables and the matrix slurries.

4) To optimize all variables to obtain desirable pumpability;

5) To perform shotcreting trail to validate this predictive approach.

The experimental program has been divided into four parts:

a) Characterization of the properties of the raw materials used in this work in terms of PSD and chemical composition;

b) Study the self-flowability, rheology, physical and mechanical properties of the experimental castables. More than 80 experiments have been carried out on castables, in terms of rheology, self-flowability, water demand, mechanical and physical properties and sample surface appearance;

c) Study the rheology of matrix slurries and correlate the rheology of the castable and the matrix to optimize all variables and obtain appropriate parameters to allow for desirable pumpability. More than 60 experiments have been performed on the matrix slurries, in terms of rheology, conductivity and exothermic profile;

d) Conduct three shotcreting trials on 3 compositions of different nature to validate the method of evaluation.

This thesis is organized and structured as a succession of articles. In total, 9 technical papers have been prepared and 7 of them are already published, one of them accepted for publication and another is ready for submission. Nine conference presentations have been given for this work. This thesis consists of 12 chapters. The main body of the work

is constituted within Chapter 4 to 11, which deal with the influence of each key variable on the rheological and other properties of the castables and matrix slurries. The seven factors include PSD, dispersant, cement, microsilica, fine fillers, water addition and aging time. Each parameter is separately dealt with in one chapter.

Chapter 1 gives the goal, objectives and scope of this work. The thesis structure is introduced and the general conclusions are announced in this chapter.

Chapter 2 provides the theoretical background of rheology and current description of the shotcreting castable. The fundamentals of rheology are included and definitions and classifications are given. The practical aspect of the rheology is also reviewed in terms of the parameters such as PSD, interparticle separation distance (IPS), solid loading index (SLI) and maximum paste thickness (MPT). The test methods and design of the castables, using the rheological approach, are presented.

Chapter 3 deals with the experimental procedure, adopted methodology and the experimental design, raw materials, set-ups, and testing methods for self-flowability, density, porosity, cold strength, exothermic profile and rheology of castable in terms of flow resistance and torque viscosity, conductivity and rheology of the matrix such as plastic yield stress and viscosity, are described.

The influence of PSD on rheology of castable is dealt with in Chapter 4. A paper of the essentialities from this part is published in *Ceramics International* Vo. 30 No. 1, 2004, pp. 47-55. Four compositions of bauxite-based low-cement castables with different PSD in terms of the q value of 0.23, 0.26 and 0.29, and the D_{max} of 5 and 8 mm are studied for both the castables and the matrix slurries.

The effect of dispersants on rheological behavior is the subject of Chapter 5. A paper based on this chapter is to be published in COM'04 – *Proceedings of 4th International*

Symposium on Advances in Refractories for the Metallurgical Industries, August, 2004, pp. 811-826, Hamilton, Canada. Seven compositions with different types and amounts of dispersant have been studied. Self-flowability and rheology of the castables and matrix slurries have been measured and analyzed.

The role of calcium aluminate cement on the castable rheology is the subject of Chapter 6. A paper on this subject has been published in *Refractories Application and News*, Vol. 9, No. 1, 2004, pp. 18-24. Two kinds of cement are used and five compositions are studied, cement CA-14 at level of 0, 2, 4 and 6 wt %, and cement CA-25R at 4 wt% Bonding water and free water content in castables with different cements are considered.

The effect of microsilica on castable rheology is provided in Chapter 7 and a paper on this work is to be published in *INTERCERAM*, Vol. 53, No. 3, 2004, pp. 166-173. Four compositions are investigated with two kinds of microsilicas with different PSD and chemistry. Microsilica-1 (Elkem 971 U) has been used at 3, 5 and 7 wt% and Microsilica-2 (Global Silica fume) at 5 wt% for comparison purposes.

The effect of fine fillers on rheology of castable is discussed in Chapter 8, based on a paper accepted and being printed by the *Canadian Metallurgical Quarterly*. Five compositions are studied with different fine fillers, Bauxite-3, A 3000 FL and A 1000 SG. The ultra-fine filler Bauxite-3 is added at 3, 9 and 15 wt % to investigate its influence on castables. The last two compositions are focused on two reactive aluminas A 3000 FL and A 1000 SG. To compare the role of fine fillers with the same amount but different source, 9 wt% additions of two aluminas is studied in each composition.

The effect of water addition on low-cement castable rheology is presented in Chapter 9, based on a paper already published in *China's Refractories*, Vol. 13, No. 3, 2004, pp. 1-12. Four castables are made with the same composition but different water addition 6.0,

6.5, 7.0 and 7.5 wt%. The self-flowability, flow resistance, torque viscosity and physical and mechanical properties are tested and compared.

The influence of aging time on castable is explained in Chapter 10, based on a paper to be submitted to *the Journal of the European Ceramic Society*. The flowability and mobility of the castable mixes may change when time is elapsing. One composition is studied at different testing times on both the castable and the matrix slurry. Conductivity of the matrix slurry and the exothermic profile of the castable are also measured to investigate the hydration process and setting behaviour and their relationship with the castable rheology.

Chapter 11 gives the results on the shotcreting trials of optimized compositions. Based on the results from Chapter 4 to 10, the variables are optimized. The castables with optimal parameters have been shotcreted. The properties including cold modulus of rupture (CMOR), apparent porosity (AP), bulk density (BD), self-flowability, rebound loss have been measured.

Finally, conclusions are presented in Chapter 12 which includes the interpretation of the experimental results and comprehensive discussions. Considerations and suggestions for further improvements to study in-depth the rheology of castables are also given. The original contributions made in this work are summarized in this chapter.

This work has been carried out to fulfill the following set of objectives:

1) To obtain a new way to test the rheology of a castable. Hence the IBB rheometer has been used to measure the rheology of the whole castable to overcome the shortcomings of considering the matrix portion alone. As a result, it has been found that two rheological parameters, flow resistance and torque viscosity could be used to describe the rheological properties of self-flow castables.

2) To establish the correlation of the castable rheology and matrix rheology. Four parameters: flow resistance, torque viscosity, plastic yield stress and viscosity have been derived to described the rheology of both the castable and matrix.

3) To optimize all parameters in a rheological approach. At last, it has been shown that a castable with q value of 0.26 and D_{max} of 5 mm, 0.12 wt% dispersant SHMP, 4 wt% cement CA-14, 5 wt% Microsilica-1 (Elkem 971 U), 9 wt % Bauxite-3 and 7 wt% water has the overall desirable rheological properties and pumpability, for a bauxite-based low-cement shotcreting castable.

4) To define some significant pumpability criteria. At the end, a "PUMPING BOX" has been designed and built, which predicts the minimum and maximum values of the flow resistance G (1 ~ 2.5 Nm) and torque viscosity H (6 ~10 Nm.s) for trouble-free pumping of a castable.

5) To conduct shotcreting trials and demonstrate that the prediction of pumpability is valid and the testing method is meaningful.

All in all the five objectives have been met. However, the physical and mechanical properties of the experimental castables have only been tested at room temperature. High temperature properties and other properties would be needed to further confirm the usefulness of the selected castables. The influence of retarders and accelerators on the castable rheology is to be identified. The pumping box should be validated with more shotcreting trials.

CHAPTER 2 – THEORETICAL BACKGROUND OF RHEOLOGY AND SHOTCRETING

In this chapter, the theoretical aspects concerning the rheology and shotcreting are covered into three separated parts. In Part 1, the fundamental concepts related to rheological properties of monolithic refractories have been reviewed, covering different models, governing equations, and classification of rheological characteristics. Based on a discussion on the parameters such as particle size distribution, interparticle separation distance, solid loading index and paste thickness index, affecting the rheological characteristics of powder-liquid and aggregate-powder-liquid systems, the fundamental links between the design of refractory castables and workability aspects are highlighted. In Part 2, the "art of shotcreting" technology is presented, with an emphasis on its characteristics, history, advantages and application. Some considerations on the future of shotcreting castables development are also discussed. In Part 3, from rheological point of view, concepts and technical routes for designing and optimizing specific properties of a good pumpable/shotcreting castable to fit the installation and hardening requirements, are presented, with a focus on the particle size distribution.

PART 1: RHEOLOGY

2.1 Introduction [8-9]

The term "Rheology" was defined by Bingham as the science of the deformation and flow of the matter. This definition was accepted when the American Society of Rheology was founded in 1929. Researches on the deformation and flow of materials can be dated back to the late 17^{th} century, e.g. the well known Hooke's Law and Newton's Law for classical extremes of Hookean elastic solids and Newtonian viscous liquids. Since nineteenth century, however, these classical extremes have been viewed as

being outside of the scope of rheology, instead, the over-riding concern has become with materials between these classical extremes, i.e. with viscoelastic behaviors, which are seen in many substances such as non-drip paint, concentrated suspensions, plastics, rubber, foodstuffs, clays, etc., behavior of monolithic refractories falls also among such examples.

Rheological studies are revealed by mathematical and/or experimental ways, quantitatively or qualitatively, and are the expression of the relationships between stress, deformation of the matter and the time, on application of external forces, in correlation with composition, texture and properties of the materials. However, conscious application of the rheology in monolithic refractories is rather recent and far from being enough, as the history of monolithic refractories as a branch of refractories family is much younger than that of rheology itself.

Monolithic refractories consist of aggregates (above 0.075 mm up to 10 mm is size), fine powders (under 75 micron), ultra-fine powders (under 5 microns) and liquid additives such water or liquid binders. They may also be incorporated with different solid or liquid admixtures, modifying their properties required for installation. For different installation methods, a specific property, related to its "workability", is required such as: good flowability and thixotropy for vibration-flow castables, good flowability under gravity for self-flow castables, good plasticity for plastic mixes, good adherence for gunning mixes, good spreadability and plasticity for mortars or coatings, etc,. These correlate in nature with the rheological characteristics of the material systems. The workability of monolithic refractories is an ill-defined concept ad yet critical to the efficiency of installation and also to the quality of the installed lining in terms of uniformity, compactness, strength, etc; and thereafter closely link to the service performance of the lining. There have been growing awareness and interests of the importance and usefulness of rheology in understanding, evaluating, optimizing workability and consequently other related properties of monolithic refractories, or even in developing

new types of monolithic refractories. In this report, some fundamental knowledge on rheology, covering different models, governing equations, and classification of rheological characteristics, are reviewed. Factors such as particle size distribution (PSD), interparticle separation distance (IPS), solid loading index (SLI) and paste thickness index (PTI), affecting the rheological characteristics of the powder-liquid and aggregate-powder liquid systems, are discussed. Finally, the concepts and technical approach, for designing and optimizing specific installation of pumpable castable are suggested.

2.2 Fundamentals on Rheology

Rheological models are idealized relationships using mathematical, mechanical or electrical analogies [9]. Rheological equations of state, also called constitutive equations, are equations relating the stress and strain with time and sometimes other variables such as the temperature [9]. The "mechanical models" consist of spring, dashpot and frictional object elements so arranged, in parallel or series that the overall system behaves analogously to a real material, although the elements themselves may have no direct analogues in the actual material. They have a practical advantage where the main features of the behavior of a material can be inferred by inspection of the appropriate model, without going into the mathematics in detail.

2.2.1 Definitions of the Rheological Terms [10]

Rheology is the study of viscous behavior as a function of shear rate (Table 2.1). An atomizer, or a nozzle on a garden hose, for example, is a high shear device. A spoon, with which one stirs coffee, is a low shear device. The behavior of fluids and suspensions over these extremes of shear rate forms the subject of rheology. Most people are familiar with non-Newtonian fluids because several common foods fall into this category. Many ceramic suspensions exhibit shear-thinning non-Newtonian behavior, which is relatively common and desirable within the ceramic process systems. The opposite behavior, known as shear-thickening behavior or dilatancy, is quite undesirable in process systems. As the solid contents increase, however, suspensions and

forming bodies become crowded and the probabilities become quite favourable for producing dilatancy.

Table 2.1 Definition of some rheological terms [8]

Term	Symbol	Definition
Stress		Force per unit area.
Strain		The measurement of deformation relative to a reference configuration of length, area or volume.
Shear		The movement of a layer of material relative to parallel adjacent layers.
Shear stress	σ	The component of stress parallel to (tangential to) the area considered.
Shear strain	γ	Relative deformation in shear.
Shear rate	γ'	The change of shear strain per unit time.
Viscosity	η	Qualitatively, the property of a material to resist deformation increasingly with increasing rate of deformation. Quantitatively, a measure of this property, defined as the σ/ D in steady simple-shear flow.
Apparent viscosity	η_a	The shear stress divided by shear rate when this quotient is dependent on shear rate. Also called shear viscosity or simply viscosity.
Elastic(ity)		A reversible stress/strain behavior.
Plastic(ity)		The capacity of a material to be moulded but also to retain its shape for a significant period under finite forces; showing flow above a yield stress.
Viscoelastic(ity)		Simultaneous existence of viscous and elastic properties in a material.
Yield stress	σ_y	The stress corresponding to the transition from elastic to plastic deformation.

Dilatancy is one of the major categories of problems facing ceramic process engineers. Constantly fluctuating raw materials' properties may stray into certain regions, and dilatancy can occur and disappear (seemingly at random) at different points in a process. Such random occurrences of dilatancy can produce inhomogeneities within the product. Suspensions and bodies can actually tear in those local regions to produce cracks or large flaws. Dilatancy can alternatively produce highly porous regions in otherwise dense bodies, which can then also produce differential shrinkage, cracks, and/or flaws. Simple models can be demonstrated by three elements as shown in Figure 2.1.

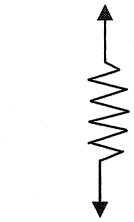
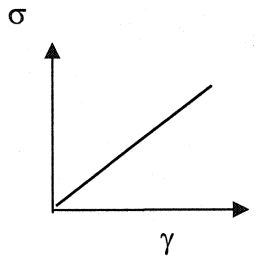
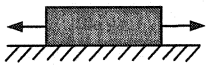
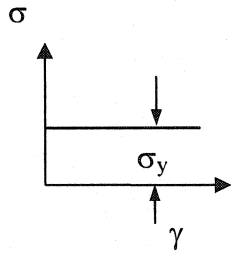
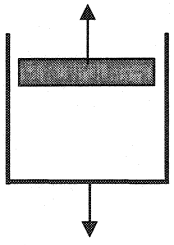
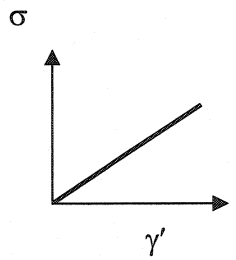
Model	Diagram	Characteristic curves	Rheological equation
Hookean solid model			$\sigma = G \cdot \gamma$ **(Equation2.1)**
St. Venant plastic model			$\sigma = \sigma_y$ **(Equation 2.2)**
Newtonian liquid model			$\sigma = \eta \cdot \gamma'$ **(Equation 2.3)**

Figure 2.1 Diagrammatic representations of three simple rheological models [8].

Model (1) represents the ideal elastic solid by a spring. In the elastic range, there is a direct proportionality between stress and strain, the constant of proportionality G being the rigidity modulus. When the applied force is removed, the elastic deformation will disappear and the solid recovers its original shape.

The analogy for the ideal plastic solid represented by model (2) is: when an applied force increases to overcome the friction between an object and a plate, the object will move. It indicates that when the applied shear stress reaches the yield stress, a plastic flow will occur during which the shear stress equals to the yield stress, being a constant.

Model (3) simulates the ideal viscous liquid, also called a Newtonian liquid, where the shear rate is simply proportional to the shear stress, as shown in Figure 2.2. Between the two parallel planes, at y = 0 and y = d, the intervening space is being filled with a liquid. The upper plane moves with the velocity v, the length of the arrows being proportional to the local velocity v_x. The resistance, which arises from the lack of slipperiness of the liquid, is proportional to the velocity with which the two planes are separated from one another. This lack of slipperiness is what has been called "viscosity", synonymous with the "internal friction" and it is a measure of the "resistance to flow". The force per unit area required to produce a motion is σ and it is proportional to the velocity gradient v/d, or shear rate γ'. The constant of proportionality η is called viscosity [10], i.e.

$$\sigma = \eta v/d = \eta\gamma' \qquad \textbf{(Equation 2.4)}$$

The characteristic of a Newtonian liquid is that the viscosity η is only a function of temperature, independent of σ or γ'. Water and some liquid binders for monolithic refractories can be treated as such liquids.

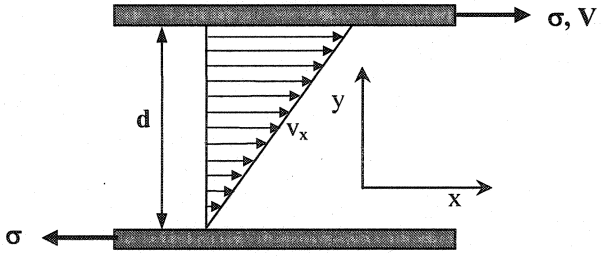


Figure2.2 Viscous flow between two planes [8].

2.2.2 Classification of Fluids [10-11]

The rheological behavior of a fluid or suspension characterizes its viscous behavior as a function of shear rate. In the field of monolithic refractories, the objects of rheology studies include the solid suspension systems with or without the aggregates. Their rheological characteristics can be expressed by the relationships between shear stress and shear rate, apparent viscosity and shear rate, or between viscosity and time under a constant shear rate. By oscillatory tests, the stress-strain relationships can be determined. There are six time-independent rheological types and two time dependent types. Time-independent fluids and suspensions behave similarly upon initial application of a shear stress as they do, for example, after 10 minutes of application over the same shear stress at the same shear rate. Changing the shear rate may produce a change in shear stress, but no variation with time. Time has no effect on the behavior of such fluids. In case of fluids and suspensions with time-dependent rheology, the apparent viscosity would change with time and shear rate variations; most crowded particulate suspensions and pastes are time-dependent fluids.

(1) Time Independent Flow Characteristics

Figure 2.3 shows the time-independent rheologies: Newtonian flow, Bingham flow, pseudoplastic flow, plastic flow, dilatant flow and dilatant flow with a yield value in two different forms [10-11]. Figure 2.3 (A) shows the six rheological behaviors plotted as shear stress versus shear rate, and Figure 2.3 (B) shows them plotted as apparent viscosity versus shear rate. Note that in Figure 2.3 (B), the Newtonian curve is the only

one that exhibits constant viscosity as a function of shear rate. The other five "non-Newtonian" rheologies exhibit variations of viscosity with shear rate changes.

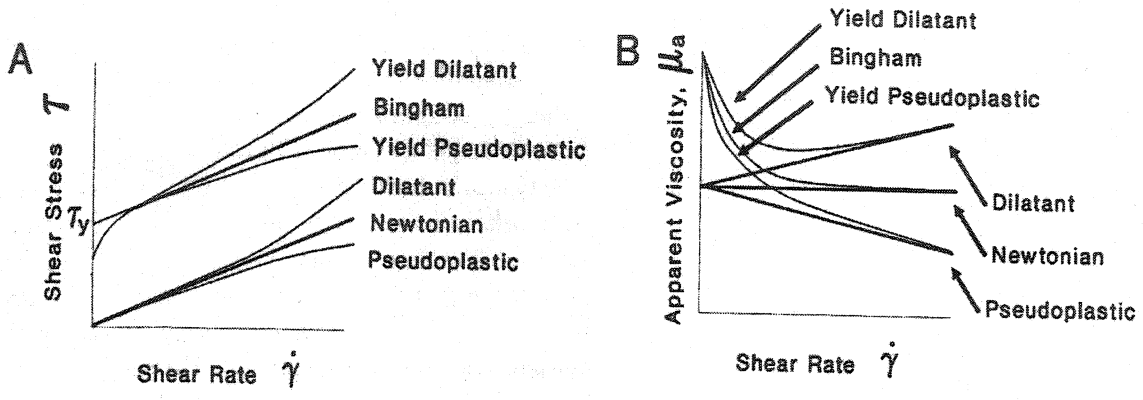


Figure 2.3 Flow patterns under low shear rate [10].

(a) Newtonian flow is characterized by a straight line from the origin when shear stress is plotted vs. shear rate. The viscosity is constant at constant temperature.

(b) Bingham flow is characterized also by a straight line, but not from the origin but starting rather from a given yield stress. The apparent viscosity (plastic viscosity) approaches a constant value with increasing shear rate.

(c) Pseudoplastic flow is characterized by a convex curve from the origin when σ is plotted versus γ'. The apparent viscosity decreases with increasing shear rate (shear thinning).

(d) Plastic flow is essentially the same as pseudoplastic flow except that there is a yield stress and sometimes called as yield-pseudo-plastic flow.

(e) Dilatant flow is characterized by a concave $\sigma - \gamma'$curve from the origin. The apparent viscosity increases with increasing shear rate (shear thickening).

(f) Dilatant flow with a yield value is essentially the same as dilatant flow except for the yield stress. The apparent viscosity decreases first to a minimum value then increases with increasing shear rate.

(2) Time dependent flow characteristics

The time-dependent rheologies such as thixotropy and rheopexy are shown in Figure 2.4. Thixotropy and rheopexy of solid-water suspensions are typical phenomena of time dependent flow characteristics.

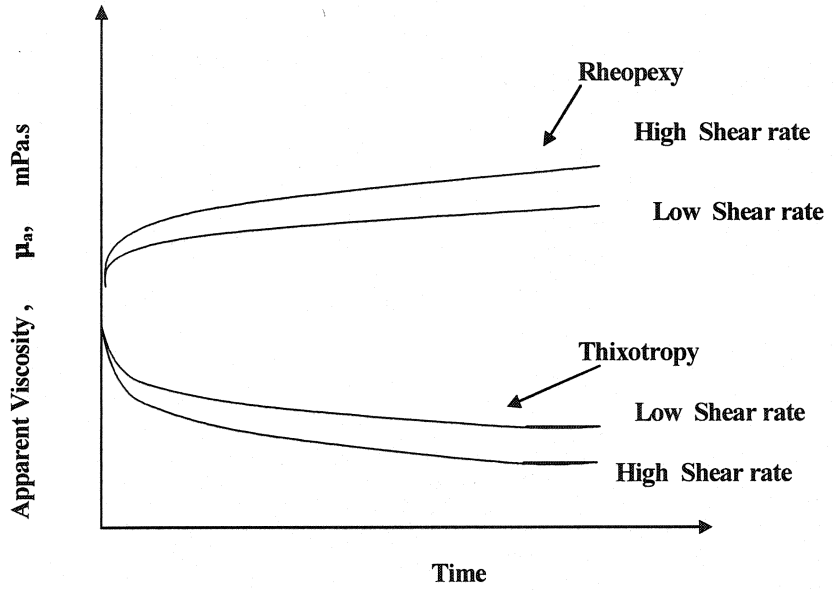


Figure 2.4 Two time-dependent rheologies showing dependent on shear rate [10].

(a) Thixotropy is defined as a decrease of the apparent viscosity with time under constant shear stress or shear rate, followed by a gradual recovery (reversibility) when the stress or shear rate is reduced or removed. Thixotropy is closely related to shear-thinning behavior and is usually expected in yield-shear-thinning suspensions because of the gelation that occurs in such suspensions, begins to break down, producing lower measured viscosities. At higher shear rate, the more the gels break down, the lower the measured viscosity becomes. Although the gel structures break down under shear, the structures will form again in time. The suspension properties, related both to particle

physics and interparticle chemistry, determine the rate at which the gels will form, which is known as the gelation rate. The gelation rate, measuring the rebuild of gel structures, will balance the shear rate, which breaks down the gel structures. The minimum viscosity achieved by a system at constant shear rate will occur at a balance point between these two phenomena. Higher shear rates will cause more gel to break down, and the balance point with gelation will be at a lower apparent viscosities.

Thixotropy is an important topic in rheology. Some detailed reviews on it are provided by J. Mewis [12] and Barnes [13]. Figure 2.5 shows the behavior to be expected from a thixotropic material by cyclic shearing test, or in other words, a loop test with the shear rate increased continuously and linearly in time from zero to a maximum and then decreased to zero in a similar way. The up-curve and down-curve do not coincide and produce a loop called "hysteresis loop". The area can be used to compare the degree of thixotropy, when other properties are similar.

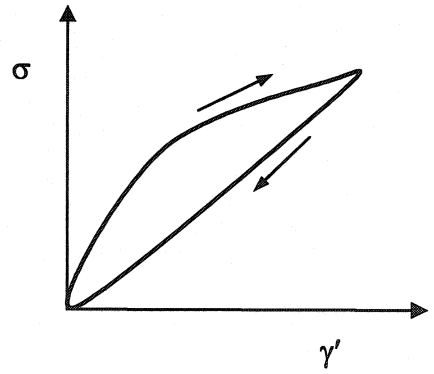


Figure 2.5 Schematic response of a thixotropic material to two shear-rate histories [12].

In monolithic refractories, a good thixotropy is required for vibration-cast type of castables. During casting under vibration, the mixes should easily flow to fill the mould, during which the trapped air should escape to avoid big pore formation in the installed body. This flowability during casting comes from thixotropy. To artificially increase the flowability, if too much water is used, the porosity of the body will be too high and

segregation may happen. In a normal case, after casting when the vibration stops, the internal structure should soon recover to avoid segregation of the coarse aggregates.

(b) Rheopexy, also called anti-thixotropy or negative thixotropy, is defined as an increase of the apparent viscosity with time under constant shear stress or shear rate, followed by a gradual recovery when the stress or shear rate is reduced or removed. Opposite to thixotropy, it is a shear-thickening behavior. It is expected there is also a hysteresis loop, but the down-curve is above the up-curve, as schematically shown in Figure 2.6, in comparison with positive thixotropy.

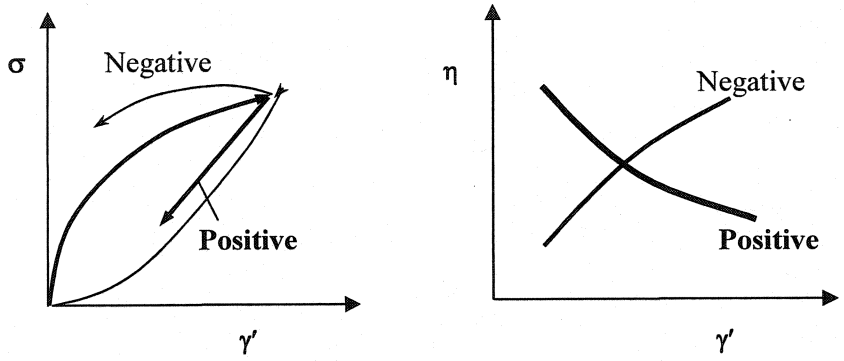


Figure 2.6 Schematic flow curves of positive and negative thixotropic materials [11].

2.3 Practical Rheology

Rheological behavior of monolithic refractories depends on both the powder-liquid (water, in most cases) system and the aggregates-powder-liquid (water) system as well. Besides, shearing history in terms of mixing equipment, mixing intensity and mixing time have also influences on the rheological properties. The main factors affecting the results are thus discussed separately hereafter.

2.3.1 Particle Size Distribution (PSD) [10]

The texture of a refractory castable is based basically on the coarse particles or aggregates touching each other. The voids between these large particles are filled with a viscous suspension consisting of a fluid (water) and solid fines, super-fines and cement.

The role of the cement is to act as "glue" which after setting, transforms the castable into a solid body. At higher temperatures the hydrated cement may also take part in different high temperature reactions. Initially, the role of the cement in the context of particle packing is, however, merely as a finely ground solid.

The PSDs within the packed particulate systems play an integral role in the processing of many ceramic products. Not only are the properties of the final products affected, such as porosity, density, and strength, but also the installation characteristics of the bodies such as plastic viscosity, casting rate, permeability and drying rate.

To describe particle packing distribution, Andreasen's work considers the packing of particles where all particle sizes are represented in a continuous distribution. Furnas's work considers the packing of discrete particle sizes. Andreasen based his experiments on the fundamental and theoretical idea that optimum particle packing requires similarity conditions to be met as the particles and their environments decrease in size. This similarity condition led to his equation [10]:

$$\frac{CPFT}{100\%} = \left(\frac{D}{D_L}\right)^n \qquad \textbf{(Equation 2.5)}$$

where, CPFT = cumulative percent of particle size finer than, %,

D = particle size, mm,

D_L = the largest particle size, mm,

n = distribution modulus.

His experimental results show that the best packing occurred between distribution moduli "n" values of 0.33 to 0.50. Funk and Dinger derived an equation from both Andreasen and Furnas shown below [10]. That takes an account the addition of a finite smallest particle size, D_S, showing that the optimum packing occurs for distributions with exponent equal to 0.37.

$$\frac{CPFT}{100\%} = \frac{D^n - D_S{}^n}{D_L{}^n - D_S{}^n} \qquad \textbf{(Equation 2.6)}$$

where, CPFT = cumulative percent of particle size finer than, %,

D = particle size, mm,

D_L = the largest particle size, mm,

D_S = the smallest particle size, mm,

n = distribution modulus.

On a log-log plot, Funk and Dinger equation is represented by a curved line while Andreasen is by a straight line. Funk and Dinger equation is complicated whereas Andreasen is easy to use and semi-empirical. The main disadvantage with Andreasen Equation is that it implies an infinite distribution with no minimum particle size. The real systems are of course finite, but anyhow the equation may be used as a tool, because of its simplicity.

2.3.2 Interparticle Separation Distance (IPS) [10, 14]

Refractory shapes are conventionally produced from powder-water blends using a large variety of refractory ceramic compositions at many levels of solids loadings. Pure fine grained Al_2O_3 may be slip cast at nearly 60 volume % solids; plastic fireclay may be cast at nearly 50 volume % solids; and some vibratory cast mixes may contain as much as 95 volume % solids. As the solid loading increases, the rheological property called "dilatancy" becomes more important and more obvious. The severity of dilatancy depends upon the PSD and the interparticle chemistry of the mix. As the solid loading for any composition increases, the greater the importance to control the PSD of the body becomes, in order to minimize viscosity at some forming shear rate.

From the volume surface area, porosity, and volume fraction of the solids in the final wet mix, we can calculate the average IPS in a suspension, assuming that all particles are touching each other in a dry body. Ignoring the different affinity for water between clays and non-clays, as water is added to the dry body, the pores volume must first be filled

before any particle separation can occur. When the pores volume is completely filled, any further water addition can then separate the particles. The separation distance is twice the thickness of the additional water spread over the surface area of the particles. The equation to calculate IPS, which is derived, is shown as Equation 2.7 [10]:

$$\mathbf{IPS} = \frac{2}{\mathbf{VSA}}\left[\frac{1}{V_s} - \frac{1}{1-P_{of}}\right] \qquad \textbf{(Equation 2.7)}$$

where, IPS = interparticle separation distance, μm,

VSA = volume surface area, (= SSA· ρ_P), calculated from the measured specific surface area (SSA) multiplied by particle density (ρ_P), m^2/cm^3,

V_s = volume fraction of solids in the mix,

P_{of} = pore fraction of the body when all particles are in contact after drying.

IPS is a major determinant of the rheology of a castable mix. Obviously if the moisture content is less than or equal to the porosity of the dry body, the mix will not flow; it will behave as a dry solid mass. Only when the moisture content sufficiently exceeds the porosity to separate the particles a minimum of 50 nm, can any reasonable fluidity be expected. For example, IPS values for traditional deflocculated whiteware casting slips are about 100 nm. Bodies with IPS distances less than 50 nm may flow, but they will exhibit high viscosity and also very severe dilatancy as shear rates increase. Bodies with different PSDs may have the same porosity but significantly different surface area, so the addition of the same amount of water will not produce the same IPS or, therefore, the same fluidity. The amount of additional water needed to impart fluidity then depends upon the PSD of the different ingredients of the body.

This is illustrated in Figure 2.7 and Figure 2.8 where hypothetical bodies are produced using the Funk and Dinger Equation 2.6. The histograms of all the bodies in Figure 2.7

on a log-log plot, differ only slightly by the volume % in each class size. Figure 2.7 compares four bodies all with the same n = 0.37 and D_s = 0.1 μm, but each with different D_L. This figure illustrates how increasing the size of the largest particle decreases the porosity due to improved packing efficiency, decreases the VSA, and thereby increases the IPS. In this case the widest size distribution with D_L = 3360μm, which has the lowest porosity and the largest IPS, should provide the highest fluidity at a given solids content.

Figure 2.8 gives the data plotted as percent porosity and volume surface area as a function of IPS at 90 volume % solids loading for distributions with D_L = 3360μm and D_S = 0.1μm. The distribution with ideal packing n = 0.37 shows a lower porosity than the distributions with n = 0.32 or n = 0.42, although all of their VSA values are in the same order. If IPS = 75 nm is selected for a fluidity target, there appears to be little difference in VSA ≈ 1.0 m^2/cm^3 between the bodies with n = 0.32 and 0.37. The body with n = 0.42 has a lower VSA of 0.5 m^2/cm^3. Therefore there appears to be no significant difference between the bodies with n = 0.32 and 0.37.

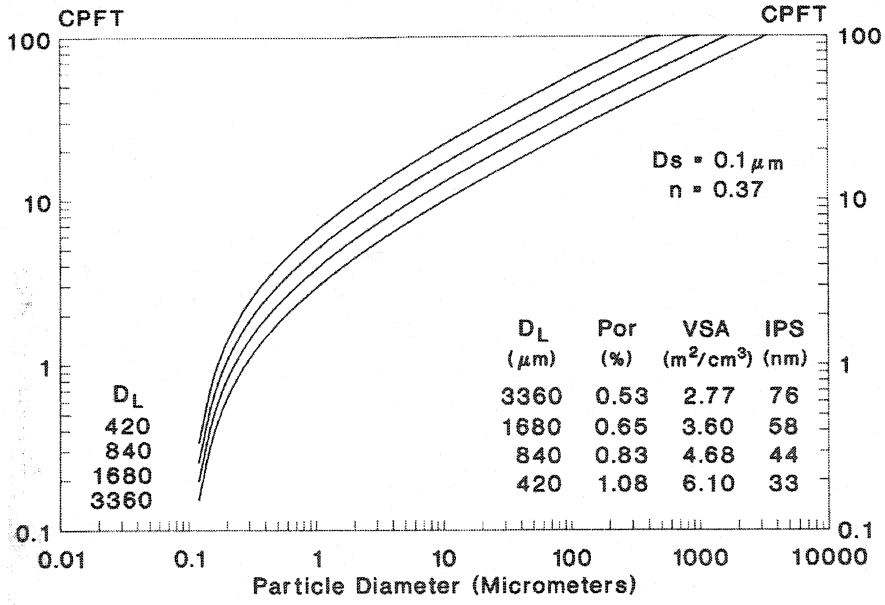


Figure 2.7 CPFT as a function of D for four hypothetical body compositions, with different largest particle size, D_L [10].

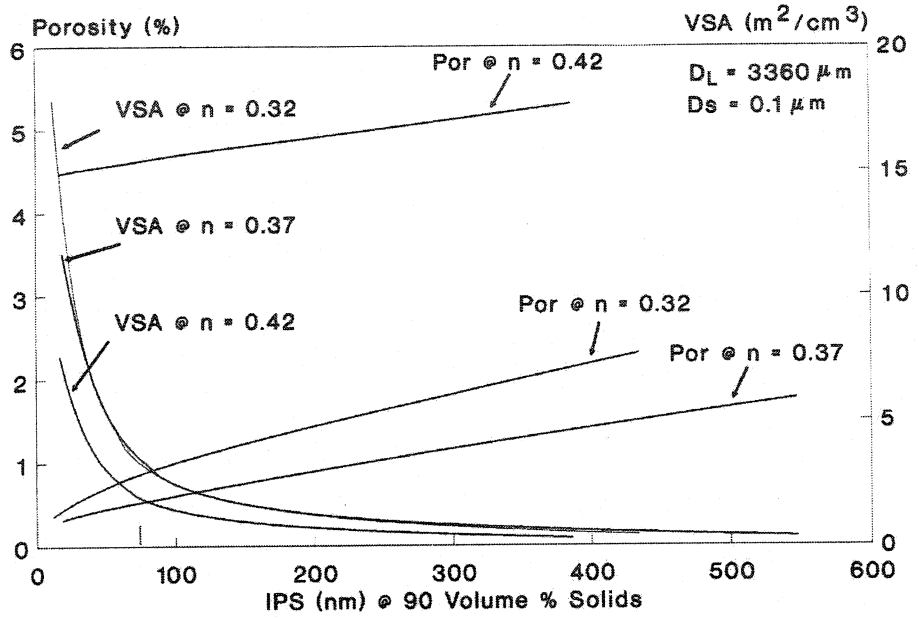


Figure 2.8 Percent porosity and volume surface area as a function of IPS at 90 volume % solids suspensions containing powder [10].

Based on the above results, the conclusions have been drawn as follows:

(a) The IPS, and not the particle packing efficiency, is the most importance criterion for designing a very highly loaded, self-lowing refractory castable mix.

(b) The IPS is determined by a combination of volume surface area, volume fraction of solids in the suspension, and the porosity of the dry body. All are important, but their significance increases with increasing the solids loading.

(c) The shear rate used in forming the body, strongly influences fluidity when the PSD modulus changes. For so called thixotropic casting or placing, the frequency of vibration is associated with the shear rate, and amplitude is associated with the shear stress. Therefore, a particular frequency and the amplitude would be optimum for a particular body. Large variations in n, D_L, or D_S, and/or additive chemistry would change the mechanical requirements for best flow behaviour. For example, if a good flow is attained at given vibrator conditions or a body with the modulus n = 0.32 and a

change in the grind produces a change in the rheogram to yield a curve similar to that for n =0.37, then the same vibrator settings may be inadequate for good forming.

2.3.3 Solid Loading Index (SLI)

Qualitatively it is easy to predict that when the concentration, counted in volume fraction, called phase volume, of the suspended material increases, more resistance arises because particles have to move out of each other's way, leading to higher viscosity. For diluted dispersed suspensions (< 10% phase volume), Einstein [15] derived a formula showing that all single particles increase the viscosity of a suspension as a simple function of their phase volume.

$$\eta = \eta_s(1 + K\phi) \qquad \textbf{(Equation 2.8)}$$

where, η_s = viscosity of the suspending medium, Pa.s,

ϕ = phase volume in fraction,

K = a constant depending on particle's shape, for spherical particles, K = 2.5.

Formula (2.8) is based on the postulates: the particles are spherical, rigid and wettable by the medium; interactions between the particles are neglected; and the liquid deformation is laminar. When interactions between the particles are included, the situation becomes more complicated, and is accounted by higher-order terms in ϕ, the common formula being

$$\eta = \eta_s(1 + a\phi + b\phi^2 + \cdots) \qquad \textbf{(Equation 2.9)}$$

It is derived that theoretically a=2.5 and b=14, but experimentally, b=5 – 8 [15]. The reason why the phase volume is so important is that the rheology depends to a great extent on the hydrodynamic forces acting on the surface of particles, generally irrespective of the particle density. The situation for concentrated suspensions is even more difficult to analyze from a theoretical point of view. The only methods available to

tackle the problem are to introduce a technique for averaging the influence of neighboring particles or alternatively to simulate the situation using computer modeling.

It is this complication that makes the rheological behaviors of concentrated suspensions to be non-Newtonian but rather plastic, pseudo-plastic and dilatant. Mooney [16] provided the desired link between viscosity and solids loading. Today the Mooney's Equation 2.10 is the most common expression linking viscosity of crowed suspensions of non-agglomerating particles to the solids loading. It relates the mixture viscosity η_M to the liquid viscosity η_L and the ratio of the solids loading to the maximum packing density. The solids loading Φ is defined as the solid volume of powder divided by the total volume. Thus, the maximum solids loading, also known as the critical solids loading Φ_C, is the inverse of the maximum packing density.

$$\eta_M = \frac{\eta_L}{(1-\frac{\Phi}{\Phi_C})^N} \qquad \textbf{(Equation 2.10)}$$

where, η_M = mixture viscosity, Pa.s,

η_L = liquid viscosity, Pa.s,

Φ = solids loading,

Φ_C = maximum packing density (critical solids loading),

N = exponent, 2 -3.5.

In many powder systems the exponent N is in the range from 2 to 3.5, and for larger particle sizes (over 10μm) N = 2 is the most appropriate. For a fixed solid content Φ, the higher the maximum solids loading Φ_C the lower the mixture viscosity. In all suspensions, the viscosity reduces as the solids loading decreases [17-18]. If the fine powder (less than 10μm) used in the suspension has a high maximum packing density, then the mixture viscosity is lower than for all solids loadings. The viscosity of particle suspensions decreases inverse proportionally to the shear rate [19]. Further, when the

particles are anisotropic, then a hysteresis problem arises. Sharp changes in strength and viscosity are observed with angular particles.

As a demonstration of the viscosity behaviour, Figure 2.9 plots the relative viscosity for mixtures of two size spheres at a constant 55% solids loading. Since bimodal powders have a maximum packing density (critical solids loading) that depends on composition, then according to Equation 10 the viscosity will shift. As it is evident, the lowest viscosity occurs at the same composition expected to give the highest packing density. Further confirmation of the link between the critical solids loading and maximum packing density is captured in Figure 2.10. This plot superimposes results from powders with different maximum packing densities, showing convergence to a normalized curve of relative viscosity versus relative solids loading (actual solids loading divided by the maximum packing density or critical solids loading).

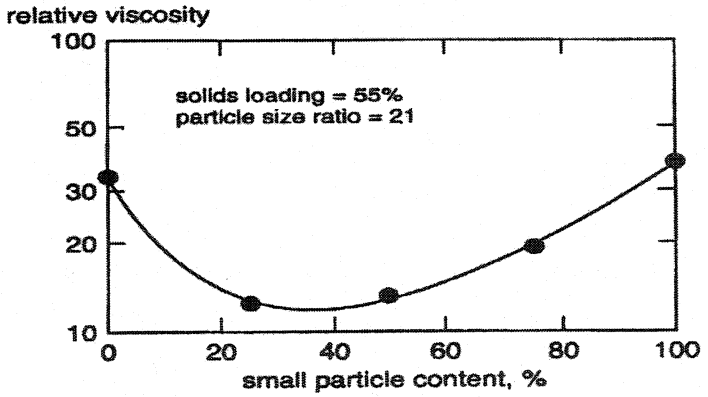


Figure 2.9 Relative viscosity versus the amount of small particles for bimodal mixtures of spheres with a large: small size ratio of 2:1 [20].

The optimal number of component particle sizes for high packing densities and low viscosities depends on the inherent packing density of the powders and the particle size ratio involved in the mixture. Bimodal mixtures give higher packing densities than tri-modal mixtures for smaller particle size ratios. In all cases, the optimal packing condition has a high proportion (by volume or weight) of the largest particles. For a

continuous PSD the packing density increases as the width of the distribution increases. Additionally, the more equiaxed and spherical the particles, the higher the packing density, but there is a limitation to the maximum density attainable. For continuous PSDs, various theories predict maximum densities as high as 96%. An experimental density has been demonstrated. Near-optimal distributions have been empirically discovered in several industries. They have a characteristic wide range of small particles. An optimal PSD for maximum density is obtained with

(a) Use of the largest mean particle size

(b) Use of round particles as opposed to angular particles

(c) A high proportion by volume of large particles

(d) A low proportion of intermediate sized particles

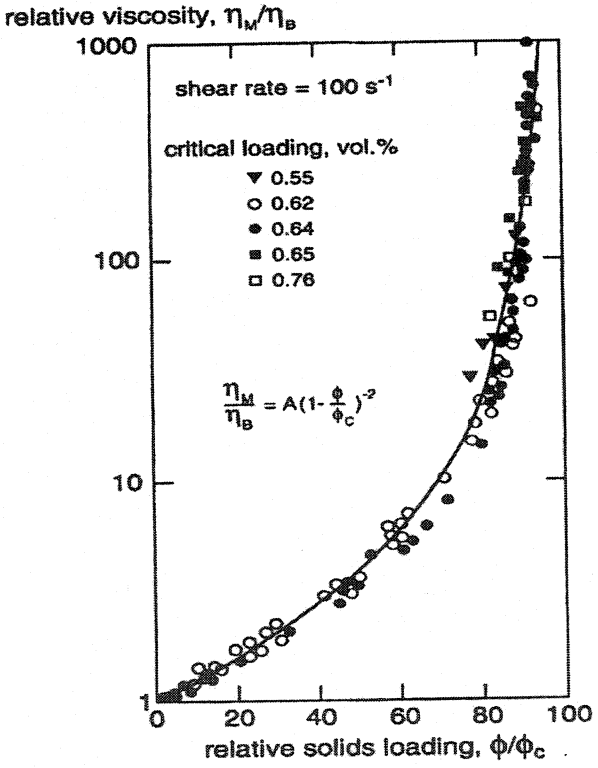


Figure 2.10 Relative viscosity versus the Mooney equation [20].

Accordingly, it is possible to identify ideal powders for various particle sizes forming process. Such a powder will have a tailored PSD for a high packing density, yet low

cost. It will consist of dense, discrete particles free from agglomeration with smooth surfaces and a nearly spherical shape. The size distribution should be wide, but skewed to follow the Andreasen equation. Generally the liquid lubrication film thickness should be sufficient to allow uninhibited particle flow, meaning the actual solids loading should be slightly below the critical solids loading. By selecting high packing density PSDs it is possible to form low viscosity suspensions with excellent flow.

2.3.4 Paste Thickness Index (PTI) and Maximum Paste Thickness (MPT) [20-21]

Most powder forming technology relies on particle lubrication from a fluid phase to assist in shaping. The fluid phase is divided into two partitions: that portion needed to fill all voids when the powder is at the maximum packing density (termed the immobile fluid) and the excessive fluid that provides lubrication (termed the mobile fluid). These are saturated suspensions with all pore space filled with fluid. It is the extra fluid from dilation to a lower packing density than the maximum packing density that ensures lubricated particle flow. Schematically, this concept is sketched in Figure 2.11. The concept of a lubricating layer, where the voids are filled between the particles with the immobile fluid and the flow between particles in lubricated layer by the mobile or excess fluid over the required liquid to fill the voids at the critical solids loading which corresponds with the maximum packing density. It is the thickness of the lubricating layer between particles that determines the viscosity of the solid-liquid suspension.

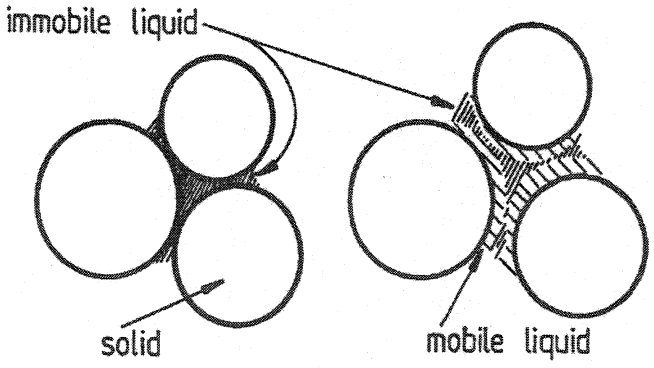


Figure 2.11 The concept of a lubricating layer [20].

A viscous suspension then consists of discrete particles with all of the pores between the particles filled with fluid. It is the lubricating layer thickness that determines the viscosity; hence, a linkage is needed between the layer thickness and the solid content in the suspension, known as the solid loading. As long as the particles are relatively large, typically not colloids, then at the critical solids loading the particles are in the "point contact", reflecting the same condition as at the maximum packing density. If the solid loading is below the critical level, meaning that the powder is below the maximum packing density, then the excess fluid lubricates the particles.

Associated with this powder-fluid structure, the points of concern are the strength and the viscosity. The strength measures the stress needed to initiate flow and the viscosity measures the stress needed to sustain the flow. The higher the desired flow rate, typically the greater the stress. Particles have a natural tendency to adhere and agglomerate, leading to a low yield strength. Flow is initiated once the applied stress exceeds the yield strength, which increases with shear strain rate and solids loading. Typically this strength is low (in the range of 100 Pa or less) and can be ignored, but it is beneficial in holding shape after forming.

It is the excess fluid, termed the "mobile fluid", which provides lubricity and lowers the suspension viscosity. The thickness of the lubrication layer δ can be estimated based on the solids loading and powder surface area on a volume basis S_v [20],

$$\delta = \frac{4(1-\Phi)}{S_v} = \frac{2}{3} D\left(\frac{1-\Phi}{\Phi}\right) \qquad \textbf{(Equation 2.11)}$$

where, δ = lubrication layer, mm,

Φ = solids loading,

D = particle size, mm,

S_v = volume surface area, m^2/cm^3.

This form assumes the particles are mono-sized spheres. If a homogeneous mixture is further assumed, then the lubricant layer thickness can be expressed as a function of the

particle size D, critical solids loading or maximum packing density Φ_C, and the actual solids loading Φ as follows [20]:

$$\delta = [(1 + \frac{1}{\Phi} - \frac{1}{\Phi_C})^{\frac{1}{3}} - 1] \qquad \textbf{(Equation 2.12)}$$

where, δ = lubrication layer, mm,

Φ = solids loading,

Φ_C = maximum packing density (critical solids loading).

As the lubricating layer increases in thickness, the viscosity and strength decrease with desirable attributes in high solids loading suspensions. It is the particle density that determines the system behaviour. Low viscosities are possible in high solids loadings if the PSD is adjusted for a high packing density.

As the separation distance between the coarse particles is markedly influenced by the matrix (less than 180 meshes) volume content and, consequently, by the concentration of fine particles, the packing model adopted is of significant importance to the flow behaviour of castables. It has been reported that the castable self-flow behaviour is only achieved when the distance between coarse particles (diameter > 100 μm), which are separated by the dispersed matrix, is superior to a minimum critical value. Bonadia et. al [21] suggested that the maximum paste thickness (MPT) can be used to determine the correlation between the refractory castable flowability and the packing model. The MPT parameter, already known in civil engineering, estimates the average distance between aggregates (coarse particles). Hence, it can be useful tool for the evaluation of packing models. Such parameter considers that part of the matrix is responsible for coating the coarse grain surfaces, where another portion fills the voids among them, and lastly, the fraction in excess accomplishes the separation between aggregates. Actually, the MPT is derived from the IPS, as suggested by Dinger and Funk [10]. The latter parameter is similar to MPT, but it is more commonly used for the fine fraction, since it considers water as the separation medium, instead of the matrix. The MPT is defined [21] as,

$$\mathbf{MPT} = \frac{2}{\mathbf{VSA}}\left[\frac{1}{V_s} - \left(\frac{1}{1-P_o}\right)\right] \qquad \textbf{(Equation 2.13)}$$

where, MPT = maximum paste thickness, μm,

VSA = volume surface area of coarse particles, m^2/cm^3,

V_s = volume concentration of coarse particles,

P_o = residual porosity considering optimum packing of coarse particles.

The original MPT equation proposed by Larrard and Sedran [22], assumes the existence of spherical particles, and does not include the porosity term. It has been found that the marked difference, usually encountered between the theoretical and experimental discrete curves, shows the importance of introducing the MPT parameter as an additional tool for castables formulation. Higher MPT values, considering the castable of having a discrete PSD, are usually responsible for enhanced flowability. However, the MPT value must have an upper limit, otherwise some thermo-mechanical properties, such as the creep at high temperature, could be seriously degraded. Since flow is a function of the MPT and of the matrix rheology, a combined analysis of these two parameters could be useful to predict the castables rheological behaviour.

2.4. Application in Castables

2.4.1 Classification of Castables by Rheology

One classification is based on the type of placement; 3 types are to be considered: weak vibration type, strong vibration type and non-vibration type. These three types include the Newtonian fluids (Time Independent) and Non-Newtonian fluids (Time Dependent) [23-24].

(1). Weak Vibration Type

The conventional castable shows the Bingham–flow (plastic flow) with low yield stress and low plastic viscosity similar to that of concrete. Moderate flowability is obtained by weak vibration. Usually shaft vibrators are used for installation.

(2). Strong Vibration Type

Low-cement castables (LCC) have high yield stress, high plastic viscosity and remarkable time dependent thixotropic flow characteristics. Relatively high-power vibration force is required to obtain moderate flowability.

(3). Non-Vibrating Type

LCC, Ultra-low cement castable (ULCC) and no-cement castable (NCC) showing self-flow behaviour fall in the category of non-vibrating type. They have very low yield stress. Fundamentally, they are placed and compacted by self-weight without external vibration force.

2.4.2 Rheology and Fluidity Test Methods Used in Castables

A growing demand for refractory castables with specific behaviours (e. g. self-flowing, pumpable, shotcreting, etc.) has stimulated studies on the development of compositions with predicable and controlled rheological properties. Since it is very difficult to directly measure the rheological behaviour of castable, some test of flowability and matrix rheology measurement are normally used to predict the fluidity of castables in the practical field.

(1). Matrix Rheology Measurement: Viscometer

In the ceramic field, the rheological behaviour of a casting slip or suspension is often studied using a viscometer. The coaxial cylinders of the viscometer have been used very often to study matrix paste rheology. The apparatus consists of two cylinders coaxially mounted; one is fixed and the other rotates at various speeds. When the solid-liquid suspension fills the space between the cylinders (the gap) and when the rotating cylinder is in motion, a torque is induced on the fixed cylinder through the sheared liquid. A relationship similar to Figure 2.12 (b) can be obtained for a Newtonian fluid [25].This kind of rheometer is a piece of equipment developed to evaluate properties (e. g., viscosity, yield stress and others) of rheological fluids and suspensions as a function of time, shearing rate, etc.

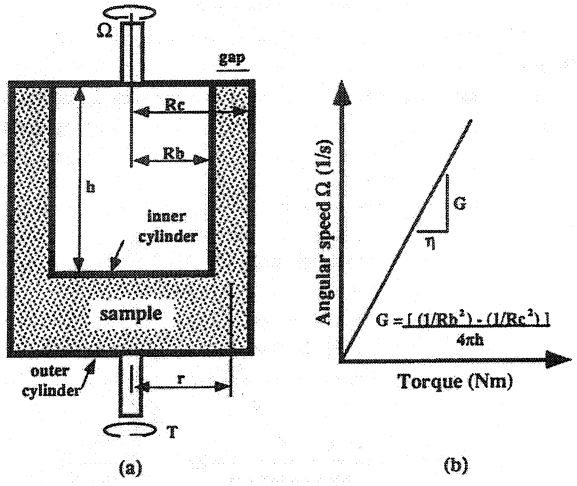


Figure 2.12 Representation of the coaxial cylinders viscometer [25].

For this apparatus, the shear stress (τ) equals the torque (T) divided by the surface area of the cylinder ($2\pi rh$) and its radius r. The relationship between the shear rate (or velocity gradient $rd\omega/dr$) and torque is [25]:

$$T/(2\pi rhr) = \eta r d\omega / dr \qquad \textbf{(Equation 2.14)}$$

where, T = torque, N.m,

η = the coefficient of viscosity, Pa.s,

r = cylinder radius, m,

h = height of the inner cylinder, m

ω = angular velocity, radians/sec.

By integrating Equation 14 between the radius of the inner cylinder, Rb, and the radius of the outer cylinder, Rc, for r and between 0 and Ω for ω and by isolating η (assuming η is independent of shear rate), the following relationship is obtained:

$$\eta = \frac{T\left(\frac{1}{Rb^2} - \frac{1}{Rc^2}\right)}{\Omega 4\pi h} \qquad \textbf{(Equation 2.15)}$$

where, T = torque, N.m,

η = the coefficient of viscosity, Pa.s,

R_b = radius of the inner cylinder, m

Rc = radius of the outer cylinder, m

h = height of the inner cylinder, m

Ω = rotor speed = $60\omega/(2\pi)$, min^{-1}.

In Equation 2.15, the ratio Ω/T is the slope of the line in Figure 2.12(b). From a constant factor $G = [(1/Rb^2) - (1/Rc^2)]/4\pi h$, the slope of the plot of Ω vs. T is equal to G/η for a coaxial cylinder viscometer with physical characteristics similar to those of Figure 2.12(a).

It is understood that the study of castable rheology is important in order to have better performance during installation. Most of the researchers worked only on rheology of fine matrix of castable and attempted to correlate the behaviour of castable mix with fine matrix rheology [4-7]. In practice, it is found that when coarse aggregate is introduced into matrix, there is a drastic change in rheological behaviour of castable. This necessitates one to consider the study of rheology of castable rather than considering the rheology of matrix.

Mobility is the ability of a fresh mix to flow and fill the formwork or other space. It is a very important characteristic not only to the cast-in-place castable but also to the shotcreting castable, because the mobility is one of the characteristics that define pumpability. Many tests have been designed to evaluate the mobility. The best known for civil concrete is the slump test. For castable, the flow table test is now used in many countries as standard tests. To evaluate the pumping property, some studies have measured the flow value or the viscosity resistance.

(2). Slump Test [25-27]

Slump measurement is the most commonly used test in concrete. The slump test consists of filling a cone with concrete in a standard way; the cone is then lifted and the slump measured after the concrete has reached an equilibrium position (Figure 2.13). The higher the slump, the highest the mobility. Originally, the slump test is developed to

measure the effect of water content on the workability of the fresh concrete. The limits of its proper application correspond to slumps between 40 mm and 180 mm. In other words, this method is not good for very stiff or very fluid concrete. Other factors beside the variation in water content may cause variations in slump measurements. Almost any change in mix composition or in the material characteristics will affect the slump.

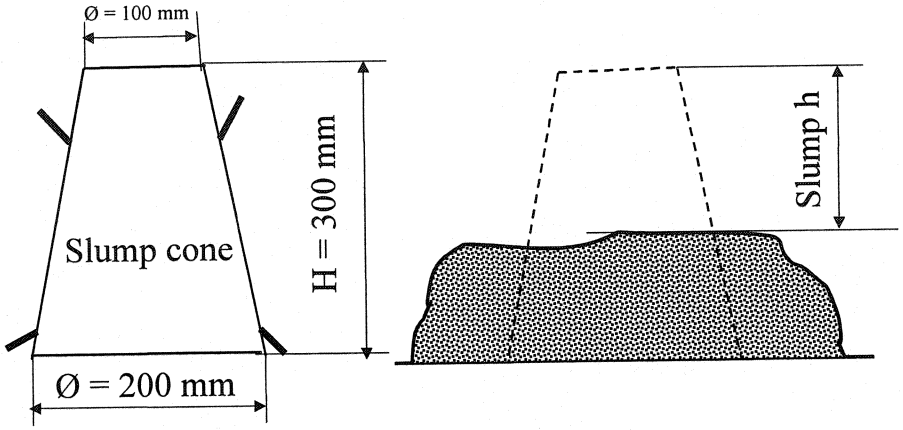


Figure 2.13 Slump test [25, 27].

Slump is a major concern when the installer is trying to build up thick sections and/or apply the gunning material overhand. Slumping is related to the cohesion-adhesion characteristics of a formulation especially as the visco-elastic characteristics change with time (measured in seconds or minutes). Dry gunned castables are the most prone to slump during installation, often due to the excess water added at the nozzle. Plastic gun mixes and shotcreting castables do not slump in this context. But they do fall out (an extreme form of slumping) at times when gunned overhead. The weight of the applied material exceeds it's adhesion to the anchor surfaces, and/or (in the case of the shotcreted castable) stiffening is too slow and the material's green tensile strength (cohesive strength) is exceeded by the force of gravity.

(3). Table Test [25, 28]

Flow table test is much like a miniature slump test but it measures the spread in mm with or without vibration (Figure 2.14). It is very a simple test. The applied vibration during

the test may encourage segregation if the mix is not properly designed: the fine matrix tends to move away from the center of the flow table, leaving the coarse material behind.

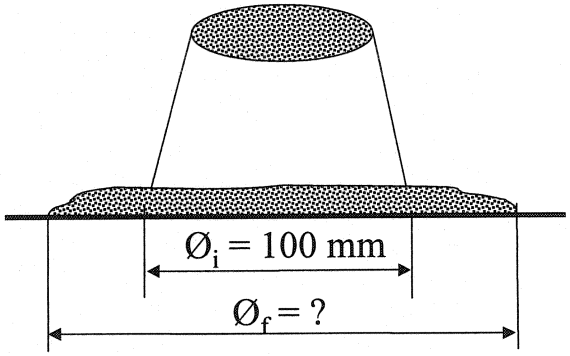


Figure 2.14 Table flow test [28].

(4). V-funnel Flow Test [29]

Blockage and plugging may occur due to bleeding or segregation. Bleeding water is rising up by pumping pressure through castable to the inner surface of hose or pipeline. Therefore, pressure bleeding test is used as an evaluation method for pumpability. Naotaka Fukami et. al. used V-funnel flow test to determine the fluidity and bleeding resistance of LCC (Figure 2.15). In repeated V-funnel flow test of LCC, the change of efflux time (the time of efflux of a specified volume through the V-funnel) decreased with the addition of thickening agent and the change of efflux time of LCC with polycarboxylic acid super-plasticizer is smaller than that with polyphosphate.

The schematic drawing of V-funnel flow test is shown in Figure 2.15. V-funnel flow test measures the efflux time of a specified volume through the V-funnel. After flow test, times of efflux are measured over 5 cycles using same mix. This flow test uses a mix having efflux time of 20 s, first time. In repeated V-funnel flow test of low cement castable, the change of efflux time decreases with adding the thickness agent and the change of efflux time of LCC with polycarboxylic acid super-plasticizer is smaller than with polyphosphate.

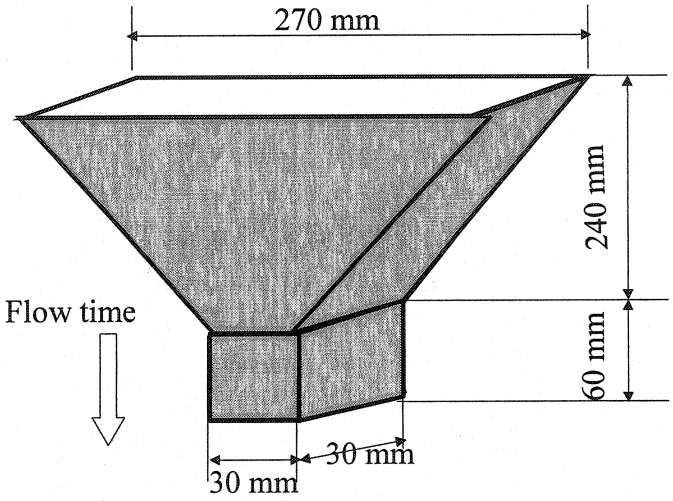


Figure 2.15 V-funnel flow test [29].

(5). Pipe Flow Test [30]

This implies measuring the velocity of free fall and/or the velocity under loaded fall of material in a pipe, which is designed with reduced diameter of the discharge port from 60 mm to 30 mm (Figure 2.16). A mixture of dense castable is filled in the model pipe with the discharge port closed by the shutter. It is held for three minutes under a load of 0.01 MPa on the top of the charge. The discharge rate (falling rate, g/s) of the material is measured when the shutter at the discharge port is opened. This experiment shows that material possessing higher falling velocity can discharge a larger amount of materials within the same period even under lower material pressure, and can be easily pumped.

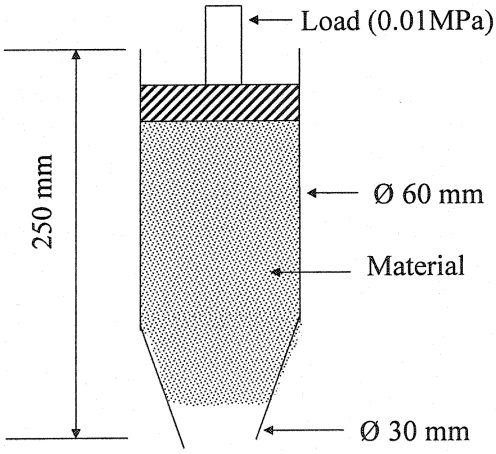
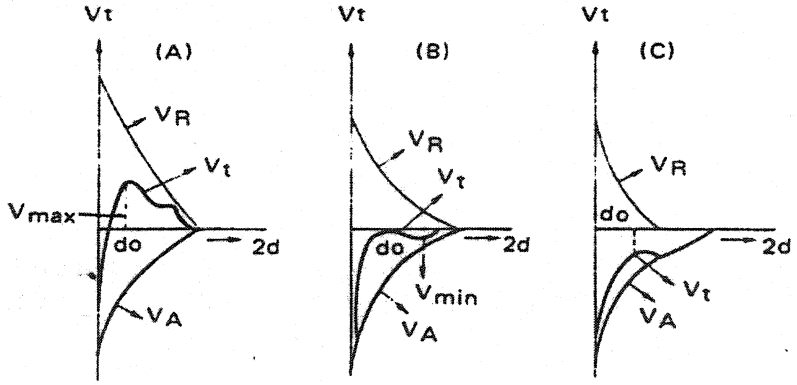


Figure 2.16 Pipe flow test [30].

2.4.3 Rheological Behaviour of Some Monolithic Refractories

The workability of monolithic refractories is firstly governed by the flow properties of the fine powder components contained in them. It is important to know and understand the rheological behavior of the powder-liquid system. A success in controlling this will enable good workability and quality of installation.

The rheological behavior of the powder-liquid system is dependent on the dispersion-flocculation state and. the stability of the system. According to DLVO theory (Moreno 1992, Mizunuma and Yamato 1991) [31-32], by adjusting the total potential energy V_t as the sum of attractive potential V_A and repulsive potential V_R, the dispersion-flocculation state can be changed, as schematically shown in Figure 2.17 [33], which can be achieved by using specific flocculants and deflocculants. This point is to be illustrated using examples of monolithic refractories, hereafter.



A: Deflocculation state; B: Critical point of flocculation; C: Flocculation state

Figure 2.17 Interaction potentials between dispersed particles [33].

(1). Refractory Mortars

Low water demand, good troweling, low dripping and suitable setting time are required for refractory mortars. To decrease the water demand and to obtain a good spreadability, specific deflocculants are added. Meanwhile, to avoid dripping, flocculants are also needed to adjust the system at a loose flocculation state in the vicinity of the critical point, as in Figure 2.17 (B).

Fujimoto et al [34], investigated the rheological properties of a binding clay suspension at a ratio of clay/water = 1 versus different additives, i.e. 0.2 % of sodium pyrophosphate (SPP), 0.2% of sodium tripolyphosphate (STP) and 0.2% of STP + 0.8% of calcium lignosulphonate (CLS) and correlated them with the workability of a silica mortar (silica sand/clay = 90/10). As shown in Table 2.2, a combination of STP as deflocculant and CLS as flocculant is necessary to engender an appreciable workability

Table 2.2 Workability in relation with rheological parameters [34]

Parameters		No additive	SPP	STP	STP+CLS
Rheological parameter	Yield value (dyne/cm^2)	290	0.2	35.5	102
	Residual stress (dyne/cm^2)	200	0.6	3.3	54.7
Workability*	Smearability	O	Dripping	×	O
	Deformability	O	Dripping	×	O
	Spreadability	O	Dripping	O	O
Water addition (%)		40	25	25	30

* O: good; ×: poor

(2). Clay-bonded Castables

Clay-bonded castable is based on the deflocculation-flocculation theory for clay-water system by cation exchange. To disperse the clay particles so as to obtain good flow under as low as possible water addition and to ensure an adequate pot life, the bivalent cations (Ca^{2+} and Mg^{2+}) adsorbed on the particle surface must be replaced by monovalent cations (Na^+, K^+ or NH_4^+) to increase the zeta potential. This can be achieved by using deflocculants like sodium polyphosphate, sodium silicate or sodium carbonate, as the negative groups to combine with the bivalent cations to form indissoluble compounds, and to facilitate the ion exchange. For setting after casting, the deflocculated system must be floculated again and coagulated by reducing V_R, for which the electric double layer must be suppressed by adding bivalent or trivalent flocculating ions (according to Schulze-Hardy rule). This should happen gradually, never before the first process anyway. For this purpose, a retardative flocculant (also called setting accelerator) to release bivalent or trivalent cations is required. Calcium aluminate cement is a good such retardative setting accelerator which can release Ca^{2+} and Al^{3+} upon addition of water. Fujimoto et al [34] suggested the clay for clay-bonded castables

should contain no montmorillonite; otherwise the deflocculant ions would be trapped in the layered structure to cause poor deflocculating effect.

(3). Clay-bonded Plastic Mixes

Refractory plastics should be easily deformed by ramming without cracking and remain the deformation after ramming. From rheology point of view, as the binder, clays that have a large hysteresis area and a high residual stress while showing negative thixotropy are most suitable, containing montmorillonite being appreciated for this purpose, according to Fujimoto et al [33]. Usually, adequate addition of flocculant, e.g. aluminium sulfate and ferric sulfate can further increase the plasticity [33].

(4). Low cement, Ultra-low Cement and Cement Free Castables

Low cement, ultra-low cement and cement free castables distinguish themselves from conventional cement bonded castables in that hydraulic bonding by cement is more and more substituted by coagulation bonding by ultrafine components, where hydraulic components act more as retardative flocculants than a real binder. The key factors to such castables include thus the option and optimization of ultrafine components, PSD and suitable admixtures such as dispersants and setting time adjusting agents. All these are for decreasing the apparent viscosity and yield stress of the matrix portion, reducing water demand and improving the flowability. For the placement and densification under vibration, negative thixotropy is required and dilatancy should be avoided. The first and direct response to these factors is the rheological behavior which can be approached by measuring $\sigma-\gamma'$, $\eta-\gamma'$ relationships and flow values by either static or dynamic methods [11, 33].

(5). Self-flow Castables

The workability for self-flow castables is different from that of the vibrating-flow castables. Instead of being applied an external shear force, the flow is caused only by gravity of the mix itself, i.e. gravitational energy. This requires the yield stress to be

extremely small while the apparent viscosity is so small. The criterion for self-flow castables is the self-flow value, which should be around 200 mm without segregation by standard flow cone method. It is more sensitive to PSD than vibration-flow castables.

(6). Gunning/shotcreting Mixes

The prerequisite of workability for such mixes is the pumpability, for which dilatancy and segregation must be avoided and good flowability under the pressure of compressed air and cohesiveness are required [35].

In a rheological sense, two systems are adaptable, such as viscous-plastic-elastic model and viscous-plastic model. In the former case, the elastic components, namely the aggregates, should be embedded with a very low contacting ratio, i.e. discontinuous, and the yield value should be low. Self-flow or pumpable castables are therefore suitable to be used as shotcrete [1, 36], but the top size of the grains should be limited, not as large as for vibratable castables. The advantage of such system is that it is easy to transport them by pumping. However, due to the low yield value and good flowability, the mix is likely to drip when reached the gunned surface. To solve this problem, instant stiffening accelerant to create "flash setting" must be incorporated when the mix is leaving from the nozzle but still in the nozzle. This becomes a technical barrier. On the other hand, thixotropy of the matrix should be carefully controlled. When too shear-thinning, the matrix paste may be squeezed to separate from the aggregates. To this point, slight dilatancy could not necessarily be harmful. In the latter case, the yield value is high. Usually chemical binders and /or soft clays are used to produce good plasticity. Owing to the viscoplasticity, the adhesion is good and dripping can hardly occur. Adding instant accelarant is thus not necessary. This makes the equipment and operation simpler and easier.

By the method of measuring the thickening time and flow resistance of gunning mix in laboratory, Eguchi Yauhiro et al [37], thought that accelerator effect is affected by

accelerator dosage, and also varied remarkably with varied dispersant. Sodium silicate and sodium aluminate cannot have thickening effect whereas polyaluminium chloride and calcium chloride show thickening effect while using polyacrylic acid as dispersant. Addition of sub-micron activated alumina powder shortens the thickening time and increases the thickening rate of flow resistance. The appearance of installed body for shotcreting mix depends upon the way which the addition of varied accelerators is made, corresponding to 3 types, illustrated in Figure 2.18.

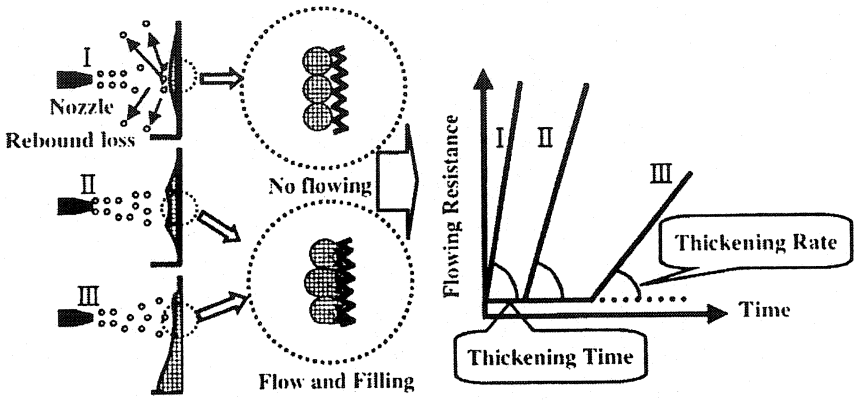


Figure 2.18 Adhesion of shotcreting mix [37].

Type I: Setting time and thickening time (flowable time) is too short. Shotcreting mix coagulates before reaching surface. It cannot flow and fill on the surface and has no adequate adhesion strength owing to the point contact. It is also considered that gunning body has high porosity and low strength.

Type II: Thickening time (flowable time) is short but measurable. Shotcreting mix coagulates after contacting the surface and hence can flow and fill on the surface. This mix has adequate adhesion strength. It is also considered that the gunning body has homogeneous structure, high strength and low porosity.

Type III: Thickening time (flowable time) is too long. When on the surface, shotcreting mix can not coagulate quickly. It can flow and accumulate on the surface, as well as type II. However, owing to the insufficient retention strength, the mix sags.

2.5. Conclusions

Some fundamental and classical aspects in rheology have been reviewed and associated with monolithic refractories in this report. It has been found that:

(1) The rheological models can simulate behaviors of different monolithic refractories. They are helpful in sorting out and elucidating phenomena, working mechanisms and problems of different types of monolithic refractories.

(1) The PSD plays a major role in governing the rheological characteristic of matrix-liquid system, which dominates the behavior of the aggregate-matrix-liquid system. It is a key to design a castable with good flowability and workability.

(1) The parameters such as the IPS, MPT and SLI are also important to predict the rheological behaviors of castable.

PART 2: SHOTCRETING

2.6 Introduction [38-48]

During the past several decades, traditional gunning application for lining and maintaining vessels has been well-known and documented. Since 90s, the pneumatic application of fully wet mixed refractories, shotcreting (a term from civil concrete industry, also known as shotcreting, wet-gunning, wet spray or shotcasting in refractory castable technology), is attracting more and more attention to the unshaped refractory users. In the UNITECR'97, the largest conference on refractory technology in the world held in New Orleans, USA on Nov. 4-7, 1997, an individual session was there for shotcreting. Eight papers were discussed on this latest placement technology.

The shotcreting method for LCC using high pressure was introduced in the United States of America in 1996. In this process, refractory ingredients (aggregates, fine powders, binder and dispersing agent) premixed with water are transported with the help of a

pump to a nozzle where some accelerators are added and projected at high velocity onto a receiving surface. Figure 2.19 shows the line diagram of a shotcreting system.

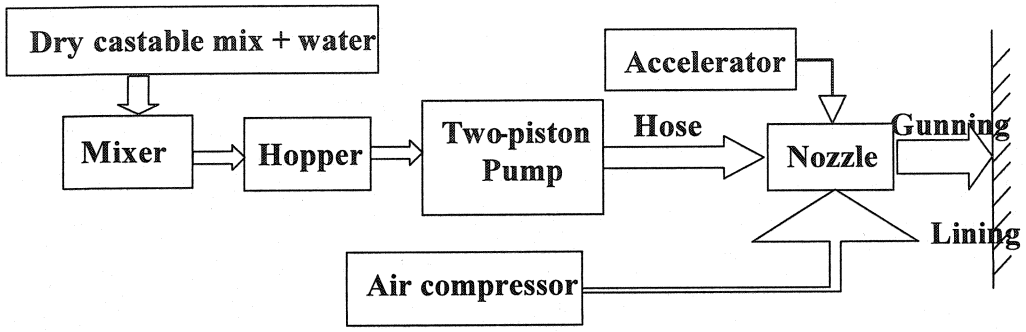


Figure 2.19 Line diagram of Shotcreting process [38-48].

Shotcreting has been available for many years. The Portland concrete industry has been shotcreting since the early 1950's. By 1965, the process progressed to use piston type concrete pumps with 32 mm to 50 mm hoses suitable for use with refractory concretes. The results of shotcreting refractory castables to dry densities greater than 2.1 g/cc were published in 1963. Thus, shotcreting of refractories has been known for over thirty-five years. Further reports in 1978 described shotcreting of refractory castables in torpedo cars to similar dry densities. With the development of LCC technology in 70's, the refractory industry realized the potential for significant improvements in properties of gun-placed material since shotcreting could encompass the longer wet mixing times needed to effectively wet and disperse the fine matrix components present in a LCC, which use fine particles of material, such as silica, alumina or chromia in combination with deflocculants to enhance flow. With substantially reduced water contents, the cement content could be reduced without adversely affecting the desired strengths. In 1986, the characteristics of wet-shotcreted, low-cement castables were reported.

Although, considerable work has been done over the last 35 years in the refinement of shotcreting refractory mixes, including LCC's, shotcreting was not accepted commercially until 1995. This acceptance has resulted from increasing restrictions on dust in the workplace, refinement in pumping equipment and development of refractory

concrete more suitable to pumping. It isn't until after the creation of self-flow technology in the U.S. in 1991 that shotcreting became a more effective installation tool. Pumping self-flow mixes over significant distances, both horizontally and vertically, paved the way for closer scrutiny of extending pumped place of refractory castables to shotcreting. National Refractories completed a successful placement of refractory concrete in a municipal boiler using a concrete boom truck to transport a self-flow castable over 26 meters vertically in April, 1991. This ushered a new method for rapid transport and placement of refractory castables. However, this method required the initial placement of expensive and time-consuming forming to hold these very fluid, heavy self-flow castables. Form leakage occasionally occurred. Additional time is necessary for proper curing of the castables and then form removal.

Also aiding in the transformation from pumping to shotcreting is the refinement of piston pump technology. A concentrated effort is made by pump manufacturers to design pumps that would provide the necessary pressure to pump heavier, more viscous refractory materials through the relatively small hose diameters needed for proper mobility. Material flow at high pressures through limited line reduction from piston to nozzle is achieved. This paved the way for shotcreting LCC mixes with limited self-flow characteristics. Hydraulic pumps with 75 mm diameter pistons are now readily available in the industry. Instruction manuals on the details of shotcreting of refractory concretes have been readily available for over ten years. The key device of the apparatus is the material pump with double pistons, a swing valve and a 3-inch diameter outlet port. Figure 2.20 shows a schematic diagram of the material pump. A swing valve between two cylinders is activated and returned by oil pressure in a scheduled order. When one cylinder sucks material, the other connects with the outlet through the swing valve. The sequential movement of the swing valve and two cylinders stabilizes the material flow for long time. The tapered caliber of a hose from 3 inch to 1.5 inch minimizes the pressure loss and a gunning rate as high as 1.5 to 3.8 m^3/hr is possible.

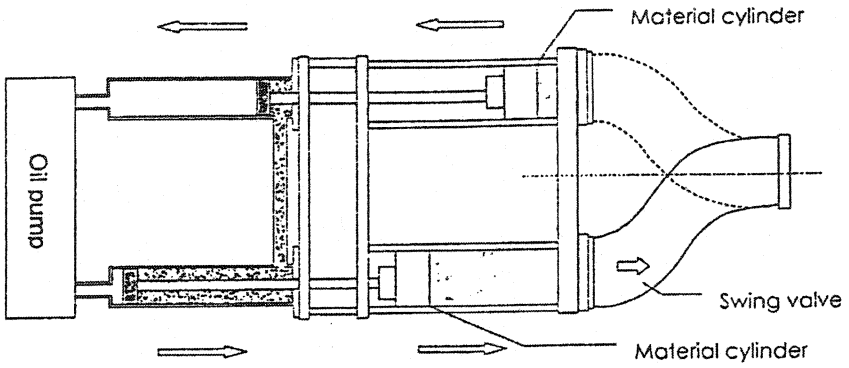


Figure 2.20 Structure of a double piston pumps [42].

In conclusion, the shotcreting technology is based on self-flow castable, high-pressure pump and LCC technology with modern installation requirements

2.7 Advantages of Shotcreting [26, 46, 47, 48]

When compared to Dry and Semi-wet process, the shotcreting process has got many advantages such as less rebound, less dust and no forms or moulds requirement. It is possible to obtain similar properties of high strength and density as that of vibrated castables with this technique. The main advantages are:

(1) The properties of the shotcreting castables are the same as that of the identical material castables

(2) No forms required for installation

(3) Less rebound and no dust scattering

(4) High efficiency, labour saving and cost reduction

(5) Suitable for complex installation

(6) Low water addition and less curing time

(7) Mechanization and automation installation and high availability

(8) Quick repair for linings

(9) Low porosity and homogeneous linings

(10) Good and easy transportation of the materials by using high-pressure pump

In Table 2.3, a comparison is presented between several refractory installation methods. Characterized by low moisture content and a dense installed body, shotcreting is regarded as the method which eliminates the disadvantages of installation by casting. Table 2.4 shows the properties of the material in comparison with those of the conventional castable.

Table 2.3 Refractory lining installation methods [48]

Installation method	Brick laying	Casting	Shotcreting
Main equipment	Not applicable ○	Mixer, form, vibrator ×	Mixer, pump △
Mixing	Not applicable ○	Mixer ×	Mixer ×
Installation labor	Much ×	Little ○	Little ○
Skill	Necessary ×	Nor required ○	Not required ○
Lining thickness	Fixed ×	Form △	Not limited ○
Curing time	Not applicable ○	Necessary ×	Short △
Drying time	Not necessary ○	Necessary ×	Necessary ×
Installation rate	0.5 Tons/hr	3-5 Tons/hr	5-10 Tons/hr
Continuous installation	×	×	×

○ Advantage △ Neutral × Disadvantage

Table 2.4 Typical properties of the materials after installation for steel ladles [48]

Installation method		Shotcreted	Cast
Chemical Composition (%)	Al_2O_3	88	91
	MgO	10	7
Bulk density (g/cm^3)	110^0C ×24h	2.80	2.91
	1500^0C×3h	2.75	2.83
Modulus of Rupture (MPa)	110^0C×24h	5.5	8.1
	1500^0C×3h	35.6	19.6
Apparent Porosity (%)	110^0C×24h	19.5	18.7
	1500^0C×3h	22.5	23.0
Permanent Linear Change (%)	1500^0C×3h	+1.25	+1.52

In the case of shotcreting, the generated dust can be substantially reduced more than in the conventional Dry and Semi-wet gunning. A measurement result of dust concentration during the gunning is presented in Table 2.5. Dust concentration is measured by the digital dust meter which is installed behind 2 m from the perpendicular wall to be gunned. By visual observation, the conspicuous dust (count per minute, CPM = 500-800) is seen in the Dry and Semi-wet gunning, but not much in shotcreting dust (CPM = 100) and the formation of mist is almost inexistent. In the newly developed full shotcreting, it is possible to decrease more the dust quantity than in the conventional gunning method. A refractory castable is being shotcreted in a rotary kiln as shown in Figure 2.21, where there is lack of dusting.

Table 2.5 Dust concentration measurement in various gunning technique [46]

Type of Castable(Bulk density, g/cm^3)	Dust concentration (CPM*)		
	Dry gunning,	Semi-wet gunning	Shotcreting
Insulation (0.8-1.3)	700	400-500	N/A
Refractory (1.90)	800	550	N/A
Low Cement (2.20-2.75)	N/A	N/A	100

CPM* (0.01 mg/m^3)



Figure 2.21 Shotcreting a refractory castable in a rotary kiln (note lack of dusting) [41].

2.8 Applications of Shotcreting Castables

2.8.1 Steel Ladle [3, 42, 49, 50, 51]

In the large steel plants in Japan, both the ladle barrel and floor are usually lined with monolithics such as Al_2O_3-MgO, Al_2O_3-spinel and Zircon by casting using forms. The shotcreting system would be promising as the installation method to replace veneering. Shotcreting is used for the initial installation in the sidewall (installed thickness of 160-270 mm), which indicated the same durability as the cast castable. The barrel and the bottom of a 25 ton molten steel ladle are usually relined by shotcreting. There are no problems with corrosion resistance or thermal spalling, as the residual thickness after use is the same as the cast castable. In addition, there is increased ladle service life, as well as cost reduction, with additional repairs that are done by shotcreting. Large differences are not found between the thermal properties of vibration-cast castables and shotcreting castables. The results of field application of shotcreting materials are as good as those of a castable of the same type. Table 2.6 shows the materials installed.

Table 2.6 Typical shotcreting material properties for steel ladles [49]

Material		Al_2O_3-MgO	ZrO_2-SiO_2
Chemical Composition (%)	Al_2O_3	88	4
	MgO	10	-
	SiO_2	1	44
	ZrO_2	-	51
Bulk density (g/cm^3)	110^0C	2.92	3.20
	1500^0C	2.87	3.00
Apparent Porosity (%)	110^0C	20.9	15.6
	1500^0C	21.7	21.8
Modulus of Rupture (MPa)	110^0C	3.8	9.0
	1500^0C	31.5	12.5
Permanent Linear Change (%)	1500^0C	+0.51	+2.43
Approximate Water Required for Pumping (%)		7.0	7.5

The performance of this shotcreting material for a 25 t molten steel ladle is shown in Table 2.7. The gunning amount is 4.0 tons and the gunning yield is more than 95%. The appearance of the gunned body and the cleanliness of the working environment are

excellent. The service life and the wear rate are the same as the conventional casting method. The installing time is half that of the conventional casting method.

Table 2.7 Comparison between shotcreted and cast lining (25 tons steel ladle) [42]

Method	Shotcreting	Casting
Lining life (heat)	42	40
Amount installed (t)	4.0	4.0
Term (h)	1	1.5
Labors consumed (personnel)	3	3
Wear rate (mm/heat)	1.57	1.61
Total installation time (h)	3.0	6.0

2.8.2 Cement Plant (Pre-heater) [41, 42, 49]

The shotcreting seems promising for the repair in pre-heaters. At one plant in Japan, 60-70 m of pumping head distance was required in an actual installation. Repairs were made in a cyclone of the suspension pre-heater, calciner and tertiary air duct inlet. The equipment was located on the ground level with successful shotcreting performance with pumping head of 60 m for upper portion of pre-heater. The shotcreted material with satisfactory performance is shown in Table 2.8.

Table 2.8 Typical shotcreting material properties cement pre-heater [49]

Material		Al_2O_3-SiO_2
Chemical composition (%)	Al_2O_3	60
	SiO_2	35
Bulk density (g/cm^3)	110^0C	2.33
	1300^0C	2.28
Apparent porosity (%)	110^0C	22.6
	1300^0C	22.3
CMOR (MPa)	110^0C	5.7
	1300^0C	21.9
Permanent linear change (%)	1300^0C	+0.25
Approximate water required for pumping (%)		7.8

2.8.3 Torpedo Ladle [49]

Torpedo ladle linings are currently changing from bricks to monolithics for the purposes of labor saving under a shortage of skilled bricklayers and refractory material cost

savings. Showing a 50% labor savings, the shotcreting seems so far to be promising. The current maintenance method using the shotcreting is to provide a veneer over the existing brick lining. The materials typically installed are shown in Table 2.9. Material A is an Al_2O_3–SiC material, characterized as low cement and high strength. Material B is an ultra-low cement material with excellent erosion resistance and volume stability used for trough materials. Both of these materials have been used in the torpedo ladles operated with rather severe condition like preliminary troweling and brick replacement. The vibro-troweled lining thickness of 50 – 100 mm is usually entirely eroded after 70 heats and always critically over its expected life of 70 – 80 heats. The linings with material A and B, by the shotcreting have shown durability of 140 – 210 heats (2 – 3 cycles) with shotcreting thickness of 50 – 150 mm.

Table 2.9 Typical shotcreting material properties for torpedo ladles [49]

Material		A	B
Chemical composition (%)	Al_2O_3	67	70
	SiO_2	14	4
	SiC	14	10
	F.C	-	3
Bulk density (g/cm^3)	110^0C	2.56	2.75
	1450^0C	2.62	2.73
Apparent porosity (%)	110^0C	18.5	21.6
	1450^0C	19.6	26.0
CMOR (MPa)	110^0C	11.0	2.5
	1450^0C	14.0	6.7
Permanent linear change (%)	1450^0C	-0.50	+0.11
Approximate water required for pumping (%)		7.5	6.8

2.8.4 Blast Furnace Trough [42, 49]

Trials of the shotcreting have been performed mainly targeting the shorter repair time on hot Blast Furnace (BF) trough. The typical repair practice shows 4 hours repair period for this trough of a 4000 m^3 blast furnace. The hot repair to the trough was made according to the schedule on a 7-meter long section from the tap-hole. Approximately 1.5 hours after casting is completed, the trough is prepared, removing the slag buildup and old refractory lining and preparing for shotcreting application. The working surface

temperature is about 800^{0}C at the time of shotcreting application. The thickness shotcreted range is from 50 mm to 155 mm in the slag line area and from 110 mm to 240 mm thickness in the metal zone, using about 2 tons of refractory for the repair.

The refractory shotcreting mix for the BF trough is shown in Table 2.10. The materials are high corrosion-resistant castable for the metal zone application, of low cement and low SiO_2 with fused Al_2O_3 and fused spinel as aggregates. When shotcreted, these materials show sufficiently quick hardening for hot surface repair by optimizing selection of flocculants and ultra-fine powders. The shotcreted refractory shows excellent adhesiveness (more than 95%) with almost no rebound loss. The shotcreted refractory surface shows an increase in temperature to greater than 250^{0}C within 30 minutes due to the effect of the hot shotcreting surface. No additional curing or drying is used and the trough will be ready for rapid preheating for tapping. The results from these installations show the shotcreting mix to have sufficient durability up to a minimum of 30, 000 tons of iron. Using similar BF trough castable as shown in Table 2.10, a maximum of 80, 000 tons of iron has been recorded by the shotcreted mix when shotcreted on a cold surface downstream of the trough. In this case, the durability measured in erosion speed is almost equivalent to that of BF castables behind forms.

Table 2.10 Typical shotcreting material properties for hot BF trough in Japan [49]

Chemical Composition (%)	Al_2O_3	74
	MgO	9
	SiC	14
	F.C	3
Bulk density (g/cm^3)	110^{0}C	2.81
	1450^{0}C	2.79
Apparent Porosity (%)	110^{0}C	18.0
	1450^{0}C	18.9
Modulus of Rupture (MPa)	110^{0}C	4.5
	1450^{0}C	7.7
Permanent Linear Change (%	1450^{0}C	+0.02
Approximate Water Required for Pumping (%)		6.5

2.9 Conclusions [41, 49, 52, 53, 54]

Nowadays, based on the mix of modern self-flow and pumping castable technology, and high-pressure pump system and related technique, shotcreting is running at the top of castable installation. The evolution of refractory castables has been reviewed and concluded as shown in Figure 2.22.

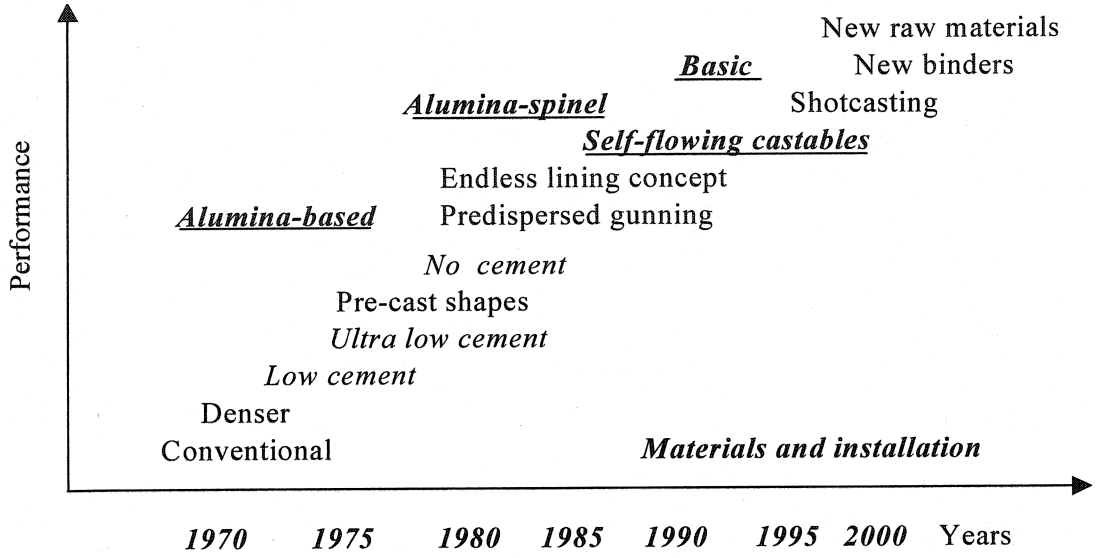


Figure 2.22 Illustration of the evolution of castables over the last 30 years [53].

Shotcreting self-flow castables provides the refractory customer with yet another method for installing monolithic materials. It is not the answer for all installations but it is a process that offers distinct advantages in regard to speed and ease of installation with minimal noise and dust. There is a tremendous potential and future for shotcreting technology, as there has been consistent research input in mix design and related technology. Though, the properties of shotcreted castable cannot be compared with cast ones at present, the difference in properties are narrowing down continuously.

However, the customer and installer need to be aware of the limitations of the process. Although no forming is required, proper anchoring placement needs to be done. The actual installation is labour-intensive with specially trained personnel needed for pumping. The setup and clean-up process can be extensive. Equipment needs are great

considering proper mixers, pumps and all of the accessory pipes, hoses, clamps, air line, accelerator lines, nozzles, etc. Backup pumps are required for large installations. Even with all of these requirements, shotcreting can still be more economical than casting considering the extensive labour and form work needed for many casting installations.
For the customer, installation contractor and the refractory salesman, there is often a reluctance to use shotcreting of self-flow castables as a placement method because it is a complicated process. Other factors important to successful shotcreting installation include:

- ✓ A clear understanding of the refractory and mixing requirements.
- ✓ A properly prepared surface and anchor system to ensure bonding of the refractory and proper depth of the lining.
- ✓ Careful planning of the material handling in relationship to mixing, pumping and conveying line system based on the logistics of the project.
- ✓ A familiarity with the conditions and safety requirements of the high-pressure pumping equipment.
- ✓ Proper and ample training and education. This is not a "do-it-yourself" application method.

PART 3: DESIGN OF SHOTCRETING CASTABLES: A RHEOLOGICAL APPROACH

2.10 Introduction [41, 42, 48, 52, 55, 56]

The design of a self-flow castable must be based on the ability of the mix to be pumped through a 50 mm (most common) or a 38 mm hose/pipe system. This castable with optimum shotcreting characteristics has a chosen aggregate top sizing that prevents plugging and reduces the rebound. Other important self-flow required features are the minimum dilatancy, cohesiveness and a low tendency for segregation. These characteristics usually become more difficult to achieve as the cement level decreases.

After experiencing the pressure and movements of pumping over significant distances, the material must remain fluid enough to break up inside the shotcrete nozzle so that proper gunning action is achieved. The accelerator must fully penetrate and activate the castable. The working time of the original wet mix must be long enough to provide for worry-free installations under normal field conditions where delays may occur for many reasons. The accelerator should provide the necessary stiffening when the castable is shotcreted onto a surface.

Most self-flow shotcreting mixes are still based on calcium aluminate cement, although the process may become attractive for non-cement systems, particularly when dealing with magnesium oxide castables. However, any self-flow mix used for shotcreting has to have three characteristics:

(1) Proper flow from the hopper to fill each cylinder under negative pressure during the reverse piston stroke.
(2) Flow through extended lengths of pipe-hose without plugging, segregating or causing excessive pump pressure.
(3) Effective reaction with an accelerator at the nozzle causing a rapid increase in viscosity so that material will stick onto the gunned surface.

The rheology has a strong relationship with the particle sizing of pumpable castables. A castable must be pseudo-plastic fluid to be pumpable, and the aggregate and matrix constituents must flow together and not be segregated. The pumpability of a castable must be evaluated by a rheometer and not by flow table because of the segregation of components that can occur. It is important to control the aggregate and matrix content of castables.

2.11 Design Shotcreting Castables by Optimizing PSD

Better pumping characteristics are pursued by optimizing the PSD of the shotcreting materials. Pumping is investigated by measuring the required pressure to pump material

mixture through a hose of 38 mm in diameter and 30 meter long. The optimal moisture content is determined for each mixture by aiming at self-flowability value of 180 mm. Table 2.11 shows the difference in pumping pressure for several PSDs.

Table 2.11 Dependence of pumping on PSD [48]

Material	A	B	C	D
Ratio of coarse / medium size particle	2/1	2/1	3/2	1/1
Maximum particle size (mm)	8	5	5	5
Moisture (wt %)	6.2	6.4	6.6	6.9
Tap flow value (mm)	182	178	183	179
Pumping pressure (MPa)	>14	13	8	4
Pumping behaviour	Bad	Bad	Excellent	Excellent

Material A, one of the conventional castables, demands an optimal moisture content of only 6.2% to obtain the expected tap flow value. Material A, however, is found unsuitable for pumping up to the nozzle tip, because it blocked the hose at an excessive pumping pressure of more than 14 MPa.

Material B with a maximum particle size of 5mm, versus 8 mm in material A, could be pumped, but required 13 MPa of pumping pressure, which is almost the maximum allowable value for the system and may possibly lead to blocking of the hose when gunning goes on for hours.

Materials C and D are derived from material B by increasing the amount of medium size particles. Due to the increase of the specific surface, caused by an increase of medium size particles, the moisture demand increases and the pumping pressure decreases considerably. Both materials C and D demonstrate excellent pumping characteristics.

Good workability is obtained with materials C and D which had continuous PSD. Material A and B are difficult to pump, although it could be pumped if it contained a sufficient amount of medium size particles which exhibited pseudo-plastic flow. This

seems to indicate that a mix with non-continuous PSD can be pumped if strong pseudo-plasticity prevents particle separation.

When materials are prepared with the maximum particle size fixed at 5 mm and their PSD between 0.045 and 5 mm conforming to that of Andreasen, increase in the q value, as shown in Figure 2.23 resulted in water demand reduction, increase in particle separation, and decrease in adhesion ratio in gunning. Pumping pressure also decreased as the q value increased. When the q value exceeded a certain value, however, it did not decrease further but increased instead. This seems to indicate that, at high q values, the content of coarse particles is high so that fine particles separated out of voids among coarse particles, which made pumping difficult. On the other hand, decrease in the q value brought about increase in water demand and increase pumping pressure. However, particle separation in this case is less, and adhesion ratio in gunning is satisfactory. Accordingly, materials that exhibit good workability with comparatively little water addition are considered to have their q values in a certain range. In order to achieve satisfactory workability with relatively little water addition, materials containing a small amount of those particles which contribute to pseudo-plastic flow need to have their PSD in conformity with the Andreasen' continuous distribution and have an appropriate q value.

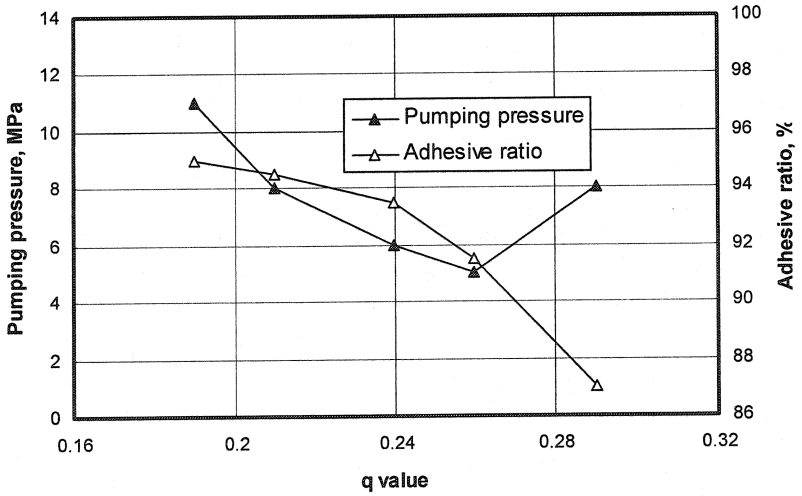


Figure 2.23 Influence of q value on pumping pressure and adhesive ratio [56].

Aggregate gradation, both large and fine, is probably the largest single influence on pumping. Uniformity of aggregate size and not having enough fines (also of the correct gradation) to create the "cream" or paste is the most common problem observed in the field. One general recommendation is to follow ASTM C33 [57], for good pumping sand. Flowability of castables, both vibration type and self-flow type, depends strongly on PSD and aggregate/powder ratio. As illustrated by Figure 2.24 [11] using a low cement castable, Fl_0, Fl_{15} and Fl_v represent respectively self-flow, flow after 15 shocks by flow table method and flow after 5 sec. of vibration by vibrating test. When q = 0.35, corresponding to about 21% of fines (-200 mesh), there is no self-flow; when q = 0.25, i.e. at about 33% of the fines, both vibration-flow and self-flow are improved remarkably; when q drops to 0.22 where the fine portion is about 40%, vibration-flow tends to be unaffected, while self-flow increases further.

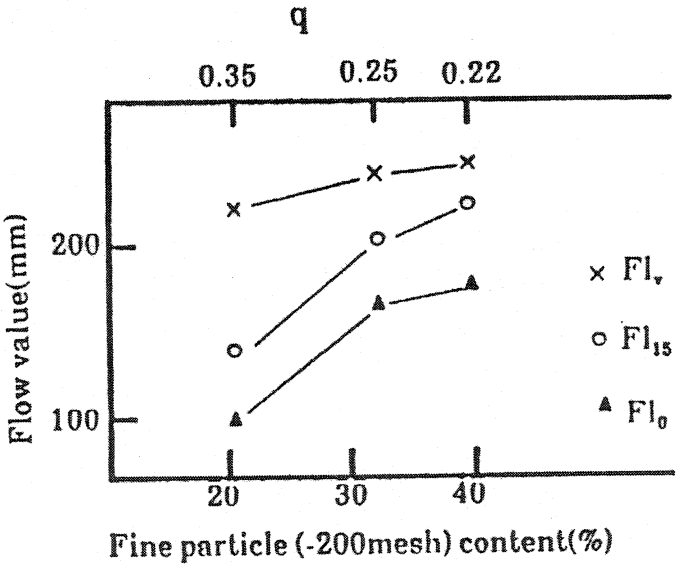


Figure 2.24 Flow values as a function of fine particle (-200 mesh) content [11].

Another study [58] on the free-flow (same meaning as self-flow) and vibra-flow of ultra-low cement Al_2O_3 based castables as a function of the q-value suggests that the PSD of typical vibratable castable would have a q-value between 0.28 and 0.30 as this gives low free-flow but high vibra-flow; for a self-flow castable, then the q-value should not be

more than 0.26 where a significant drop in free-flow is experienced. To achieve lower water addition and better flowability, PSD of the castables should be carefully optimized. This is especially important to self-flow castables.

The aggregates in castables are usually discontinuous, whilst the matrixes are continuous. Therefore, the rheological characteristics of the matrix portion have decisive effect on the aggregate-powder-water system. Usually, the flowability of castables increases with the decrease in yield stress and apparent viscosity of the matrix. Figure 2.25 and Figure 2.26 [11] give an example showing the decisive effect of the matrix. As shown in Figure2.26, at 5% of water addition, matrix A is lower in η than B. A behaves as a pseudo-plastic flow pattern, while B represents a mixed pattern comprising Newtonian, pseudo-plastic and dilatant flows. B shows an intensive dilatancy at a lower level of water addition, i.e. 5%, leading to a poor flowability for castable B at this water addition in comparison to castable A, other things being equal.

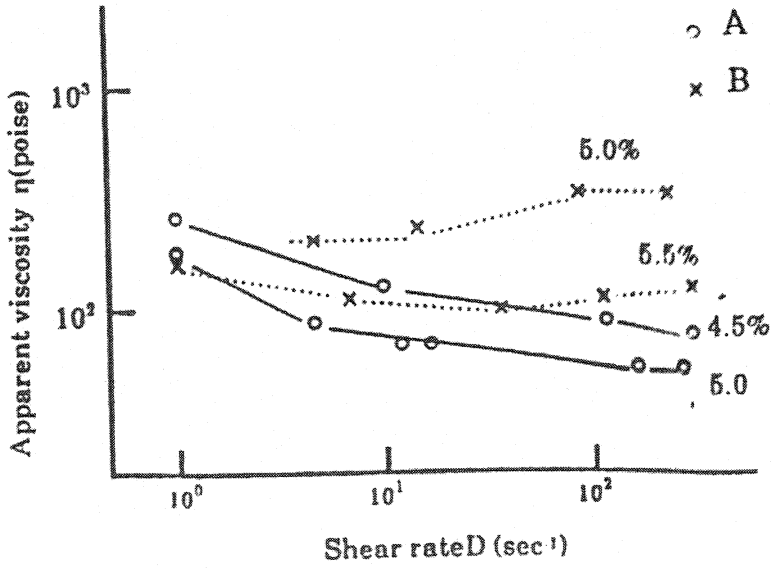


Figure 2.25 Rheological behavior of matrix A in comparison with matrix B [11].

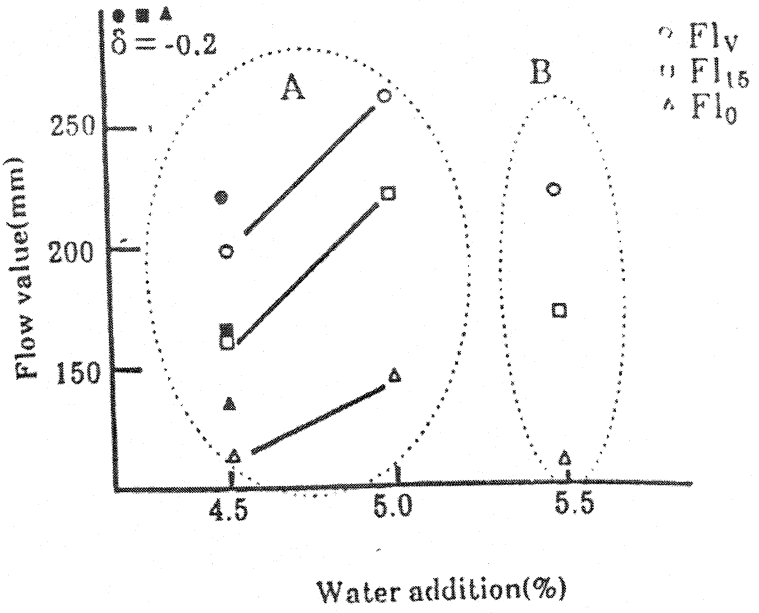


Figure 2.26 Flow values of the low cement castables with matrix A and B [11].

Stable pumping can be realized by optimizing PSD of castables. Figure 2.27 shows the relation between the grain size distribution and the pumping character of low cement castables. Stable pumping can bone when the top size is 5 mm and the volume ratio of grains less than 1 mm in diameter is 60 to 80 %. Castable outside the above grains size distribution need a large amount of mixing water to avoid choking in the hose. Pumping condition: flow rate 80 kg/min, distance 15 m.

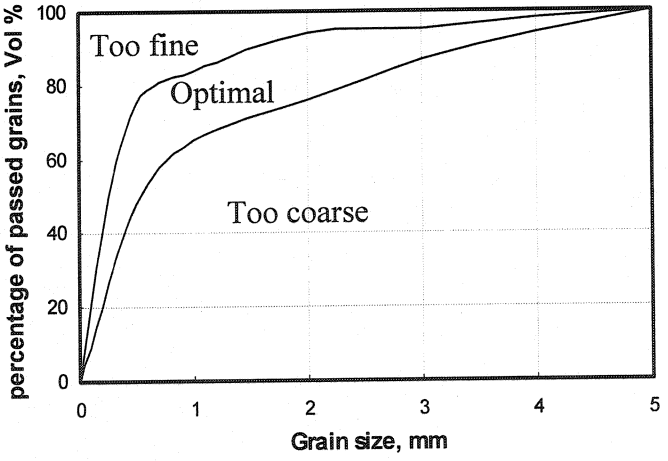


Figure 2.27 Relation between grain size and pumping behaviour of material [42].

2.12 Design of Shotcreting Castables by Optimizing Additives [55]

Rheological properties of a commercial 70% alumina shotcreting castable are evaluated by a special rheometer, and its matrix is studied by viscosimetry technique and the founding is:

(a) Exists a correct amount of additive for projection to initiate a satisfactory coagulate effect on the concrete, that must well be determined to prevent loss of material during the application.

(b) Inorganic additives, such as, sodium silicate and sodium aluminate, had shown instability as coagulant because they had allowed that the concrete recovered high free flow with time. Determined minimum amounts for use of these additives had been of 0.4 % for sodium silicate and 0.6 % of sodium aluminate.

(c) The organic additive showed to be the steadiest for shotcreting, showing a strong coagulation of the concrete for a minimum amount of 0.6 wt%.

(d) The mechanism of reduction of the flow occurs by coagulation and not directly by the acceleration of the hydration reactions of the cement (setting time).

(e) Inorganic additives had presented a gradual slow increase of the values of the yield stress instead of the organic additive that presented an instantaneous increase of the yield stress from the amount of 0.6 wt%.

(f) Among the additives evaluated for the shotcreting castables, the efficiency and the coagulation stability can be classified in the following order: organic > sodium silicate > sodium aluminate

It is desirable in field applications to accelerate hardening in the case of a thick lining on a perpendicular wall and to delay it when a towelling finish is required. Thus it is necessary to select the optimum kind and quantity of activators for each installation condition.

Based on above discussions, it has been concluded that rheological study is very important issue for shotcreting castables. Therefore, rheology and shotcreting is the general topic covered in the whole work.

CHAPTER 3 – EXPERIMETNAL PROCEDURE

The experimental program, raw materials, composition of the castables to be investigated, sample preparation and tests methods to characterize the developed shotcreting castables, are to be presented in this chapter.

3.1 Experimental Program

The whole work has been planned in four stages, as illustrated in Figure 3.1.

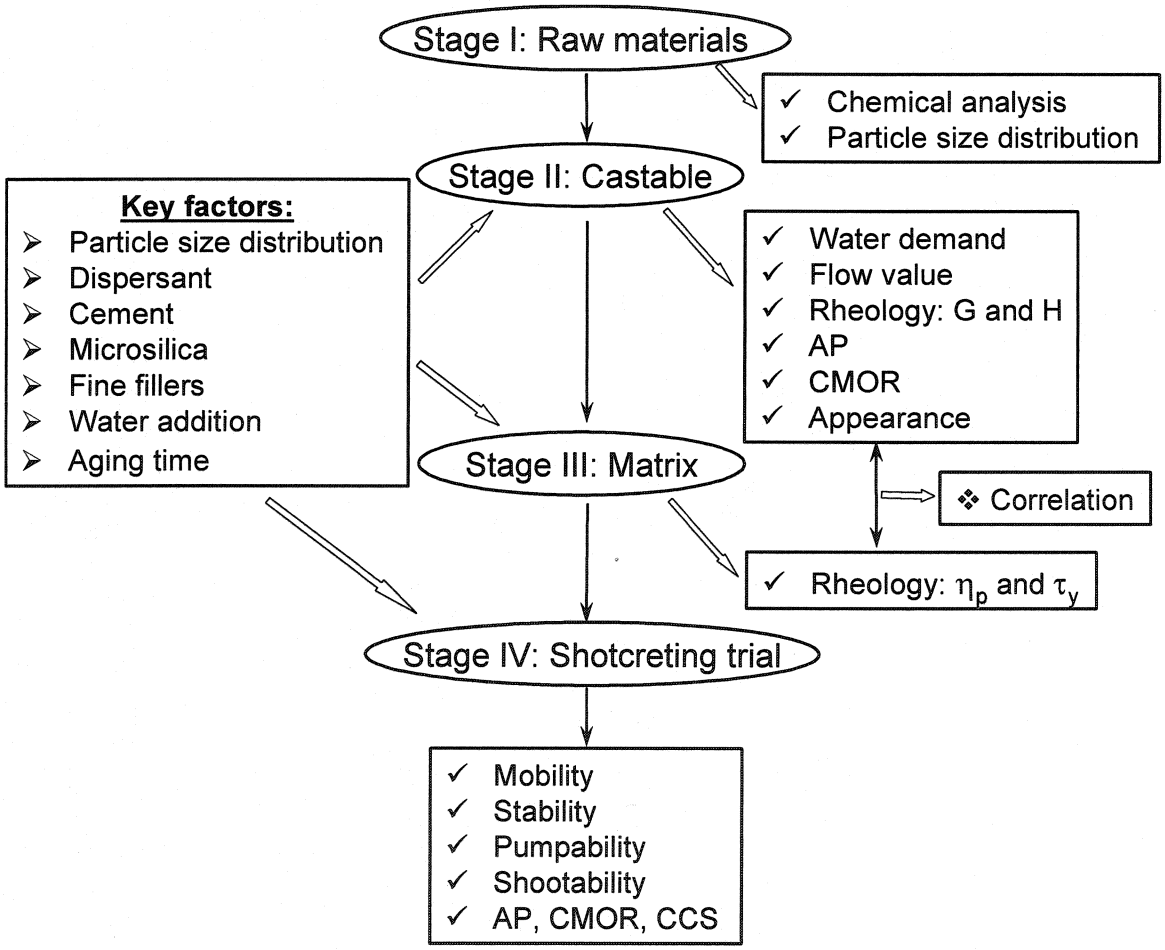


Figure 3.1 Experimental programs.

In stage I, all raw materials, including bauxites, cements, microsilicas, reactive aluminas, have been characterized for chemical composition and particle size distribution.

In stage II, the influence of different variables on the rheology of low-cement bauxite-based castables has been studied. The variables, which have been taken into account, are: water demand, flowability, AP, CMOR, flow resistance, torque viscosity.

In stage III, the rheology of only the fine matrix portion of the low-cement bauxite-based castables has been carried out to find out the influence of the same variables, which correlates with castable rheology. The rheology is characterized through the plastic yield stress and plastic viscosity. The factors include particle size distribution, cement, microsilica, fine fillers, water addition, dispersant and aging time.

In stage IV, with the optimized composition of the castables defined in the two previous stages (stage II and III), mixes have been shotcreted in the field to verify the validity of the present approach.

3.2 Raw Materials

The raw materials used in the present work include bauxite, alumina, microsilica, calcium aluminate cement and dispersants.

3.2.1 Bauxite

Bauxite used for refractory is a stable product, after calcination in a rotary kiln. Calcined bauxite is high in alumina content and low in impurities (particularly iron oxide) and it contains corundum (alpha alumina) as its principal component, mullite and a small quantity of glass phase [59]. In this work, Chinese high-grade bauxite with a nominal density of 3.4g/cm^3 has been used, as supplied by Henan Gengsheng Refractories Co., Ltd., China. The chemical composition determined by X-ray spectra-fluorescence, is shown in Table 3.1. As coarse aggregates, the size fractions used in this work are 5-3 mm, 3-1 mm and 1-0.21 mm. The particle size distribution of aggregates is shown in Table 3.2.

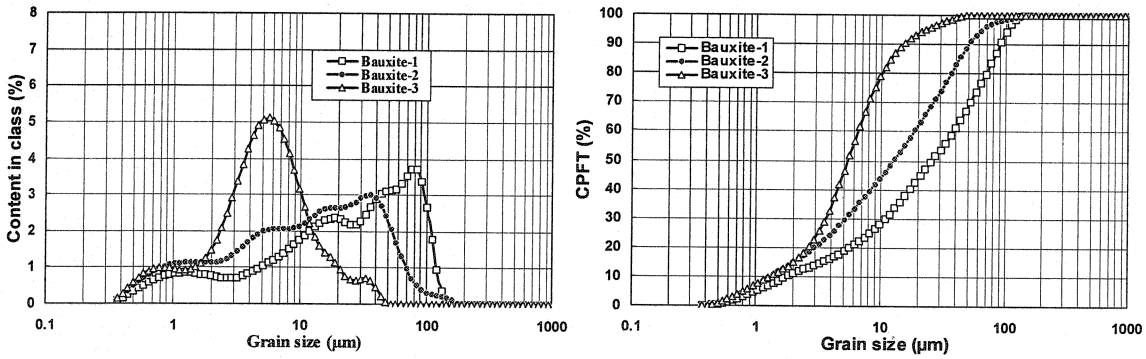
Table 3.1 Chemical composition of Chinese bauxite

Chemical composition	Al_2O_3	CaO	SiO_2	Na_2O	K_2O	Fe_2O_3	MgO	TiO_2	P_2O_5
%	85.1	0.21	5.26	<0.10	0.22	1.61	0.96	5.89	0.38

Table 3.2 Particle size distribution of bauxite aggregates fractions

Size fraction (mm)		8 - 5	5 - 3	3 - 1	1 - 0.21
CPFT (%)	8	100	100	100	100
	6.3	30	100	100	100
	5.0	2.6	95	100	100
	4.3	1.5	53	100	100
	3.0	0	5	94	100
	1.8	0	0	36	99
	1.0	0	0	5	95
	0.5	0	0	1	38
	0.088	0	0	0	10
	0.045	0	0	0	5

As fine grade, three kinds of bauxite fines have been considered: Bauxite-1, Bauxite-2 and Bauxite-3, with the same quality but different particle size distribution. The PSD of fine matrix components has been determined using COULTER LS200 particle size analyzer. The PSD of the bauxite fines is shown in Figure 3.2. Figure 3.2(a) represents the differential whereas 3.2(b) represents the cumulative volume distribution. The median (d_{50}) particle size is 25.6, 12.8 and 5.5 μm for Bauxite-1, Bauxite-2 and Bauxite-3, respectively. All the bauxite fines have mono-modal size distribution and the submicron (d<1μm) content is around 7.0 vol %.



3.2 (a) 3.2 (b)

Figure 3.2 Particle size distributions three bauxite powders Bauxite-1, 2 and 3.

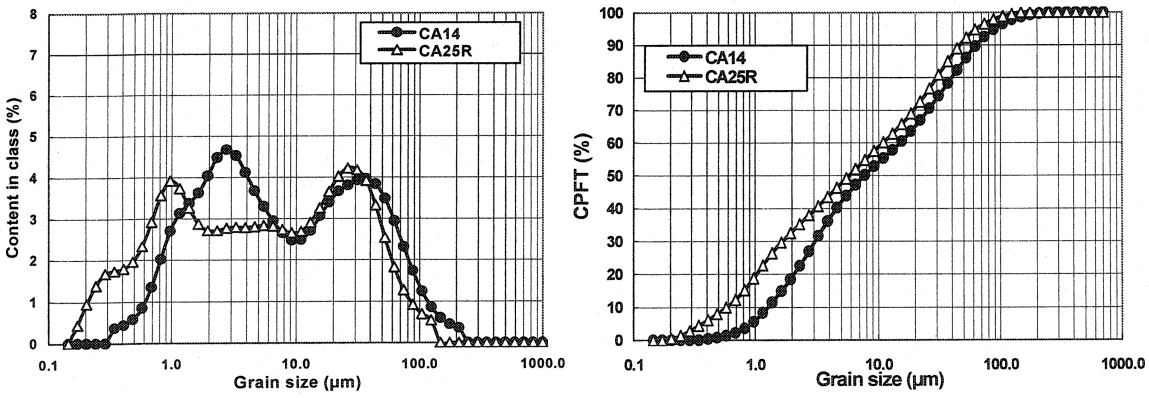
3.2.2 Calcium Aluminate Cements

Two kinds of cements, CA-14 and CA-25R, supplied by Alcoa Industrial Chemicals (currently Almatis), USA, are used as hydraulically setting binder. Both are commonly used for monolithic refractories. CA-14 is designed to be used in low and ultra-low cement castables. It provides excellent strength and long casting life (working time) with high alumina and microsilica containing monolithic castables. CA-25R is commonly used in conventional and low cement castables, which require high early strength development and good strength at intermediate temperatures [60]. Their chemical composition is given in Table 3.3.

Table 3.3 Chemical and mineralogical composition of cements

Chemical composition	Al_2O_3	CaO	SiO_2	Na_2O	Fe_2O_3	MgO	Mineralogical composition
CA-14 (%)	73.08	26.5	0.18	0.18	0.061	0.34	CA, CA_2, α- Al_2O_3
CA-25R (%)	81.88	17.5	0.15	0.41	0.059	0.26	CA, CA_2, $C_{12}A_7$, α- Al_2O_3

The PSD of CA-14 and CA-25R has been provided by the producer as shown in Figure 3.3. Figure 3.3(a) represents the differential volume % whereas 3.3(b) represents the cumulative volume % of PSD and their median (d_{50}) sizes are 8.0 and 3.7 microns for CA-14 and CA-25R respectively. Both of them are bi-modal in size distribution and the cumulative percentage finer than 325 mesh / 44 microns is 88.6 for CA-25R and 81.6 for CA-14.



3.3 (a) 3.3 (b)

Figure 3.3 Particle size distribution of cements CA-14 and CA-25R

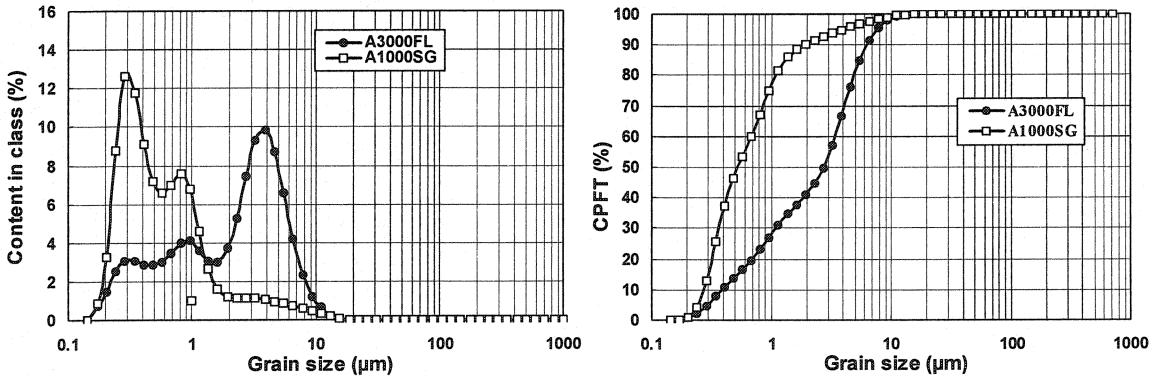
3.2.3 Reactive Alumina

Reactive alumina A-1000SG and A-3000FL from Alcoa (Almatis) have been used as ultrafine fillers. Their typical properties are given in Table 3.4 [61].

Table 3.4 Properties of reactive aluminas

Reactive alumina	Chemical composition (%)							SSA (m^2/g)	α-Al_2O_3 (%)
	Al_2O_3	CaO	SiO_2	Na_2O	Fe_2O_3	MgO <	B_2O_3 <		
A-1000SG	99.8	0.025	0.045	0.04	0.014	0.003	0.003	9.0	> 95
A-3000FL	99.8	0.02	0.02	0.07	0.02	0.02	0.003	2.5	> 95

The aluminas are produced by calcining Bayer process aluminium trihydroxide in rotary kilns. During calcination, the combined water is driven off and the oxide formed passes through several intermediate phases to obtain finally the stable α-alumina structure. By controlling the temperature and time of calcination, soda content, and processing parameters, a long list of calcined aluminas are available for selection, in terms of crystal, particle size and distribution, soda level, reactivity, etc. [62-63]. The PSD data of the two kinds of reactive alumina A 1000SG and A 3000FL are provided by the producer and shown in Figure 3.4. Figure 3.4(a) represents the differential volume distribution and 3.4(b) the cumulative volume distribution of them. The median (d_{50}) size is 0.42 and 2.7μm for A-1000SG and A-3000FL, respectively. Both are bi-modal in size distribution. They are commonly used in refractory castables to enable good flowability and mechanical properties. The submicron (d<1μm) fraction contents are 76.3% and 27.3% for A-1000SG and A-3000FL, respectively.



3.4 (a) 3.4 (b)

Figure 3.4 Particle size distributions of A-1000SG and A-3000FL.

3.2.4 Microsilica

Microsilica is amorphous, ultra-fine in size (submicron), very high in specific surface area, spherical in shape, and reactive with cement and water to form SiO_2-cement-bond in castables. The chemical composition of two microsilicas is given in Table 3.5. The SiO_2 content of Microsilica-1 (Elkem 971U, Elkem Materials, Norway) is higher than that of Microsilica-2 (Globe Metallurgical Inc., USA) and the carbon content is reverse. It is obvious that Microsilica-1 is purer than Microsilica-2 but with the same specific surface area.

Table 3.5 Properties of microsilicas

		Microsilica -1 (Elkem 971U)	Microsilica-2
Chemical composition (%)	Al_2O_3	0.4	0.28
	CaO	0.13	0.4
	SiO_2	98.2	96.2
	Na_2O	0.08	<0.10
	K_2O	0.31	0.56
	Fe_2O_3	0.05	<0.10
	MgO	0.15	0.22
	P_2O_5	0.05	0.04
	Carbon	0.5	1.21
	L.O.I	0.5	2.19
Density (g/cm^3)		2.2	2.1
SSA (m^2/g)		≥ 20	≥ 20
pH Value		5.7	7.3
Moisture content (%)		0.21	0.7
Physical state		Grey powder	Dark grey powder
Producer		Elkem Materials, Norway	Globe Metallurgical Inc., USA

3.2.5 Dispersant

Three dispersants have been used as dispersing agent and the details are shown in Table 3.6:

Table 3.6 Specification for dispersants [64-66]

Dispersant	Dispersant I	Dispersant II	Dispersant III
Synonyms	Castament® FS-20	SHMP, Calgon	Darvan 811D
Chemical composition	multi-component polycarboxylate copolymer	Sodium hexametaphosphate $(NaPO_3)_6$	sodium polyacrylate copolymer
Physical state	Yellowish-brownish powder	White powder or flake	White to yellow powder
Bulk density (g/cc)	0.3 - 0.6	0.9 - 1.1	0.50 - 0.75
Moisture (mass %)	4.0 maximum	6.0 maximum	8.0 maximum
pH-value	3.0-5.0 (20 % solution)	6.7-8.0 (1% solution)	6.0-9.0 (1% solution)
Producer	SKW Polymers GMBH	Anachemia Canada	R. T. Vanderbilt company, Inc.

3.3 Compositions of the Castables

The castable compositions are presented in the successive chapters, at each step when it is pertinent to do so.

3.4 Experimental Set-ups to Measure Rheology and Exothermic Profile

3.4.1 IBB Rheometer V1.0 for Castable Rheology

The IBB Rheometer V1.0 has been used to measure the rheology of the castables (Figure 3.5).

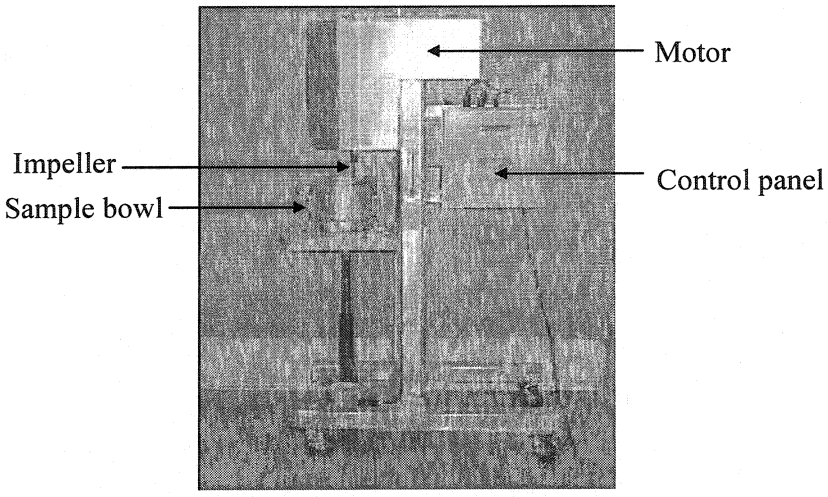


Figure 3.5 Photograph of IBB Rheometer V1.0.

It consists of a sampling bowl (inner diameter ∅ = 168mm and height h = 200mm) and a 3/4 HP motor, which drives an H-shaped impeller (height h = 85mm and width w = 53mm) with a planetary motion inside the bowl. The line diagram of sampling bowl and impeller is presented in Figure 3.6. Originally, developed for the rheological measurements in concretes [25, 67, 68], this rheometer can be a useful tool for rheological research of refractory castables. The major advantage of this kind of technique is that the rheological measurements are made directly on a castable, whereas a viscometer can only measure the rheology of the fine matrix of a castable.

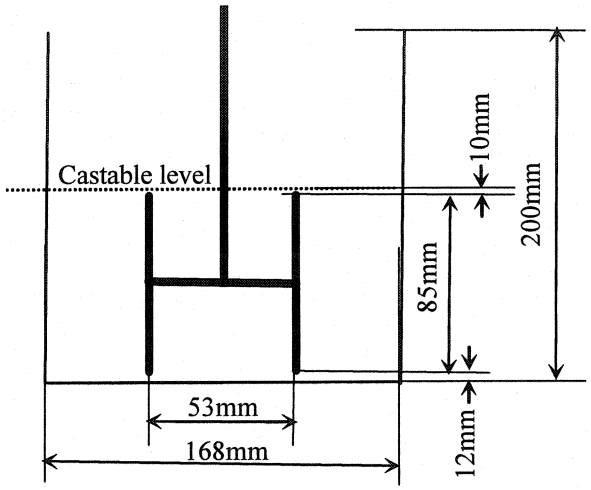


Figure 3.6 Line diagram of bowl and impeller of IBB rheometer.

Since castables are normally Bingham fluids the torque T, required to drive an impeller, the flow resistance G, the impeller angular speed N and the torque viscosity H are all related through the following equation [25]:

$$\mathbf{T = G + (H \times N)} \qquad \textbf{(Equation 3.1)}$$

where, T = the torque, required to drive an impeller, Nm,

G = the flow resistance, Nm,

N = the impeller angular speed, s^{-1},

H = the torque viscosity, Nm.s.

In Equation 3.1, T and G are in Nm, H and N are in Nm.s and rev/s respectively. By proper calibration of rheometer, the G and H parameters can be used to calculate the values of two fundamental rheological properties: yield stress, τ_0 and apparent viscosity, η, which are directly related to the castable mobility and other flow-related properties. All the castable rheological tests are carried out at 20 °C (environmental temperature) and the mixes are not protected from evaporation.

3.4.2 CVO 120 High Resolution Rheometer for Matrix Rheology

A Bohlin rheometer (CVO 120 High Resolution) is used to measure the rheology of the matrix portion of castable (Figure 3.7). It has an automated gap setting and control system, and interchangeable temperature control system, run by a computer. This rheometer is very powerful tool for suspension rheology characterization with very broad shear rate range from 0.05225 to 3344 s^{-1} and wide temperature range from -150 to 550°C. Its advantage comes from being able to work with low viscosity materials and mobile particulate suspensions with good repeatability and accuracy.

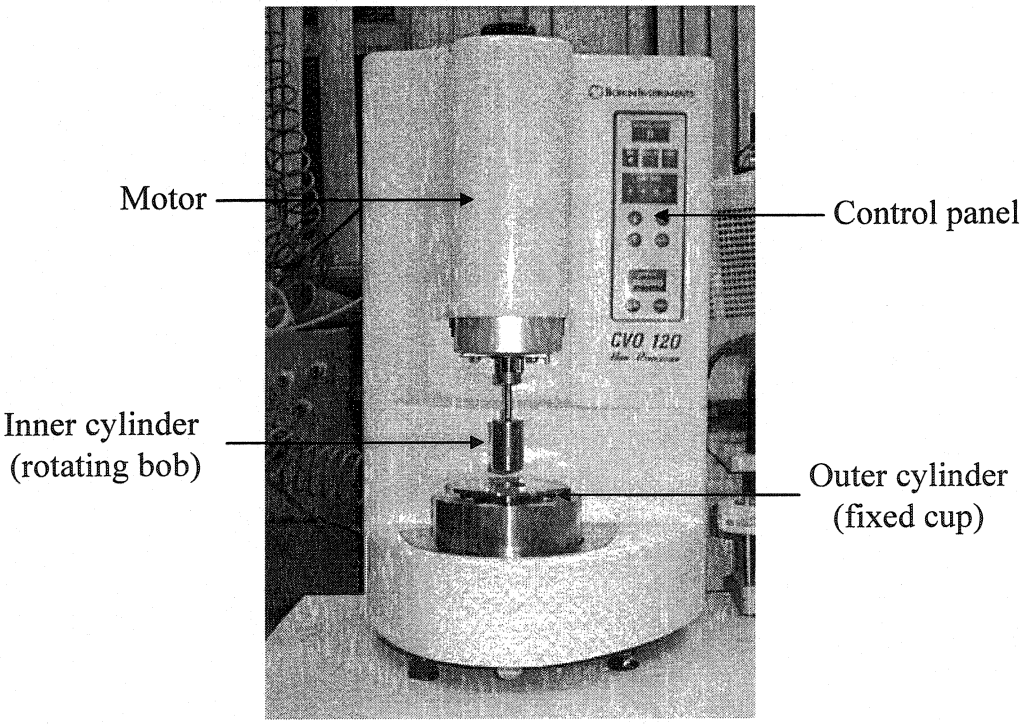


Figure 3.7 Photograph of CVO 120 High Resolution rheometer.

The concentric cylinder (cup /bob) measuring system is chosen to evaluate the matrix rheology. The line diagram of impeller is shown in Figure 3.8. This system consists of a rotating bob (inner cylinder) located in a fixed cup (outer cylinder) with the sample contained in the annular gap between them. The model C25 is applied with a 25-mm-diameter and 37.5-mm-height bob and a coaxial 27.5-mm-diameter and 49.9-mm-working-height cup [69]. The sample is placed into the annular gap between the outer cylinder and the rotor. A motor drives the inner cylinder. A viscosity related torque, caused by the resistance of the sample to shearing, act on the inner cylinder. The shear stress (τ) at different shear rate (γ) by varying the rotation speed can be measured and then apparent viscosity (η) is calculated and recorded by computer using the formula:

$$\eta = \tau / \gamma \qquad \textbf{(Equation 3.2)}$$

where, τ = the shear stress, Pa,

γ = shear rate, s^{-1},

η = apparent viscosity, Pa.s.

In Equation 3.2, η, τ and γ are in Pa.s, Pa and sec^{-1}, respectively. The stepped shear is used for flow characterisation tests. Individual shear rate values are selected. Each shear is applied for set time (The delay time is set to 30s and the integration time to 20s.). The shear rate, shear stress and apparent viscosity are recorded for each value. The start shear and end shear are 0.1 s^{-1} and 400 s^{-1}, respectively, with total 30 individual upward points and 30 downward points distributed on a log scale. The total 60 individual points are then joined up in a "dot to dot" fashion to produce the flow curve and the viscosity curve. One slurry test lasts 50 min.

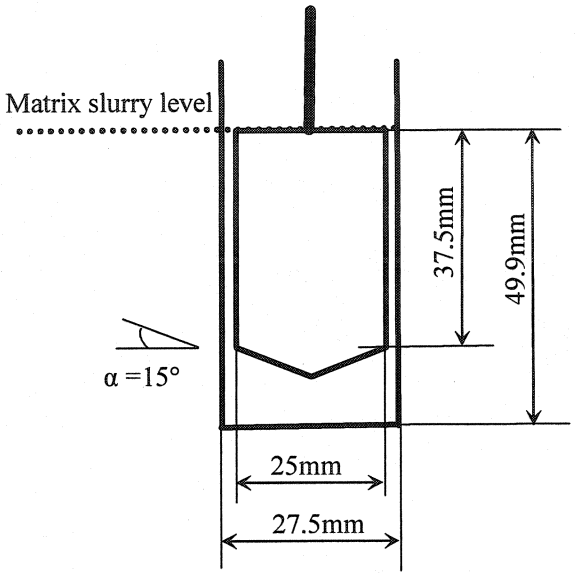


Figure 3.8 Line diagram of the impeller of CVO 120 rheometer [69].

3.4.3 Testing Set-up for Exothermic Profile Measurements

An insulating box is used for exothermic profile measurements. The line diagram of the set-up is shown in Figure 3.9. Two thermocouples are used simultaneously to measure the temperature at 10 seconds intervals. One is inserted into the mix and the other to measure room temperature. All data are stored in an automatic recorder.

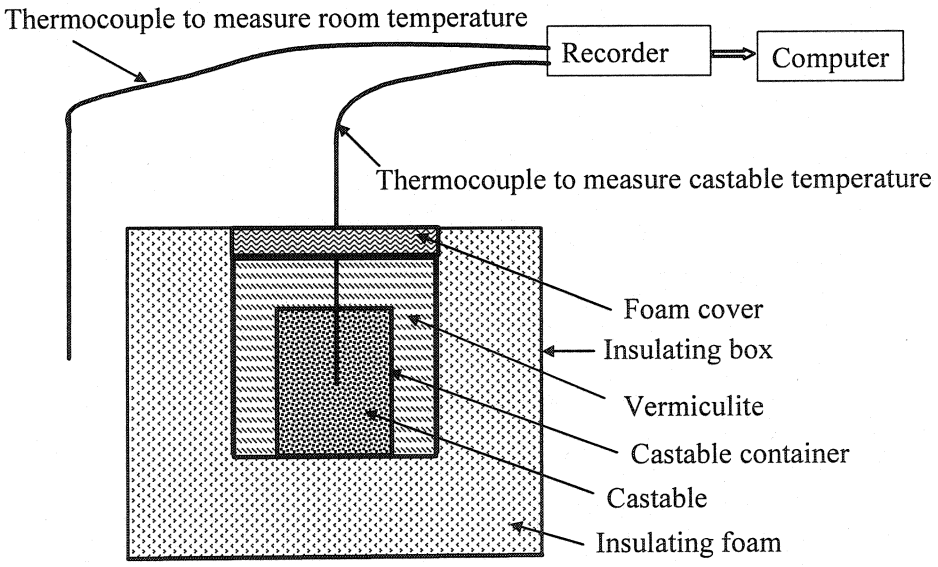


Figure 3.9 Line diagram of the set-up for exothermic profile measurement.

3.5 Sample Preparation

According to the composition, a castable mix is batched and first dry mixed for 5min in a Hobart mixer, model N50 or D340, depending on the quantity, and then water is added to the mix in a two-step procedure. At first, 80% of total water amount is added and mixed for 3min. The remaining water is then added and further mixed for another 3min at the same speed.

Samples are cast by vibration, self-flowing, pumping or shotcreting. The vibrated samples are cast on vibration table working at 0.4mm of amplitude and 60 Hz of frequency. The self-flow samples are cast only by gravity, without external force. After casting, the samples are cured for 24 h in mould at room temperature (19-22 °C) and for another 24 h after demoulding, at room temperature, and then dried at 110 °C for 24h.

Prism of 160×40×40 mm are made for the determination of BD, AP, PLC and CMOR.

3.6 Test Methods

3.6.1 Flowability, Flow Decay and Water Demand

Flowability is represented by flow value, which is measured by the flow cone conforming to ASTM C1445-99 [28] method. Self-flowability measurements are performed as per ASTM C1446-99 [70]. For flow decay test, 4 kg castable mix is made and stored in an airtight container. The self-flowability is measured at every 10 min (sample of around 0.5 kg drawn from container) and the castable is put back into container after measurements and mixed with the remaining castable with a spatula. The container is sealed airtight to prevent moisture evaporation. This procedure is repeated until the castable ceases to self-flow.

Water demand is counted as an extra to the weight of the dry mix. It is so controlled as to enable the castable to reach enough self-flowability value at reasonable water addition.

3.6.2 Mechanical and Physical Properties: BD, AP, PLC and CMOR

BD and AP measurements are performed as per ASTM C 830-00 [71]. PLC is determined according to ASTM C1407-98 [72]. CCS and CMOR are determined by the conventional three-point bending method conforming to ASTM C 133-97 [73], using universal testing machine (model TTCML, Instron Engineering Co., USA).

3.6.3 Castable Rheology

For castable rheological measurements, 8 kg of fresh castable mix is poured into the bowl and the torque-speed relationship is observed at intervals of 5min for a total duration of 185 min. During testing, the rotation speed of impeller through the bowl with castable is changed step-wise, and in each step the required torque and the impeller speed are measured.

3.6.4 Matrix Rheology

For matrix rheological measurements, 205 grams of fine matrix (corresponds to fine matrix of 0.5 kg of castable) is wet-mixed by a CAFRAMO mixer at constant speed of 200 /s for 5 min. The water addition and dispersant dosage are kept the same as in the castable. The fresh matrix slurry is stored in a small sealed container during testing. The Bohlin Rheometer is set in an isothermal mode at 20 °C for all tests. Matrix slurry (12 ml) is injected into the cup of the rheometer by a syringe and then some mineral oil with very light density and low viscosity is added on the top of the sample in the cup as a barrier to prevent moisture evaporation. This oil is immiscible to the sample and remained on the top during testing. Measurements are performed with a table of step-wise shears to get up/down sweep at intervals of 1h for single test. Six tests are performed on the slurry for the duration of 6h. The sample slurry for each test is taken from the container and filled in the rheometer after cleaning the cup. The shear stress vs. time test of the matrix slurry is also performed for 15 min at different shear rate level of 0.3139, 3.094, 12.93, 30.49, 127.4 and 300.5 /s, respectively. The data for all experiments are automatically recorded by a computer.

3.6.5 Conductivity

For conductivity measurement, fine matrix slurry is made with 41.0 g dry fine matrix in 102.5 g water (water/ solid content =2.5) and conductivity is measured using pH and Conductivity Meter (Hanna Instruments, Canada) at 20 °C. The measurements are made for 12 hrs at 5 min intervals.

3.6.6 Exothermic Profile

For exothermic profile measurements, 3.5 kg fresh castable mix is put into an airtight box, which is placed in an insulated box as shown in Figure 3.10. The box is covered and held at 20 ± 1.0 °C. The castable temperature and room temperature are measured by thermocouples and the values are displayed on a recorder, as function of time after start of mixing (zero) until complete hydration.

3.6.7 Bonding Water Measurements for Cement Hydration

The castable samples are cast, and then covered with plastic film and cured at 20^0C for 24 hours, demoulded and dried for 24 hours at 110^0C and fired at 1000^0C for 5 hours. The samples are weighed after demolding, drying and firing by an electronic balance. The weight loss percentage is taken as the free water and cement hydration bonding water.

CHAPTER 4 - PARTICLE SIZE DISTRIBTUTION

Particle size distribution (PSD) is one of the most important parameters to achieve desirable workability of monolithic refractories while designing a castable. Using two rheometers, the influence of particle size distribution on castable rheology is investigated in terms of the rheological parameters: flow resistance (G) and torque viscosity (H) and matrix rheology with plastic yield stress (τ_y) and plastic viscosity (η_p). Two parameters: interparticle separation distance (IPS) and maximum paste thickness (MPT) have been calculated. The correlation between these parameters is analyzed and reported.

4.1 Introduction

Nowadays, the self-flow castables are designed with a continuous distribution of refractory particles using either Andreasen's equation or Funk and dinger's equation, which consider the existence of the smallest particle diameter (D_s) [21, 74, 75]. For practical reasons, the Andreasen's equation is most often used, and the same is used for the present work. When using Andreasen packing model, with the same D_{max}, the castable with smaller q value contains higher matrix volume fraction. Meanwhile, with the same q value, the castable with a smaller D_{max} value contains greater portion of fine particles than with a bigger D_{max}. The well-designed castable with an ideal PSD permits:

(1) To achieve high packing efficiency and maximum packing density.
(2) To obtain appropriate interaction among particles to ensure workability.
(3) To get desirable physical and mechanical properties, such as density, porosity, and modulus of rupture etc,

It is well known that the rheology of castable mix depends upon the state of dispersion, agglomeration, collision and friction between the particles. These effects are understood

through this work. Results on rheograms are collected by changing PSD as a variable to show the influence of PSD on castables as well as matrix slurries in terms of coarse to matrix (C/M) ratio and water to matrix (W/M) ratio.

4.2 Compositions

The composition details are given in Table 4.1. In this work, 3 q values are considered. The influence of D_{max} on rheology is also evaluated. With a D_{max} of 5 mm, the q values of CM-1, CM-2 and CM-3 are 0.23, 0.26 and 0.29, respectively. The D_{max} of composition CM-4 is 8 mm and q value is 0.26 to be compared with CM-2. 5 wt% microsilica and 4 wt% cement are fixed for each composition with 0.12 wt% SHMP as the binder system. The details of raw materials have been described in Chapter 3.2.

Table 4.1 Details of castable mixes to study the effect of particle size distributions

Castable		**CM-1**	**CM-2**	**CM-3**	**CM-4**
Coarse aggregate (wt%)		55	59	63	61
Fine matrix (wt%)	Bauxite-1	13	11	10	10
	Bauxite-2	13	12	10	10
	Bauxite-3	10	9	8	10
	Cement CA-14	4	4	4	4
	Microsilica-1 (Elkem 971U)	5	5	5	5
Dispersant SHMP (wt%)		0.12	0.12	0.12	0.12
Andreasen modulus (q value)		**0.23**	**0.26**	**0.29**	**0.26**
D_{max} (mm)		**5**	**5**	**5**	**8**
C / M ratio		**1.22**	**1.44**	**1.70**	**1.56**
W / M ratio		**0.16**	**0.17**	**0.19**	**0.18**

4.3 PSD of the Castables

The PSD of the four compositions are shown in Figure 4.1. It shows CM-1 contains more fine particles than the others. CM-3 contains the least fine particles among them.

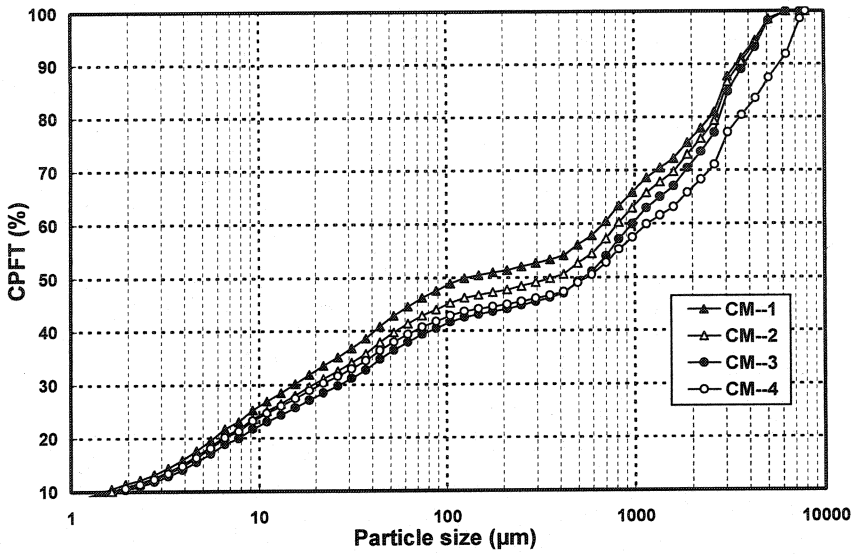


Figure 4.1 PSD of the four compositions with different q value and D_{max}.

4.4 Water Demand and Self-flowability

The self-flowability of the four compositions as a function of water is shown in Figure 4.2. The compositions CM-2, CM-3 and CM-4 have shown more self-flow for 6 wt % water compared to CM-1. The same trend is observed with 6.5 wt % water. The possible reason is the more specific surface area associated with CM-1 compare to the other compositions, which needs more water to coat and then make the castable flow. With 7 wt % water addition, the self-flow of all compositions are almost same and further addition of water does not improve flow (segregation observed) in all cases and hence not shown. Considering the minimum self-flowability as 100% for pumpable castable, the water amount for the present investigation has been fixed at 7 wt % for the rheology measurements.

With 7.0 wt% water, the self-flowability of different compositions measured immediately after mixing (0 min) is compared with the values measured after 30 min (30 min) in Figure 4.3. It is noted that at 0 min, self-flowability for all compositions looks similar at around 120%. After 30 minutes, the self-flowability of castable CM-1 has shown considerable increase in self-flowability while observing little increase for composition CM-2. In case of composition CM-3 and CM-4, there has been a decrease

in self-flowability which is the result of segregation. In the case of CM-1, additives dissolve well with elapsed time and coat the surface of fine particle and disperse them well and then improve flowability. Other compositions with relatively less fine particles get dispersed well during mixing itself and hence not showing any improvement in flowability with time. It should be noted that the compositions CM-4 and CM-2 differ only in D_{max} value. This indicates that it would be better to limit the maximum particle size below 8mm for pumpable castables, under such conditions, with 7 wt% water.

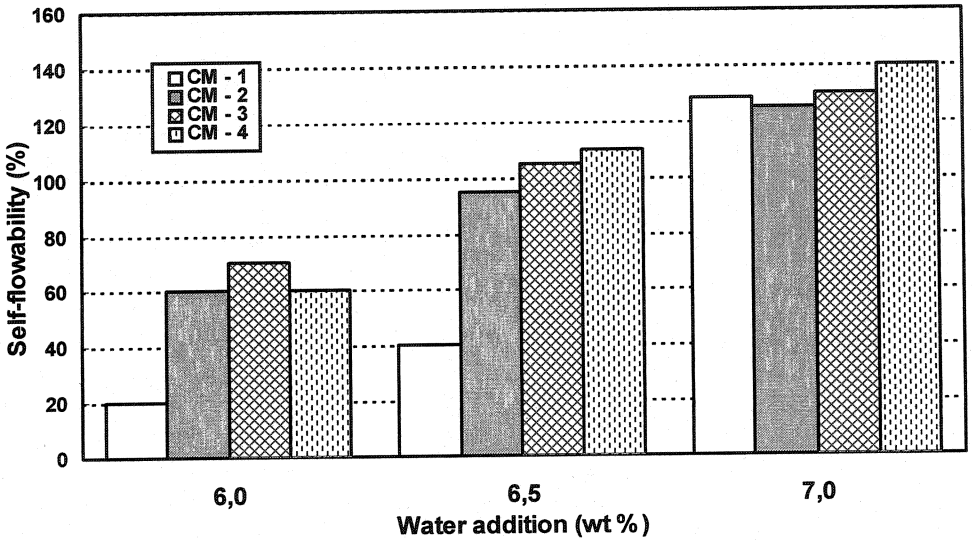


Figure 4.2 Self-flowability vs. water addition.

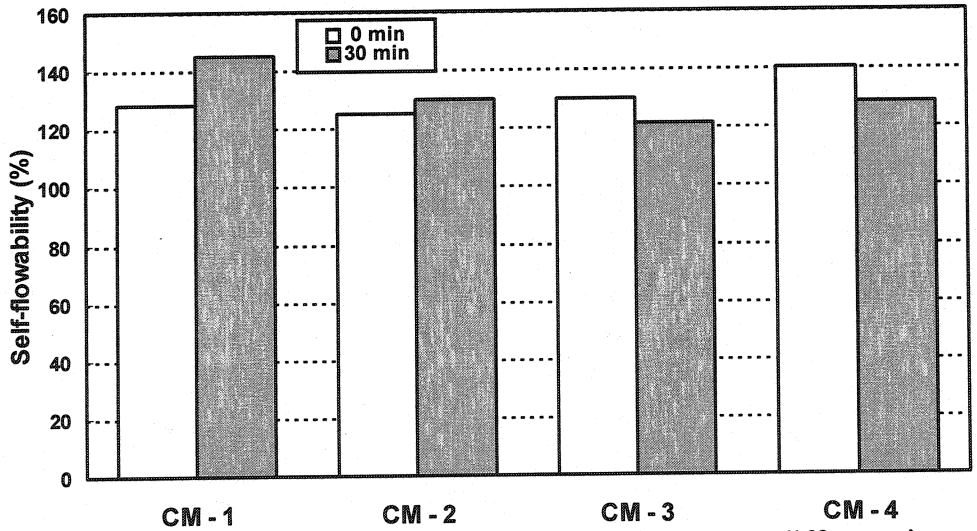


Figure 4.3 Comparison of self-flowability of castables at different time.

4.5 Castable Rheology

4.5.1 Torque vs. Speed

The rheological measurements on the four castables CM-1, 2, 3 and 4 with different torque and speed are shown in Figure 4.4, 5, 6 and 7, respectively. The rheometer results of CM-2 are considered for explanation (Figure 4.5). The hysteresis loops in Figure 4.5 represent the relationship between torque and impeller speed for castable mix after 0, 5, 10, 15, 20, 25, 30, 35, 40 and 45min of rheological testing. At 0 min (immediately after mixing) that is on the first ramping up, the forward cycle reveals pseudoplastic nature of the mix, while the reverse cycle displays almost Bingham behaviour (Newtonian Fluid with Yield). In the forward cycle, the rate of torque increase is decreasing with testing speed and the mix is getting more homogenized. Once it reached a maximum testing speed, the homogeneous mix behaves almost linearly in the reverse cycle. In the same test, after 5min, there has been a drastic reduction of the hysteresis loop's area when compared to the initial loop. The loops area remains almost the same then after 10, 15, 20, 25, 30, 35, 40 and 45min but shift downward (i.e., rate of torque decrease with speed decreases) from 0 to 20min, and then remains almost constant.

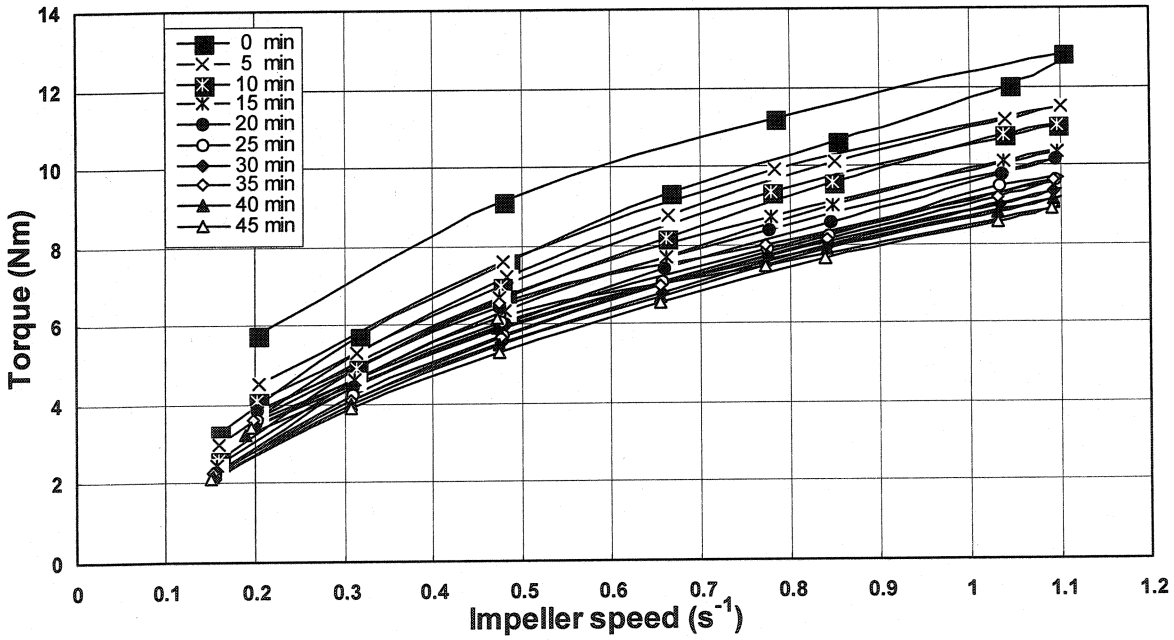


Figure 4.4 Torque vs. impeller speed for CM-1.

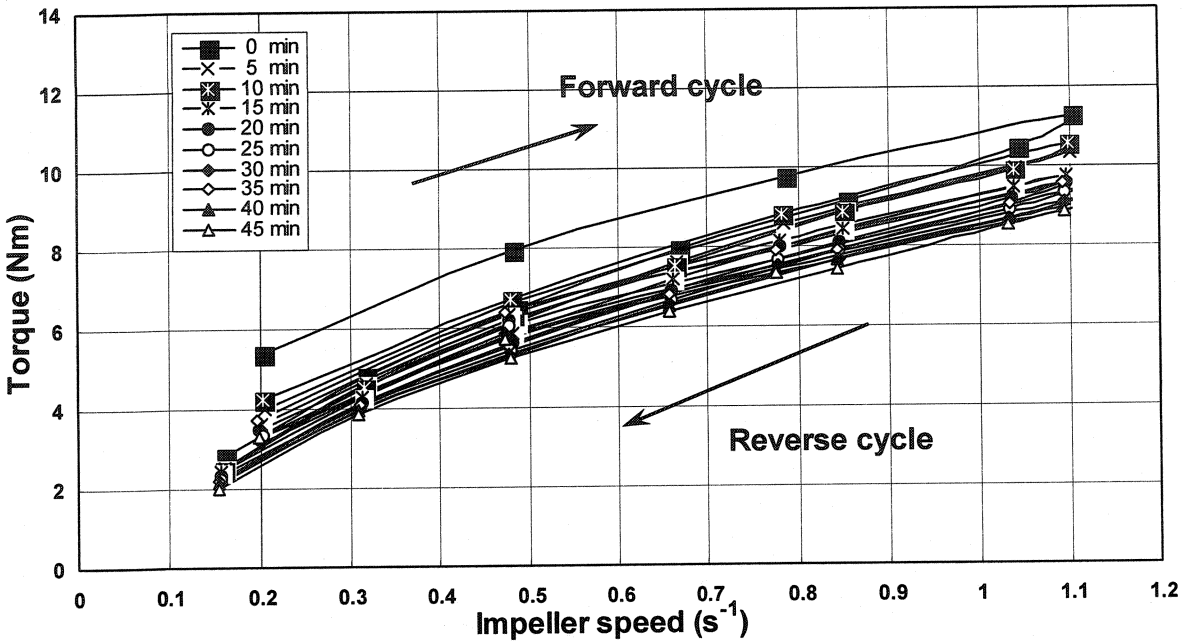


Figure 4.5 Torque vs. impeller speed for CM-2.

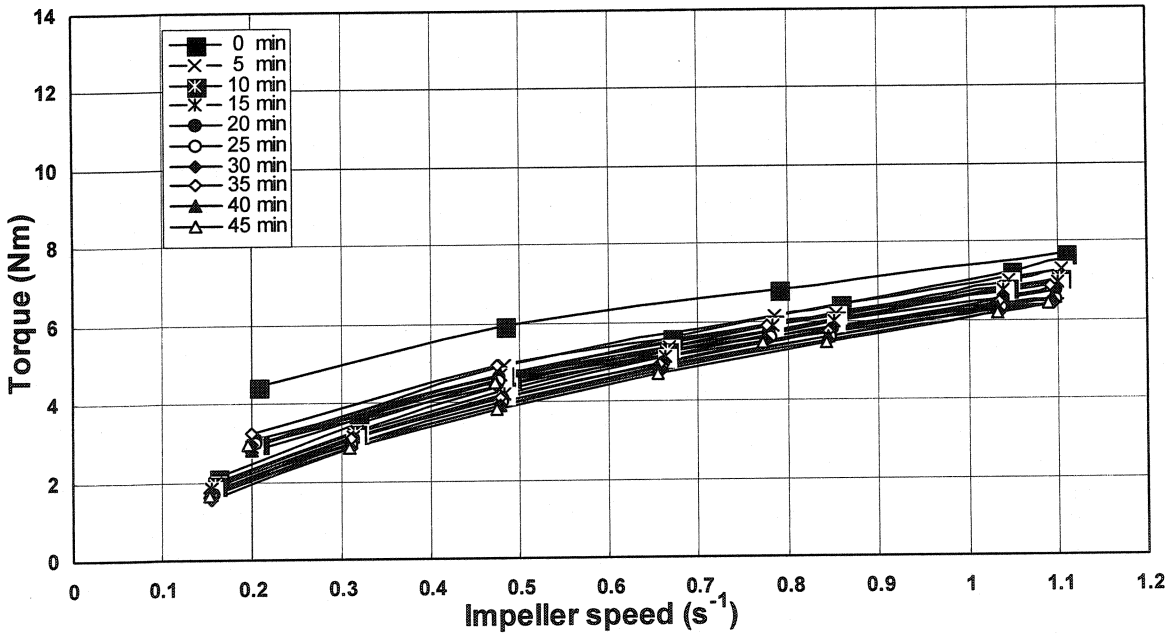


Figure 4.6 Torque vs. impeller speed for CM-3.

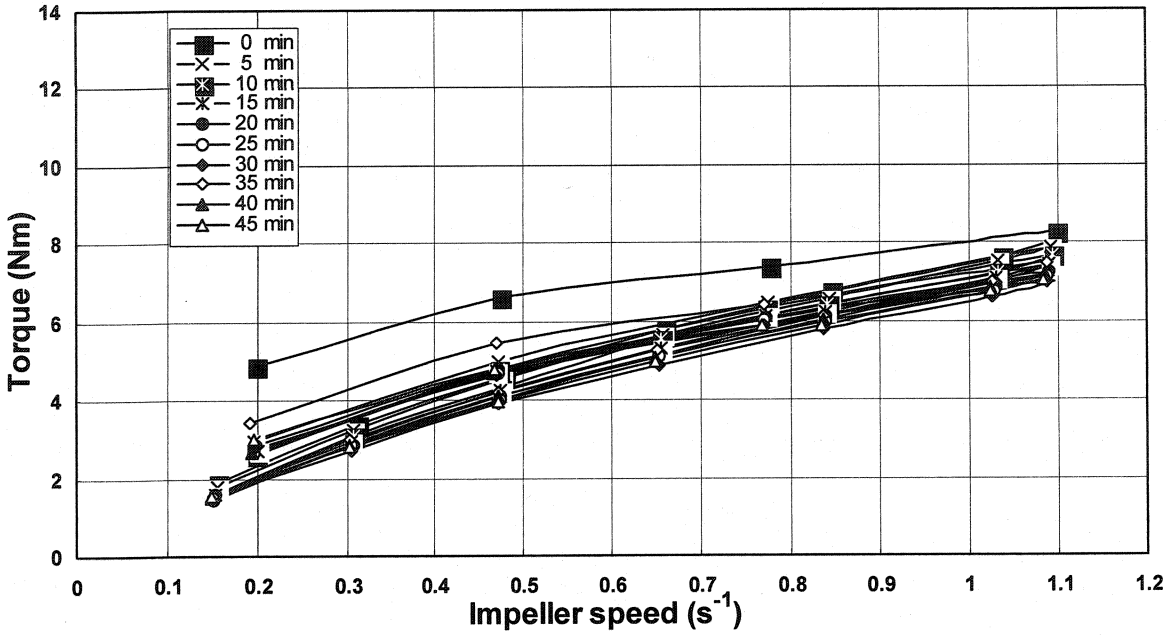


Figure 4.7 Torque vs. impeller speed for CM-4.

At the beginning of the test, the mix may not be considered as completely mixed and gains in homogeneity with mixing speed. The shearing stress helps break agglomerates, and to fill the voids and improve dispersibility, due to the post mixing action of the impeller. Once the mix has been sheared at a level of $1.1s^{-1}$, the mix is in a more homogeneous state and then shows Bingham behavior in the reverse cycle. Further on, in the testing cycle, the mix is more and more homogeneous and reaches after 20min a state where further homogenization with mixing action is not noticeable.

The same kind of behaviour has been observed for the other compositions but with different rates of change of torque with speed. The torque (T_{max}) of the four compositions at the highest impeller speed of 1.10 s^{-1} in 1st loop (0 min) is given in Table 4.2. In the case of CM-1, 2 and 3, the T_{max} is 12.83, 11.29 and 7.67 Nm, respectively. The loops of these three compositions compress and shift downwards more and more. In the case of CM-4, the torque is 8.25 Nm and loops compress more than CM-2, with the same q value but different D_{max}.

Table 4.2 T_{max} for the 4 compositions at the impeller speed of 1.10 s^{-1} in 1st loop

Composition	CM--1	CM--2	CM--3	CM--4
T_{max} (Nm)	12.83	11.29	7.67	8.25

4.5.2 Equivalent Apparent Viscosity

The relationship between equivalent apparent viscosity and impeller speed of CM-2 with testing time is shown in Figure 4.8, always closely typical to a Bingham fluid. The values of equivalent apparent viscosity are calculated from the instantaneous torque divided by impeller speed. Although not a fundamental parameter, as the apparent viscosity, the equivalent apparent viscosity can be converted to apparent viscosity of the chosen system with proper conversion factors [25]. The trends are similar for the other compositions and hence not shown.

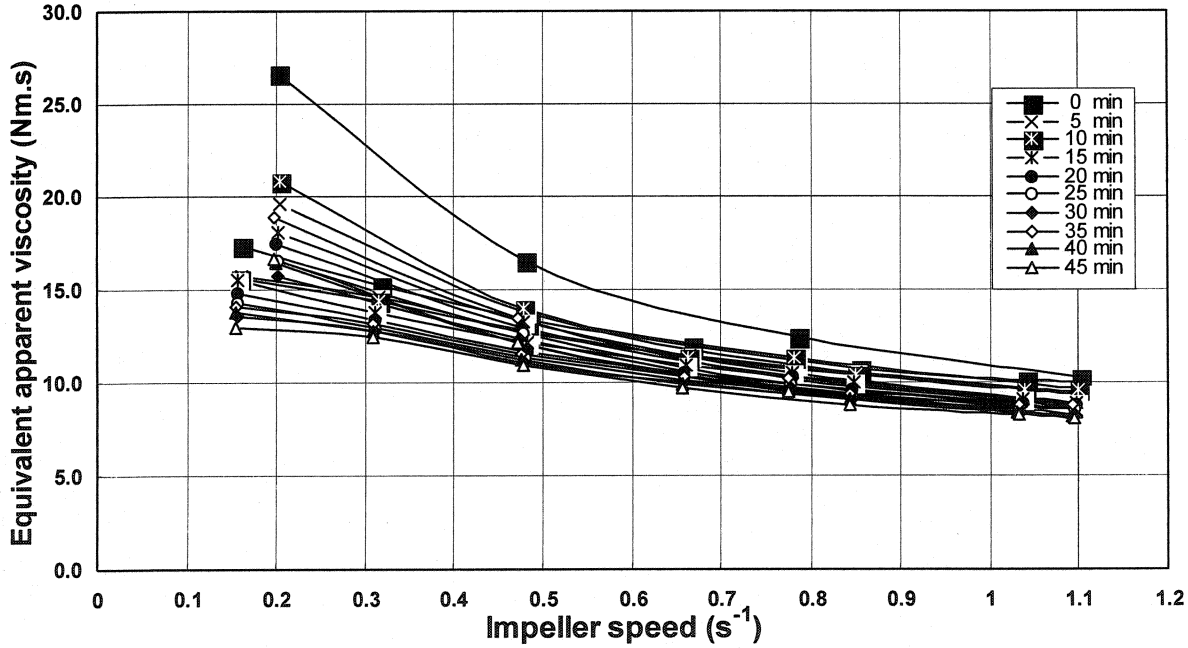


Figure 4.8 Equivalent apparent viscosity vs. impeller speed for CM-2.

4.5.3 Thixotropy

Thixotropy is defined as the decrease of viscosity (softening) with time at a constant shear rate [10]. Though the mixes are behaving as Bingham fluid, when analyzed as a

function of time at constant impeller speed, the mixes displayed thixotropy as illustrated in Figure 4.9. In Figure 4.9, CM-1 (a) and CM-1 (b) represents the equivalent apparent viscosity, which is calculated (the specific torque values divided by the specific impeller speed)for the higher (1.10 s^{-1}) and lower speed (0.48 s^{-1}) respectively (in the reverse cycle) in each five minute cycle for composition CM-1. The same nomenclature is valid for CM-2, CM-3 and CM-4. The equivalent apparent viscosity is decreasing and stabilizing with time at constant shear rate in all cases. The values of equivalent apparent viscosity for the constant speed 0.48 s^{-1} are higher than those at 1.10s^{-1}. The equivalent apparent viscosity of CM-1 is the highest and then follows as CM-2, CM-4 and CM-3. All compositions show shear-thinning and thixotropy behaviours.

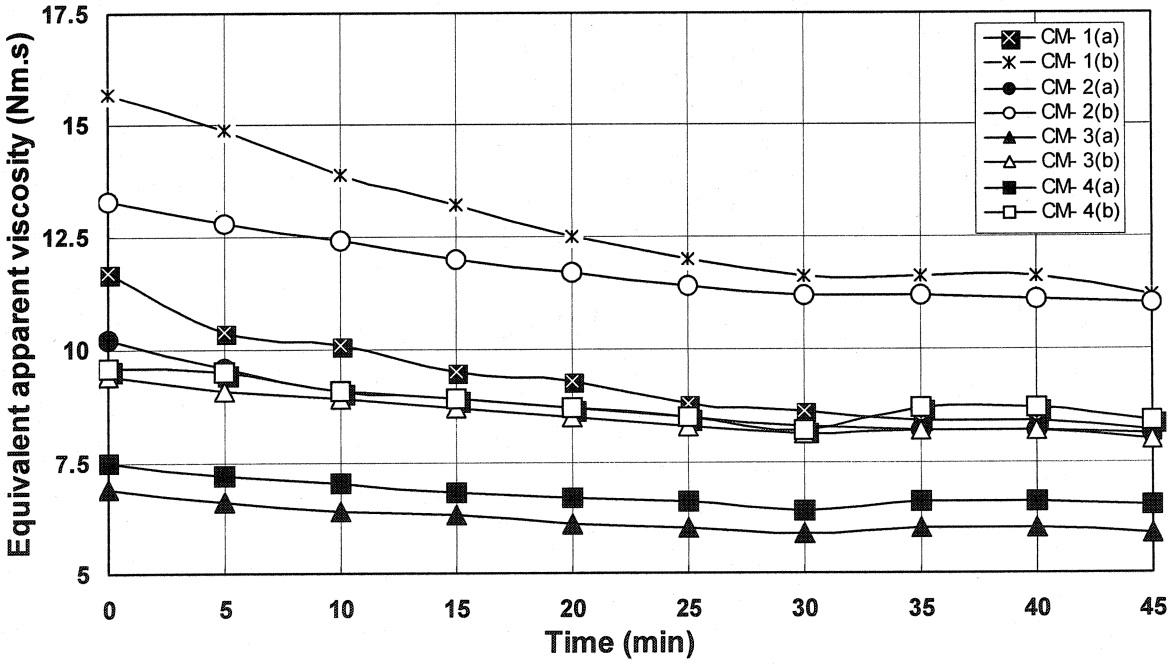


Figure 4.9 Equivalent apparent viscosity vs. time at high (a) and low (b) impeller speed.

Thixotropy is closely related to shear-thinning behavior and it is usually observed in yield-shear-thinning suspensions because of the gelation behavior that occurs in such suspensions begin to break down, producing lower measured viscosities [10]. The higher the shear rate, the more gel broke down, and the lower is the measured viscosity.

Although gel structures break down under shear, the structures will re-form again with time. Suspension properties, relating both to particle physics and interparticle chemistry, determine the rate at which the gels will form, which is known as the gelation rate. The rate of gelation, which rebuilds gel structures, will balance shear rate, which breaks down the gel structures. The minimum viscosity achieved by a system at constant shear rate will occur at a balance point between these two phenomena. Higher shear rates will cause more gel to be broken, and the balance point with gelation will occur at a lower apparent viscosities.

4.5.4 Flow Resistance and Torque Viscosity

The method of evaluation of G and H values using the test results for mix CM-2 at 0 min. is shown in Figure 4.10. The intercept G and the slope H are being obtained by a linear regression analysis using six points in the reverse cycle (i.e., from high speed to low speed) as they represent the behaviour of the homogenized castable mix [25]. The G and H value are for mix CM-2 at 0 min are 1.86 Nm and 8.65 Nm.s, respectively.

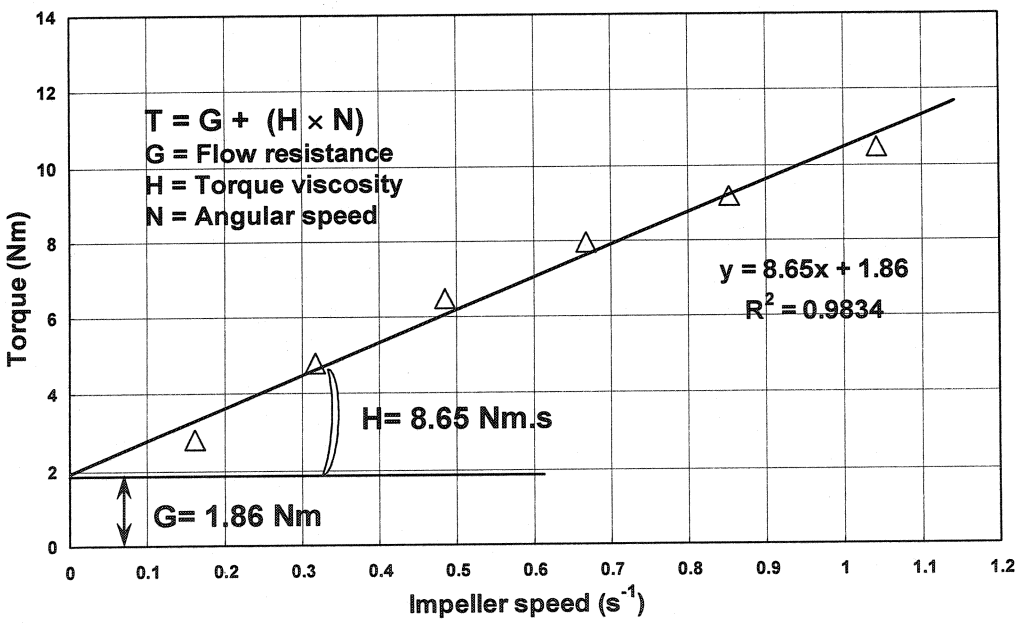


Figure 4.10 Calculation methods of G and H for CM-2 at 0 min.

The calculated methods of G and H for all compositions are the same as shown in Figure 4.10. The calculated values of the four compositions are given in Table 4.3.

Table 4.3 G and H values for all the compositions

Time (min)	Flow resistance G (Nm)				Torque viscosity H (Nm.s)			
	CM- 1	CM- 2	CM- 3	CM- 4	CM- 1	CM- 2	CM- 3	CM- 4
0	2.28	1.86	1.5	1.18	9.9	8.65	5.8	6.58
5	2.06	1.73	1.37	1.1	9.44	8.47	5.67	6.52
10	1.69	1.62	1.34	0.93	9.33	8.27	5.56	6.54
15	1.65	1.56	1.28	0.9	8.68	8.02	5.53	6.36
20	1.49	1.52	1.19	0.92	8.47	7.78	5.45	6.13
25	1.46	1.46	1.17	0.85	8.07	7.58	5.27	6.11
30	1.43	1.42	1.07	0.88	7.8	7.43	5.26	5.84
35	1.42	1.41	1.16	0.89	7.7	7.41	5.24	6.05
40	1.41	1.4	1.2	0.89	7.61	7.4	5.22	6.14
45	1.36	1.33	1.16	0.92	7.38	7.34	5.11	5.95

The G values of different compositions with testing time are shown in Figure 4.11. At 0 min, the G value is higher for CM-1 followed by CM-2, CM-3 and CM-4, respectively. G decreases drastically for the initial 20 minutes and remains constant during further testing period. In case of CM-1, around 40% reductions are observed by 20 minutes while only 28% for other three compositions. Although the value of G can be drastically changed by choosing the proper type and amount of dispersant, only the ratios C/M and W/M have been considered here, as defined in Table 4.1. The relationships between the ratios C/M, W/M and G can be understood by comparing Table 4.1 and 3. It is observed that G is decreasing as the ratios increase, except for C/M ratio of 1.56 (CM-4). In CM-4, the maximum particle size is 8 mm rather than 5 mm and for this mix segregation has been observed. The reason for segregation is that C/M ratio for CM-4 is less than for CM-2, with same q of 0.26, due to broader distribution of CM-4 than CM-2. The reason for decrease of G with ratios is that more addition of water with decreasing fine matrix and given q reduces the force required for yielding the castable system. It is also observed that the G decreases with testing time, which is due to the additional mixing. Though the test is conducted to study the rheology, it gave additional mixing energy to

the castable system as discussed earlier. The castable system with additional energy requires only less force to yield. Each G value reaches a constant value after 20 minutes, indicating that system has attained saturation stage in mixing and G cannot be further reduced. The 40% reduction of G in case of CM-1, which is due to the lowest C/M ratio, means that the castable has got more fines in the system and the additional mixing is drastically favoured when compare to other compositions

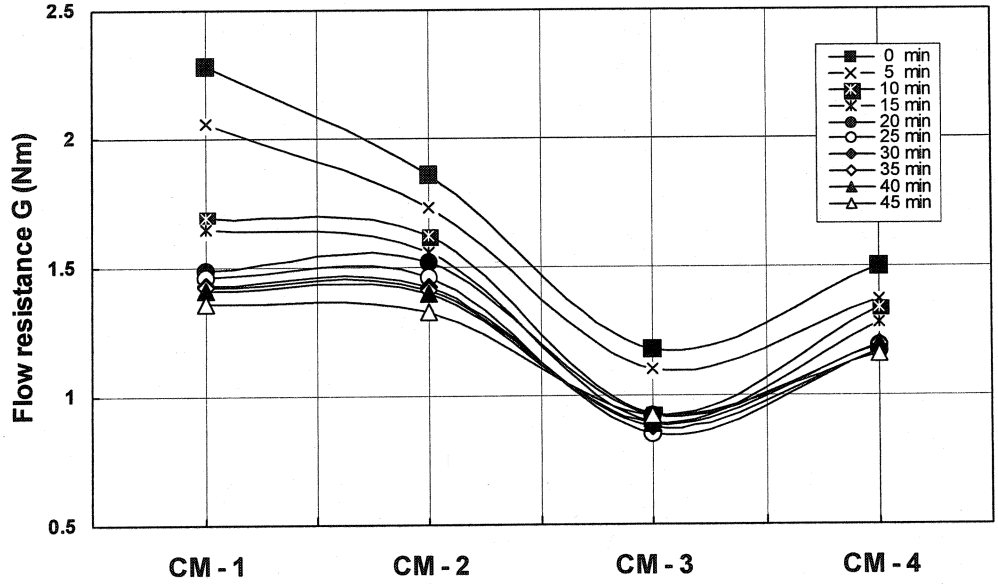


Figure 4.11 Flow resistance vs. PSD.

The H values of different compositions with testing time are shown in Figure 4.12. The H value is the highest for CM-1 followed by CM-2, CM-4 and CM-3 respectively. The trends of H and G values are different for composition CM-1 and CM-2. H decreases by 25% and 15% from the initial value in the first 20 minutes, and remains constant further on. In case of CM-3 and CM-4, the H values are almost constant with time and are around 50% lesser than for CM-1 and CM-2. This has a direct impact on the design of castables in practice. H has to be at optimum value to maintain the coherence of the castable system at given C/M and W/M ratios. It is observed that above the C/M ratio of 1.44 there has been a drastic reduction in torque viscosity, H. This means that an optimum amount of fine particles and sufficient viscosity are required to avoid segregation by maintaining coherence, integrity and stability of the castable mix.

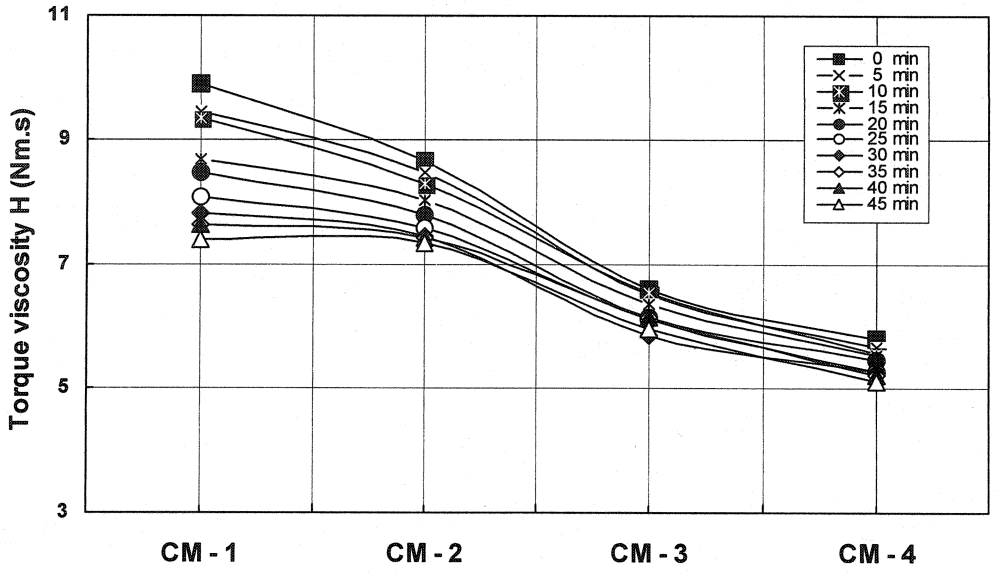


Figure 4.12 Torque viscosity vs. PSD.

Both H and G are decreasing with increasing q value but the rate of decrease is more for H (Table 4.1). This indicates the variation of bauxite fines in the matrix has influenced more the torque or apparent viscosity than the flow resistance or yield stress. In the present study, the type and amount of dispersant have been fixed and hence no drastic rate of change of G has been observed.

4.6 Matrix Rheology

4.6.1 Shear Stress vs. Shear Rate

The shear stress as a function of shear rate of the matrix slurry of the four castables CM-1, 2, 3 and 4 is shown in Figure 4.13. The shear stress in the forward cycle (shear rate increasing) is higher than rate in the reverse cycle (shear rate decreasing) and then forms a hysteresis loop. The shape of the loop looks like a bow and almost similar for each matrix slurry. The loops for the matrix slurries shift downwards from CM-1 to CM-2 and then to CM-3, with q value of 0.23, 0.26 and 0.29, respectively. The loop of CM-2 is located in the middle of CM-1 and CM-3. In the case of CM-4, the loop is slightly lower than CM-2.

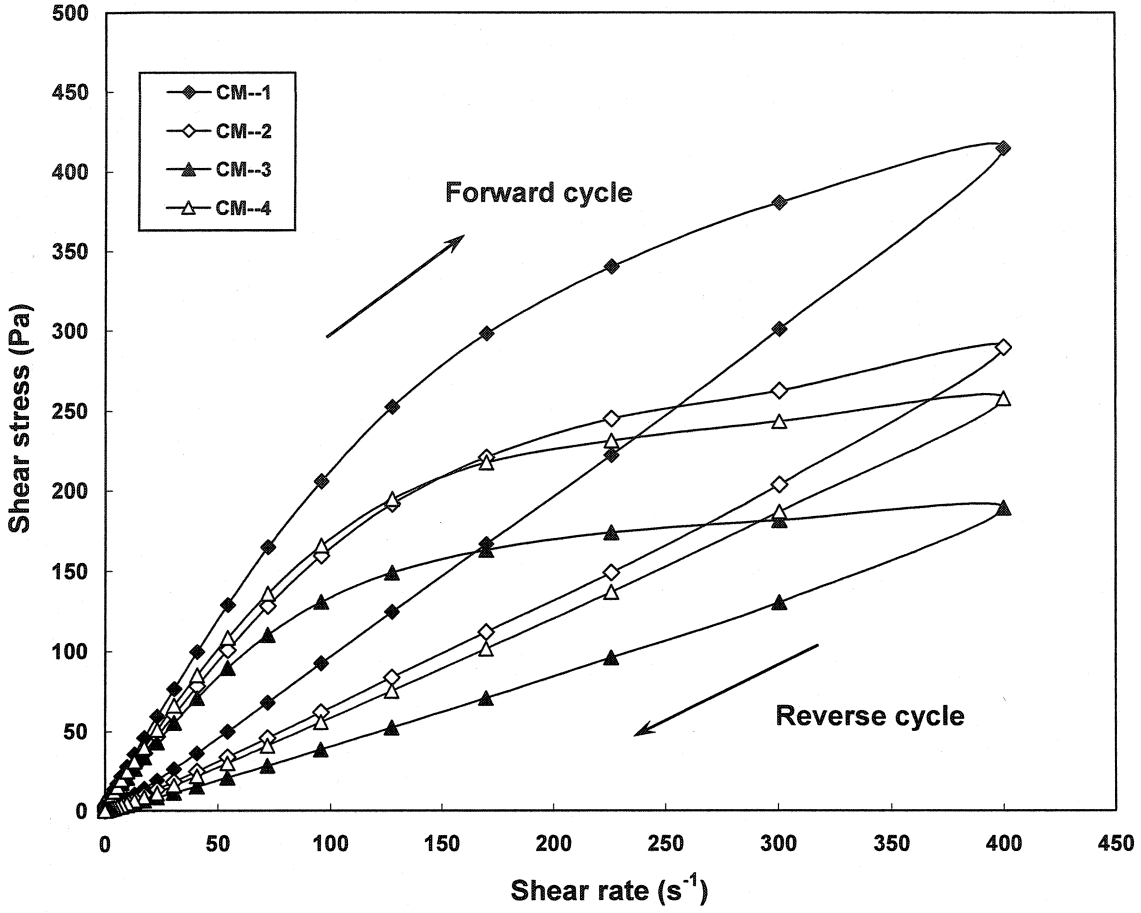


Figure 4.13 Shear stress vs. shear rate for all the matrix slurries.

The shear stress (τ_{max}) at the highest shear rate of 400 s^{-1} of all the matrix slurries is given in Table 4.4. The same trend has been found for the torque (T_{max}) at the highest impeller speed of 1.10 s^{-1} at 0 min, as given in Table 4.2. The τ_{max} decreases with q value increasing from 0.23 to 0.29 for the same D_{max}. In the case of CM-4, the τ_{max} is slightly lower than CM-2 and this is due to the less solid content of CM-4 compared to CM-2 (Table 4.4). The forward cycle reveals pseudoplastic nature of the slurry, while the reverse cycle displays almost Bingham behaviour.

Table 4.4 τ_{max} and solid content of the matrix slurries at the highest shear rate of 400 s^{-1}

Matrix slurry	CM--1	CM--2	CM--3	CM--4
τ_{max} (Pa)	414	290	189	258
Solid content (%)	67	65	63	64

4.6.2 Apparent Viscosity vs. Shear Rate

The apparent viscosity as a function of shear rate of the matrix slurry of the four castables CM-1, 2, 3 and 4 is shown in Figure 4.14. The apparent viscosity as a function of shear rate of the matrix slurry of the four castables CM-1, 2, 3 and 4 is shown in Figure 4.14. The apparent viscosity in the forward cycle (shear rate increasing) is higher than rate in the reverse cycle (shear rate decreasing). The apparent viscosity of CM-1 is the highest and that of CM-3 is the lowest. The apparent viscosity of CM-2 and CM-4 are similar and rank in the middle of CM-1 and CM-4. This is related to solid content of the matrix slurries under study (Table 4.4). In the forward cycle, the apparent viscosity of the four matrix slurries decrease sharply within 5.0 s^{-1} and remains similar till 100 s^{-1} and finally slightly decreases till to 400 s^{-1}. In the reverse cycle, the apparent viscosity remains similar from the shear rate of 400 s^{-1} to 1 $^{-1}$ and then increase till the shear end.

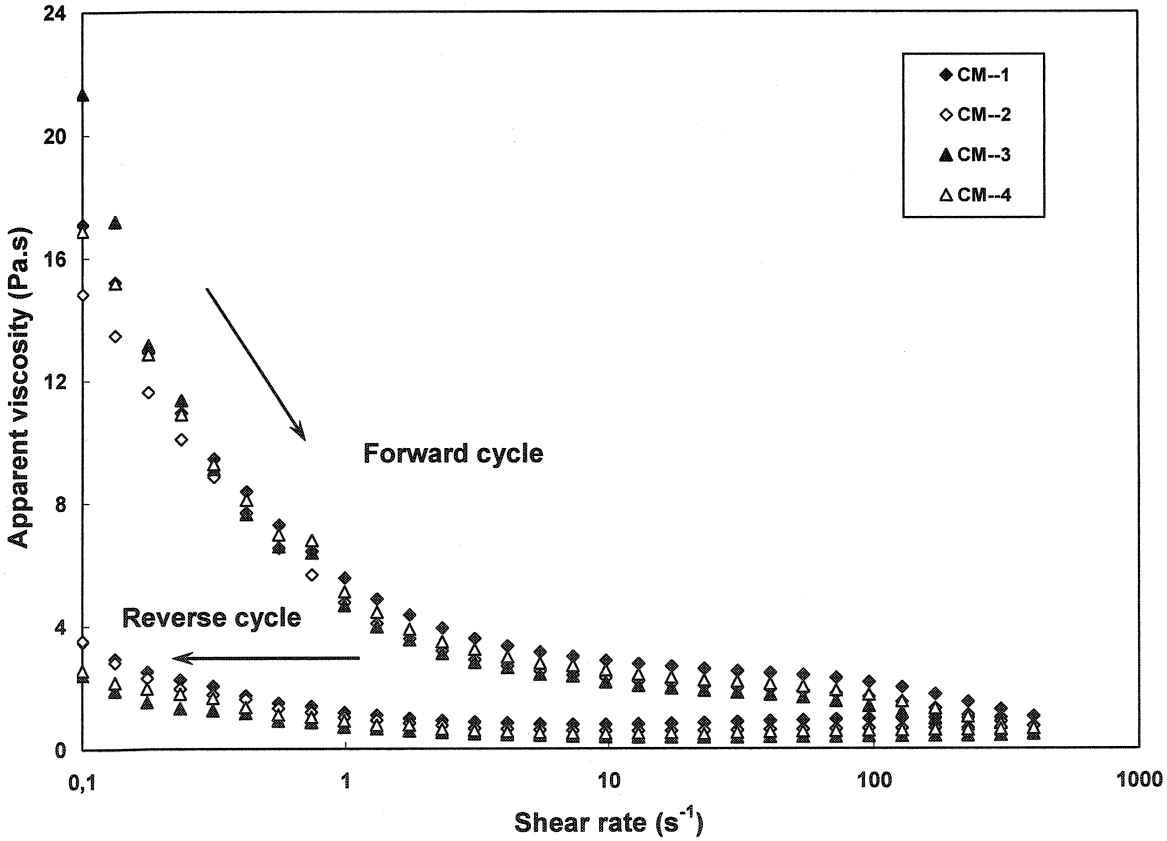


Figure 4.14 Apparent viscosity vs. shear rate for all the matrix slurries.

4.6.3 Thixotropy

As shown in Figure 4.14, the apparent viscosity decreases as the shear rate increases. The matrix slurry shows shear thinning behaivor because of the gelation behavior that occurs in such suspensions begin to break down, producing lower measured viscosities [10]. The shear stress in the forward cycle is different with the reverse cycle. This difference can be considered to quantitatively calculate thixotropy degree of matrix slurry, using the following formula [76]:

$$\Delta T = \Sigma (\tau^{up} - \tau^{down}) \qquad \textbf{(Equation 4.1)}$$

where, at the same shear rate,

ΔT = Thixotropy degree, Pa,

τ_{up} = the shear stress in the forward cycle, Pa,

τ_{down} = the shear stress in the reverse cycle, Pa.

The loop's area of rheogram is mathematically calculated to quantify the thixotropy degree, using the following formula:

$$S = 0.5*\Sigma (\gamma_{i+1} - \gamma_i) (\Sigma (\tau^{up}_{i+1} - \tau^{up}_i + \tau^{down}_{i+1} - \tau^{down}_i) \qquad \textbf{(Equation4.2)}$$

where, S = the loop's area, Pa/s.

γ_i = the shear rate at the i^{th} point, s^{-1},

γ_{i+1} = the shear rate at $i+1^{th}$ point, s^{-1},

τ^{up}_{i+1} = the shear stress at $i+1^{th}$ point in forward cycle, Pa,

τ^{up}_i = the shear stress at i^{th} point in forward cycle, Pa,

τ^{down}_{i+1} = the shear stress at $i+1^{th}$ point in reverse cycle, Pa,

τ^{down}_i = the shear stress at i^{th} point in reverse cycle, Pa.

The thixotropy degree and loop's area of the four matrix slurries are shown in Figure 4.15. The thixotropy degree ranking goes from CM-1 to CM-2 and CM-3. In the case of CM-4, it is slightly higher than CM-2. The same trend is found for the loop's area.

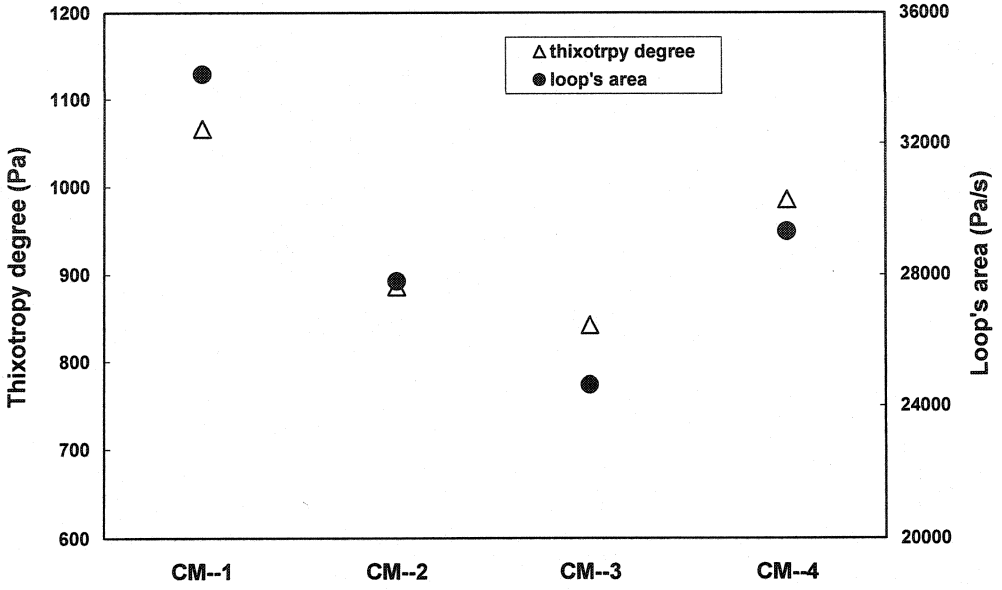


Figure 4.15 Thixotropy degree and loop's area for all the matrix slurries.

These results show clearly that for a castable, the amount of fine particle regulate the degree of thixotropy to be observed. With more fine particles in a castable, the mix will have a higher thixotropic characteristic, and vice verse. The loop area results go into the same direction. The higher the amount of fine particles, the more the hysteresis is. This means the more difficult it is to entrain all the particles at the same speed.

4.6.4 Plastic Yield Stress and Plastic Viscosity

The plastic yield stress and viscosity of the four matrix slurries are calculated from shear rate of 0.556 to 54.024s^{-1} in the forward cycle, as shown in Figure 4.16. For a typical plastic flow curve, the plastic yield stress, τ_y, corresponds to the intercept of the extrapolated straight line to ordinate (τ-γ plot) and the slope corresponds to the plastic viscosity η_p, of chosen system. The correlation coefficient is close to 1 and the lines show typical Bingham behaviour of flow curve [63]. The calculation method of plastic yield stress and plastic viscosity are followed by the equation 4.3.

$$\tau = \tau_y + \eta_p \times \gamma \qquad \textbf{(Equation 4.3)}$$

where, τ = the shear stress at the specific shear rate in the forward cycle, Pa,
τ_y = plastic yield stress, Pa,
η_p = plastic viscosity, Pa.s,
γ = shear rate, s^{-1}.

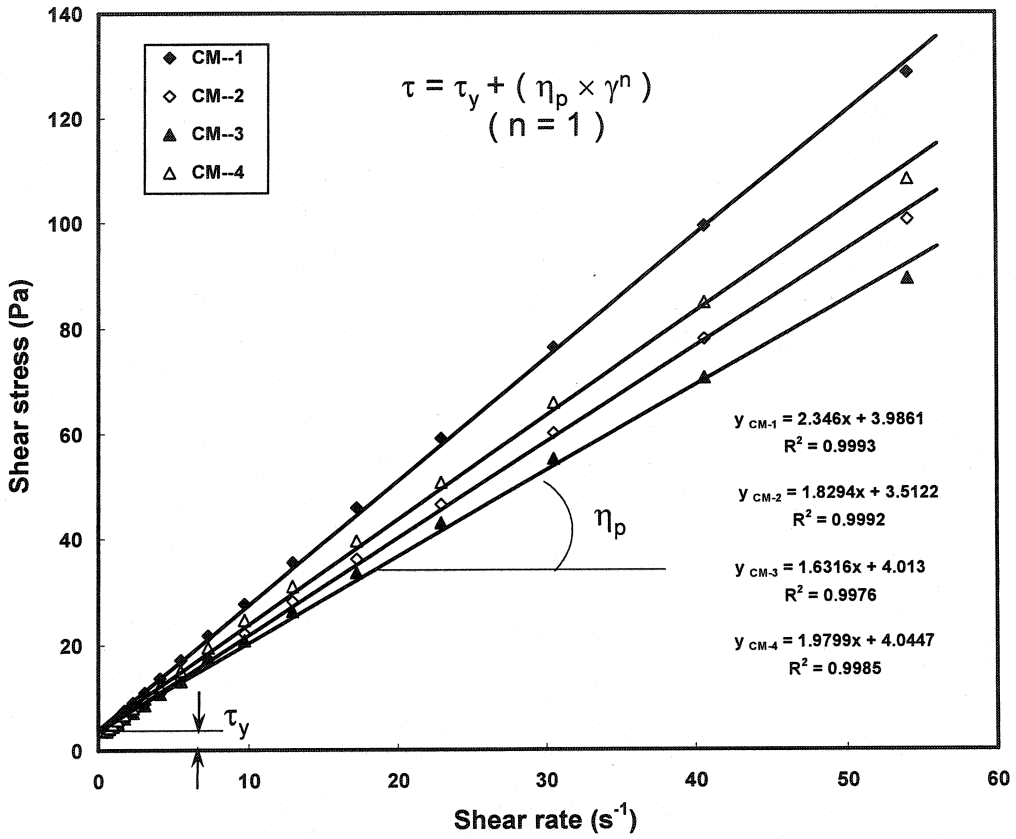


Figure 4.16 Plastic yield stress and viscosity for all the matrix slurries.

The plastic viscosity and yield stress of the four matrix slurries are given in Table 4.5. The plastic viscosity of CM-1 is the highest and then followed by CM-2 and CM-3. In the case of CM-4, the plastic viscosity is close to CM-2. The plastic yield stress of all the compositions is similar. From flowability point of view, both τ_y and η_p should be low. For a castable, however, they should never be too low, when water addition is adjusted to reach a minimum. For a suspension with higher packing fraction at a certain consistency, various deflocculants will have an impact on these two parameters. When other things being equal, the lower they are, the better the flowability is expected. The

results show that not only plastic yield stresses have a very low value, but also all of them equal to 4 Pa, which in fact cannot be used to predict the yield stress of a castable mix. This is because in the matrix slurry, the solid content is only 62-67 vol %, the particles are much smaller and the excess free water is much higher than in castables.

Table 4.5 Plastic viscosity and yield stress of the four matrix slurries

Composition	CM--1	CM--2	CM--3	CM--4
Plastic viscosity (Pa.s)	2.346	1.829	1.632	1.98
Plastic yield stress (Pa)	3.986	3.512	4.013	4.045

4.7 IPS of the Matrix Slurries and MPT of the Castables

In Chapter 2, the calculation methods of IPS of matrix and MPT of castables have already been described as Equation 2.7 and 13. The IPS and MPT of CM-1, 2, 3 and 4 are given in Table 4.6.

Table 4.6 IPS of the matrix slurries and MPT of the castables

Composition	CM--1	CM--2	CM--3	CM--4
IPS (nm)	86.0	87.9	90.1	88.8
MPT (μm)	144.8	123.8	105.8	146.0

In the case of CM-1, 2 and 3, the IPS of matrix slurry of the four castables increase with q value increases as 0.23, 0.26 and 0.29. The IPS of matrix slurry of CM-4 is in the middle of CM-2 and CM-3. On the reverse, the MPT of CM-1, 2 and 3 decreases with q value increasing. In the case of CM-4, the MPT is the highest among four compositions.

4.8 Mechanical and Physical Properties

The CMOR and AP of all compositions are almost similar, as shown in Table 4.7, which are around 7-9 MPa and 18-19% with 7wt % water addition. The physical and mechanical properties of green body are not affected by changing PSD. This is due to maintaining cement and microsilica content. The CMOR of all castables at 45 min is slightly lower than those at 0 min. In the case of AP with time, CM-1 remains the same

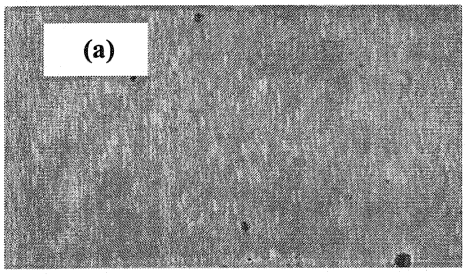
and CM-2 slightly decreases because of degassing during self-flow casting. The AP of both CM-3 and CM-4 increases slightly as a result of segregation to be shown later on.

Table 4.7 CMOR and AP of all the compositions

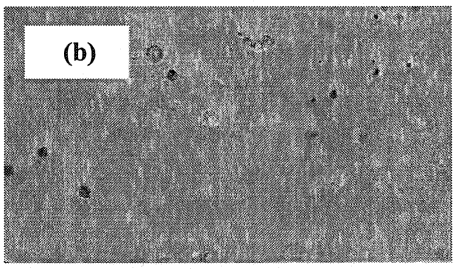
Composition	CMOR (MPa)		AP (%)	
	0 min	45 min	0 min	45 min
CM - 1	8.1	7.4	18.7	18.7
CM - 2	9.3	8.7	18.2	17.8
CM - 3	9	8.1	17.9	18.2
CM - 4	9.2	7.9	18.1	18.4

4.9 Appearance of the Castable Samples

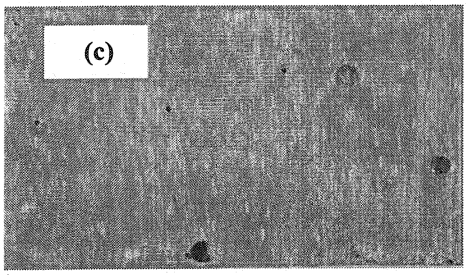
The appearance of castables at different time for different composition is shown in Figure 4.17(a)-(h). The appearance of the fresh (0min.) castable for compositions CM-1 and CM-2 are very good, whereas dewatering and bleeding has been observed for compositions CM-3 and CM-4. After 45 minutes of mixing, some bubbles appear on the surface of castable compositions CM-1 and CM-2. Total segregation is observed with composition CM-3 and CM-4.



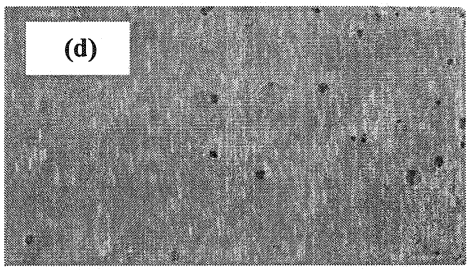
CM-1 (0 min)



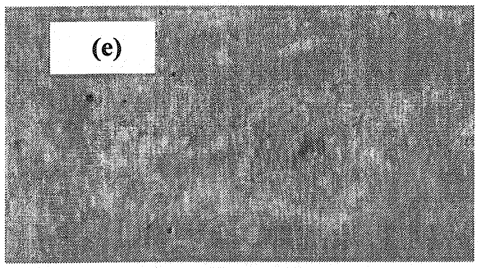
CM-1 (45 min)



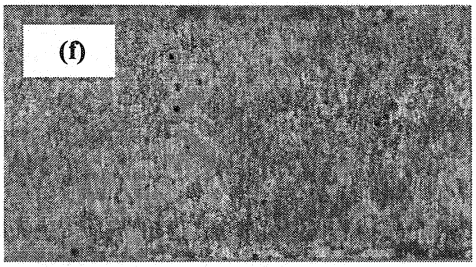
CM-2 (0 min)



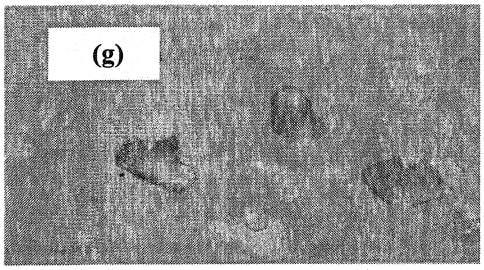
CM-2 (45 min)



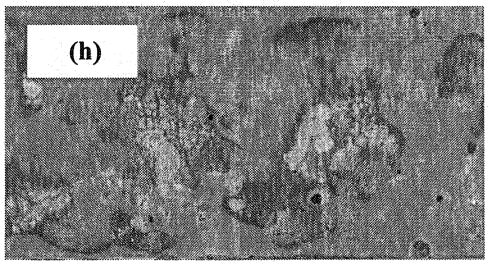
CM-3 slight dewatering (0 min)



CM-3 serious segregation (45 min)



CM-4 slight dewatering (0 min)



CM-4 serious segregation (45 min)

Figure 4.17 (a)-(h) Appearance of samples CM-1, 2, 3 and 4 at different time.

4.10 Optimization of the Castables

Normally, a castable with good flowability is considered as pumpable and this is not necessarily so. Though castables are considered as a simple mixture of aggregates, fines and binders they are complex in terms of rheological behaviour. A test of flowability alone does not describe completely by such a behaviour. In this paper, CM-1, CM-2, CM-3 and CM-4 show the similar self-flowability with 7 wt% water (Figure 4.2 and 3), but all of them are not good pumpable castables. For good pumpability, a castable must possess optimum combination of torque viscosity and flow resistance in order to flow well and to avoid blockage and segregation. The relationship between G and H is shown in Figure 4.18. The composition CM-1 is having good flow resistance (no segregation) but very high torque viscosity. CM-2 provides almost similar flow resistance but lesser torque viscosity than CM-1. Between CM-3 and CM-4, values of G are higher and H lower, but both CM-3 and CM-4 have been found to segregate (Figure 4.17). This indicates that the values of G and H should be above a critical value to avoid

segregation; hence composition CM-2 appears to be the optimum combination in terms of rheological behavior.

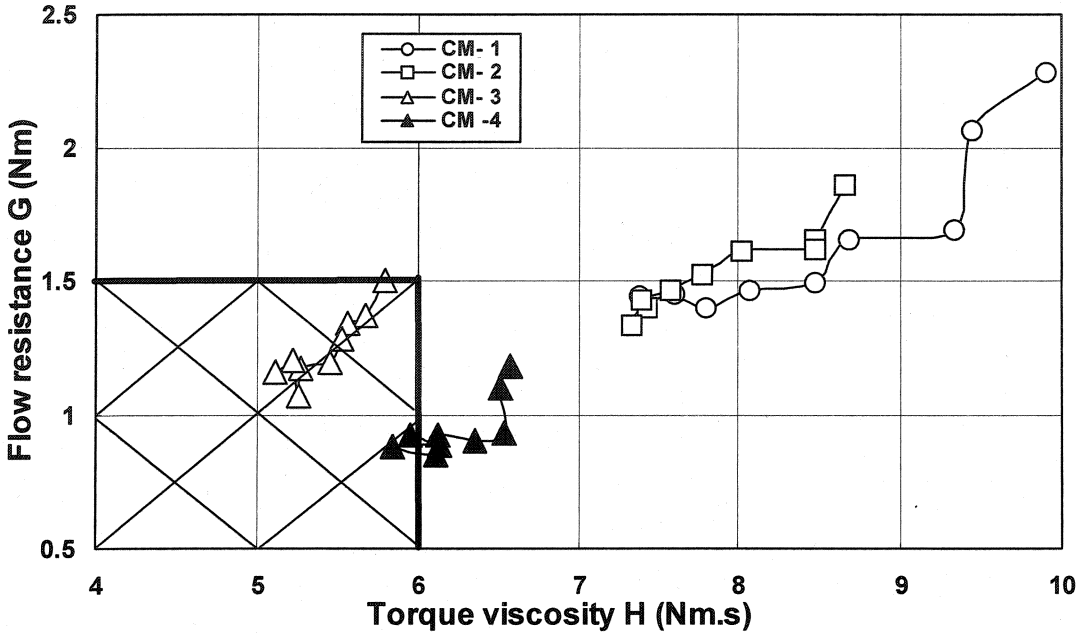


Figure 4.18 Flow resistance vs. torque viscosity.

4.11 Conclusions

The rheological behavior of bauxite based low-cement castable has been studied using two rheometers. The conclusions based on this investigation are:

a) The rheometer has been found to be an effective tool to measure the rheology of castable mix directly. Two important properties torque viscosity (H) and flow resistance (G) have been evaluated using this rheometer. The mixes have shown Bingham behavior for single cycle of rheometer test and thixotropy has been observed when analyzed with testing time at constant impeller speed.

b) Though self-flowability is found to be same for all compositions at water amount of 7 wt%, they have shown different flow resistance and torque viscosity. This confirms that only flow measurement is not sufficient to define the castable behavior.

c) G and H have got direct correlation with q value, D_{max}, C/M ratio and W/M ratio under the present set of conditions, the maximum particle size should not exceed 8mm (with q of 0.26 and W/M ratio of 0.17) for achieving good G and H values.

d) The composition CM-2 has been found to have optimum values of H and G under the given condition.

CHAPTER 5 - DISPERSANT

The effect of amount and type of dispersants on the rheological behaviour of bauxite-based low-cement castables has been studied in details. The rheological properties: flow resistance and torque viscosity are indeed strongly influenced by the amount and type of dispersants. In the present investigation, a mix containing sodium hexametaphosphate, at an optimal level, is observed to be rheologically superior under the given experimental conditions.

5.1 Introduction

Dispersants (deflocculants), accelerators and retarders are frequently used as additives in refractory castables. Deflocculants are used for better dispersion of fine matrix in the castable whereas the accelerators are used to reduce the setting time and the retarders to increase it.

Normally, low-cement castables, as any other cement-containing castables, are composed of coarse and fine fractions of refractory materials (aggregates and fines), aluminous cement particles and water. Castables are lyophobic particle/ liquid (water) dispersion systems, which will agglomerate if left standing for a long time. The agglomerated state of the lyophobic particle/liquid dispersion systems is more stable than the dispersed state. The stability of dispersed state can only be retained using a dispersing agent and/or under the action of a mechanical force. The common dispersing agents used in castable technology are sodium hexametaphosphate (SHMP), sodium tripolyphosphate (STPP), sodium pyrophosphate and sodium tetra polyphosphate. Those are all inorganic in nature. Several organic dispersants are also available, namely sodium polyacrylate, sodium naphthalene sulfonate formaldehyde condensate, polymelamine sulfonic acid, sodium polymethacrylate etc [7, 77].

The agglomerated structure is changed to a dispersed structure when sheared at a given rate with some appropriate dispersing agents. The decrease or increase of apparent viscosity is connected to such a structural change [23].

The stability of suspension can be described by means of potential energy curves as a function of the separation between particles, which has been quantified for the electrostatic repulsion, as proposed by DLVO (Derjaguin-Landau-Verway-Overbeek) [10, 31, 32, 78, 79]. According to DLVO theory, the stability of dispersion of colloidal system is determined by the summation of two terms:

$$\mathbf{V_T = V_R + V_A} \qquad \textbf{(Equation 5.1)}$$

where, V_R = electrostatic repulsive force,

V_A = attractive force (London Van der Waals force),

V_T = total force [32].

The other mean for stabilizing a suspension is polymeric stabilization, which is related to the action of macro-molecules. Polymeric stabilization may be achieved by two different mechanisms: a) steric stabilization where the macro-molecules are attached to the particle surface and b) depletion stabilization in which the macromolecules are free in suspension. It has been generally accepted that all adsorbed polymers may provide steric stabilization, if two requirements are satisfied: (1) strong anchoring to the particle surface, and (2) sufficient extension of the adsorbed long-chain into solution to prevent the particles from approaching more than 10-20 nm to each other. The steric repulsion is due to a loss in configurational entropy that occurs when polymer chains of two particles interpenetrate. It is assumed that combination of both electrostatic and steric mechanism can result in better stabilization. This combination is referred to as electrosteric (stabilization of suspension due to the actions of both electrostatic and steric effect)

stabilization. The electrostatic component may originate from a net charge on the particles surface, and/or charges associated with the anchored polymer, that is polyelectrolyte. The double layer provides a high potential energy barrier at large distances, and at short range the steric stabilization prevents contact between particles.

The effect of accelerator and retarder in a castable is also to be considered. When calcium aluminate cement (CAC) is dissolved in the water the cement grains dissolve and release calcium ions Ca^{2+} and $Al(OH)_4^-$ into the solution. Retarder and accelerator primarily modify the Ca^{2+}/ Al $(OH)_4^-$ ratio of the system. The higher the Ca^{2+}/ Al $(OH)_4^-$ ratio, the faster the hydrate formation, and vice versa. Retarders influence the kinetics of hydration by modifying (usually slowing down) the dissolution of the anhydrous cement particles. The mechanism involves reduction of dissolution by absorption on the cement grain and/or combination with calcium ions. Retarder tends to decrease the Ca^{2+}/ Al $(OH)_4^-$ ratio by reacting with Ca^{2+} ions and thereby diminishing their activity. Accelerator influences the dormant period of hydration by promoting nucleation and thereby accelerating the hydration. The accelerator reacts with $Al(OH)_4^-$ thereby increasing the Ca^{2+}/ Al(OH)4– ratio in solution. This promotes rapid hydrate formation, which results in a decrease of setting time [80]. The commonly used retarders are citric acid, trisodium citrate, tartaric acid and sodium gluconate. Lithium salts are the common accelerators for CAC.

In summary, the workability of castables is governed by the flow properties of the fine powder components contained in them. It is important to know and understand the rheological behavior of the powder-liquid system. A success in controlling this will enable good workability and quality of installation. The rheological behavior of the powder-liquid system is dependent on the dispersion-flocculation state, viz. the stability of the system. According to DLVO theory by adjusting the attractive potential V_A and repulsive potential V_R, the dispersion-flocculation state can be changed [33], by using

specific flocculant and deflocculant. At the end, the placement of castable is influenced strongly by the rheological behavior of castable, which in turn is a function of type and amount of dispersants for a given mix. In this context, the present investigation attempts to study the role of different type and amount of dispersants on the rheological behavior of a bauxite-based low-cement castable.

5.2 Compositions

The details of raw materials have been described in Chapter 3.2. The q value is 0.26 and D_{max} is 5 mm for this part of the work. The cement and microsilica contents are fixed at 4 and 5 wt % respectively. The amount of water for rheometer measurements is fixed at 7 wt% for all compositions and the reason for this will be discussed in section 5.3. In this investigation, the composition is fixed and chosen as composition CM-2 (see Chapter 4), and only the dispersants are different. Three dispersants: FS-20 (polycarboxylate copolymer), SHMP (sodium hexametaphosphate) and Darvan 811D (sodium polyacrylate copolymer) are used. The details are given in Table 5.1.

Table 5.1 Details of castable mixes to study the effect of dispersants

Castable		**DS-1**	**DS - 2**	**DS-3**	**DS-4**	**DS-5**	**DS-6**	**DS-7**
Aggregate (wt%)		59	59	59	59	59	59	59
Fine matrix (wt%)	Bauxite-1	11	11	11	11	11	11	11
	Bauxite-2	12	12	12	12	12	12	12
	Bauxite-3	9	9	9	9	9	9	9
	Cement CA-14	4	4	4	4	4	4	4
	Microsilica (Elkem 971 U)	5	5	5	5	5	5	5
Dispersant (wt%)	**SHMP**	**0.08**	**0.12**	**0.16**	**0**	**0**	**0**	**0**
	Darvan 811D	**0**	**0**	**0**	**0.05**	**0.08**	**0.12**	**0.16**

5.3 Water Demand and Self-flowability

In the case of FS-20, when the amounts added correspond to 0.08, 0.12 and 0.16 wt% of dry mix and with 6.0 wt % water addition, the vibration flowability is 15, 100 and 110% respectively. After around 2 minutes, the mixes are setting very fast and cannot flow anymore, even with more dispersant or water addition. It has been concluded that this

dispersant does accelerate the setting for this kind of bauxite-based low-cement castle and it is not suitable for application even with high dosage. No further discussion on FS-20 is undertaken in the present work.

At 0.04 wt% level of SHMP or Darvan 811D, with 6.0 wt % water, the vibration flowability is 85 and 90% respectively. After around 2 minutes, the mixes stop flowing. When more SHMP or Darvan 811D is added, the mixes flow well for long periods of time. This indicates that the addition of 0.04 wt % is not enough to deflocccculate the wet mix. At 0.05 wt% of SHMP, the mix behaves in the same way as with 0.04 wt%, but in the case of Darvan 811D at 0.05 wt%, the flowability is much higher than with 0.04 wt%. It is found that Darvan 811D performs better than SHMP at low addition levels in the selected castable system.

The self-flowability of selected composition containing SHMP and Darvan 811D, as a function of water content is shown in the Figure 5.1. In the case of mixes DS-1, 2 and 3, with 0.08, 0.12 and 0.16 wt % SHMP, the self-flowability attains similar values at 6 wt% water addition level. If water addition is increased to 6.5 wt%, the self-flowability of DS-1 and DS-2 surpasses that of DS-3. Similar trend is observed at 7.0 wt% water addition. Each 0.5 wt % of water addition could increase by about 40 % the self-flowability. On the other hand, increasing SHMP addition does not change the self-flowability.

Among the mixes DS-4, 5, 6 and 7, DS-4 has shown the highest self-flowability with 6.0 wt% water addition and DS-7 has shown the lowest flow value. The same trend is observed at 6.5 wt% water addition. At 7.0 wt% water addition, the self-flowability of DS-4, 5 and 6 are similar, while DS-7 still exhibits the lowest value. It is concluded that increasing dispersant addition does not bring any increase in self-flowability, and in the considered castable systems, the amount of Darvan 811D should not exceed 0.12 wt%.

With 7.0 wt% water, the flow values measured in the beginning of the test (0 min) and 30 min of rheological testing, are almost similar for all mixes containing SHMP. In the case of mixes with Darvan 811D, the flow drops to zero in 30 min. (Figure 5.2). This is reflected in rheological measurements, which will be discussed later. The water addition is fixed at 7% in all rheological tests in order to reach optimal self-flowability of 110-120% and to avoid possible segregation in the mix.

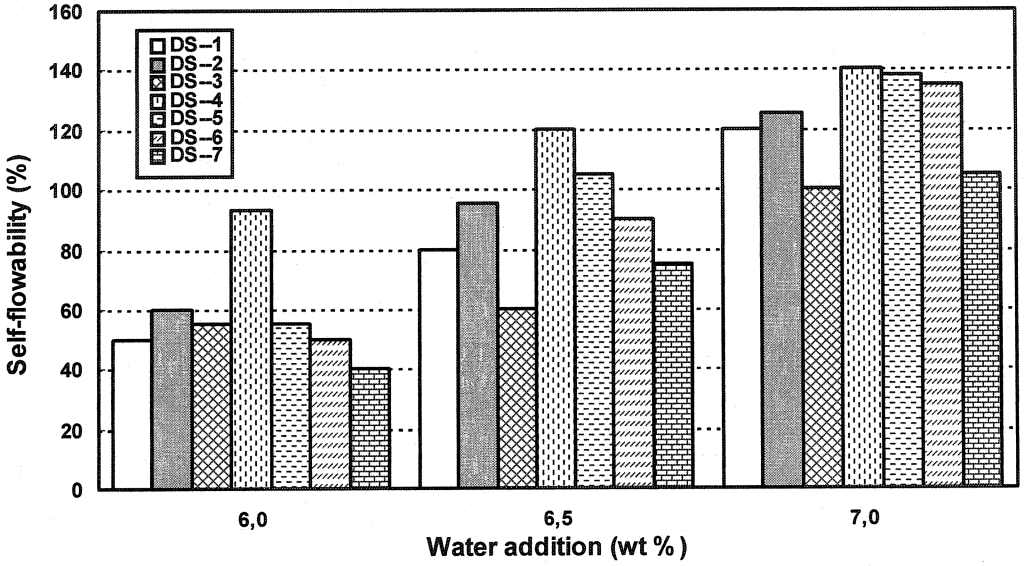


Figure 5.1 Self-flowability vs. water addition.

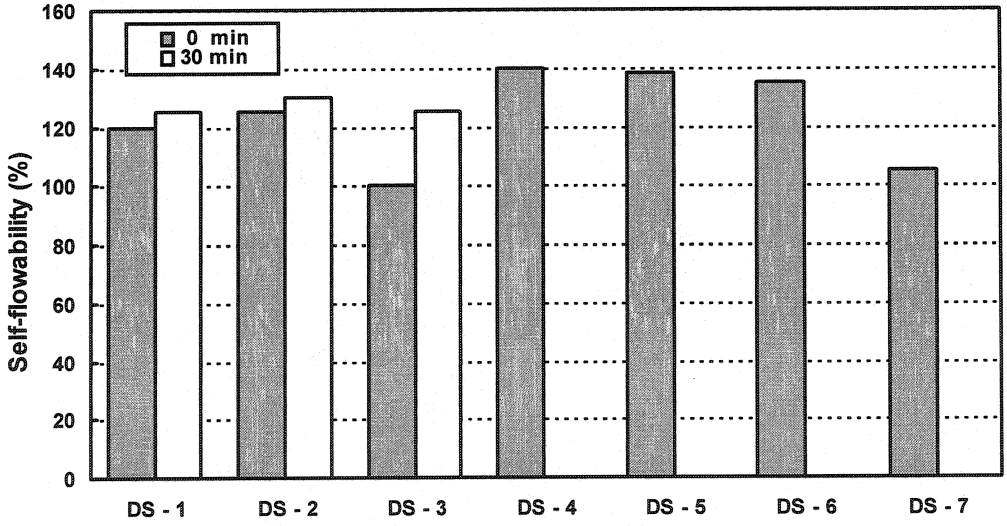


Figure 5.2 Comparison of self-flowability of the castables at different time.

5.4 Castable Rheology

5.4.1 Torque vs. Speed

The rheological measurements of three castables DS-1, 2 and 3 with different torque and speed are shown in Figure 5.3, 4 and 5, respectively.

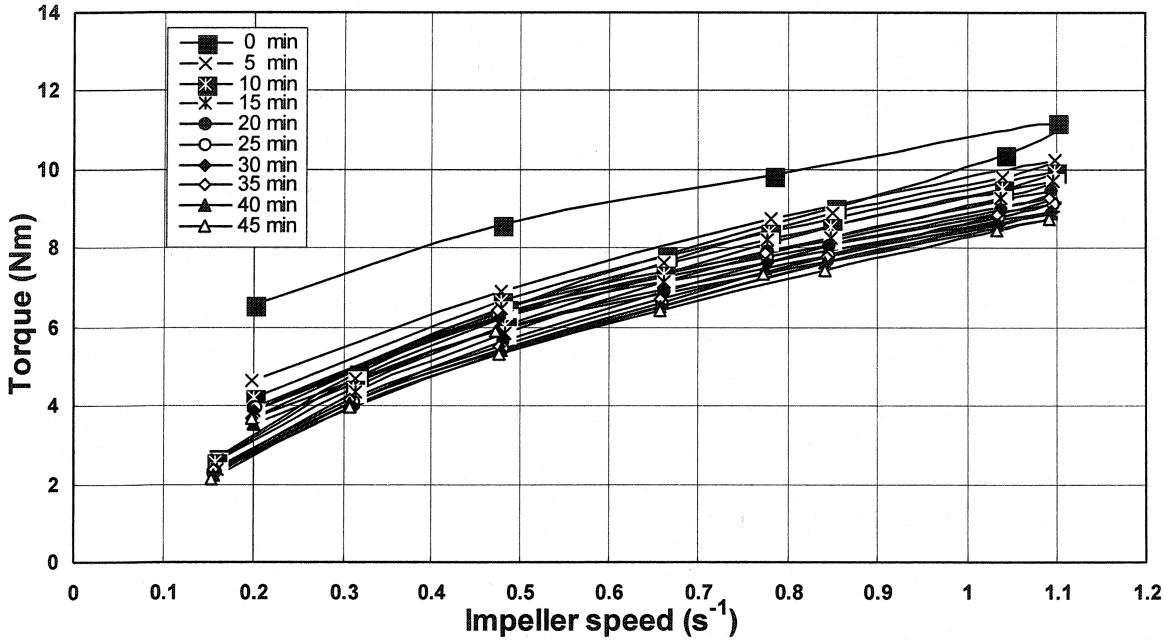


Figure 5.3 Torque vs. impeller speed for DS-1.

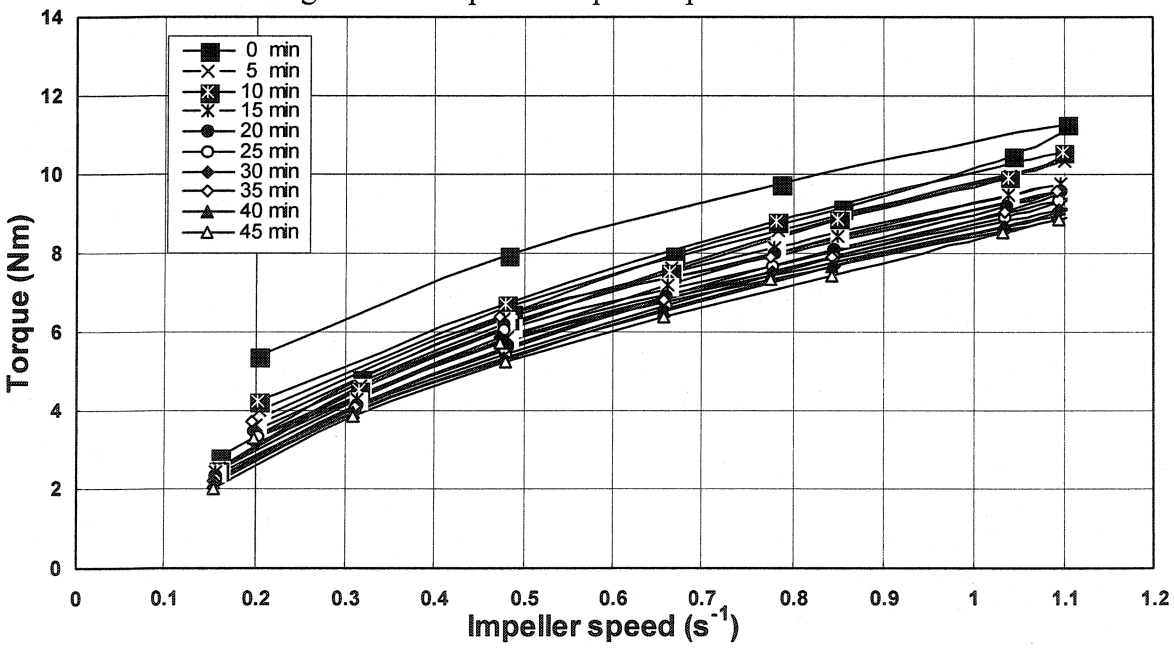


Figure 5.4 Torque vs. impeller speed for DS-2.

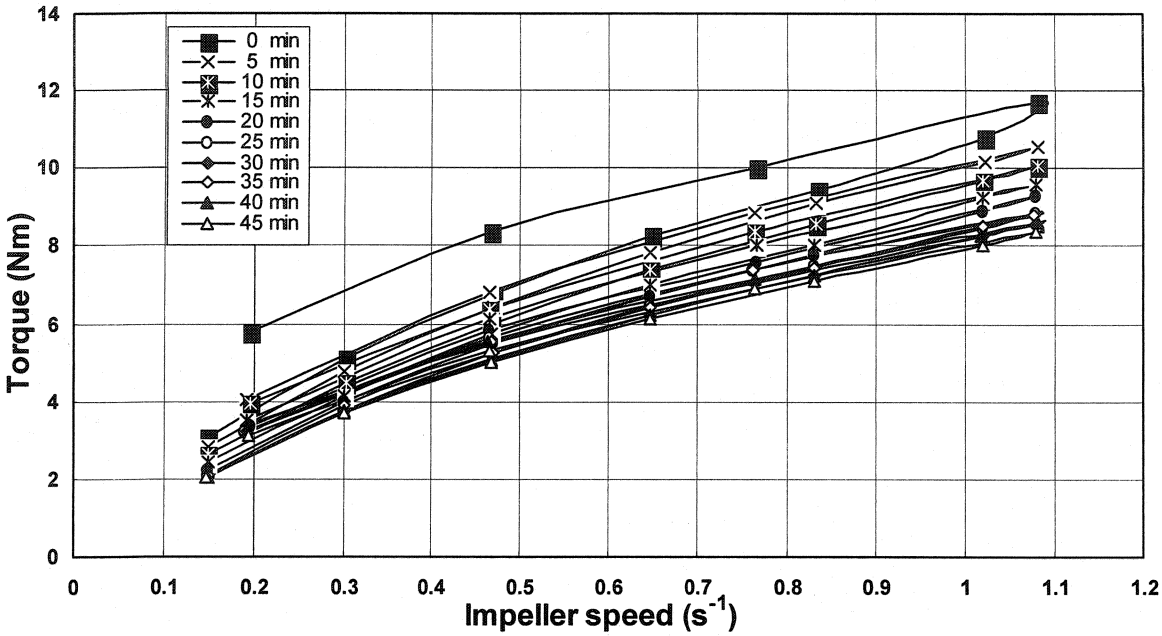


Figure 5.5 Torque vs. impeller speed for DS-3.

The nature of curves deserves similar explanation as in Chapter 4.5.1. For mixes DS-1, 2 and 3 with SHMP, the mix cannot be considered as completely mixed in the beginning of the test, and it gains in homogeneity with increasing mixing speed. The shearing stress helps to break the agglomerates, to fill the voids and to improve dispersibility, due to the post mixing action of the impeller. Once the mix reaches the maximum speed, the mix is in a homogeneous state and it shows Bingham behavior in the reverse cycle. Further on, in the testing cycle, the mix is more and more homogeneous so that after 20 minutes it reaches a state where further homogenization through mixing is not possible, and follows almost similar path during testing. The same kind of behaviour has been observed for the compositions DS-2 and DS-3.

The test results for the four compositions DS-4, 5, 6 and 7 with Darvan 811D are shown in Figure 6, 7, 8 and 9, respectively. Rheological behaviour follows similar trends as in the case of SHMP containing mixes (Bingham fluid), however, the test could not be continued after 35 min of testing (Figure 5.6). Moreover, the testing time of DS-5, DS-6 and DS-7 reduced to 25, 15, and 5 min respectively. Those mixes have been kept for

rheological study but are not fully characterized later due to their poor castability. In the case of DS-4, 5, 6 and 7 with Darvan 811D, the castables are setting very fast before homogenization.

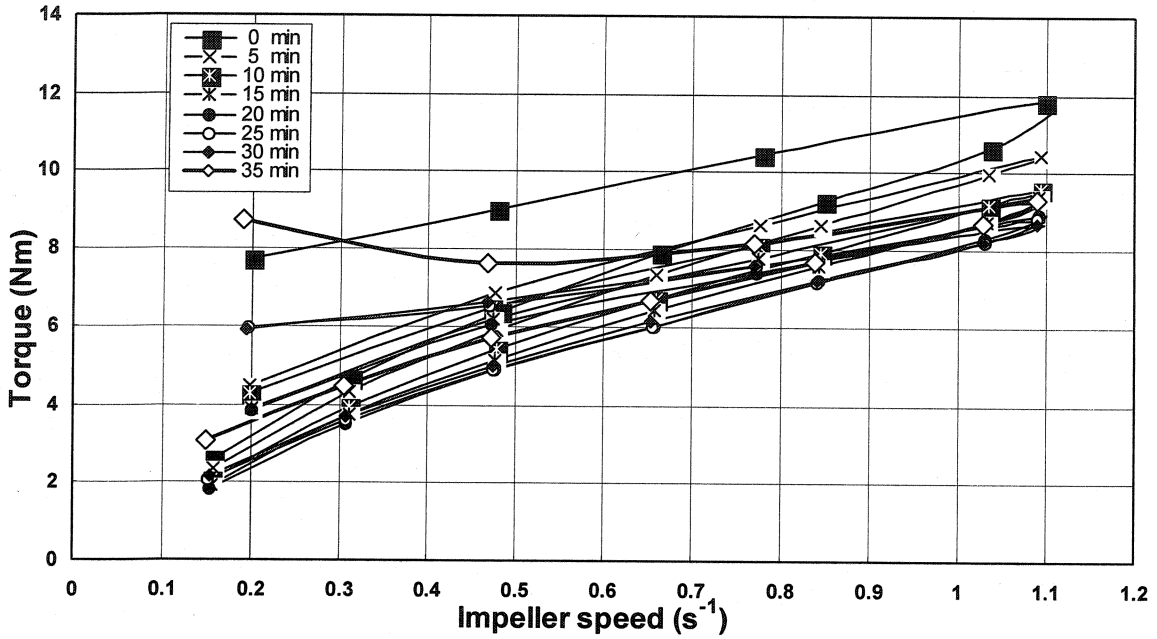


Figure 5.6 Torque vs. impeller speed for DS-4.

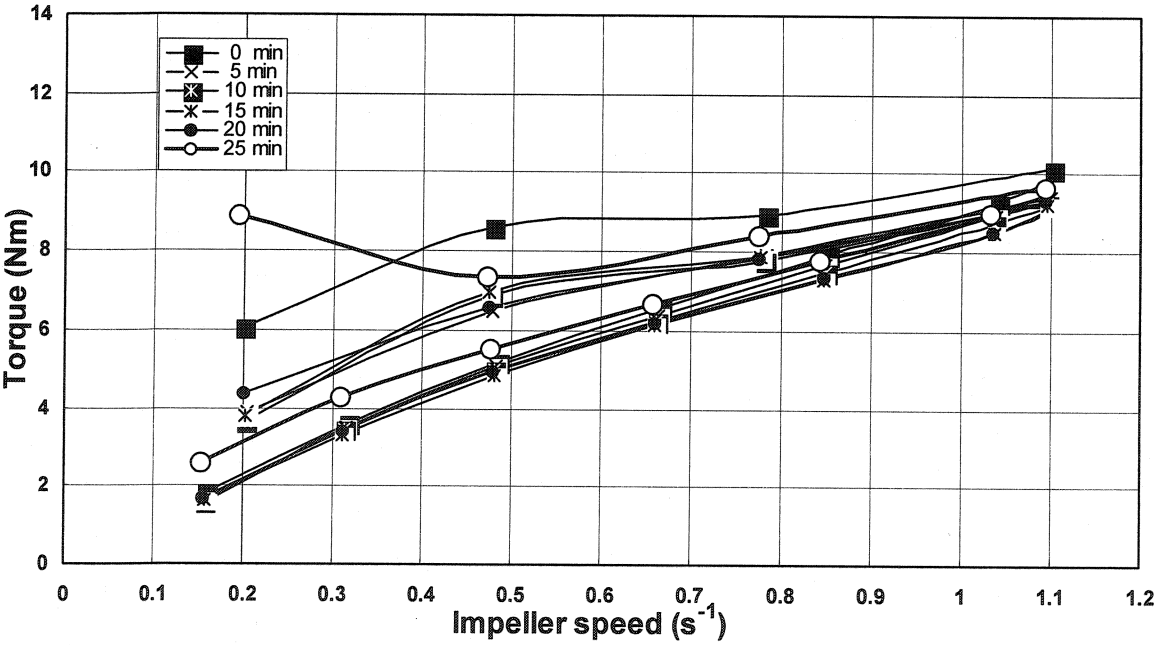


Figure 5.7 Torque vs. impeller speed for DS-5.

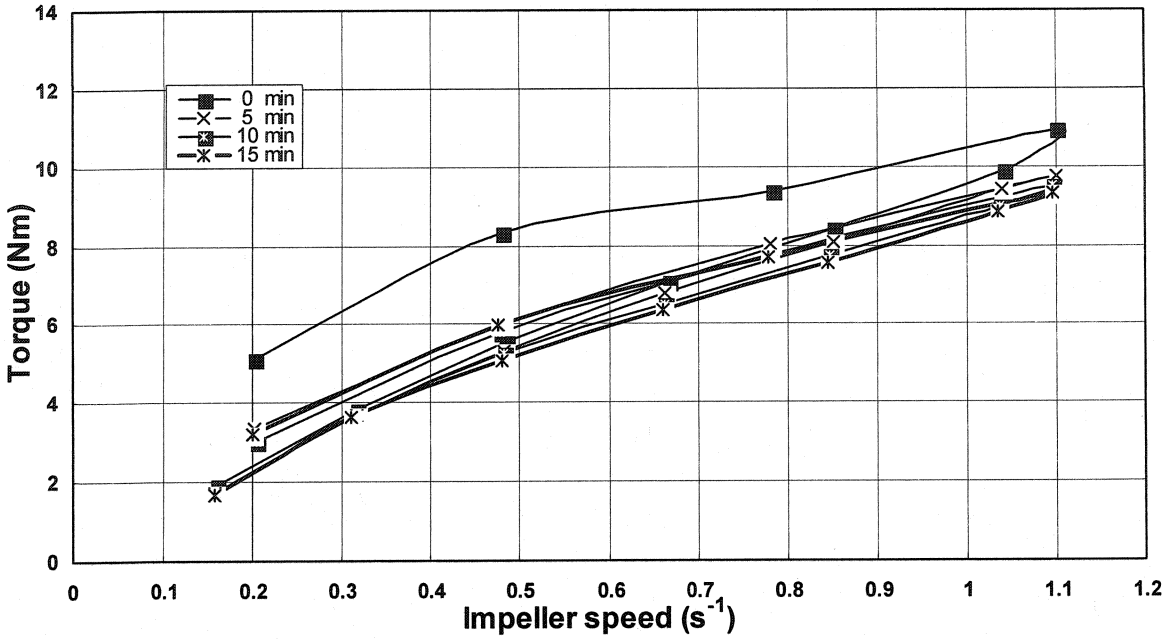


Figure 5.8 Torque vs. impeller speed for DS-6.

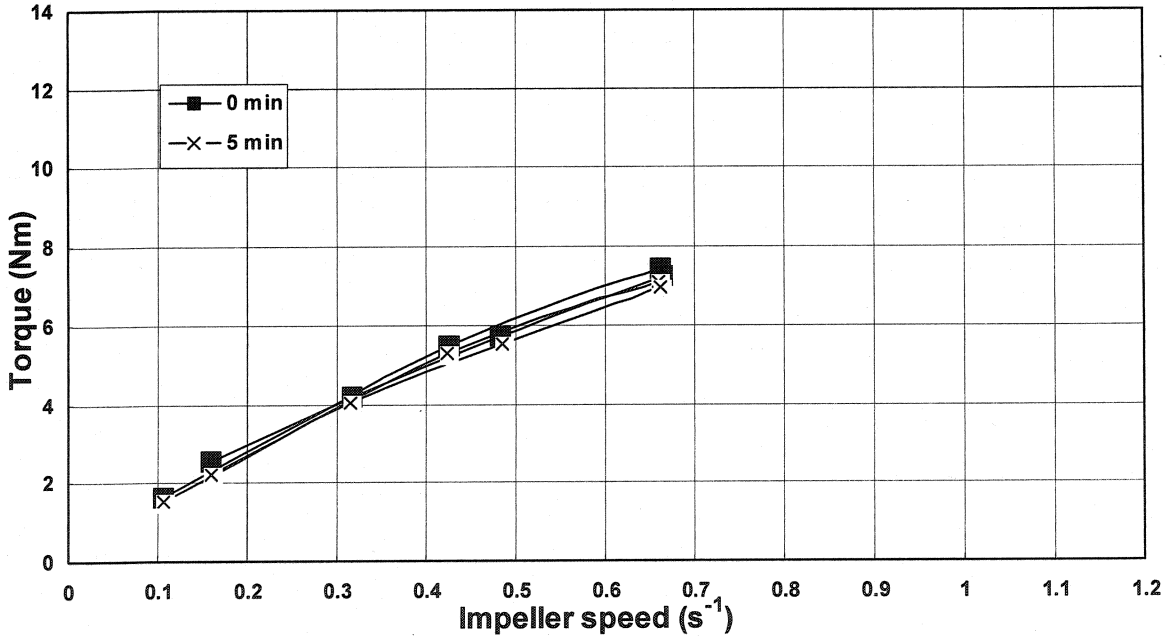


Figure 5.9 Torque vs. impeller speed for DS-7.

The torque (T_{max}) of the first 6 compositions, at the highest impeller speed of 1.10 s^{-1} at 0 min, is given in Table 5.2. The T_{max} remains similar with DS-1 and DS-2. The T_{max} of DS-3 is slightly higher than those two compositions with SHMP as dispersant. In the

case of compositions with Darvan 811D, the T_{max} is the highest for DS-4 and the DS-5 is the lowest. DS-6 is in the middle among those three compositions. DS-7 can not be tested at the highest impeller speed of 1.10 s^{-1} because the castable mix becomes too stiff, too soon after mixing.

Table 5.2 T_{max} of the 6 compositions at the impeller speed of 1.10 s^{-1} at 0 min

Composition	DS--1	DS--2	DS--3	DS--4	DS--5	DS--6	DS--7
T_{max} (Nm)	11.19	11.29	11.73	11.84	10.10	10.95	--

5. 4.2 Equivalent Apparent Viscosity

The relationship between equivalent apparent viscosity and impeller speed is shown in Figure 5.10 for DS-1, which follows closely a Bingham fluid behaivor. The shear-thinning trends are the same for the other compositions and hence not shown.

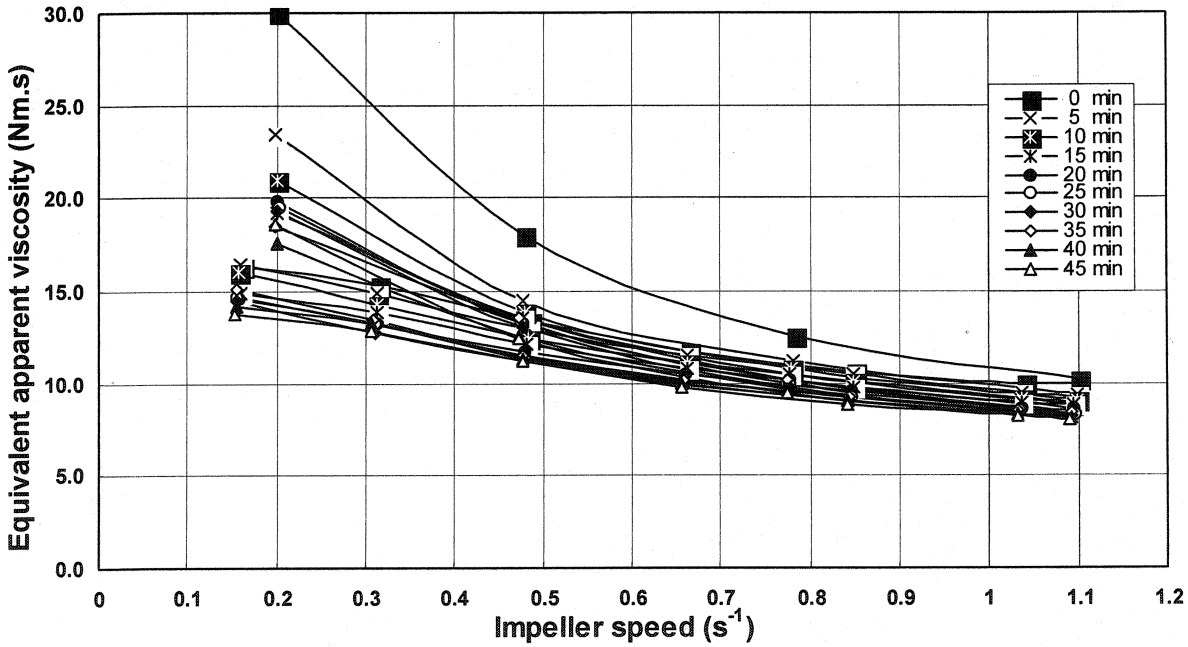


Figure 5.10 Equivalent apparent viscosity vs. impeller speed for DS-1.

5.4.3 Thixotropy

In Figure 5.11, DS-1(a) and DS-1(b) represents the equivalent apparent viscosity calculated for the higher (1.10 s^{-1}) and lower speed (0.48 s^{-1}) respectively (in the reverse

cycle) in each five minute cycle for the mix DS-1. Similar nomenclature is valid for other mixes. The values of equivalent apparent viscosity for the constant speed 0.48 s^{-1} are higher than those of 1.10 s^{-1}.

The equivalent apparent viscosity values of DS-1 at both high and low speeds are lower than for DS-2 and DS-3. As the testing time increases, the values converge to same level after around 20 min of testing time. After 20 min, the values diverge again, and the equivalent viscosity of DS-1 becomes higher. It follows that mix with more dispersant additions needs more mixing time to dissolve and enhance the dispersion. The enhanced dispersion reduces the equivalent apparent viscosity of DS-2 and DS-3 and it falls below that of DS-1. In case of DS-4, 5 and 6, the equivalent apparent viscosity of DS-4 is the highest, followed by DS-6 and then by DS-5. The higher value for equivalent apparent viscosity of DS-4 may be due to stronger and faster flocculation of ultra-fine particles due to insufficient additive content. The sudden increase in the equivalent apparent viscosity values of DS-4 and DS-5 is due to only setting or coagulation.

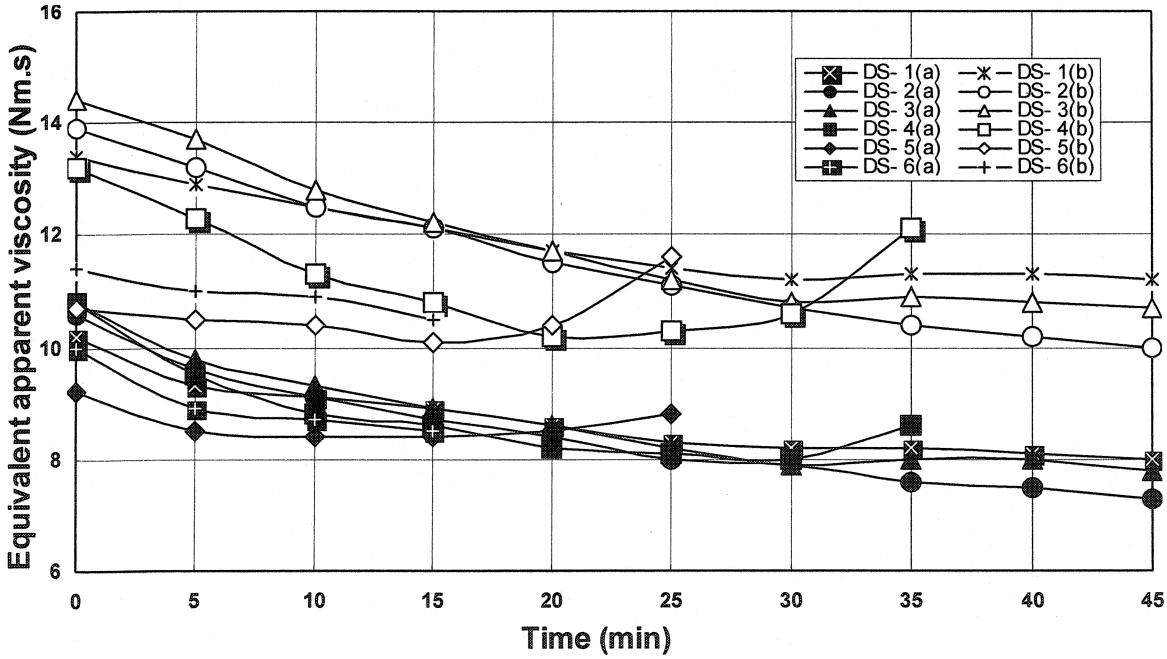


Figure 5.11 Equivalent apparent viscosity vs. time at high and low impeller speed.

5.4.4 Flow Resistance and Torque Viscosity

The method of evaluation of G and H values using the rheometer test results has been described in Chapter 4.5.4. The G and H values are given in Table 5.3.

Table 5.3 G and H values for all the compositions

Time (min)	Flow resistance G (Nm)							Torque viscosity H (Nm.s)						
	DS-1	DS-2	DS-3	DS-4	DS-5	DS-6	DS-7	DS-1	DS-2	DS-3	DS-4	DS-5	DS-6	DS-7
0	1.82	1.86	2.34	1.62	0.85	0.86	1.11	8.66	8.65	8.75	9.07	8.34	8.96	9.36
5	1.78	1.73	2.02	1.42	0.69	0.74	0.82	8.28	8.47	8.47	8.6	8.26	8.7	9.51
10	1.74	1.62	1.85	1.24	0.73	0.85		7.97	8.27	8.07	7.97	8.02	8.2	
15	1.6	1.56	1.68	1.11	0.76	1.25		7.87	8.02	7.76	7.72	7.76	7.99	
20	1.54	1.52	1.5	1.06	0.86			7.66	7.78	7.62	7.31	7.71		
25	1.57	1.46	1.39	1.32	1.86			7.37	7.58	7.36	6.93	7.09		
30	1.52	1.42	1.37	1.45				7.24	7.43	7.12	6.85			
35	1.53	1.41	1.38	2.41				7.26	7.41	7.15	6.33			
40	1.55	1.4	1.37					7.24	7.4	7.13				
45	1.5	1.33	1.39					7.12	7.34	6.86				

The flow resistance G is an indication of self-flowability of a particular mix, the correlation between the two terms is shown in Figure 5.12. G has shown linear relationship with self-flowability. The mixes with high self-flowability (Darvan 811D containing) have given low G values.

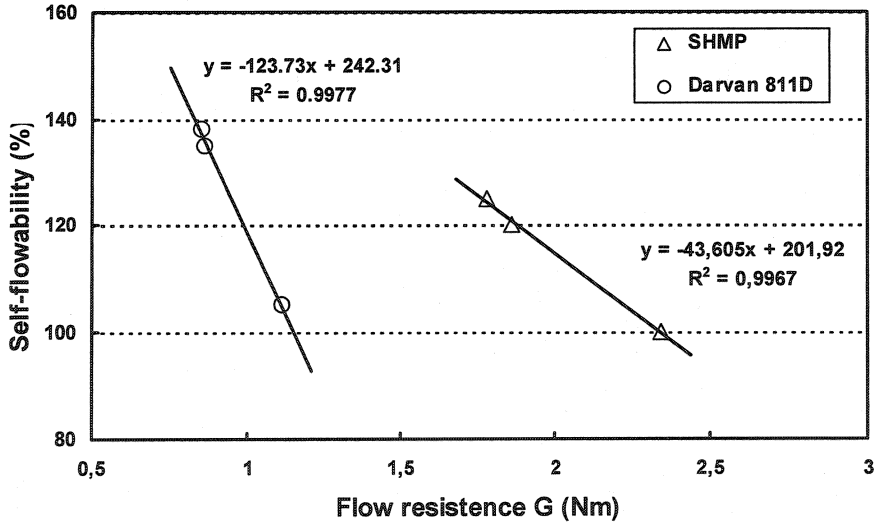


Figure 5.12 Relationship between self-flowability and flow resistance of castables.

The relationships between dispersant amount and G can be further understood in Figure 5.13. At 0 min, the value of G increases with an increase of SHMP (DS-1, 2 and 3). This trend is observed till 20 min of testing, after that G reaches almost similar value. This is due to additional mixing and homogenizing effect during rheological testing. With different amount of Darvan 811D, G values go through a minimum value at 0.08%. The higher G values at 0.05 wt % is due to an insufficient amount of additive; the proper dispersion takes place at 0.08 and is still valid at 0.12 wt% levels. The increase G with 0.16 wt% is due to excessive deflocculant content and accelerated setting.

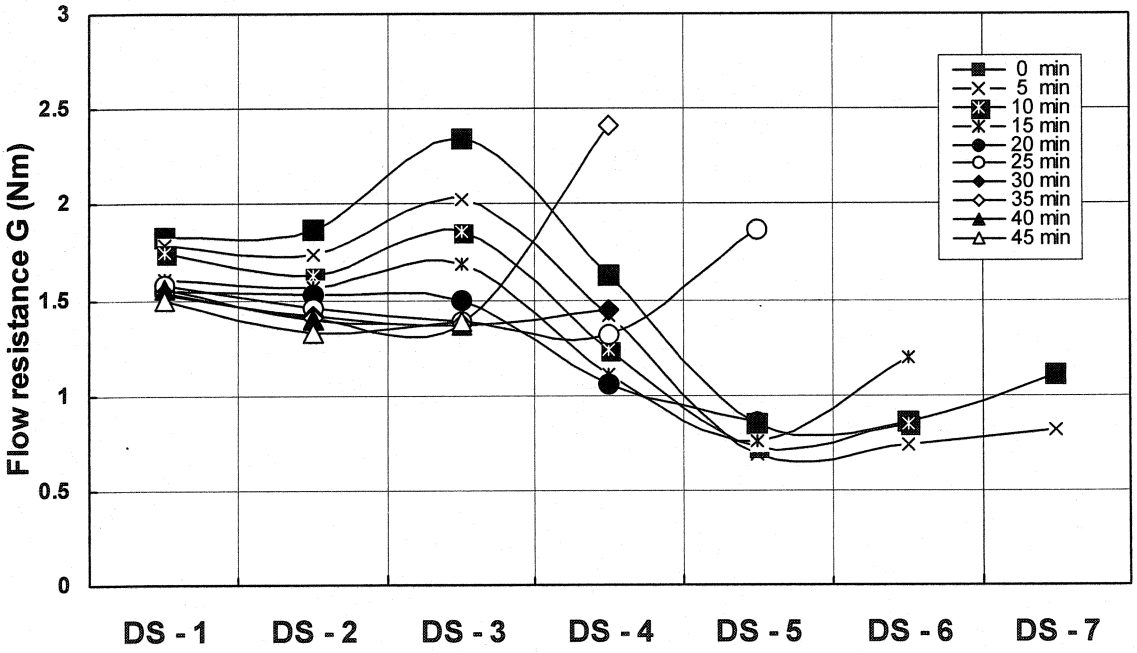


Figure 5.13 Flow resistance vs. dispersant.

The relationships between dispersant and H are illustrated in Figure 5.14. The H values of all compositions are similar and decrease slowly during the testing period. This clearly indicates that G is more dependent on dispersant than H. The decrease in H with testing time is attributed to the homogenizing effect due to additional mixing during testing. The observed increase in H with 0.16 wt% Darvan 811D is due to setting or coagulation.

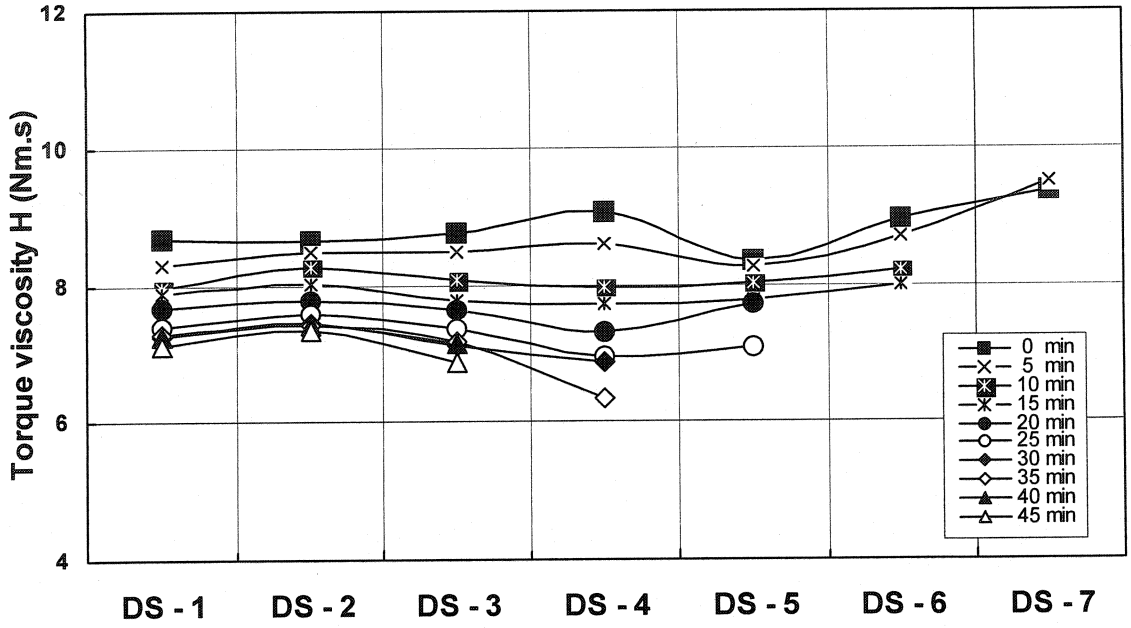


Figure 5.14 Torque viscosity vs. Dispersant.

5. 5 Matrix Rheology

5.5.1 Shear Stress vs. Shear Rate

The shear stress as a function of shear rate for the matrix slurry part of the 7 castables (DS-1 to DS-7) is shown in Figure 5.15. The similar explanation can be given to the trend of curves, as in Chapter 4.6.1. The shape of loops is the same but the loop slightly shifts up or down for each matrix slurry.

The shear stress (τ_{max}) at the highest shear rate of 400 s^{-1}, for all the compositions is given in Table 5.4. In the case of DS-1, 2 and 3, the τ_{max} of DS-2 is the highest. DS-1 and DS-3 are similar. In the case of castables with Darvan 811D, the τ_{max} decreases with Darvan 811D content.

Table 5.4 τ_{max} of the 7 compositions at the highest shear rate of 400 s^{-1}

Composition	DS--1	DS--2	DS--3	DS--4	DS--5	DS--6	DS--7
τ_{max} (Pa)	266	290	258	291	283	273	263

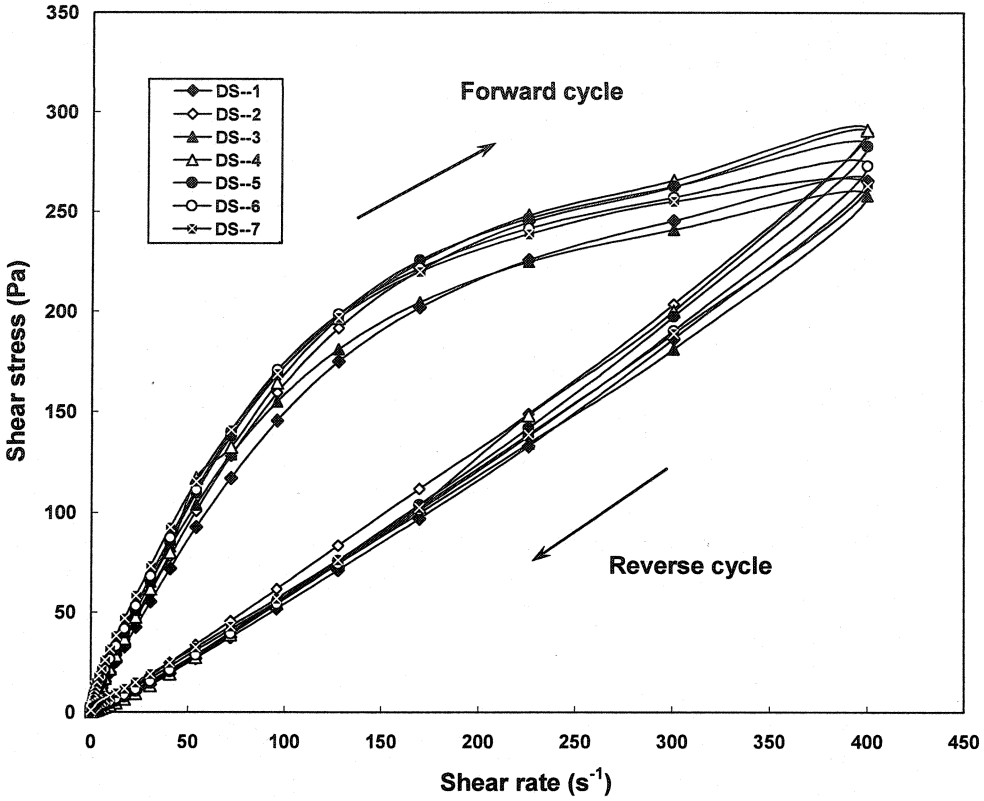


Figure 5.15 Shear stress vs. shear rate for all matrix slurries.

5.5.2 Apparent Viscosity vs. Shear Rate

The apparent viscosity as a function of shear rate of the matrix slurry part is shown in Figure 5.16. The apparent viscosity in the forward cycle (shear rate increasing) is higher than rate in the reverse cycle (shear rate decreasing). The apparent viscosity increases with the dispersant amount used. The apparent viscosity of the castables with Darvan 811D is higher than those with SHMP, at the same addition level. In the forward cycle, the apparent viscosity of the matrix slurries containing Darvan 811D decrease sharply up to a shear rate of 5.0 s^{-1}, then stabilizes up to 100 s^{-1} and finally decreases slightly after. In the reverse cycle, the apparent viscosity remains similar between shear rate of 400 s^{-1} and 10 s^{-1}. At low values, under 10 s^{-1}, the viscosities slowly increase again. It has been found that the apparent viscosity of DS-7 is significantly higher than the others in both forward and reverse cycles. The apparent viscosity of DS-4 fluctuates at low shear rate, because of the added amount, 0.05 % is insufficient.

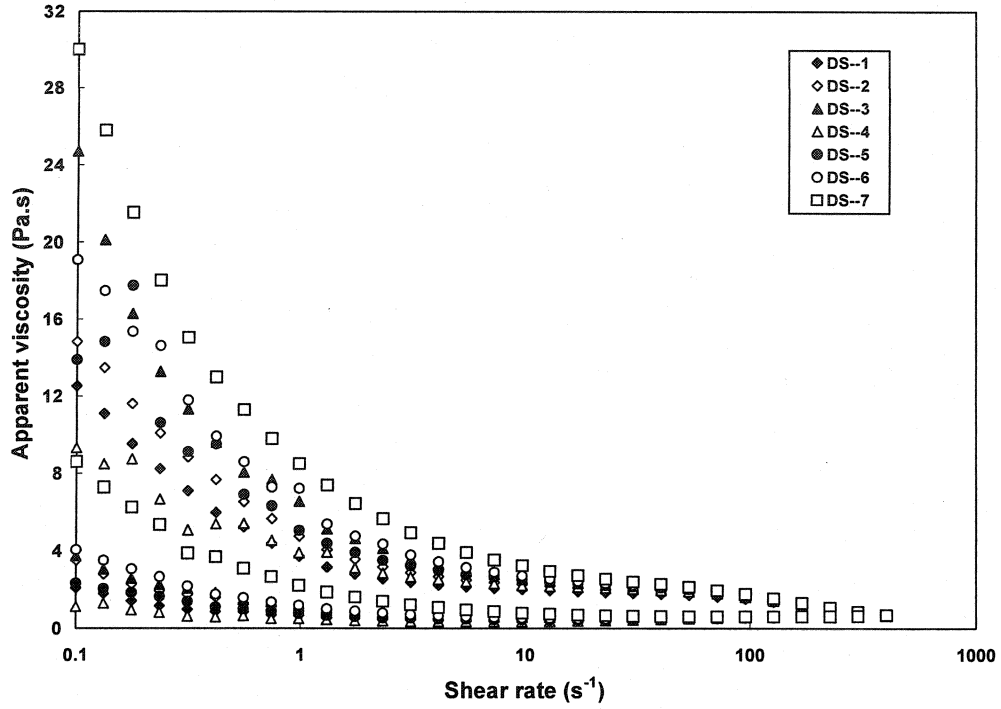


Figure 5.16 Apparent viscosity vs. shear rate for all the matrix slurries.

5.5.3 Thixotropy

The degree of thixotropy, defined in Chapter 4.6.3, for the mixes with SHMP or Darvan 811D, does increases in proportion to the amount of dispersant used. The evolution is shown in Figure 5.17. The loops' area calculated values also follow the same trend.

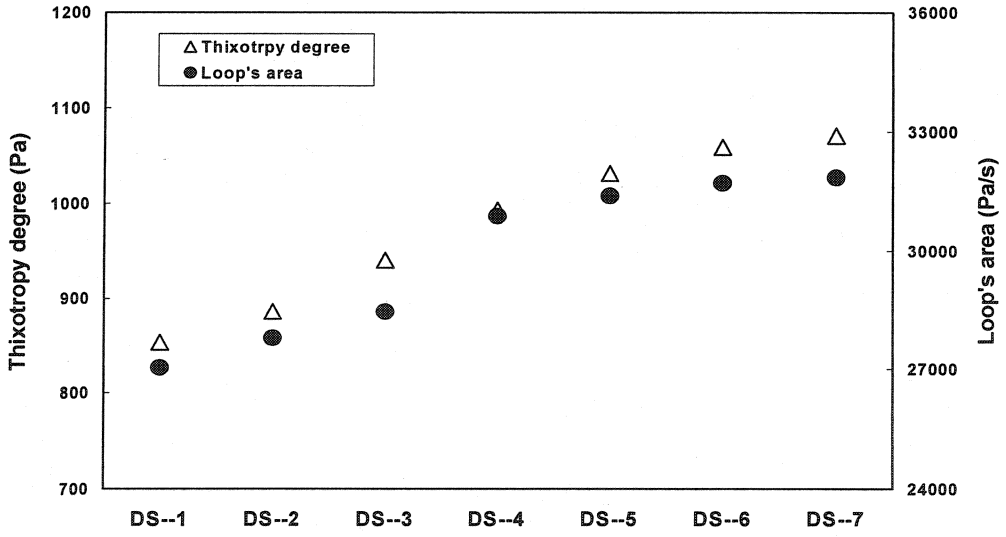


Figure 5.17 Thixotropy degrees and loop's area for all the matrix slurries.

5.5.4 Plastic Yield Stress and Plastic Viscosity

The calculated values of plastic yield stress and viscosity of the 7 matrix slurries are given in Table 5.5. The calculation method has been described in Chapter 4.6.4. The plastic viscosity remains similar with all slurries. The plastic yield stress significantly increases as dispersant amounts increase. The plastic yield stress of the castables with SHMP is slightly higher than the castable with Darvan 811D at the same addition level.

Table 5.5 Plastic viscosity and yield stress of the 7 matrix slurries

Composition	DS--1	DS--2	DS--3	DS--4	DS--5	DS--6	DS--7
Plastic viscosity (Pa.s)	1.702	1.829	1.885	2.046	1.992	2.005	2.054
Plastic yield stress (Pa)	2.415	3.512	5.615	1.531	3.983	5.599	8.774

5.6 Mechanical and Physical Properties

The CMOR and AP of the compositions with dispersant SHMP DS-1, DS-2 and DS-3 are given in Table 5.6. With the same amount of water addition, the CMOR and AP values are similar (8-9 MPa and 17-18 % respectively). The AP of DS-3 is slightly higher than the others because of better degassability. The physical and mechanical properties of DS-4, 5, 6, and 7 with Darvan 811D have not been tested due to their poor castability.

Table 5.6 CMOR and AP of the compositions DS-1, 2 and 3

Composition	CMOR (MPa)		AP (%)	
	0 min	45 min	0 min	45 min
DS - 1	8.3	8.0	18.2	17.7
DS - 2	9.3	8.7	18.2	17.8
DS - 3	8.8	8.0	18.6	18.6

5.7 Appearance of Samples

The appearance of the castables with SHMP cast after initial mixing shows some degas bubbles on the surface, except for DS-3, as shown in Figure 5.18. Mixes with SHMP, has shown good self-flow and the appearance of the samples is good although some degassed bubbles appear on the surface cast after 45 minutes. This is a normal phenomenon for castables hence it is not shown here. The glassy surface has been found

with the castable DS-7 at 0 min. The castable with Darvan 811D shows the similar surface at 0 min, hence not shown. The castables samples with Darvan 811D can not be made after 45 min since the mixes set very quickly.

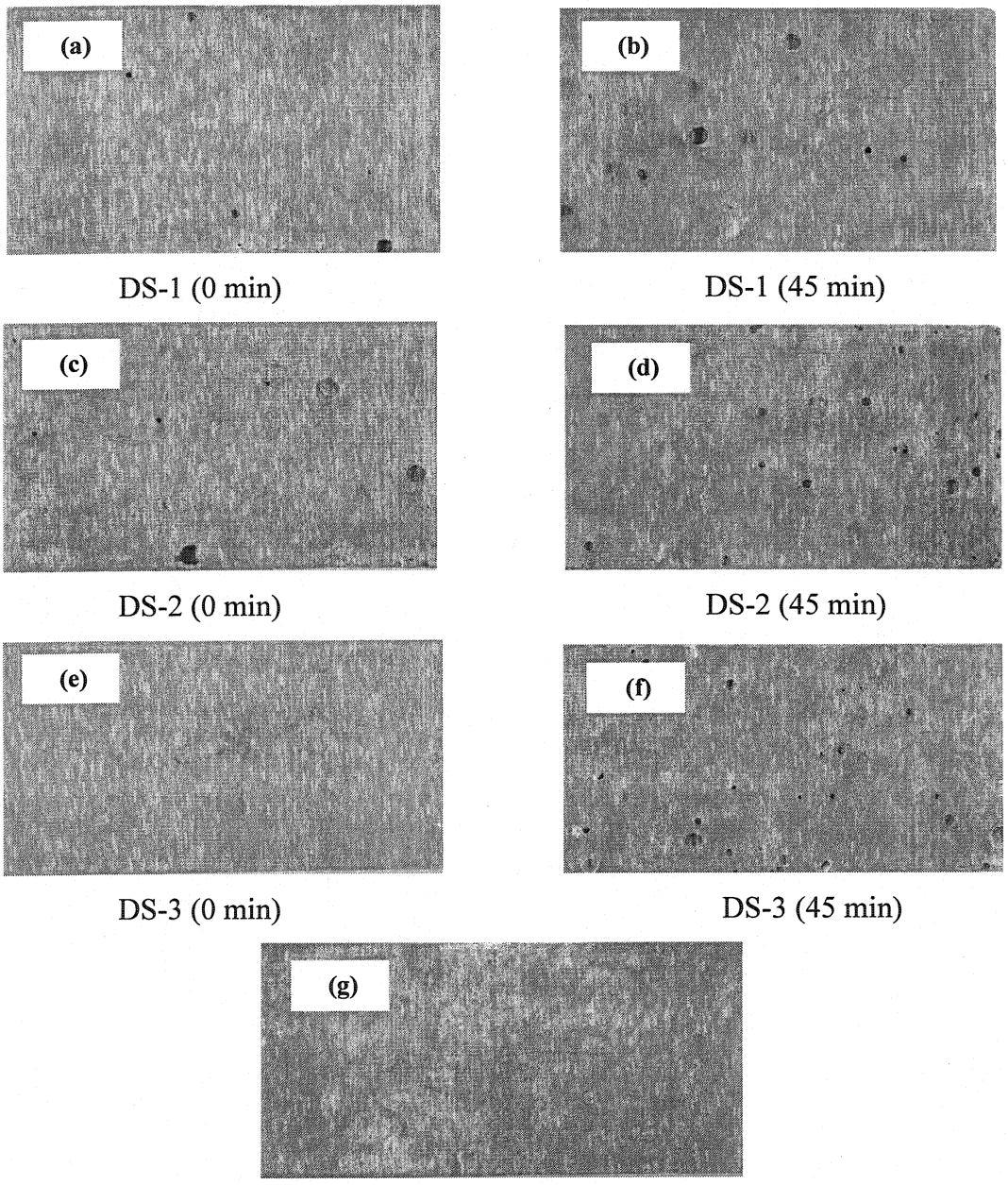


Figure 5.18 (a)-(g) Appearance of samples DS-1, 2, 3 and 7 at different time.

5.8 Dispersants and Rheology

LCC consists of aggregate, fine fillers, alumina cement and deflocculant. The reduction of water content through the action of specific additives during mixing results from the repulsion between the particles due to the increase of zeta potential, and it is referred to as deflocculation [40]. Accordingly, for a constant apparent viscosity of the suspension, the required amount of water can be reduced by the deflocculant, or for a constant solid concentration, the apparent viscosity can be reduced by the deflocculant. The material, reducing apparent viscosity or water requirement of the slurry is referred to as a deflocculant. Coagulation is the reverse of deflocculation. If material contains both electrolytes for deflocculation and coagulation and it is mixed with water, then the two electrolytes may start acting at the same time and increase the viscosity without deflocculation resulting in poor fluidity. The two electrolytes, therefore, must differ in the rate of dissociation or dissolution. The deflocculant must dissolve first and the coagulant must provide the necessary time lag for successful mixing. Deflocculation occurs when the state of the charged ions on the surface of particles change with the addition of an electrolyte. Therefore the pH of the aqueous solution of sodium phosphate acting as an electrolyte has an important effect on deflocculation.

There are three kinds of deflocculants used in castables: anion-, cation- and non-ion types. SHMP is an anion-type dispersant, which ionizes the anion-group when dissolved in water. In low-cement castable, cement and alumina particles hydrate during mixing with water and release Ca^{2+} and Al^{3+} ions, as follows [76]:

$$CaO{\cdot}Al_2O_3 + 4H_2O \rightarrow Ca^{2+} + 2Al^{3+} + 8OH^- \quad \textbf{(Equation 5.2)}$$

$$CaO{\cdot}2Al_2O_3 + 7H_2O \rightarrow Ca^{2+} + 4Al^{3+} + 14OH^- \quad \textbf{(Equation 5.3)}$$

$$Al_2O_3 + 3H_2O \rightarrow 2Al(OH)_2^+ + 2OH^- \quad \textbf{(Equation 5.4)}$$

The anionic groups dissolving from dispersant have a very strong affinity (attractive) force with the two cations Ca^{2+} and Al^{3+}, and they form a monomolecular film

surrounding the cement and bauxite particles, which lessens agglomeration, connection, collision and friction of fine particles, to obtain a well dispersed system.

The dispersant amount in a castable maybe deficient, sufficient or excessive. If the amount of dispersant is not sufficient, the cement and other fine particles agglomerate quickly and the mix sets very fast. Less than 0.05wt% is insufficient for SHMP, and it is 0.04 wt % in the case of Darvan 811D. On the contrary, if the amount of dispersant is excessive, the dispersant dissolves and releases excessive ions in a short time to accelerate the cement hydration and setting reaction. This also leads to the flash setting of the castable mix. More than 0.16wt% is excessive for both SHMP and Darvan 811D in this work. With sufficient amount of dispersants, appropriate dissolution and ionization rate leads to satisfactory dispersability and rheology of the castable. During mixing and testing, the dispersant dissolving and ionizing may change from unsaturated to saturated and then to over-saturated conditions. With time, the castable with the sufficient addition of appropriately selected dispersant reaches saturation state where the viscosity is at the lowest level and it remains stable.

5.9 Optimization of Castables

In this work, all castables show a satisfactory self-flowability with 7.0 wt % water addition (Figure 5.1), but not all of them are pumpable castables. For good pumpability, a castable must possess an optimum combination of torque viscosity and flow resistance in order to flow well and to avoid blockage, segregation and setting. The relationship between G and H is shown in Figure 5.19. The compositions DS-4, 5, 6 and 7 exhibit low G values initially, but the G values rise sharply when the flash setting is observed. For DS-1, DS-2 and DS-3, both G and H values are high. The values of G and H should be above a critical value to avoid segregation, but below a key value to avoid blockage, hence compositions DS-1, DS-2 and DS-3 appear to be the optimum combination. This means that an optimum amount and type of dispersant are required to avoid blockage

inside pipes and sufficient viscosity is required to avoid segregation by maintaining flowability, coherence, integrity and stability of the castable mix. Darvan 811D may be applicable for this bauxite-based low-cement castables with a retarder and it requires further research. SHMP should not be used at more than 0.16 wt%. The excessive additive in the mix is associated with negative effects.

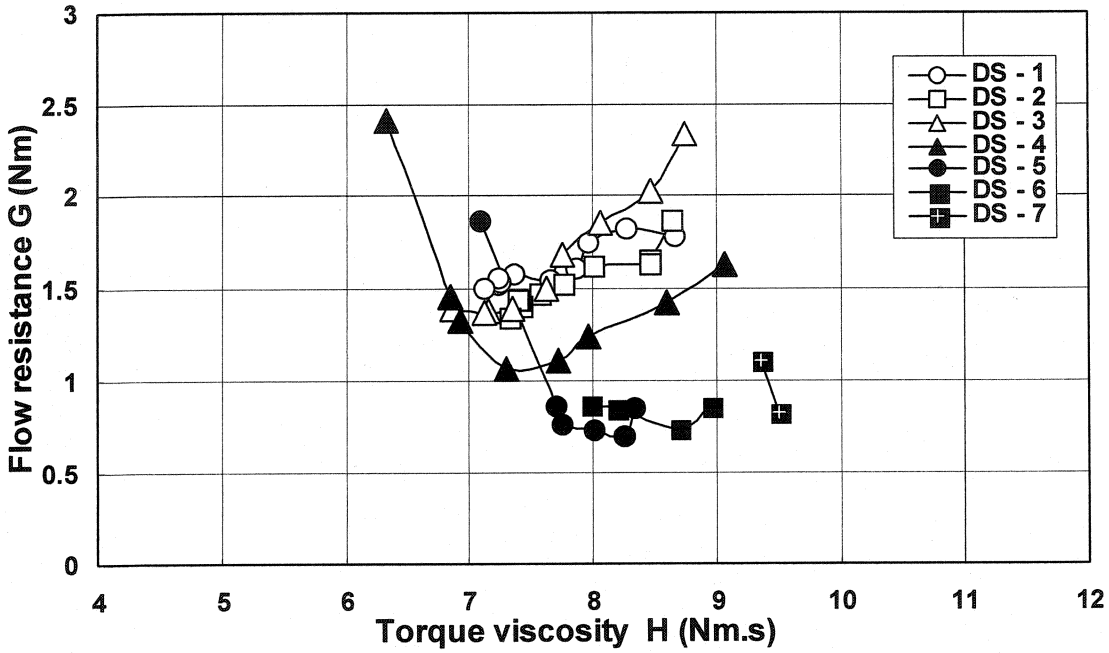


Figure 5.19 Flow resistance vs. torque viscosity.

5. 10 Conclusions

The rheological behavior of bauxite based low-cement castable has been studied using a rheometer. The conclusions based on this investigation are as follows:

a) The type and amount of dispersant affect considerably the flowability of mixes. In particular, when SHMP (sodium hexametaphosphate) is used, the self-flowability remains the same at all addition levels. With the dispersant Darvan 811D, the mixes exhibit flash setting. As the amount of Darvan 811D is increased, the setting time becomes shorter.

b) Mixes with both SHMP and Darvan 811D exhibit Bingham behavior.

c) G is influenced by the type and amount of dispersant under the present set of conditions. The optimum amount of 0.08-0.16 wt% SHMP (sodium hexametaphosphate) has been found for achieving good G and H values.

d) The compositions DS-1, DS-2 and DS-3 have been found to possess optimum values of H and G under the given conditions. For the mixes DS-4 to 7, some retarders would have to be used systematically.

CHAPTER 6 - CALCIUM ALUMINATE CEMENT

In this chapter, the influence of type and amount of calcium aluminate cement on the rheological behavior of bauxite based low-cement castable with fixed amount of microsilica and water addition is studied in details. Two measured rheological constants, namely flow resistance and torque viscosity, have revealed the fact that castable rheology is strongly influenced by the type and amount of calcium aluminate cement under the specified experimental conditions.

6.1 Introduction

The first commercial calcium aluminate cement (CAC) was produced as a sulphate-resisting construction cement by Climents Lafarge in 1913, in a cupola, although the hydraulic characteristics of calcium aluminate (the principal mineral in cement) were discovered by Vicat as far back as 1846. The initial low-moisture and low-cement castable composition as adopted by the industry in later years were first introduced in 1974. Although the initial concept of LCCs was presented as early as 1962, it was not adopted by the industry because the necessary purer varieties of CAC were not available [40, 59]. The commercial development and application of CACs, as the most important hydraulically bonding agent, is one of the milestones of the modern castable technology. The manufacture and commercial availability of high purity CACs have been essential to obtain many advantages such as high refractoriness, early strength development and adjustable setting time. The characteristics of mineral constitutions, hydration, dehydration, setting and development of strength and hydrates change on heating have been defined very clearly [40].

Nowadays, low-cement self-flow castables are being widely used in high temperature furnaces because they can be easily installed and display high density and strength [81-82]. Different CAC can be used as a binder, the most common being differentiated by their alumina content (nominally 70 and 80 % Al_2O_3) for high-alumina castables.

Different cements with different phases show varying hydration behaviour. Among the mineral constitution of CAC, CA (C= CaO, A= Al_2O_3) has the highest strength and has a relatively high melting point of 1600^0C. It takes some time for initial setting and then set fast. Relatively, it is the most important component and the principal hydraulic compound in a CAC, which influences the main properties of the cement. Although CA_2 can withstand temperatures above 1700^0C, it takes an exceedingly long time to set and it is relatively low in strength. It occurs in a smaller quantity as an auxiliary mineral in CAC. As a single phase, $C_{12}A_7$ has short initial (5 minutes) and final (7 minutes) setting time with very quick hydration and hardening, and is mixed, in a small quantity, into various CACs to control the setting time [40]. Variables such as curing temperature, certain additives (dispersant, retarder or accelerator), water to cement ratio, are influencing the hydration mechanism of cement with a given chemistry and fineness. The effect of temperature on hydration behavior of calcium aluminate cement is shown in Table 6.1.

Table 6.1 Effect of temperature on hydration-reaction products of a typical 70 % alumina CAC [40]

Curing temperature (°C)	Hydration products of CA phase	Physical properties	
		Density (g/cm^3)	Solid volume change from CAH_{10} (%)
< 21	$CAH_{10} + AH_3$ (gel)	1.72	--
21 - 35	$C_2AH_8 + AH_3$ (gel)	1.95, 2.42	- 37
> 35	$C_3AH_6 + AH_3$ (crystalline)	2.52, 2.42	- 53

In castables, CAC does not only act as bonding agent, but also fine filler in the structure. LCC contains coarse aggregates and fine matrix. The fine matrix is generally composed of microsilica, fine aluminas, cement, and fine powder of bauxite, grog. etc. Though cement is added to castable to get hydraulic bonding and strength, it is considered as a fine matrix component from the particle size distribution point of view before cement hydration takes place with addition of water. Usually, the percent of CAC particle finer

than 325 mesh / 44 microns is about 80%, which brings some important influence on the flowability and rheological properties of castables.

In cement containing castables, part of the added water is utilized for hydration of cement. This water is referred to as bonding water or water of crystallization. It is considered being combined as H_2O molecules or as OH – groups [40, 59]. The remained water in the castable is existing as free water. This free water is helping in dissolving other additives and mainly wetting the surface of particles. It is very important that enough fine matrix paste fills the voids between particles to get high packing density and surrounds the aggregates to form a lubricating layer to make castable flow well.

To control the hydration rate of CAC and then workability of castable, certain additives are to be added for dispersion, and retardation or acceleration purposes. In this work, only one type of dispersant has been used. The focus will be on the influences of the nature and amount of CAC cement being used, in the same typical bauxite-based self-flow castables. Since CAC acts as both fine filler and hydraulical binder, the evolution of the rheology of the mixes with time is to be monitored with the rheological characteristics of the mixes: its flow resistance (G) and torque viscosity (H). It is with the appropriate selection of those two characteristics that it will be possible to minimize and control the aggregate bleeding (or segregation of fine matrix) and to obtain optimal properties.

6.2 Compositions

For this chapter, the composition details for this step are given in Table 6.2. The details of raw materials have been described in Chapter 3.2. Based on the previous results already considered, the q value and D_{max} are fixed at 0.26 and 5 mm, respectively. The microsilica is fixed at 5 wt%. The amount of water is adjusted to obtain self-flowability values over 100%. A total of five castable compositions have been considered with different amount of CAC content, as shown in Table 6.2.

Table 6.2 Details of the castable mixes to study the effect of cements

Castable		CA - 1	CA - 2	CA - 3	CA - 4	CA - 5
Aggregate (wt%)		59	59	59	59	59
Fine matrix (wt%)	Bauxite-1	11	11	11	11	11
	Bauxite-2	14	13	12	11	12
	Bauxite-3	11	10	9	8	9
	Cement CA-14	**0**	**2**	**4**	**6**	**0**
	Cement CA-25R	**0**	**0**	**0**	**0**	**4**
	Microsilica-1 (Elkem 971U)	5	5	5	5	5
Dispersant SHMP (wt%)		0.12	0.12	0.12	0.12	0.12

6.3 PSD of Castables

The PSD of the 5 compositions are shown in Figure 6.1. As shown, their PSDs are similar, chosen on purpose to elicit the role of cement only.

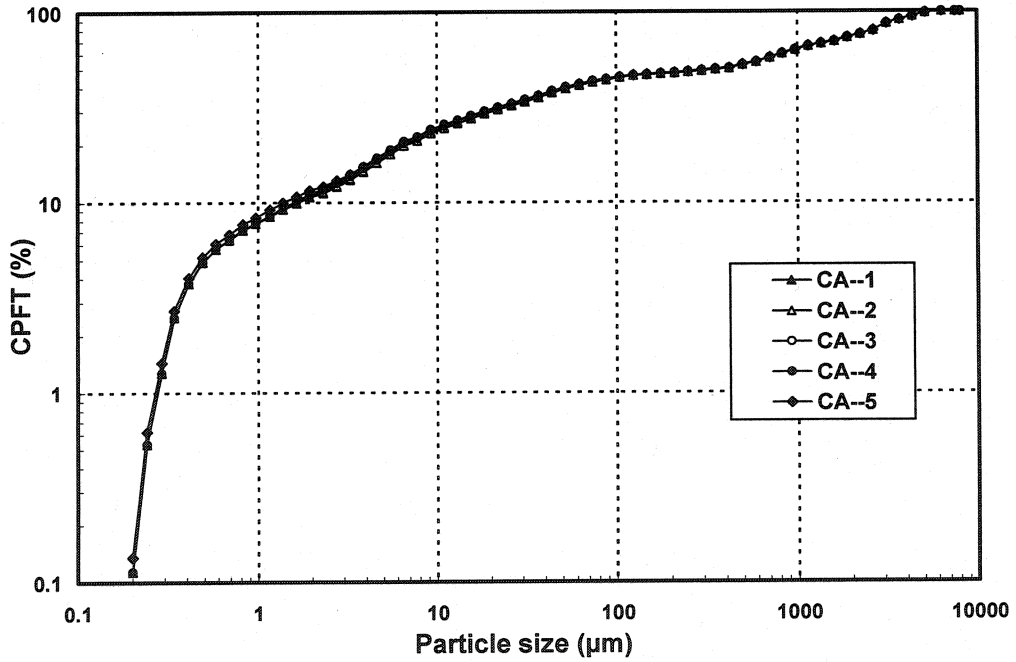


Figure 6.1 PSD of the 5 compositions with different cements.

6.4 Water Demand and Self-flowability

The self-flowability values, in %, for each composition as a function of water addition are shown in Figure 6.2. For each water amount, the self-flowability values for the 5

compositions are almost similar. With 6.0, 6.5 and 7.0 wt% water, self-flowability values are fixed at around 40, 80 and 120% respectively, hence the amount and type of CAC have not shown any marked influence on self-flowability. With 7.0 wt% water, similar self-flowability values are measured immediately after mixing and after 30 minutes (optimum working time), as shown in Figure 6.3.

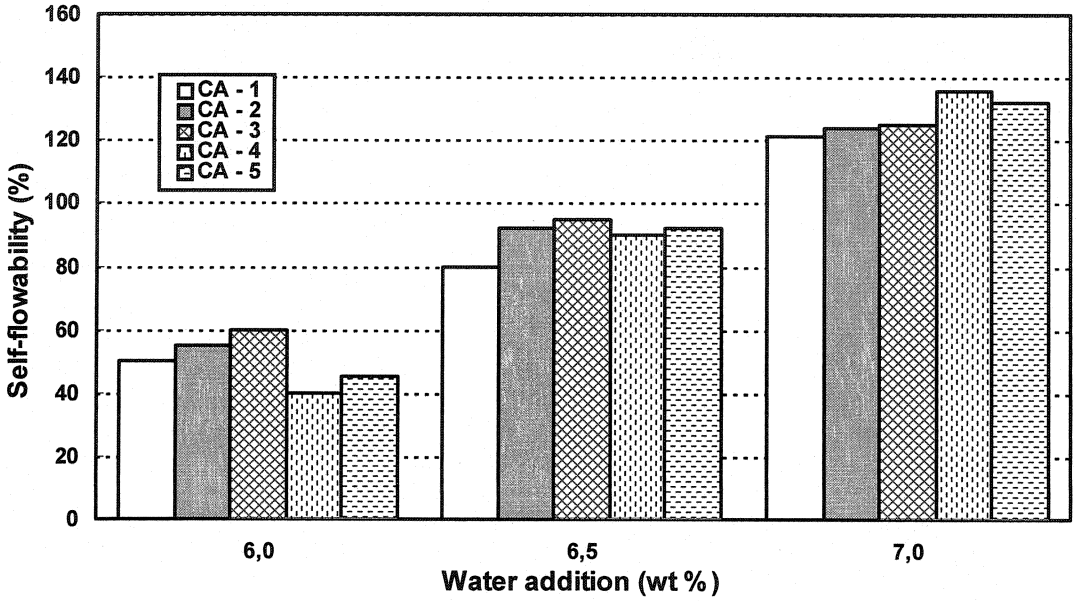


Figure 6.2 Self-flowability vs. water addition.

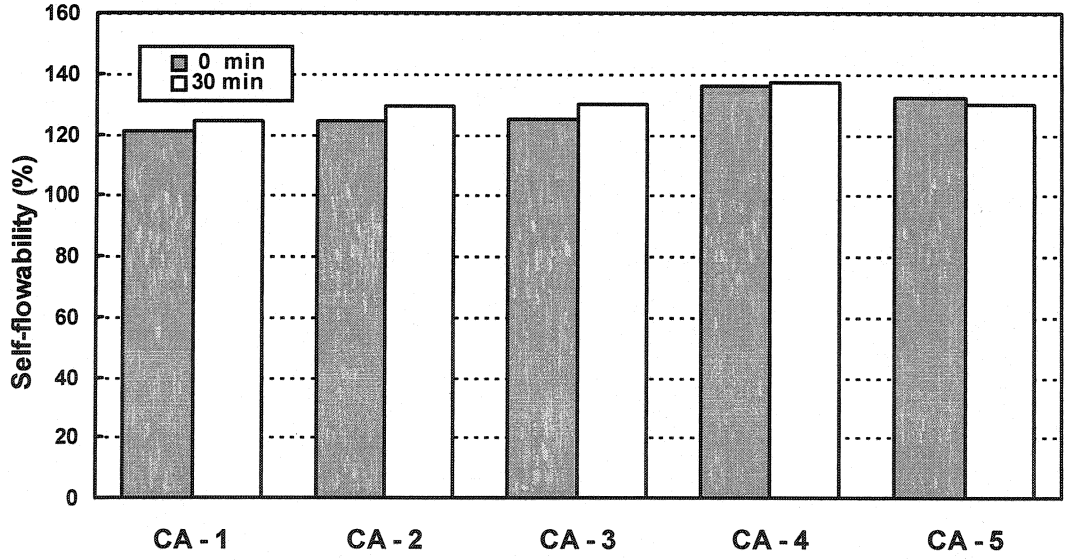


Figure 6.3 Comparison of self-flowability of the castables at different time.

6.5 Castable Rheology

6.5.1 Torque vs. Speed

The rheological test results of castables CA-1, 2, 3, 4 and 5 are shown in Figure 6.4-8, respectively. The rheograms have shown similar behavior, as explained in Chapter 4.5.1.

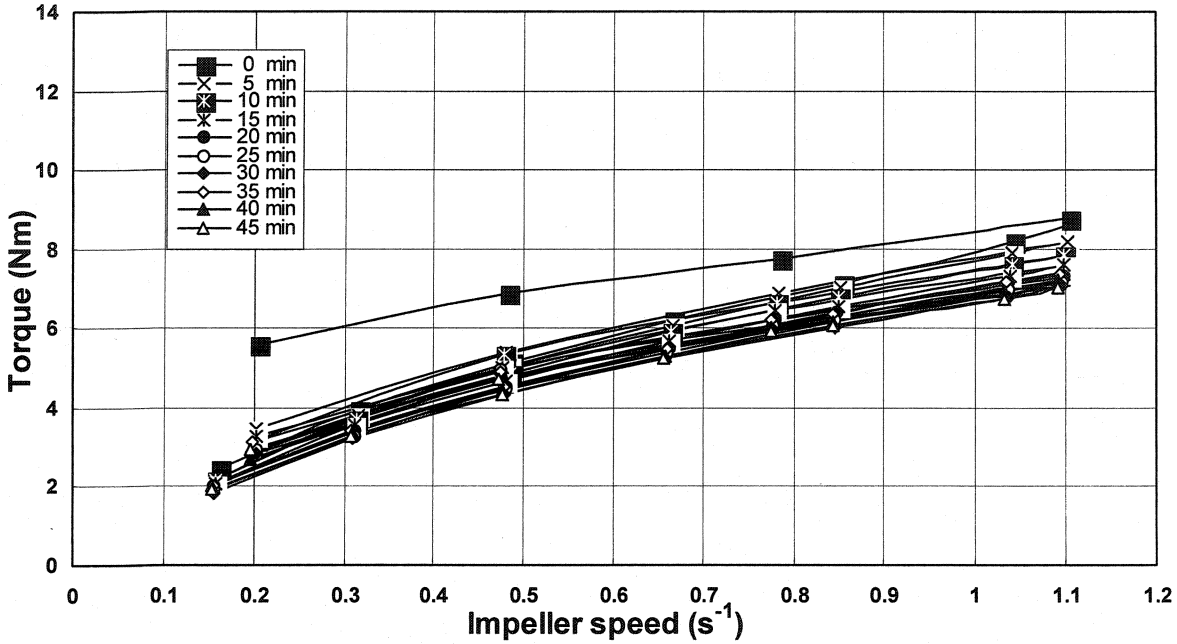


Figure 6.4 Torque vs. impeller speed for CA-1.

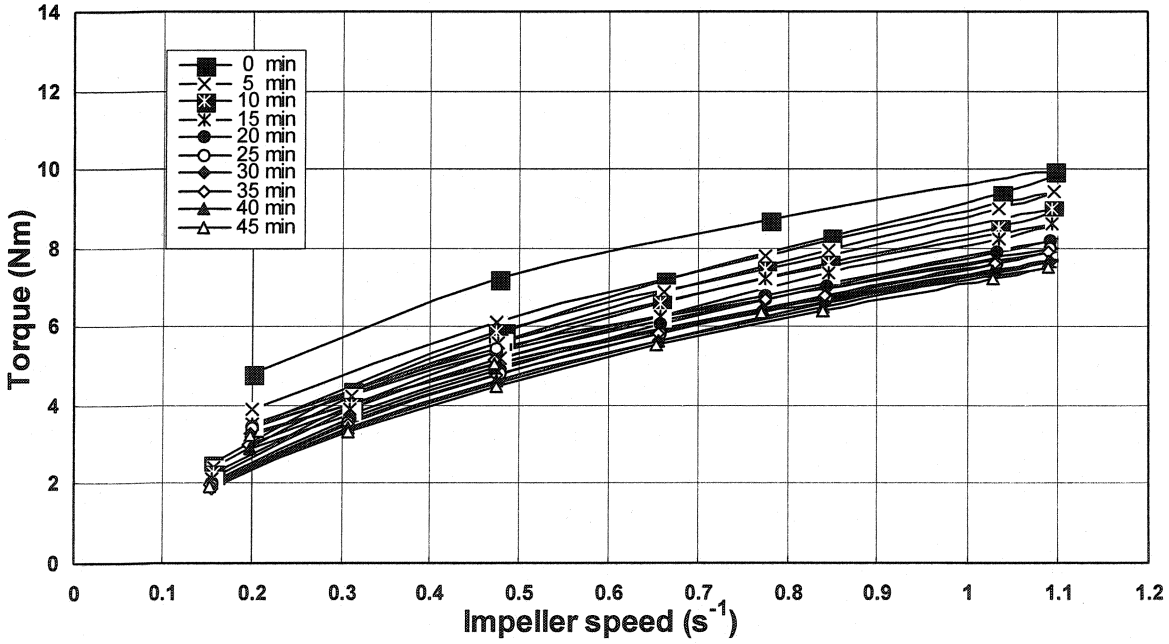


Figure 6.5 Torque vs. impeller speed for CA-2.

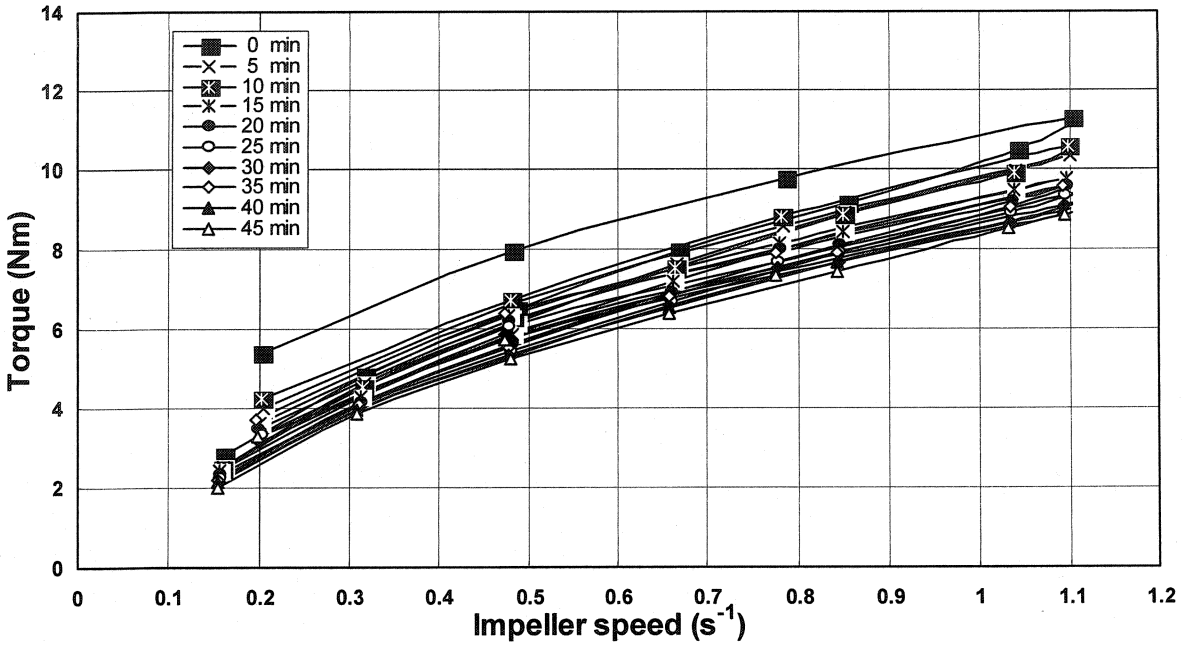


Figure 6.6 Torque vs. impeller speed for CA-3.

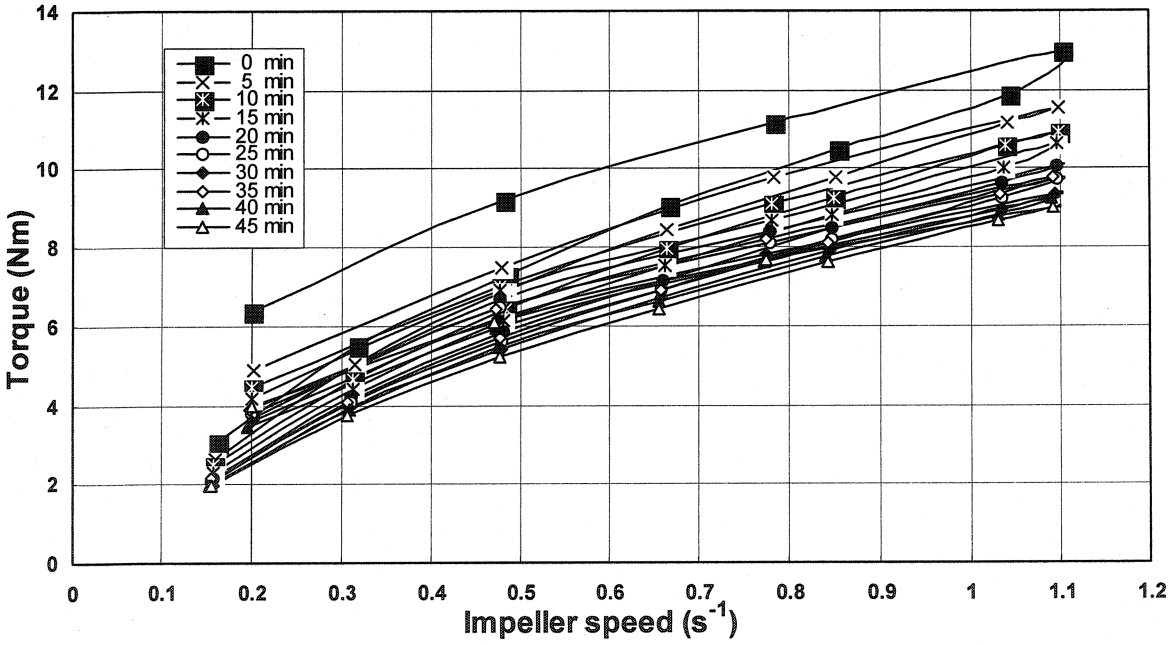


Figure 6.7 Torque vs. impeller speed for CA-4.

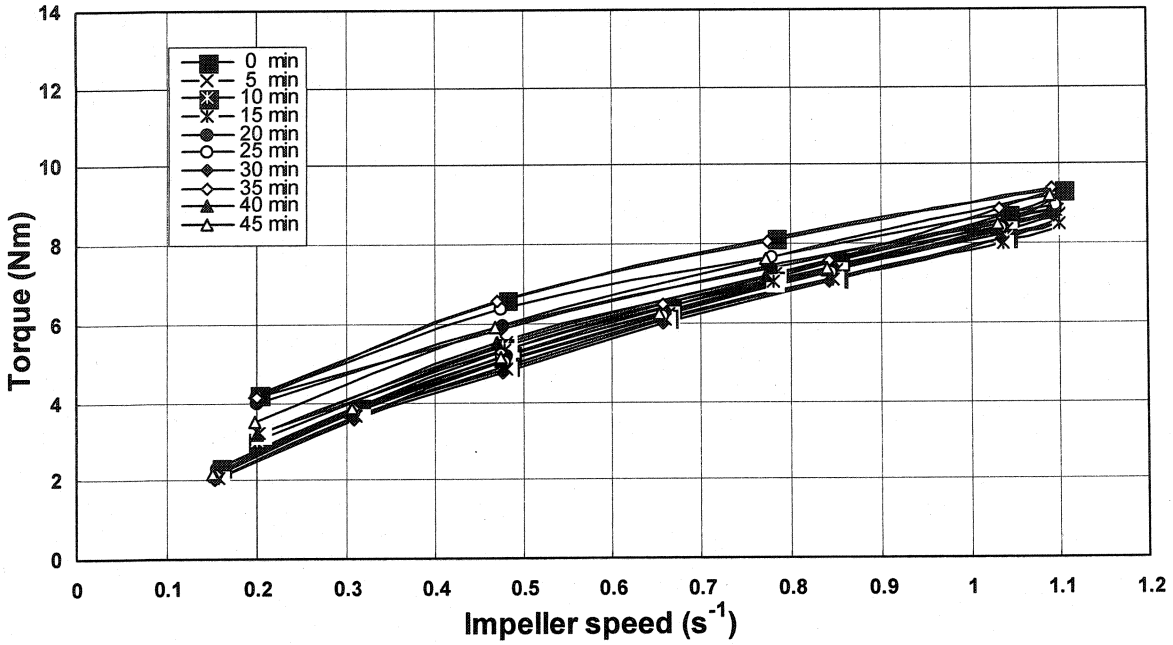


Figure 6.8 Torque vs. impeller speed for CA-5.

The same kind of behaviour has been observed for all compositions but with different rates of change of torque with speed. With an amount of cement CA-14 increasing, the loops scatter more and more. The torque (T_{max}) for the five compositions at the highest impeller speed of 1.10 s^{-1} at 0 min is given in Table 6.3. The T_{max} increases with cement CA-14 amounts. In the case of CA-5 with cement CA-25R, the torque is 9.36 Nm and lower than CA-3 with CA-14 at the same addition level of 4 wt%, showing the influence of CAC chemical and mineralogical compositions, as given in Table 3.3.

Table 6.3 T_{max} of the 5 compositions at the impeller speed of 1.10 s^{-1} at 0 min

Composition	CA--1	CA--2	CA--3	CA--4	CA--5
T_{max} (Nm)	8.76	9.98	11.29	13.00	9.36

6.5.2 Equivalent Apparent Viscosity

The relationship between equivalent apparent viscosity and impeller speed is shown in Figure 6.9 for composition CA-4, always closely typical to a Bingham fluid. The trends are the same for the other compositions and hence not shown.

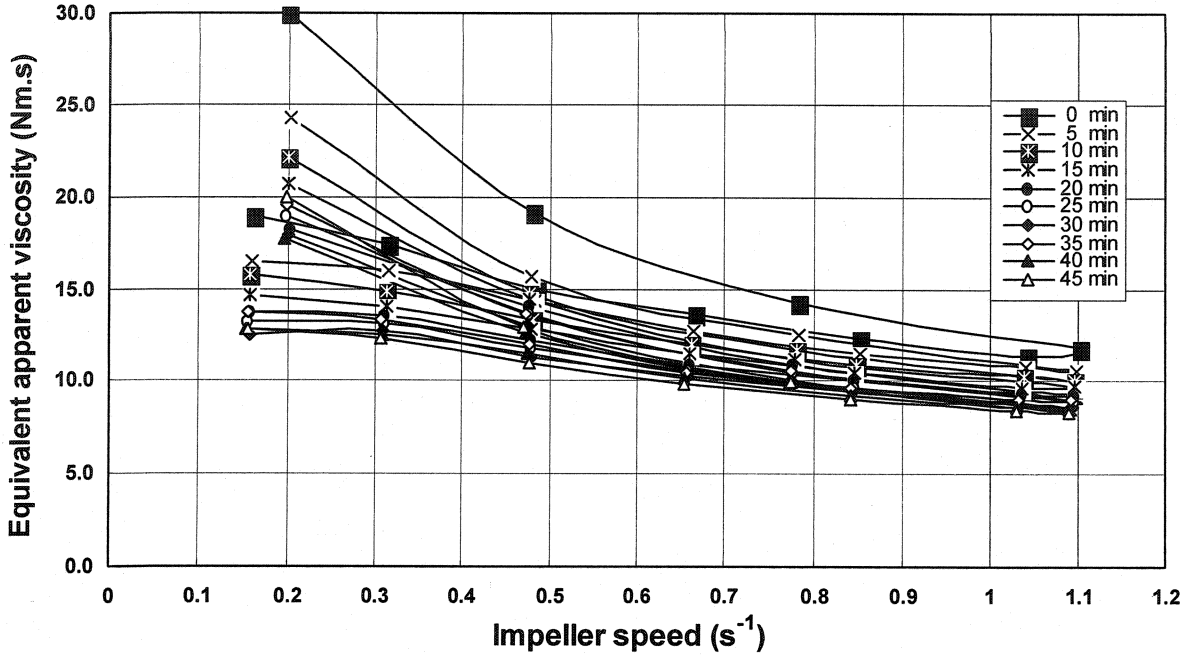


Figure 6.9 Equivalent apparent viscosity vs. impeller speed for CA-4.

6.5.3 Thixotropy

Though the mixes are acting as Bingham fluids, when analyzed as a function of time at constant impeller speed, the mixes displayed thixotropy (Figure 6.10). At the constant speed, the equivalent apparent viscosity is decreasing with testing time and stabilizes at 30 min of testing. The rate of reduction of equivalent apparent viscosity is more when the cement is increased from 0 to 6 wt%, which is the results of the influence of amount of hydrates present in castable. The equivalent apparent viscosity is increasing with the cement amounts, for CA-1 to CA-4, and nearly parallel to each other between sets of lines. When the cement CA-14 is replaced with CA-25, castable CA-5 shows a slight increase and fluctuation after 15 min, which might correspond to the quick setting of $C_{12}A_7$ that cement contains, being present in different percentages in the two CAC considered, as given in Table 3.3.

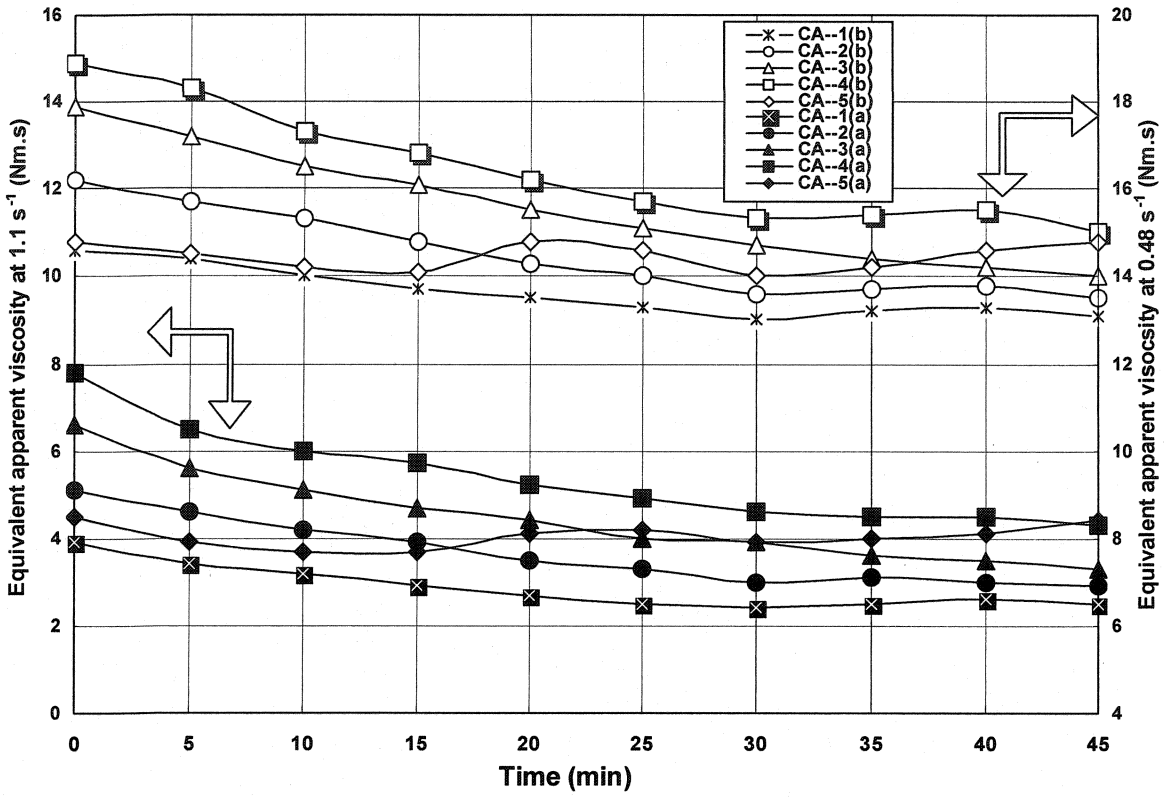


Figure 6.10 Equivalent apparent viscosity vs. time at high (a) and low (b) impeller speed, for mixes CA-1 to CA-5.

6.5.4 Bonding Water and Free Water

To further confirm the cement hydration, after cast, the castable sample with cement CA-14, CA-1, 2, 3 and 4, covered with plastic film and cured at 25^0C for 24 hours, demoulded and dried for 24 hours at 100^0C and fired at 1000^0C for 5 hours. It is observed that the bonding water and free water are proportional to the amount of cement with opposite trends, under the given experimental conditions (Figure 6.11). An increase of bonding water dictates the amount increase of hydration and gelatinous phases associated with cement hydration. The influence of mixing water on bonding water and free water has been tested with mix CA-3. It is noted that the bonding water remains same at 1.1 wt % even when the mixing water is changed from 6.0 to 7.5 wt%.

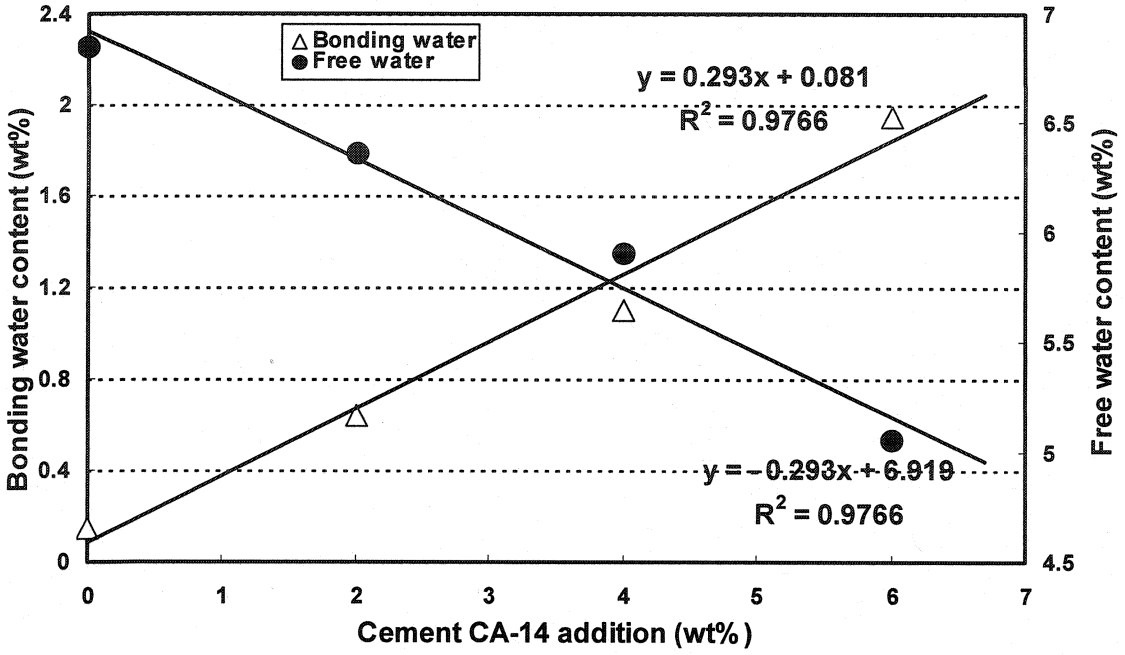


Figure 6.11 Bonding water and free water content of castables CA-1, CA-2, CA-3 and CA-4, with different cement CA-14 addition.

6.5.5 Flow Resistance and Torque Viscosity

The method of evaluating G and H values, using the IBB rheometer test results, has been described in Chapter 4.5.4. The calculated values of G and H are shown in Table 6.4.

Table 6.4G and H values for all the compositions

Time (min)	Flow resistance G (Nm)					Torque viscosity H (Nm.s)				
	CA - 1	CA - 2	CA - 3	CA - 4	CA - 5	CA - 1	CA - 2	CA - 3	CA - 4	CA - 5
0	1.75	1.73	1.86	2.02	1.49	6.38	7.79	8.65	9.97	7.17
5	1.54	1.65	1.73	1.68	1.32	6.46	7.49	8.47	9.64	7.06
10	1.58	1.57	1.62	1.55	1.31	6.15	7.15	8.27	9.15	6.9
15	1.51	1.47	1.56	1.45	1.36	5.95	6.95	8.02	8.75	6.75
20	1.46	1.37	1.52	1.33	1.59	5.79	6.72	7.78	8.46	6.86
25	1.37	1.35	1.46	1.28	1.4	5.75	6.43	7.58	8.17	7.02
30	1.31	1.26	1.42	1.2	1.26	5.61	6.29	7.43	7.96	6.86
35	1.3	1.27	1.41	1.22	1.25	5.62	6.28	7.41	7.9	6.8
40	1.31	1.28	1.4	1.21	1.29	5.58	6.24	7.4	7.81	6.5
45	1.32	1.27	1.33	1.22	1.35	5.55	6.07	7.34	7.6	6.55

As shown in Figure 6.12, the flow resistance of the castables at 0 min, is increasing with increasing cement content. This is due to more hydrates and gel formation with increasing cement content. After 5 min, the influence of cement is not more visible and the G values remain the same independently of the cement content. This trend remains but with a decrease in G values with testing time. As explained earlier, the more amount of gel with more cement content in the matrix lead to increasing G values with cement at 0 min. After initial test (0 min), the gel structure is broken and the mix reaches lower values of G. This breaking of gel goes on with tests and thus reducing G continuously.

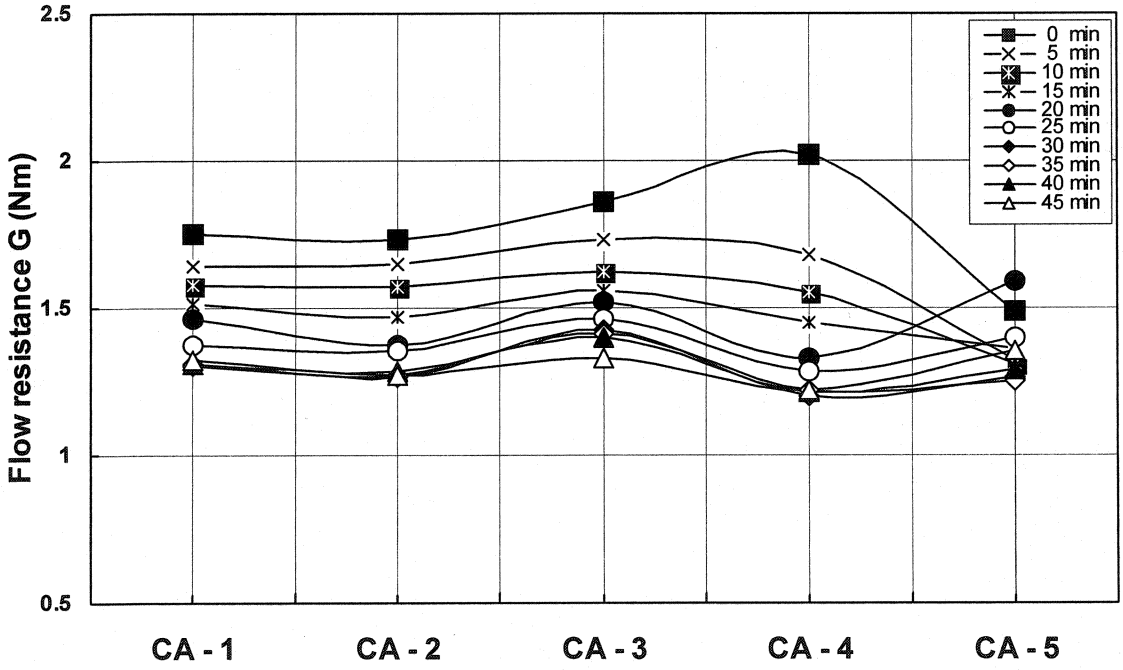


Figure 6.12 Flow resistance vs. cement.

The relationship between the torque viscosity, H values, for the 5 compositions, and the cement content, from 0 to 6 wt%, using CA-14 cement, and using CA-25R (4 wt %) are shown in Figure 6.13. As the amount of CA-14 cement increases, more water is being used in the hydration reaction and less free water is left. This leads to the mixes with reduced interparticle distance and causes an increase collision of particles. As noticed before the H values decreases with time initially and do stabilize after 20 minutes. The

difference in H between CA-3 and CA-5 may be due to the fact the CA-25R is finer than CA-14 cement as shown in Chapter 3 (Figure 3.3).

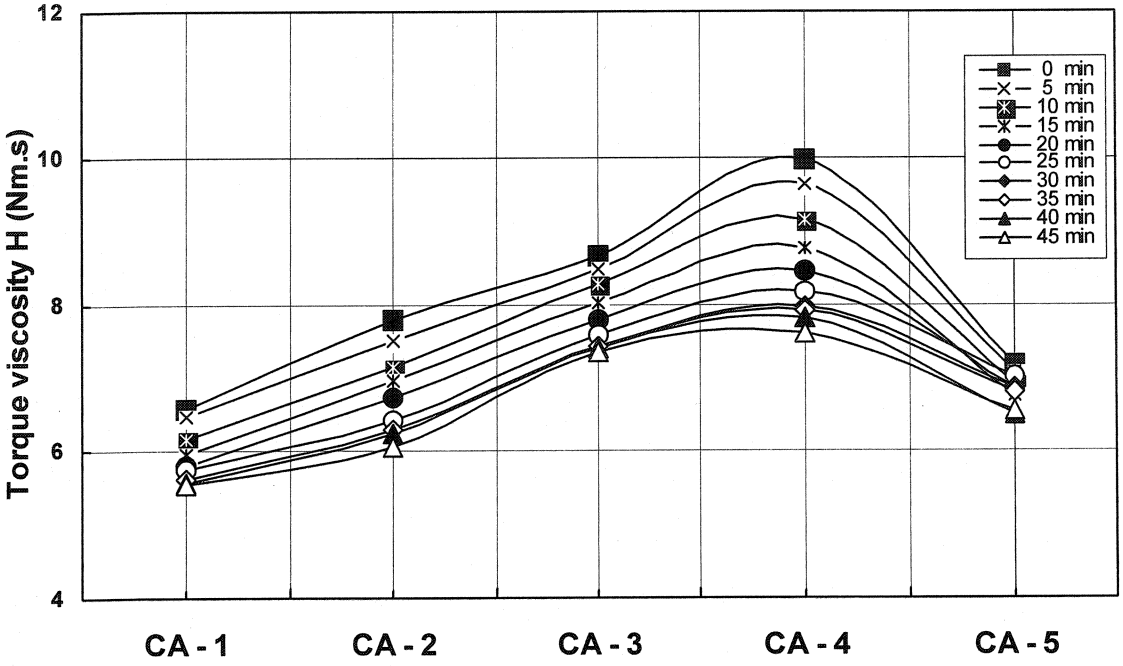


Figure 6.13 Torque viscosity vs. cement.

6.6 Matrix Rheology

6.6.1 Shear Stress vs. Shear Rate

The shear stress as a function of shear rate of the matrix slurries of the 5 castables is shown in Figure 6.14. The shear stress in the forward cycle (shear rate increasing) is higher than rate in the reverse cycle (shear rate decreasing) and then forms a hysteresis loop. As previously observed with the whole castable mix, the forward cycle reveals the pseudoplastic nature of the slurry, while the reverse cycle displays almost Bingham behaviour. The loops shift downwards as the cement CA-14 content increases. The loop of CA-5 is ranked at the highest place. The loops of CA-1 and 2 are similar.

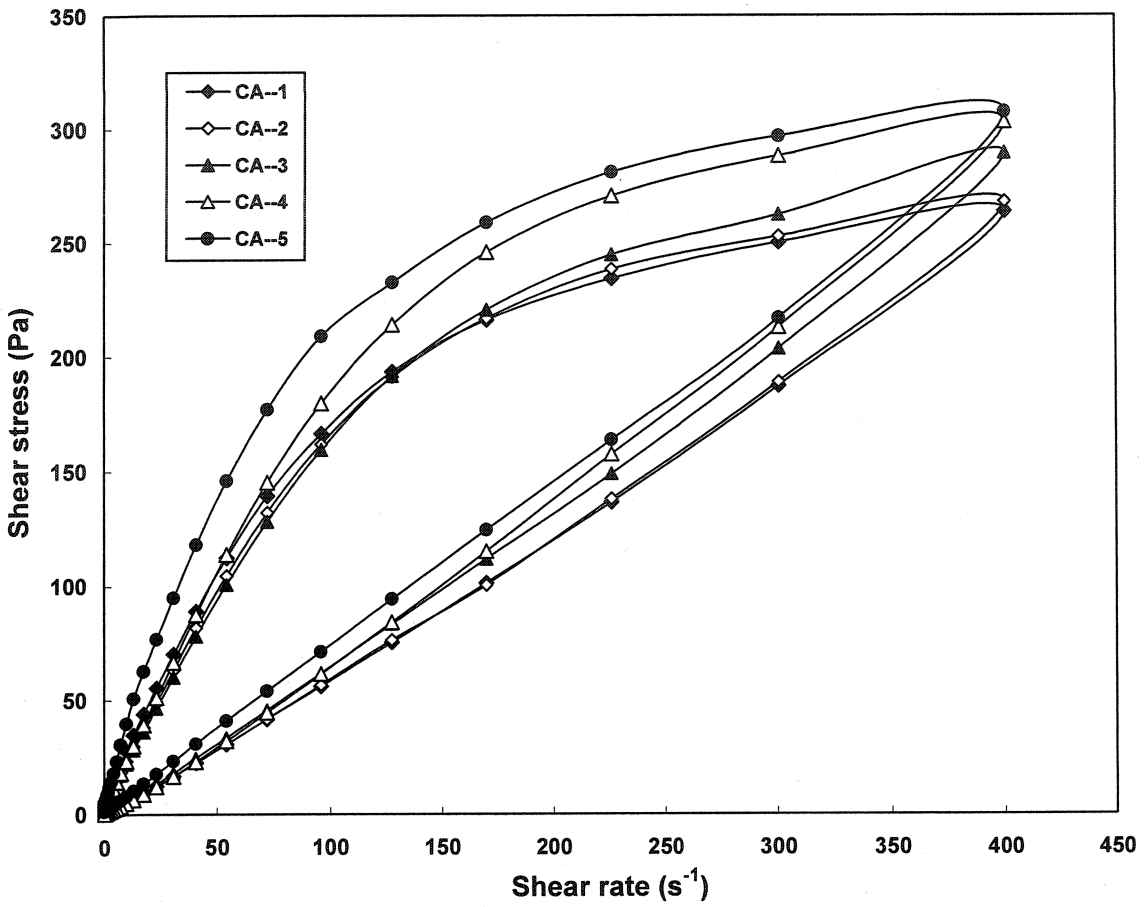


Figure 6.14 Shear stress vs. shear rate for all the matrix slurries.

The shear stress (τ_{max}) at the highest shear rate of 400 s^{-1}, for all the compositions is given in Table 6.5. The τ_{max} increases with the amount of cement CA-14 being used. It resembles the trend with T_{max} as given in Table 6.3. In the case of CA-5 with 4 wt% CA-25R, the τ_{max} is the highest among all castables.

Table 6.5 τ_{max} of the 5 compositions at the highest shear rate of 400 s^{-1}

Composition	CA--1	CA--2	CA--3	CA--4	CA--5
τ_{max} (Pa)	264	268	290	303	308

6.6.2 Apparent Viscosity vs. Shear Rate

The evolution of apparent viscosity as a function of shear rate of the matrix slurries of the 5 castables is shown in Figure 6.15. The apparent viscosity value for CA-2, 3 and 4 is similar. In the case of CA-1, without any cement addition, the apparent viscosity

fluctuates before 1 s^{-1} and is higher than CA-2, 3 and 4 in the forward cycle and remains similar as those three compositions. With cement CA-25R, the apparent viscosity of CA-5 is the highest among the 5 compositions considered and significantly increases after 1 s^{-1} in the reverse cycle, because of the early setting effect. In the forward cycle, the apparent viscosity of the three matrix slurries 2, 3 and 4 with cement CA-14, decreases sharply within 5.0 s^{-1} and remains similar till 100 s^{-1} and finally slightly decreases from 100 s^{-1} to 400 s^{-1}. In the reverse cycle, the apparent viscosity of those three compositions remains similar from the shear rate from 400 s^{-1} to 1 $^{-1}$ and then increases till the shear rate falls to zero. In the case of CA-5, the same trend has been found as the others but with different rates.

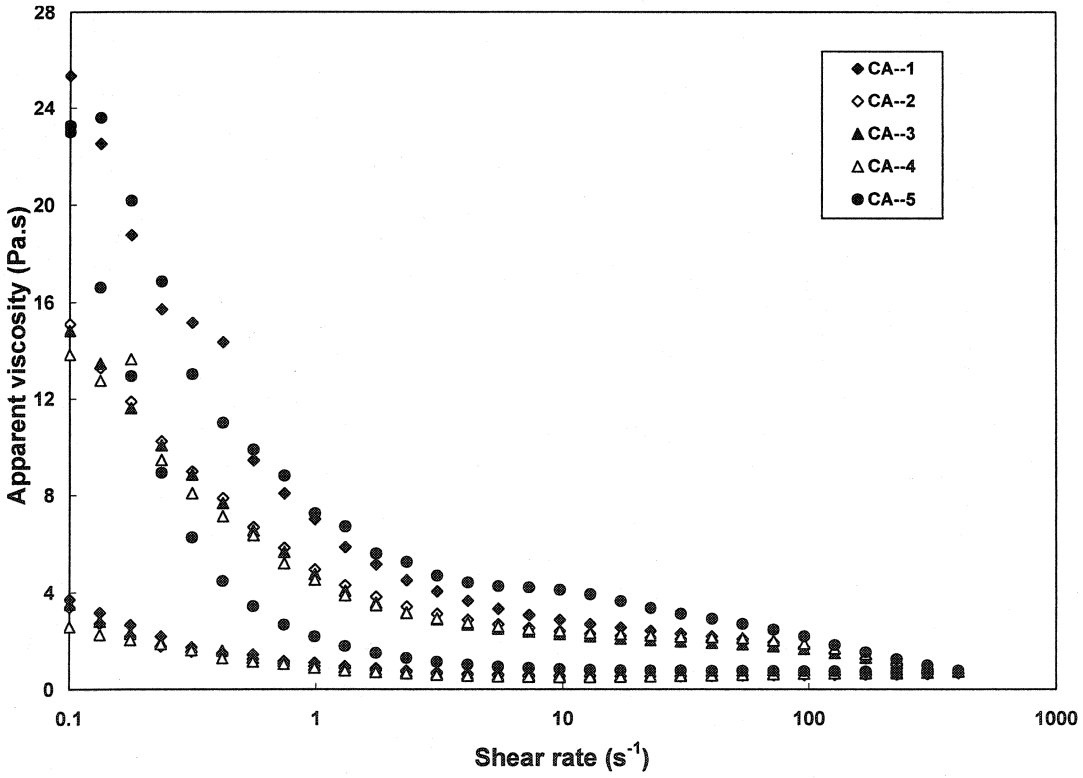


Figure 6.15 Apparent viscosity vs. shear rate for all matrix slurries.

6.6.3 Thixotropy

Following the calculation method described in Chapter 4.6.3, it appears that the thixotropy degree of CA-3 is the lowest and that of CA-5 is the highest among the 5 compositions, as shown in Figure 6.16. The loops' area hysteris follows the same trend.

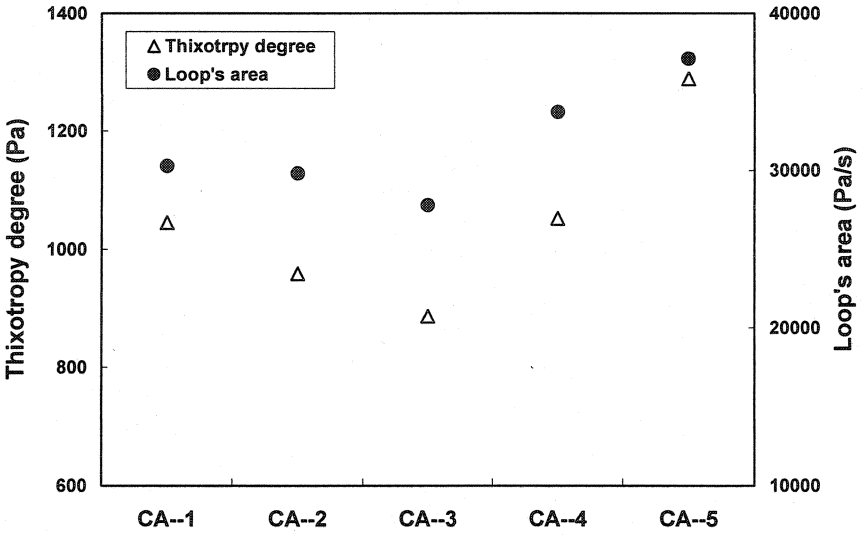


Figure 6.16 Thixotropy degree and loop's area for all the matrix slurries.

6.6.4 Plastic Yield Stress and Plastic Viscosity

The calculation method of the plastic viscosity and yield stress of all the matrix slurries has been defined in Chapter 4.6.1. The plastic viscosity remains similar for the slurries added with cement CA-14, but the plastic yield stress decreases as cement CA-14 amount increases, as shown in Table 6.6. In the case of CA-5, both the plastic viscosity and yield stress are the highest among the 5 compositions. A good reason is that CA-25R is co-ground with cement clinkers and reactive alumina, which possesses a very high surface area.

Table 6.6 Plastic viscosity and yield stress of all the matrix slurries

Composition	CA--1	CA--2	CA--3	CA--4	CA--5
Plastic viscosity (Pa.s)	2.029	1.906	1.829	2.075	2.72
Plastic yield stress (Pa)	6.414	3.890	3.512	2.744	8.155

6.7 IPS of Matrix and MPT of Castables

The calculation methods of IPS of the matrix slurries and MPT of the castables have already been described as Equation 2.7 and 13. The IPS and MPT values for CA-1, 2, 3, 4 and 5 are given in Table 6.7. When cement CA-14 amount increases, the IPS of the matrix slurries decreases. The MPT of the castables is reverse. In the case of CA-5, the IPS value is the lowest among the 5 matrix slurries. This is the reason why both the

plastic viscosity and yield stress are the highest among the 5 compositions, as shown in Table 6.6.

Table 6.7 IPS of the matrix slurries and MPT of the castables

Composition	CA--1	CA--2	CA--3	CA--4	CA--5
IPS (nm)	88.8	88.6	87.9	87.2	85.2
MPT (μm)	122.5	123.1	123.8	124.5	123.8

6.8 Physical and Mechanical Properties

The CMOR and AP of all the compositions are shown in Table 6.8.

Table 6.8 CMOR and AP of all the compositions

Composition	CMOR (MPa)		AP (%)	
	0 min	45 min	0 min	45 min
CA - 1	2.8	2.6	19.2	19.8
CA - 2	5.8	4.1	18.7	19
CA - 3	9.3	8.7	18.2	17.8
CA - 4	12.2	12.4	16.9	17.2
CA - 5	5.2	4.9	20.4	19.8

Figure 6.17 illustrates the relationship between CMOR and cement content. Using CA-14 cement, CMOR values increase by around 1.5 MPa for each 1 wt% CA-14 addition. With the same amount of CA-25R cement, only half of the CMOR values can be achieved as compared to CA-14.

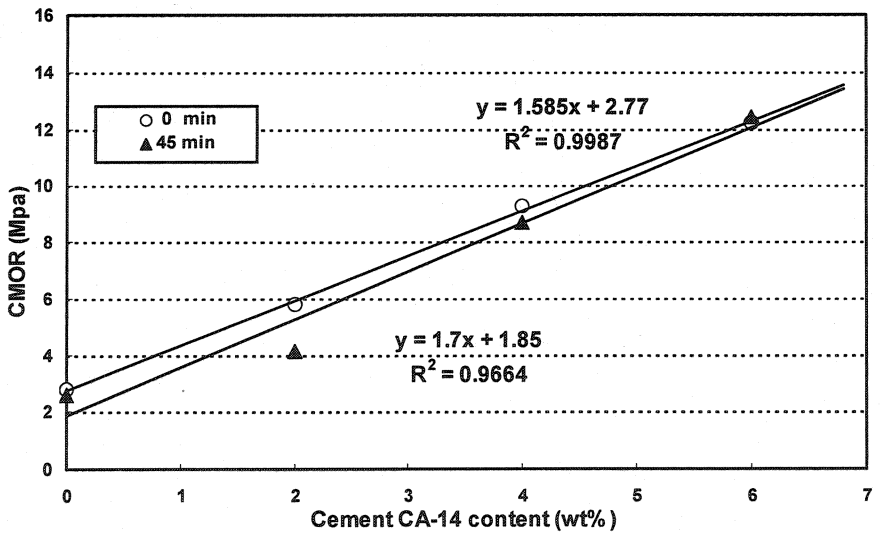


Figure 6.17 CMOR of castables CA-1, CA-2, CA-3 and CA-4 at different time.

The relationship between cement and AP of all compositions is shown in Figure 6.18. As expected, the AP values decrease as a function of the cement content, at around 0.25 % for each 1 wt% CA-14 added. The role of CA-14 and CA-25R on the AP is also very clear, in favour of CA-14 resulting in a difference of about 2 % AP, between the two types of cement.

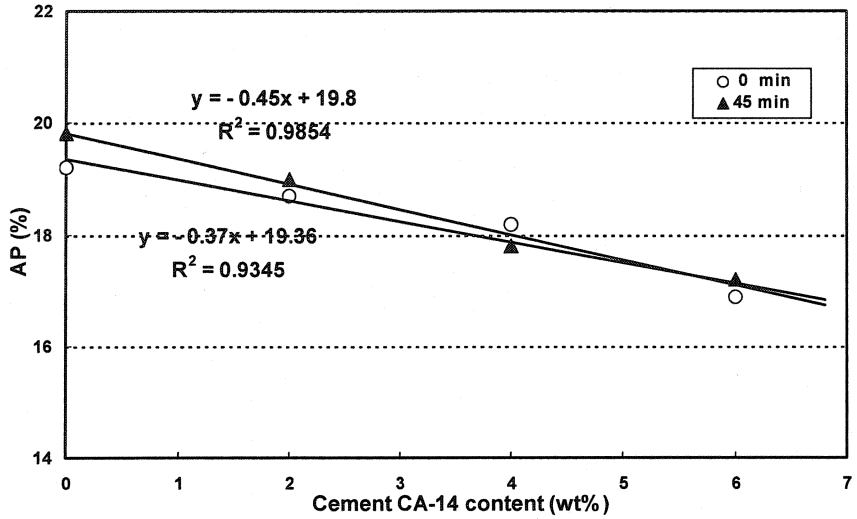
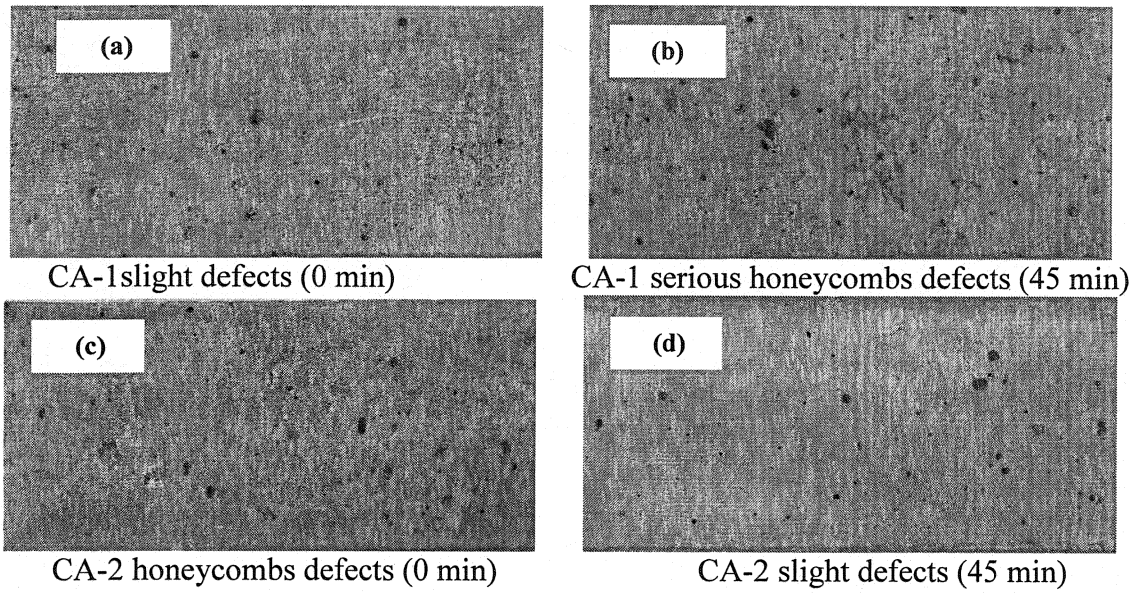


Figure 6.18 AP of castables CA-1, CA-2, CA-3 and CA-4 at different time.

The CMOR and AP values are characteristic of the structure of cast body. With 7 wt% fixed water, different cement content gives different water to cement ratio. More cement content means that more water is needed for the cement hydration and less free water is left, hence less AP and higher CMOR values. With 7 wt% fixed water, different cement content gives a different water to cement ratio. More cement content means that more water is demanded to participate the cement hydration which develops more strength. With less free water to be evaporated, the castable body becomes denser and hence the CMOR increases and AP decreases, after drying at 110^0C. Even the same amount of cement addition, but different type of cement which owns different ingredients such as CA or CA_2, will show different effects on the rheological and mechanical properties. The free water fills the voids between particles to form slurry surrounding the aggregates. It is also important to consider that above certain amount, free water may separate the aggregates after filling the voids and then bring negative impacts to the mechanical properties of castables.

6.9 Appearance of Samples

A honeycomb structure has been found on the side showing the thickness of CA- 1 and 2, as shown in Figure 6.19 at 0 and 45 min of testing time respectively. The appearance of the other castables at different time with 4and 6 wt% cement is very good, hence not shown here.



CA-1slight defects (0 min)

CA-1 serious honeycombs defects (45 min)

CA-2 honeycombs defects (0 min)

CA-2 slight defects (45 min)

Figure 6.19 (a)-(d) Appearance of samples CA-1 and 2 cast at different time.

6.10 Optimization of Castables

The relationship between G and H is shown in Fig. 6.20. It shows a linear relationship with testing time. G became independent after initial test and yet H is dependent on cement. The compositions CA-1 and CA-2 are having relatively low flow resistance and torque viscosity, but are affected by some casting defects (honeycomb structure in Figure 6.19). This indicates that the values of G and H should be above a critical value to avoid such defects. In case of CA-5, the values of G and H are influenced by some setting effects and only CA-3 and CA-4 samples can be considered as good pumpable castables. This means that proper type and amount of cement are required to avoid blockage inside pipes, with sufficient viscosity to avoid segregation while maintaining flowability coherence, integrity and stability of the castable mix.

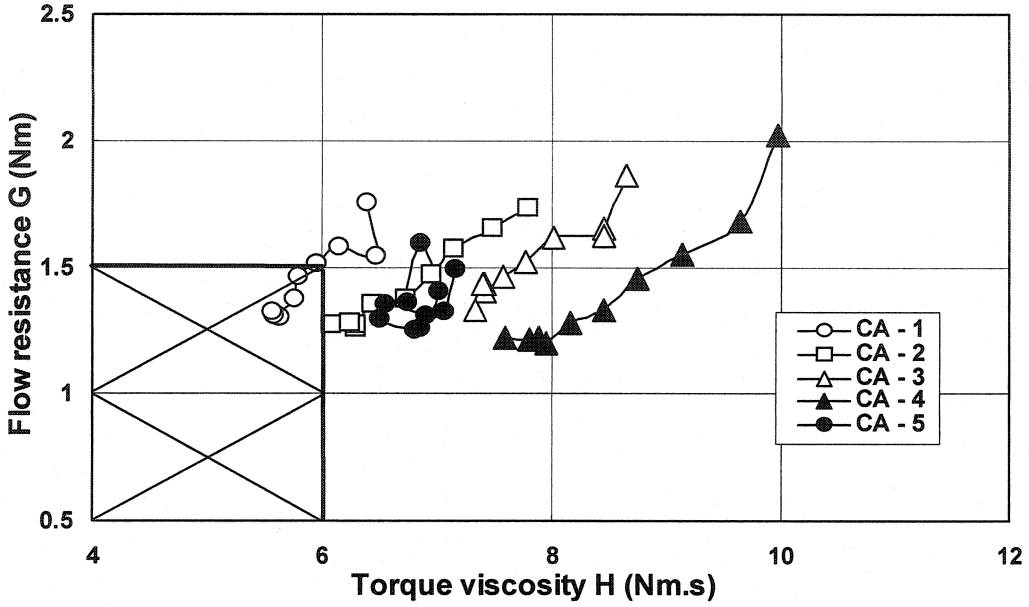


Figure 6.20 Flow resistance vs. torque viscosity

6.11 Conclusions

The rheological behaviour and physical properties of bauxite based low-cement self-flow castables with different type and amount of cement have been studied in this work. The conclusions based on this investigation are that, among the 5 mixes considered:

a) All the mixes are described as suspensions following a Bingham behavior and are thixotropic in nature.

b) The G values are not strongly influenced by the type and amount of CAC, as well as their self-flowability values. The H values have shown strong dependency on the amount of CAC due to cement hydration leading to different free water left in the mix.

c) The CMOR and AP values show an increase of around 1.5 MPa and a decrease of 0.25 % respectively with each 1 wt% CA-14 cement addition. Under the same condition, at the same amount of cement, 4 wt%, CA-14 samples have shown higher CMOR and lower AP than that of CA-25R samples.

CHAPTER 7 - MICROSILICA

In this chapter, the effects of varying types and amounts of microsilica on self-flowability, rheological, mechanical and physical properties of bauxite-based low-cement castables are studied. The two basic rheological properties, flow resistance (G) and torque viscosity (H), are measured over time and the importance of selecting the right microsilica quality and content will be demonstrated. The chemistry of microsilica is found to affect the rheological behaviour of the chosen castables.

7.1 Introduction

LCC technology is widely used because it helps to produce castables with excellent characteristics: low porosity, high density, exceptional hot strength, corrosion-erosion and thermal spalling resistances. It is linked to the use of ultra-fine particles that fill void spaces between aggregate particles and thus improve packing and bonding. In a castable, the density obtained with classical grain size distribution is limited by the inter-granular voids, which are filled with excess water during mixing. Packing density can be increased by filling voids, using ever-finer particles with diameter ratio of approximately 10:1. Voids between successive particle size fractions are thus filled with increasingly fine powder down to 0.01 μm diameter. The remaining micro-pores are filled with gel of hydrated cement. The ultra-fine particles generally include microsilica, calcined alumina, reactive alumina, TiO_2, ZrO_2, Cr_2O_3, etc. [83]. The use of microsilica started in the 1960s, and since then it has been one of the most popular ultra-fine powders for use in castable technology, especially in modern LCC technology.

The term "microsilica", used frequently in the commercial and industrial literature, is less specific and descriptive than the term "condensed silica fume". In fact, microsilica is a mineral composed of ultra-fine amorphous spheres of silicon dioxide SiO_2, produced during the manufacture of silicon or ferrosilicon. This process involves the reduction of high-purity quartz in electric arc furnaces at temperatures of over 2,000°C. The

microsilica is formed when SiO gas, given off as the quartz reduces, mixes with oxygen in the upper regions of the furnace. Here the SiO is oxidized to SiO_2, condensing as pure spherical particles of microsilica. This is known as silica fume or microsilica. The average particle is well below 0.5 μm in diameter, meaning that each micro-sphere is 100 times smaller than an average cement grain. In a typical mix, with a 10 % dosage of microsilica, there will be between 50,000 and 100,000 microsilica particles per grain of cement. Microsilica particles are spherical in shape and range from 0.02–0.45 μm in diameter for a mean particle diameter of 0.15 μm and a surface area of 15–25 m^2/g [59, 84, 85].

Microsilica is used to enhance the performance of refractory castables and to reduce cement content in castables. Since the 1990s, many reports have been published on the effects of microsilica on the properties of castables [86-95]. The five impacts of microsilica on a castable can be summarized as follows:

(1). Improved flowability and lower water addition, when used as fine fillers

(2). Better packing to maximise density and reduce porosity

(3). Optimized $MgO\text{-}SiO_2\text{-}H_2O$ bonding in basic cement-free castables, when used as a bonding agent

(4). Improved mechanical properties at low and intermediate temperature in cement-bonding castables

(5). Maximised hot strength by reaction with alumina to form mullite in alumino-silicate castables and forsterite phase to enhance slag-resistance and high-temperature properties in basic castables.

The research on microsilica containing castables over the past two decades identified it as a packing filler, water reducer, fluidity-enhancer, strength builder, etc. While the facts surrounding the role of microsilica in castables appear to be well understood, there is one important area of research that remains unexplored, i.e. rheology (the study of viscous behaviour as a function of shear rate) [10, 96]. Improvements in technology have shifted the installation mode of castables from vibration to self-flow, pumping and

shotcreting. This development not only demands instruments to carry out the installation, but also a basic understanding of the behaviour of castables when subjected to modern techniques.

It may be argued that the measurement of self-flowability, a common research method worldwide, is itself an indicator of rheology. A number of essential questions must first be answered when pumping and/or shotcreting of an aluminous silicate castable containing microsilica is planned. Does the increase of microsilica only increases flow and reduces the water amount? What is its measurable role on rheology? Are all castables containing various amounts of microsilica rheologically identical? Will they exhibit similar behaviour during pumping or shotcreting? To answer all these questions, it is necessary to simulate practical conditions in a rheological test. This part of the work will concentrate on rheology of castables containing different types and amounts of microsilica

7.2 Compositions

The composition details for this step are given in Table 7.1. The details of raw materials have been described in Chapter 3.2. Based on the previous work, the q value and D_{max} are fixed at 0.26 and 5 mm, respectively. In this work, the CAC is fixed at 4 wt%. The influence of the type and amount of microsilica are tested, varying the amount from 3 to 7 wt% and comparing two different microsilicas available, at 5 wt% level.

Table 7.1 Details of castable mixes to study the effect of microsilicas

Castable		**MS-1**	**MS-2**	**MS-3**	**MS-4**
Aggregate (wt%)		59	59	59	59
Fine matrix (wt%)	Bauxite-1	11	11	11	11
	Bauxite-2	12	12	12	12
	Bauxite-3	11	9	7	9
	Cement CA-14	4	4	4	4
	Microsilica-1 (Elkem 971U)	**3**	**5**	**7**	**0**
	Microsilica-2	**0**	**0**	**0**	**5**
Dispersant SHMP (wt%)		0.12	0.12	0.12	0.12

7.3 PSD of Castable Compositions

The PSD of the three compositions MS-1, 2 and 3, with increasing amount of microsilica, are shown in Figure 7.1. The aggregates are the same for all the compositions. Adding with more microsilica, increases more ultra-fine particles of less than 10 μm into the overall compositions.

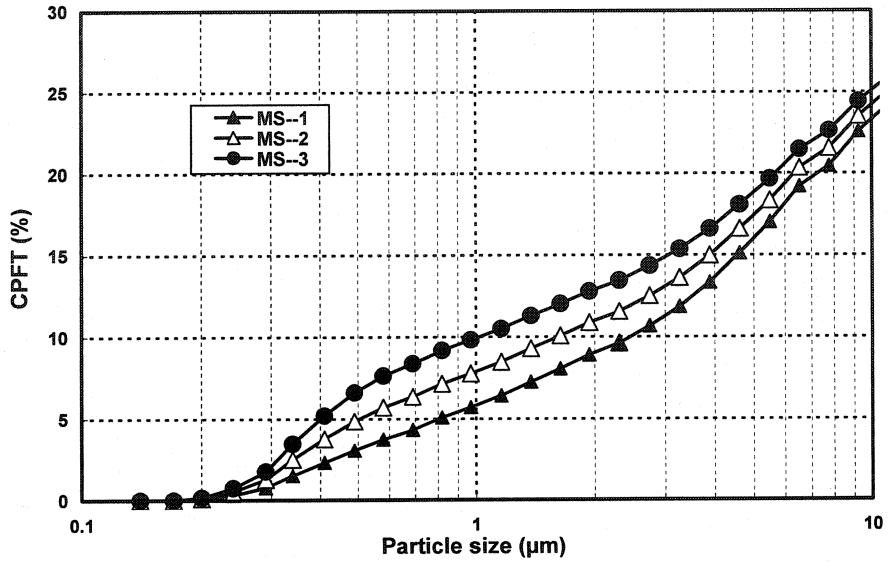


Figure 7.1 PSD of the 3 compositions with different amount of microsilicas.

7.4 Water Demand and Self-flowability

The flowability is a function of water addition. With 5.5 wt% water addition, the vibration flowability of MS-3 is about 110%, but MS-1, 2 and 4 can not flow under vibration. Adding 0.5 wt% more water is insufficient for MS-1 and MS-4 to flow under vibration, but MS-2 and 3 start to self-flow at the level of 6.0 wt% water.

The self-flowability of chosen compositions as a function of water addition is shown in Figure 7.2. In case of 6.0 wt% water, self-flowability of MS-2 and MS-3 is around 25 % and 70 % respectively, while MS-1 and MS-4 have not shown any self-flowability. With 6.5 wt% water, the self-flowability of MS-2 increases dramatically to nearly 90 % and is almost the same as that of MS-3. Both MS-1 and MS-4 begin to self-flow but self-flowability remains lower, at around 30 %. With 7.0 wt% water addition, MS-3

exhibited the highest self-flowability, followed by MS-2, MS-4 and MS-1. The self-flowability of MS-2 is almost comparable with that of MS-3 and nearly twice as high as MS-1. Although the mix MS-1 took much longer to wet-mix and is not self-flowing, it exhibited very high vibration flowability of 138 %. With 7.0 wt% Microsilica-1, the mix MS-3 is very sticky and adhesive. This study also examined the flowability of a mix without microsilica. The mix separated into many smooth-surfaced hard balls throughout the mixing process. The mix exhibited 100 % vibration flowability with 8 wt% water only but the flow stops faster, hence the mix composition is not shown.

Though microsilica addition improves self-flowability and reduces the amount of water addition required, the mix with 5 wt% microsilica displayed optimum flow and non-sticky characteristics. MS-3 has flown well but is found to be too sticky. With the same amount of microsilica (5 wt%), MS-2 flows better than MS-4, indicating the importance of the source and purity of microsilica.

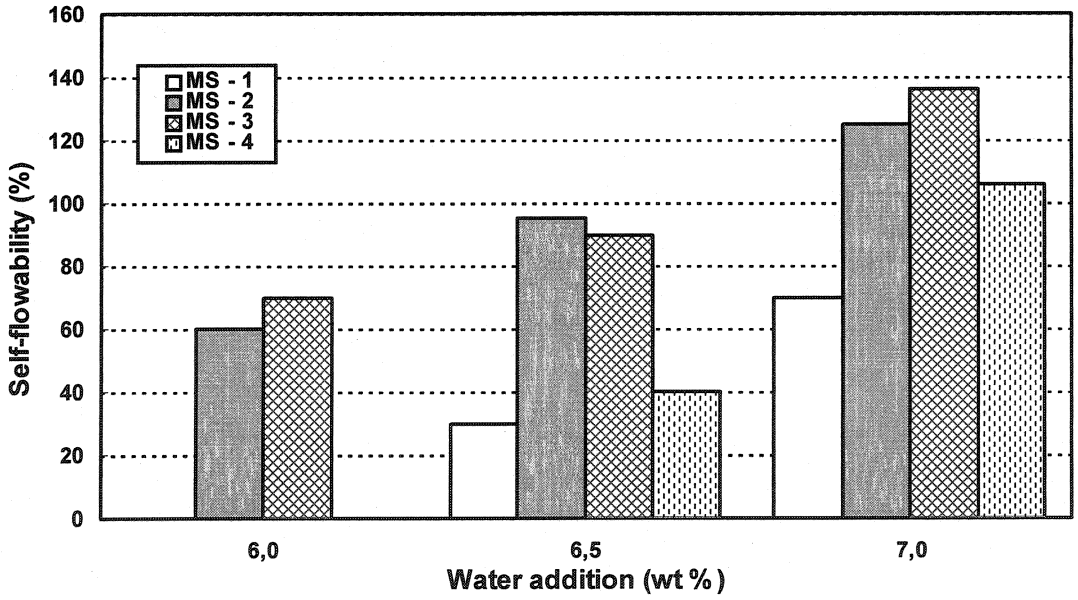


Figure 7.2 Self-flowability vs. water addition.

With 7.0 wt% water, comparing the self-flowability measured immediately after mixing with the self-flow values measured after 30 min (optimum working time), all compositions exhibited similar behaviour, except for MS-1, which hardens after 30 min

(Figure 7.3). This may be due to fast setting of MS-1, which contained less microsilica particles to surround cement grains and prevent hydration [88]. Given a minimum self-flowability of over 100 % for pumpable castables, and the fact that more water will cause segregation, the water amount for the present investigation has been fixed at 7 wt% [97].

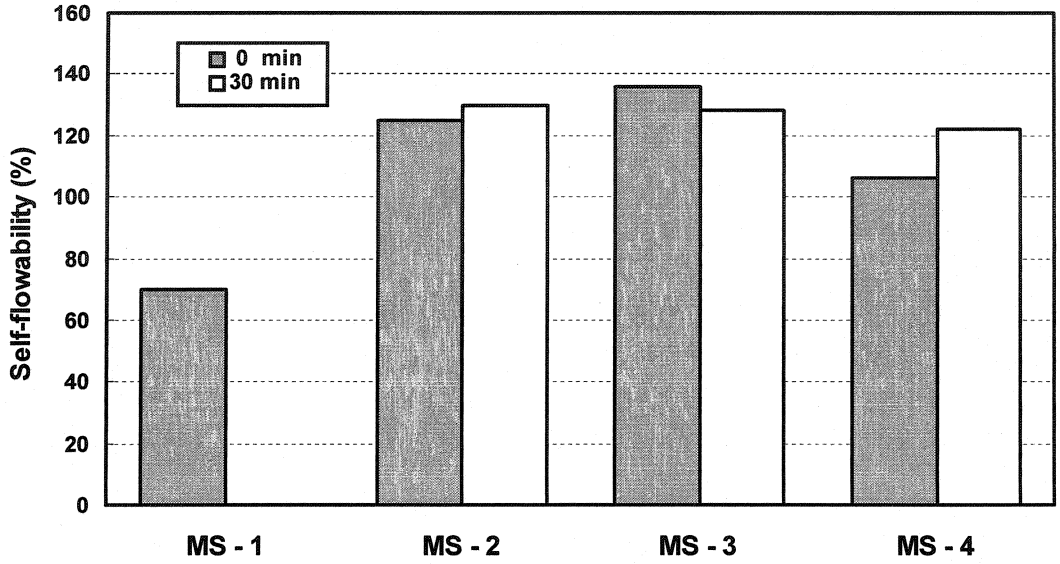


Figure 7.3 Comparison of self-flowability of the castables at different time.

7.5 Castable Rheology

7.5.1 Torque vs. Speed

The rheometer results are shown in Figure 7.4, 5 and 6 for compositions MS-2, MS-3 and MS-4 respectively. Rheological measurements on MS-1 could not be carried out as it is hard and stiff with very low self-flowability, and no further discussion on this mix is presented here. The similar nature of the rheograms of compositions MS-2 and MS-3 is achieved, as explained in Chapter 4.5.1. In the case of MS-4, the rheometer blocked at maximum speed during the first test. The second test (5 min), conducted immediately after the first attempt, is completed successfully. This indicates that mix MS-4 requires more energy for homogenization than the 3 other mixes considered in this chapter.

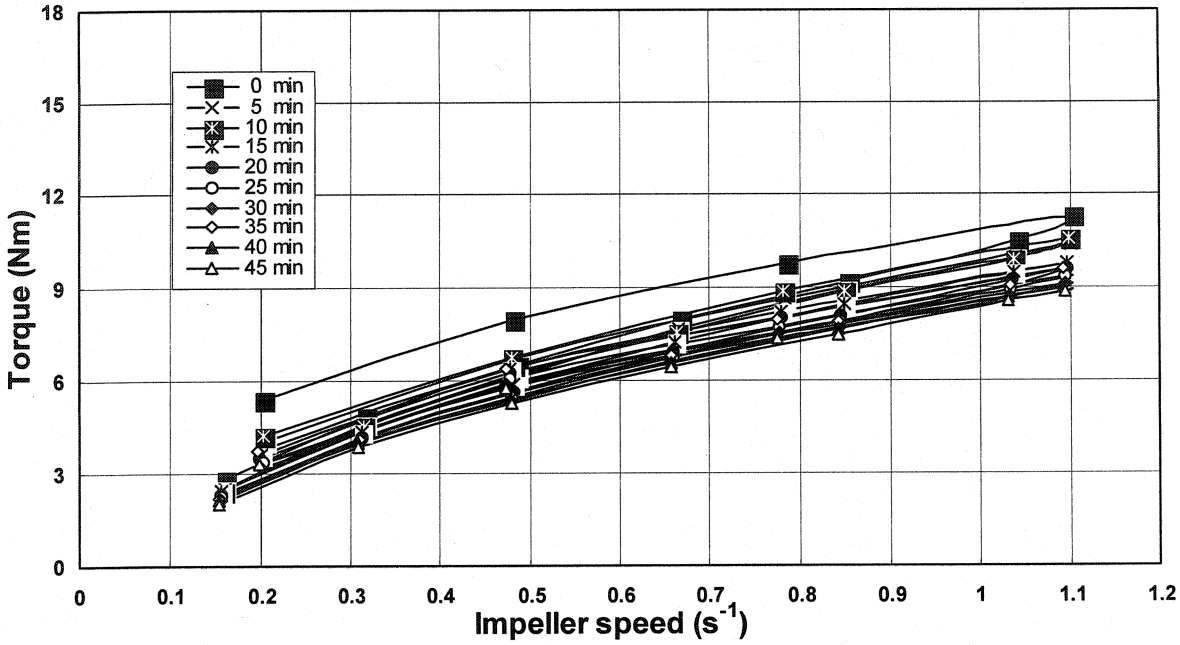


Figure 7.4 Torque vs. impeller speed for MS-2.

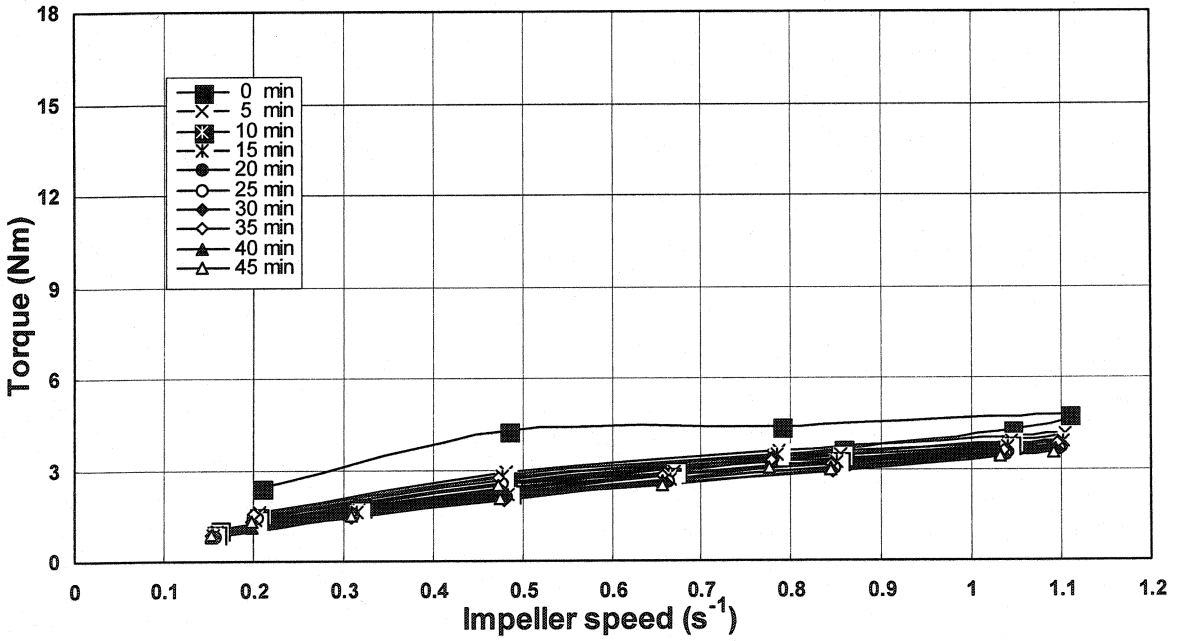


Figure 7.5 Torque vs. impeller speed for MS-3.

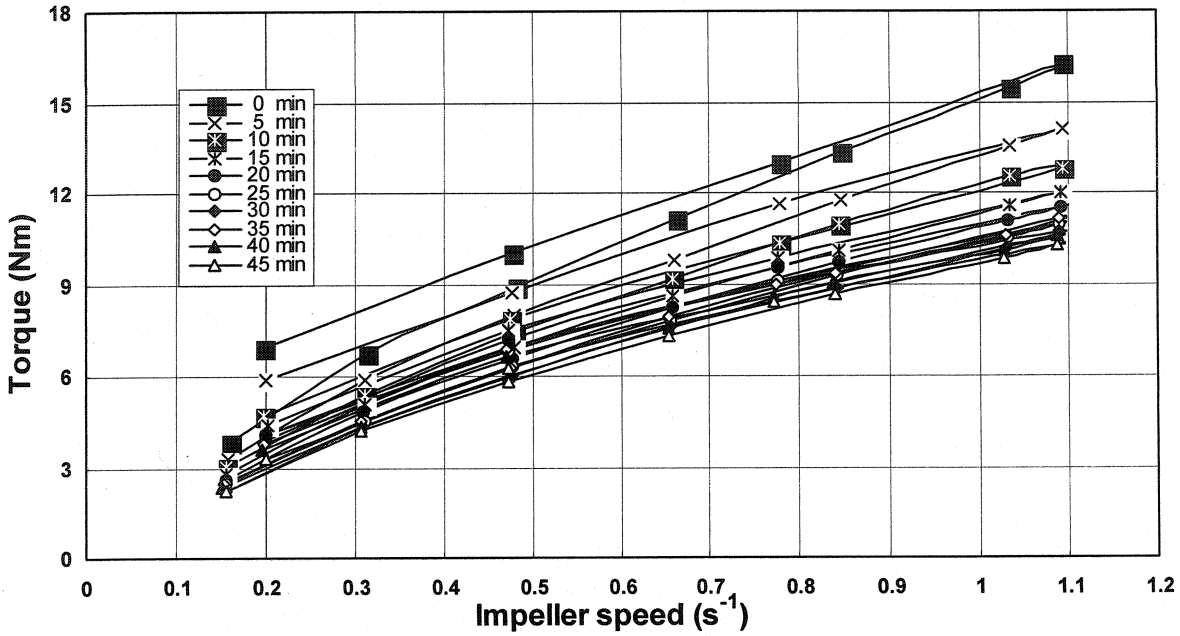


Figure 7.6 Torque vs. impeller speed for MS-4.

The same kind of behaviour has been observed for all compositions but with different rates of change of torque with speed. The loops of MS-3 compress together and overlap after 5 min, but the loops of MS-4 remain significantly and scatter at all time. The torque (T_{max}) of the three compositions MS-2, 3 and 4 at the highest impeller speed of 1.10 s^{-1} at 0 min is given in Table 7.2. In the case of MS-2 and 3, the T_{max} drastically decreases as microsilica addition increases. In the case of MS-4, the T_{max} is much higher than MS-2 with the same amount of the microsilica, indicating the different nature of the two microsilicas then used.

Table 7.2 T_{max} of the 3 compositions at the highest speed of 1.10 s^{-1} at 0 min

Composition	MS--2	MS--3	MS--4
T_{max} (Nm)	11.29	4.75	16.25

7.5.2 Equivalent Apparent Viscosity

The relationship between equivalent apparent viscosity and impeller speed for MS-2 as shown in Figure 7.7, is always very close to that of a Bingham fluid. The trends are the same for the other compositions and hence not shown.

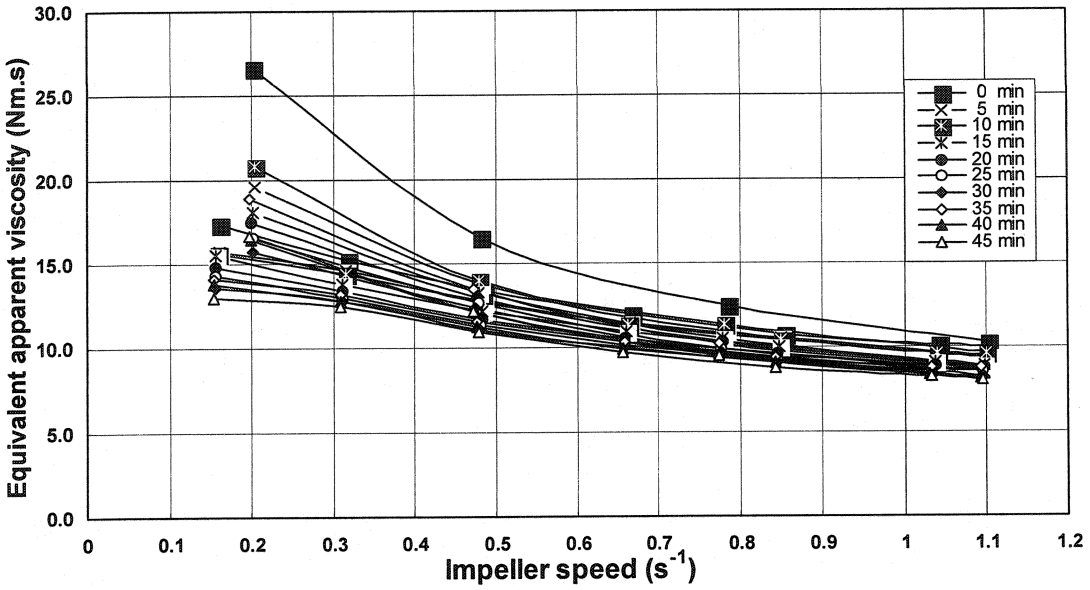


Figure 7.7 Equivalent apparent viscosity vs. impeller speed for MS-2.

7.5.3 Thixotropy

In Figure 7.8, MS-2 (a) and MS-2 (b) show the equivalent apparent viscosity calculated for the higher (1.10 s^{-1}) and lower speeds (0.48 s^{-1}) respectively (in the reverse cycle) in each five-minute cycle for mix MS-2. The values of equivalent apparent viscosity for the constant speed 0.48 s^{-1} are higher than those of 1.10 s^{-1}. All the composition has shown thixotropic effect. The equivalent apparent viscosity is decreasing and stabilizes after 20 min of testing. The set of lines of equivalent apparent viscosity between high and low speed are nearly parallel to each other. The difference between equivalent apparent viscosity values of high and low speed is expressed as a degree of thixotropy. The greater the difference, the higher the degree of thixotropy. In this study, mix MS-2 is found to be more thixotropic than MS-3. A possible explanation for this is the presence of more microsilica in MS-3, which might have covered cement grains more completely. This may have lowered the degree of hydration and conversion of cement grains [88], which is a major contributor to formation of the gel structure in castables. When MS-2 and MS-4 are compared (compositions with the same amount of microsilica but different source), MS-4 is found to be more thixotropic. It is assumed that the presence of free carbon might have covered the particles, leading to inertia and lower dispersibility.

Further investigations are required to confirm this mechanism. In all, both the amount and chemistry of microsilica influence the thixotropic behaviour of castables. In the present study, thixotropy arising due to cement hydration is well understood in Chapter 6, while the contribution from microsilica remains unclear.

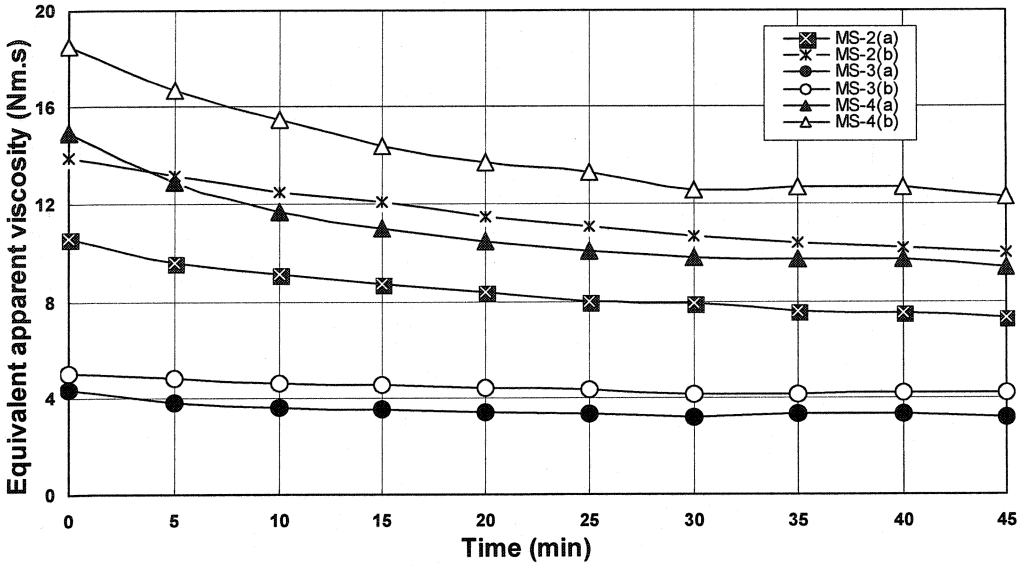


Figure 7.8 Equivalent apparent viscosity vs. time at high (a) and low (b) impeller speed.

7.5.4 Flow Resistance and Torque Viscosity

G and H values have been evaluated as described in Chapter 4.5.4. The calculated values of G and H are shown in Table 7.3.

Table 7.3 G and H values for three compositions

Time (min)	Flow resistance G (Nm)			Torque viscosity H (Nm.s)		
	MS - 2	MS - 3	MS - 4	MS - 2	MS - 3	MS - 4
0	1.86	0.59	2.29	8.65	3.61	13.05
5	1.73	0.58	1.98	8.47	3.33	11.57
10	1.62	0.56	1.79	8.27	3.22	10.83
15	1.56	0.51	1.72	8.02	3.17	9.98
20	1.52	0.51	1.57	7.78	3.04	9.6
25	1.46	0.48	1.49	7.58	3.04	9.21
30	1.42	0.48	1.33	7.43	2.92	9.01
35	1.41	0.49	1.35	7.41	2.92	8.95
40	1.4	0.5	1.34	7.4	2.93	8.91
45	1.33	0.51	1.34	7.34	2.94	8.68

The relationship between microsilica and G is plotted in Figure 7.9. As can be seen, G decreases as microsilica addition increases. The G values of MS-2 and MS-4 decrease for the initial 20 min and remain constant for the remaining test period. The reason for the decrease of G with microsilica addition is that the presence of more microsilica with the same fine mix reduces the force required for yielding the castable system (ball bearing action of spherical microsilica particles). It is also observed that G decreases with testing time, which is due to the additional mixing. Though the test is conducted to study the rheology, it also shows the effect of additional mixing energy, as discussed earlier. The castable system with additional energy requires less force to yield. The G value becomes constant after 20 min, indicating that the system has attained its saturation stage in mixing where G cannot be further reduced. It is also observed that after 20 min there is a reduction of 18 % and 31 % in G for mix MS-2 and MS-4 respectively. The G values are higher for MS-4 than for MS-2 during the first 20 min and then remain roughly similar for the remaining test duration. The reason for this trend is the presence of free carbon and its chemistry. Though the G values are higher for MS-4 than for MS-2 in the beginning, both reach roughly a similar level after 20 min of rheological testing. This again confirms the fact that MS-4 with Microsilica-2 needs more mixing time to become dispersed. In the case of MS-3 with 7.0 wt% Microsilica-1, the G values are the lowest among all compositions and remain the same throughout the test period. This again indicates the ball-bearing effect of microsilica for flow under shear.

The relationship between microsilica and H is plotted in Figure 7.10. The H values of MS-4 are the highest, followed by MS-2 and MS-3. The H values of all compositions decrease for the initial 20 min and remain constant during further testing. After 20 min, there is a reduction of about 10 % and 26 % for mixes MS-2 and MS-4 respectively. The presence of more microsilica gave better lubrication in MS-3 at a higher shear rate and thus led to a lower viscosity compared with MS-2. When comparing MS-2 with MS-4 of same microsilica content but different source, the different behaviour is attributed to the

impurity in microsilica and its effect on dispersion. The results are in line with literature [98].

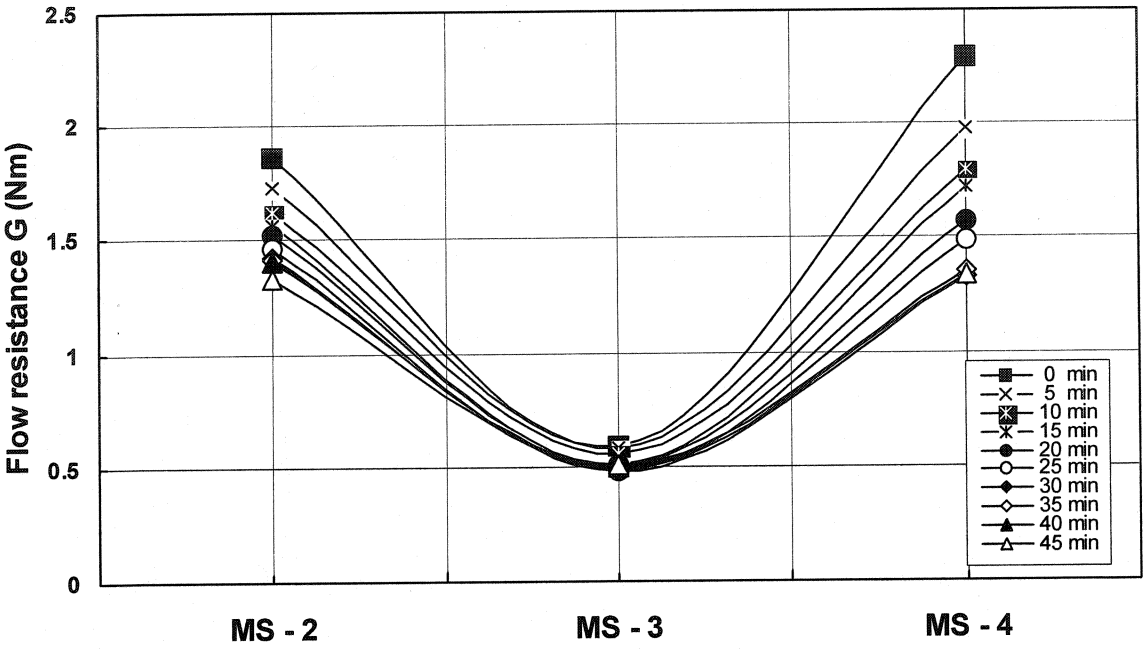


Figure 7.9 Flow resistance vs. microsilicas.

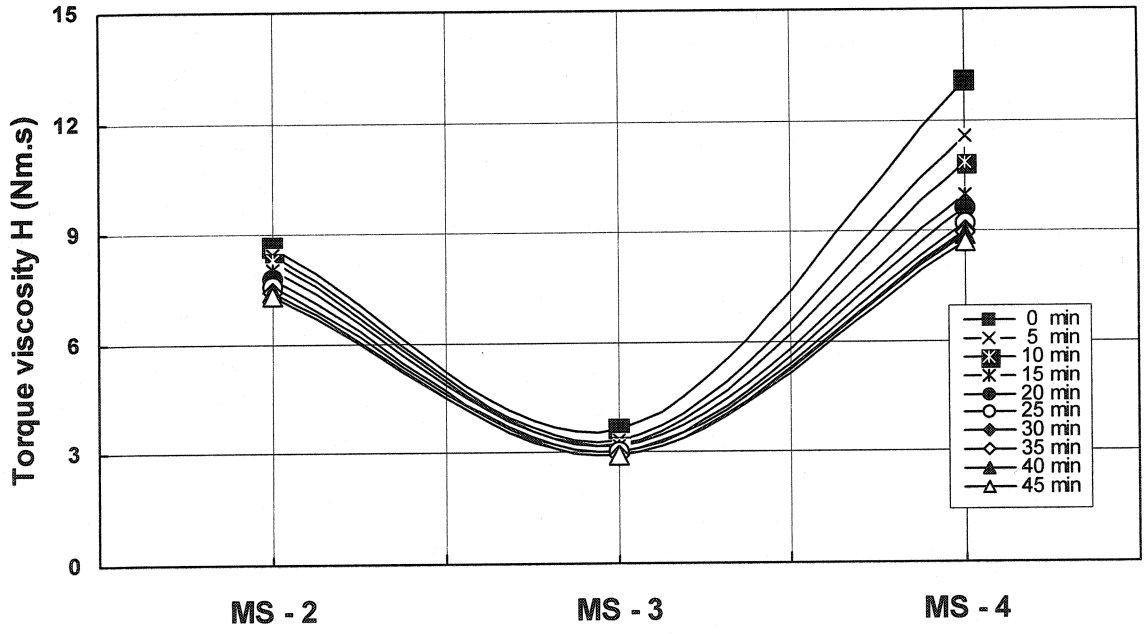


Figure 7.10 Torque viscosity vs. Microsilicas.

7.6 Matrix Rheology

7.6.1 Shear Stress vs. Shear Rate

The shear stress as a function of shear rate of the matrix slurries of the four castables is shown in Figure 7.11. The shear stress in the forward cycle (shear rate increasing) is higher than rate in the reverse cycle (shear rate decreasing) and then forms a hysteresis loop. The forward cycle reveals the pseudoplastic nature of the slurry, while the reverse cycle displays a Bingham behaviour. In the case of the compositions MS-1, 2 and 3, at different content of Microsilica-1 (Elkem 971U), the loops looks similar and but shift downwards, at higher microsilica content. The loop for MS-4, with Microsilica-2, is ranked at the highest place, when compared to MS-2 with Microsilica-1, at the same level.

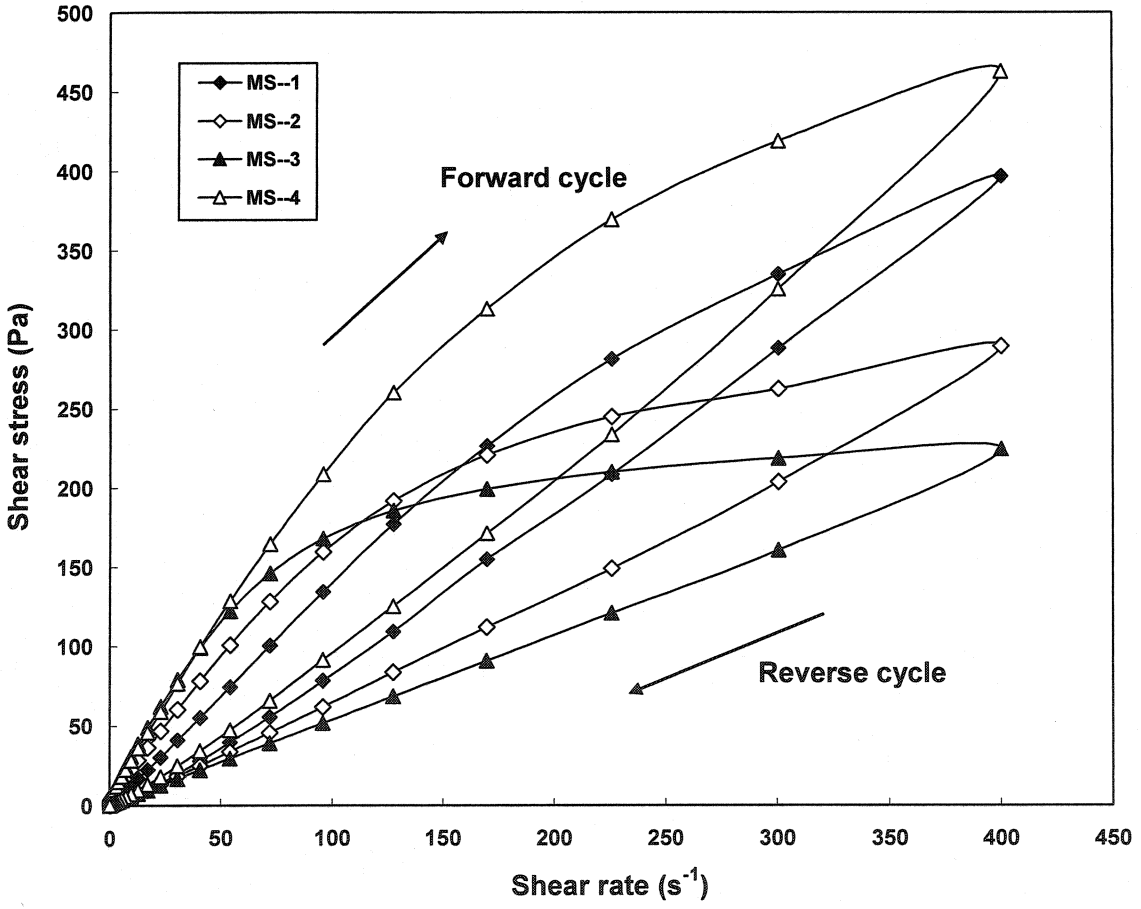


Figure 7.11 Shear stress vs. shear rate for all the matrix slurries.

The shear stress (τ_{max}) at the highest shear rate of 400 s^{-1}, is given in Table 7.4. The τ_{max} decreases with Microsilica-1 (Elkem 971U) addition increasing. In the case of MS-4 with 5 wt% Microsilica-2, the τ_{max} is the highest. As shown in Table 7.2, the trends for the castables and the matrix slurries are the same.

Table 7.4 τ_{max} of the 4 compositions at the highest shear rate of 400 s^{-1}

Composition	MS--1	MS--2	MS--3	MS--4
τ_{max} (Pa)	397	290	224	463

7.6.2 Apparent Viscosity vs. Shear Rate

The apparent viscosity as a function of shear rate of the matrix slurries of castables MS-1, 2, 3 and 4 is shown in Figure 7.12.

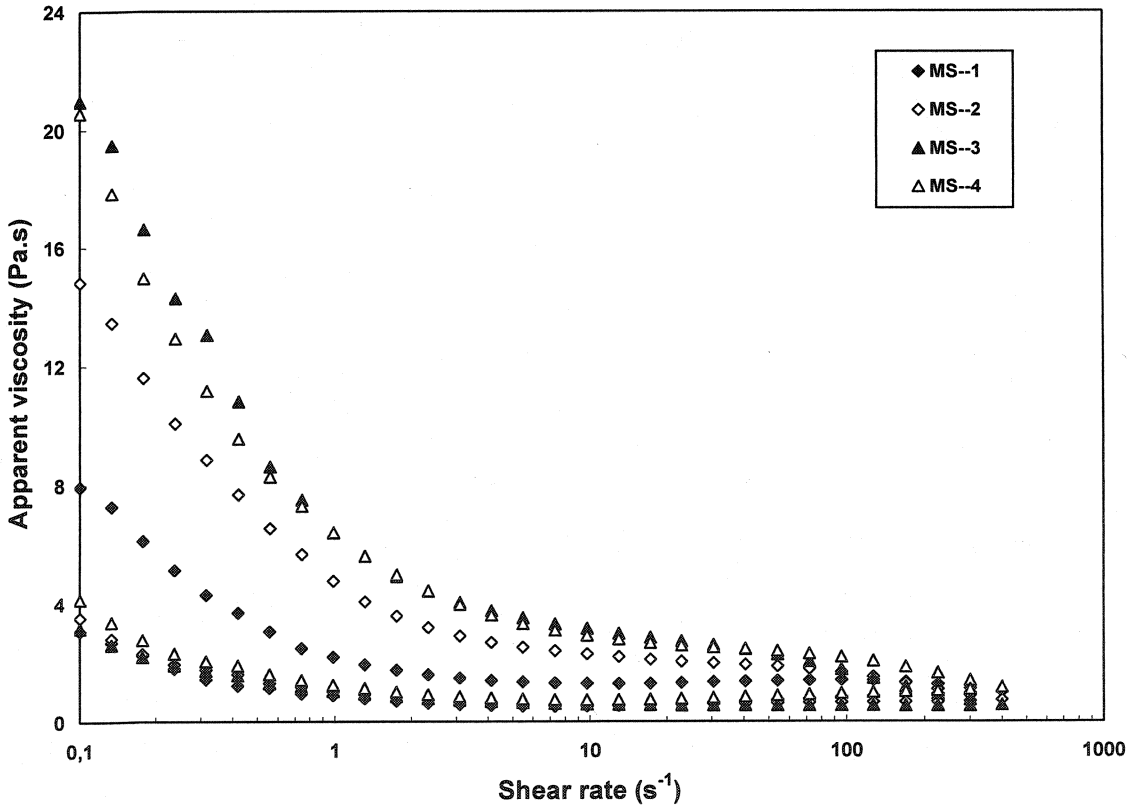


Figure 7.12 Apparent viscosity vs. shear rate for all the matrix slurries.

The apparent viscosity in the forward cycle (shear rate increasing) is higher than the rate in the reverse cycle (shear rate decreasing). In the forward cycle, the apparent viscosity

decrease sharply from 0 to 5.0 s^{-1}, remains similar till 100 s^{-1} and finally slightly decreases till to 400 s^{-1}. The apparent viscosity of MS-3 is the highest, followed by MS-4, 2 and 1, respectively. In the reverse cycle, the apparent viscosity of all the compositions remains similar from the shear rates 400 s^{-1} to 1 $^{-1}$ and then slightly increase at very low shear rates, below 1 $^{-1}$.

7.6.3 Thixotropy

The thixotropy degree and loops's area of the four matrix slurries MS-1 to MS-4 are shown in Figure 7.13. The two parameters have been calculated as described in Chapter 4.6.3. The thixotropy degree increases as the Microsilica-1 (Elkem 971U) content increases. In the case of MS-4 with microsiclia-2, the thixotropy degree is the highest among all the slurries. The loops' area also shows the same trend.

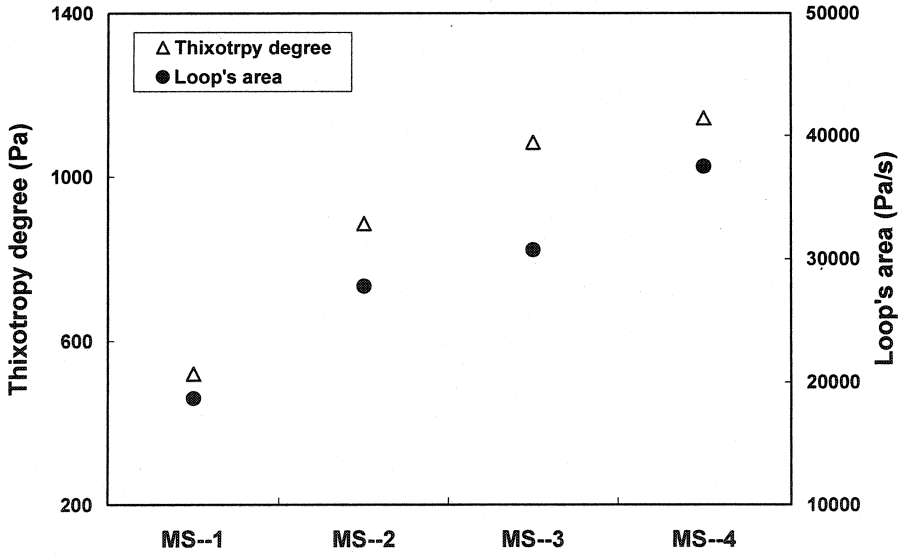


Figure 7.13 Thixotropy degree and loop's area for all the matrix slurries.

7.6.4 Plastic Yield Stress and Plastic Viscosity

The calculation method for plastic viscosity and yield stress has been described in Chapter 4.6.4. The plastic viscosity and yield stress of the matrix slurries increase as Microsilica-1 increases, as shown in Table 7.5. In the case of MS-4, the plastic viscosity is the highest and plastic yield stress is slightly higher than MS-2 with the same amount of microsilica, but different in nature.

Table 7.5 Plastic viscosity and yield stress of all the matrix slurries

Composition	MS--1	MS--2	MS--3	MS--4
Plastic viscosity (Pa.s)	1.346	1.829	2.263	2.321
Plastic yield stress (Pa)	0.186	3.512	6.192	4.874

7.7 IPS of Matrix and MPT of Castables

The calculated values of IPS and MPT of MS-1, 2 and 3 are given in Table 7.6. The IPS of the matrix slurries significantly decrease when the microsilica content increases. On the contrary, when increasing microsilica, the MPT of the castables increases. The IPS and MPT of MS-4 is considered being the same as MS-2 with same amount of microsilica and specific surface area.

Table 7.6 IPS of the matrix slurries and MPT of the castables

Composition	MS--1	MS--2	MS--3
IPS (nm)	129.4	87.9	58.9
MPT (μm)	121.1	123.8	126.6

7.8 Mechanical and Physical Properties

The CMOR and AP of all compositions are given in Table 7.6. With the same amount of water addition, and even if MS-1 sample is made by vibration, its CMOR average value is the lowest and its AP value the highest. This relates to the flowability discussed in Section 7.4. The CMOR and AP values for MS-2, MS-3 and MS-4, which are cast by sell-flowing, are similar, at around 8-10 MPa and 18 %, respectively.

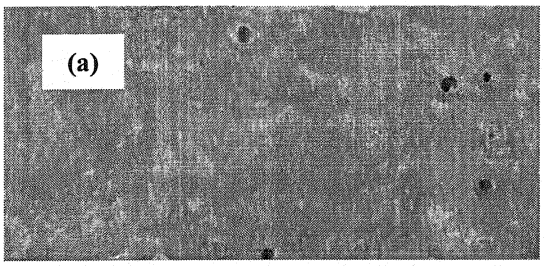
Table 7.7 CMOR and AP of all the compositions

Composition	CMOR (MPa)		AP (%)	
	0 min.	45 min.	0 min.	45 min.
MS-1 (vibration cast)	6.3	--	19.8	--
MS-2	9.3	8.7	18.2	17.8
MS-3	8.7	8.1	17.6	18.4
MS-4	8.6	9.8	17.8	17.9

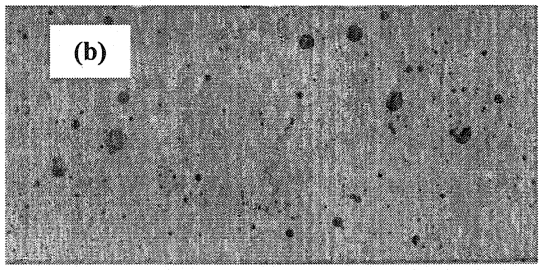
7.9 Appearance of Samples

Figures 7.14 (a)-(n) shows the appearance of castables as a function of test time. MS-1 samples are vibration cast while the others are self-flow castables. Although the MS-1

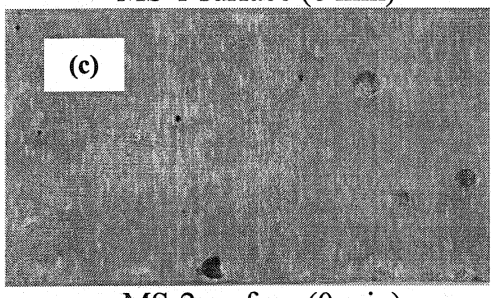
material is exposed to vibration after mixing, there are many casting defects on the side surface (b) showing the height of the sample, and more than on the top surface (a). The appearance of MS-2 samples is good both after 0 and 45 min, with some degassed bubbles on the top surface of the samples cast after 45 min (e). Composition MS-3 shows a large number of severe casting defects (honeycomb structure) on the lateral surface cast after 0 and 45 min. In the case of MS-4, there are some casting defects on the lateral surface after 0 min which, however, decreased after 45 min. The top surface coloration is due to the segregation of the undispersed fine carbon particles in Microsilica-2.



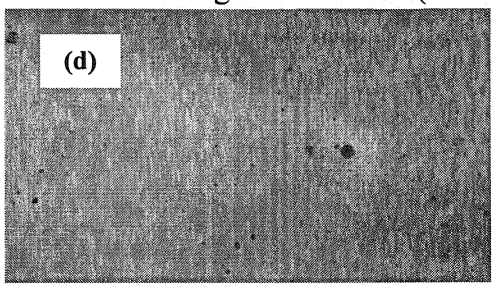
MS-1 surface (0 min)



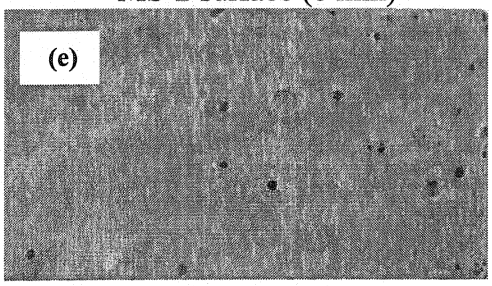
MS-1 side with degassed bubbles (0 min)



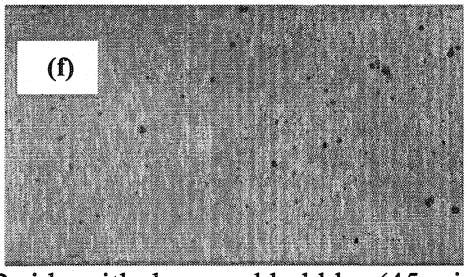
MS-2 surface (0 min)



MS-2 side with degassed bubbles (0 min)



MS-2 surface (45 min)



MS-2 side with degassed bubbles (45 min)

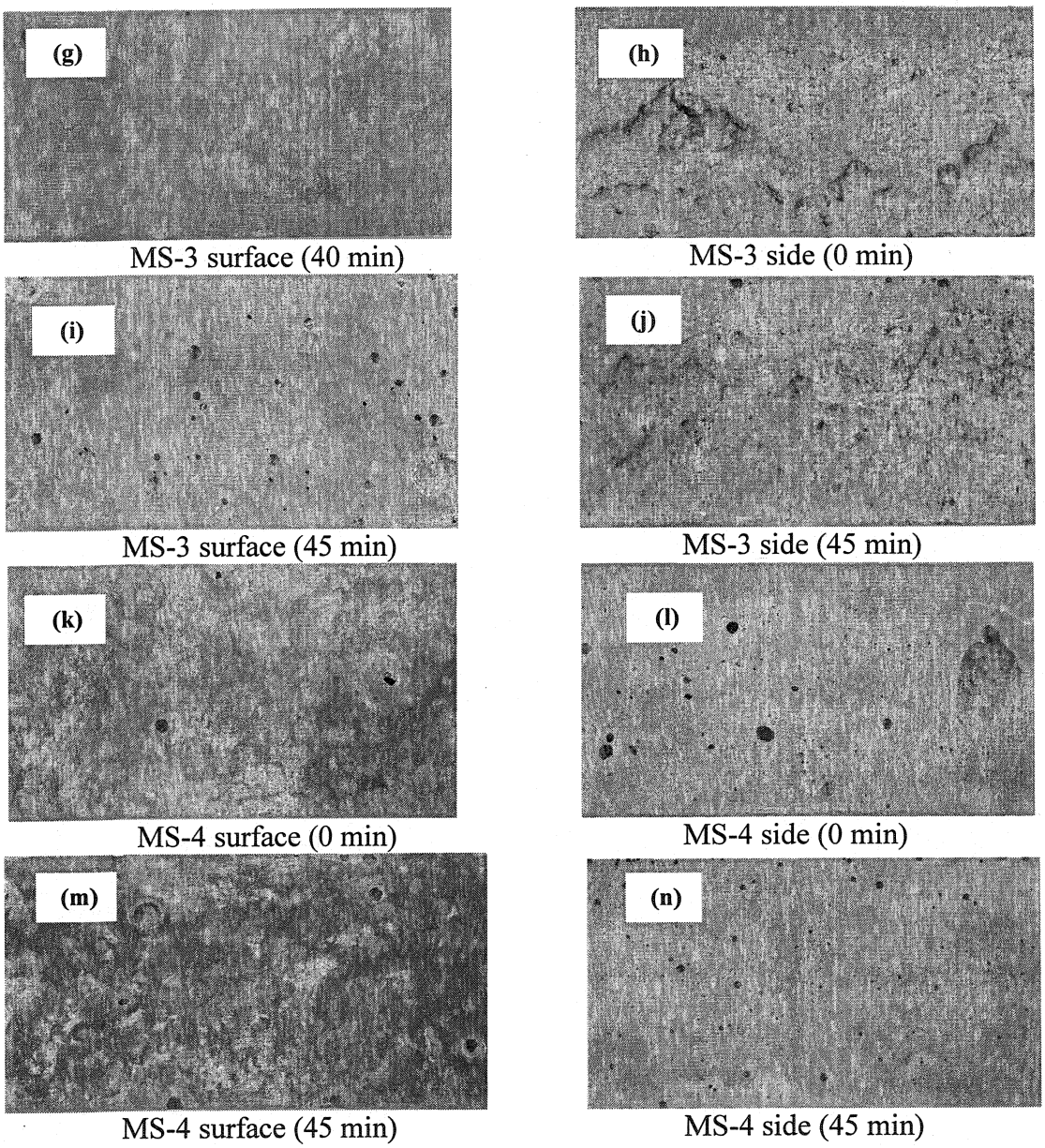


Figure 7.14 (a)-(n) Appearance of samples MS-1, 2, 3 and 4 cast at different time.

7.10 Optimization of Castables

In this work, MS-3 and MS-4 showed good self-flowability with varying amounts of water (Figure 7.2), but both are ranked poorly in terms of pumpability. As already shown in the previous chapters, for good pumpability, a castable must possess an optimum combination of torque viscosity and flow resistance in order to flow well and

to avoid blockage and segregation. The relationship between G and H is shown in Figure 7.15. With composition MS-3, G and H are too low, and segregation phenomena have been observed (Figure 7.14). In the case of MS-4, the G values are very high initially and the very high torque viscosity may lead to blockage. MS-2 provides higher G and H than MS-3, and lower G and H than MS-4. This indicates that the values of G and H should be above a critical value to avoid segregation and below a key value to avoid blockage. Hence composition MS-2 appears to provide the optimum combination. As can be seen, there is a drastic decrease in G and H with 7.0 wt% Microsilica-1, and with 3.0 wt% Microsilica-1, the mix does not flow well. With 5 wt% of Microsilica-1, optimal values of G and H are obtained. This means that an optimum amount and type of microsilica are required to avoid blockage inside pipes and sufficient viscosity is required to avoid segregation by maintaining flowability, coherence, integrity and stability of the castable mix.

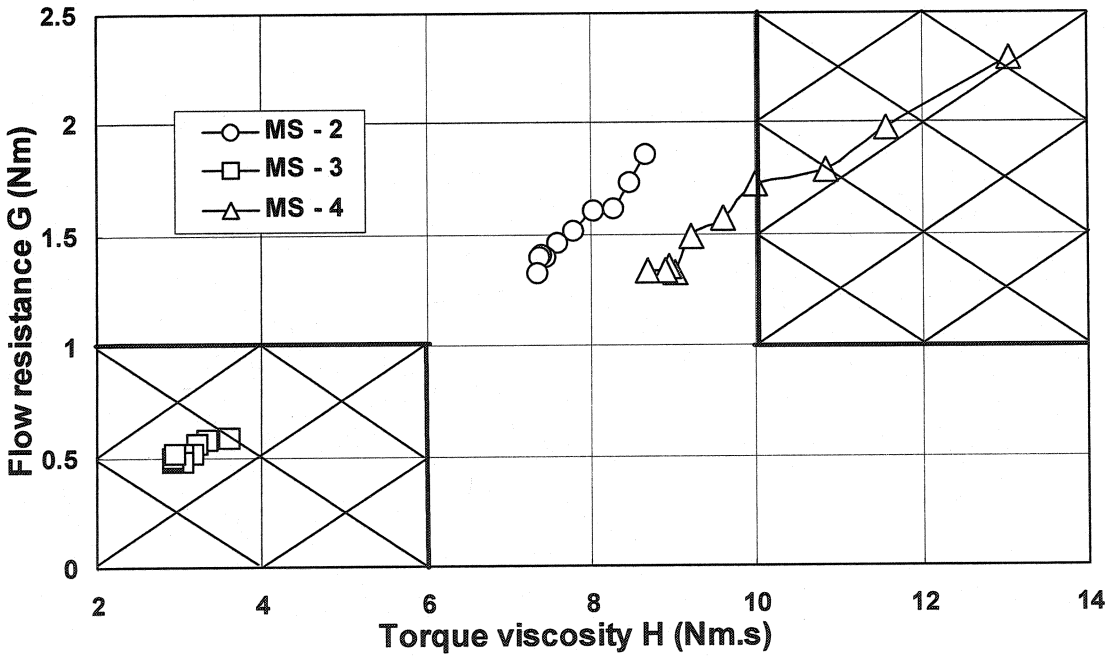


Figure 7.15 Flow resistance vs. torque viscosity

7.11 Conclusions

The rheological behaviour of bauxite-based low-cement castables and their matrix slurries have been studied using the proper rheometer. The conclusions based on this investigation are:

a) Type and amount of microsilica play a major role in the flowability of castables. In this study, Microsilica-1 showed better performance with respect to flowability, than Microsilica-2, containing carbon as a major impurity.

b) All the mixes displayed Bingham behaviour. Increasing microsilica content does not mean better rheology. It is observed that the castable with 5 wt% microsilica is rheologically more favourable than the mix with 7 wt% microsilica under given conditions.

c) The chemistry of microsilica (presence of soda and carbon) influences the rheological properties of mixes.

CHAPTER 8 - FINE FILLERS: REACTIVE ALUMINA

In this chapter, the influences of the type and amount of fine-filler materials bauxite and reactive alumina, on the rheological behavior of bauxite-based low-cement castables, with fixed amount of microsilica and calcium aluminate cement, have been investigated. The two rheological parameters measured, i.e. flow resistance G and torque viscosity H, have revealed that insufficient fine fillers result in serious segregation, but excessive fine fillers cause high rigidity and viscosity of the mixes. The correlation of the measured rheological parameters with workability and pumpability of the castables are discussed.

8.1 Introduction

Aggregates, fine fillers such as reactive alumina and microsilica, additives such as deflocculants, accelerators and retarders, and calcium aluminate cement (CAC) are generic elements for modern dense castable systems [82]. Dense castable can be considered as a mix in which coarse aggregates are surrounded by the matrix paste of reactive fillers. Matrix paste can also be seen as a suspension of small solid particles in water with a solid content usually 60-75 vol. %, while the castable itself contains up to 80-90 vol. % solid.

Some castables may be self-flowing but not necessarily pumpable. A pumpable castable should have adequate pumpability and workability [25, 99]. The pumpability of a castable refers to its mobility and stability under pressure within an enclosed hose [25]. Mobility and stability are related to rheological properties of a castable but may act differently. The degree of mobility of a castable can be referred to self-flowability, which indicates the degree of self-levelling of the castable under its own weight after mixed with water. It is relatively easy to measure mobility by flow table test using a cone described as ASTM C 1445-99 [70, 100]. However, the stability of a castable, which can be defined as the capacity to maintain its initial homogeneity during

transporting, handling and placing, is a complex parameter to measure, for which no standard test has yet been defined.

Attempts to predict the pumpability from self-flowability test alone have not always been successful, both mobility and stability are to be kept in balance for a good pumpable castable. Mobility can be improved by increasing the fine matrix content of the castable and/or the water addition. However, excessive amount of fine matrix or water addition may result in higher shrinkage and creep, and lower strength and spalling resistance in use. On the other hand, production of castables with higher fine matrix content is less economical, requiring more energy for powder-grinding. An important consideration in designing pumpable castable is the proper selection of PSD to insure a good packing efficiency and additives to achieve adequate mobility. Stability can be influenced by factors such as additives and nature of raw materials, and is harder to control. Workability, among other issues, means also adequate working time for castable placement, which can be adjusted by properly using accelerator or retarder. Working time is usually estimated by flow decay testing [77, 101]. If the above-mentioned properties for castables cannot be optimized, some difficulties are to be expected during placement.

A general problem encountered during pumping a castable is the blockage in the hose due to quick setting and/or segregation of the castable. Quick setting of a castable during placing may be caused by an increase of temperature in the hose due to excessive castable-wall friction, warm working environment or inappropriate selection of additives. Setting time can be controlled by selecting appropriate additive type and dosage during development of the castable. Lubrication is needed to reduce friction during the pumping. In practice, the grout (matrix paste) acts generally as lubrication. In Figure 8.1, the castable moving into the hose is represented as a solid plug, surrounded by a lubricating layer that is formed by fine matrix of the castable.

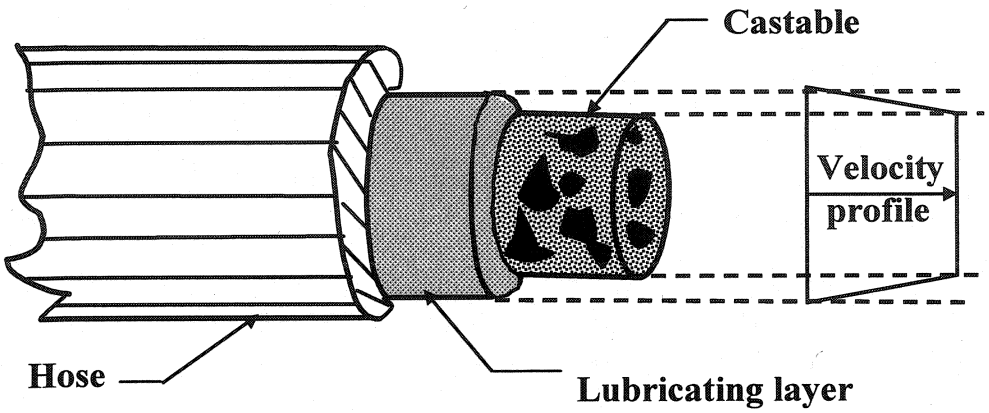


Figure 8.1 Plug flow of a castable in hose [25].

Segregation is a phenomenon of separation of matrix and aggregates, and it can be avoided by choosing proper aggregate-to-matrix and water-to-matrix ratios. These parameters directly influence the viscosity and flow of the castable. Many researchers have attempted to correlate the rheology of a castable with that of its fine matrix [6, 8], while neglecting the influence of coarse aggregates. Figure 8.2 illustrates how segregation leads to local expulsion of matrix paste and causes the aggregates to come into direct contacting with the hose, resulting in high frictional resistance and/or hose expansion. A "saturated" castable, containing enough matrix paste to fill all voids among the aggregates is easier to pump than an "unsaturated" (insufficient matrix content) one. Local transition from saturated to unsaturated state may take place during pumping, causing blockage in the hose. Therefore, the study on the rheological behaviour of a castables is very important with respect to field placement. In particular, proper selection of fine fillers and understanding their role and influence can help solve placement-associated problems.

In this work, the influence of fine fillers on pumpability is investigated in terms of the rheological parameters G (flow resistance) and H (torque viscosity). Optimization of flow resistance and torque viscosity with respect to pumpability is also reported.

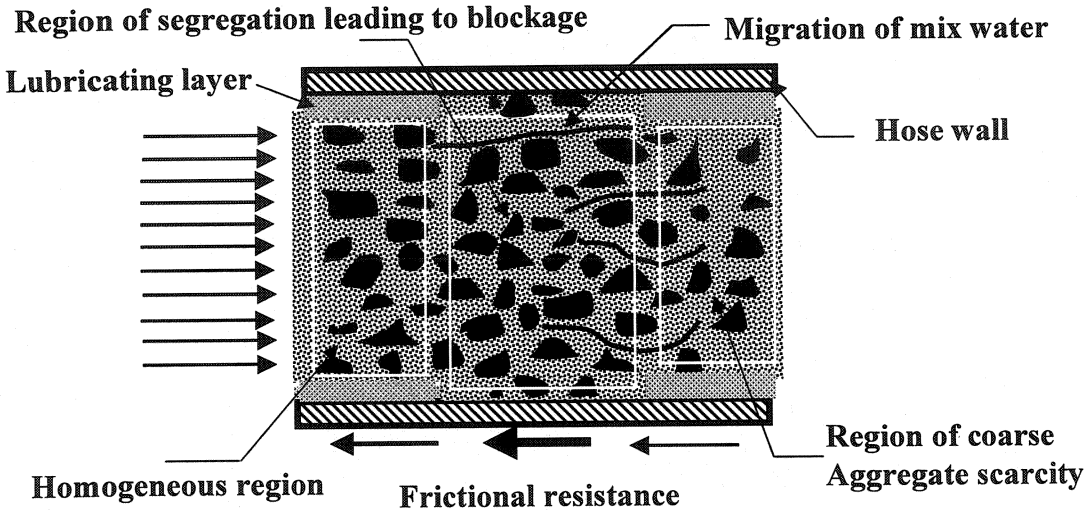


Figure 8.2 Schematic show of the segregation of a castable in hose [25].

8.2 Compositions

The composition details for this step are given in Table 8.1. The castables are still with the same q value of 0.26 and D_{max} of 5 mm. The cement and microsilica contents are fixed at 4 and 5wt%, respectively, such a formulation providing satisfactory result, as shown in previous chapters. The coarse aggregate content is fixed at 59wt% for all the castable compositions. The dispersant addition is fixed at 0.12 wt%.

Table 3.11 Details of castable mixes to study the effect of fine fillers

Castable		FM - 1	FM - 2	FM - 3	FM - 4	FM - 5
Aggregate (wt%)		59	59	59	59	59
Fine matrix (wt%)	Bauxite-1	11	11	11	11	11
	Bauxite-2	18	12	6	12	12
	Bauxite-3	**3**	**9**	**15**	**0**	**0**
	A 3000FL	**0**	**0**	**0**	**9**	**0**
	A 1000SG	**0**	**0**	**0**	**0**	**9**
	Cement CA-14	4	4	4	4	4
	Microsilica 971U	5	5	5	5	5
Dispersant SHMP (wt%)		0.12	0.12	0.12	0.12	0.12

8.3 PSD of Castable Compositions

The aggregates are the same for all compositions shown in Table 8.1. In this chapter, only the effects on PSD of different amounts of fine fillers: Bauxite-3, reactive alumina

A 3000FL and A 1000SG are considered. Figure 8.3 illustrates the PSD curves for compositions FM-1, 2 and 3, with increasing amount of ultra-fine particles Bauxite-3, which affects the percentages of particles between 1 and 100 μm in the matrix portion.

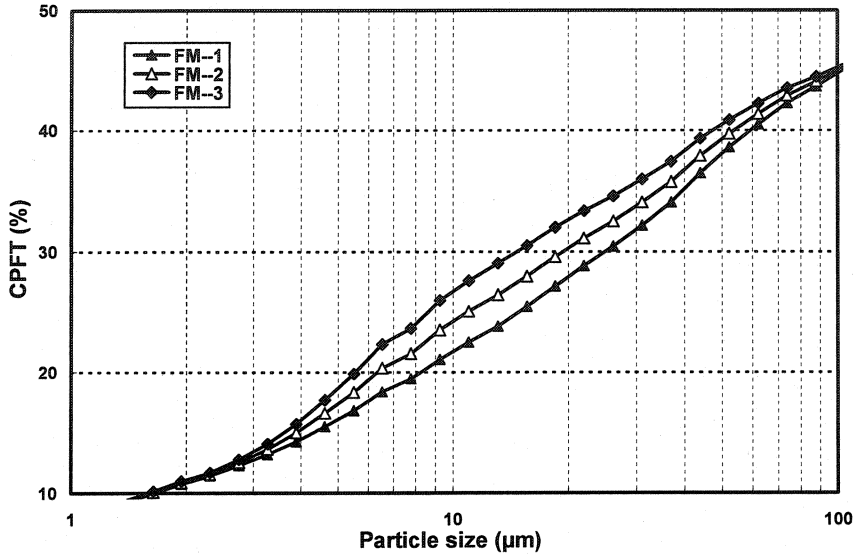


Figure 8.3 PSD of FM-1, 2 and 3 between 1 and 100 μm with different Bauxite-3.

Figure 8.4 compares the different PSD curves in the region between 1 and 10 μm for compositions FM-2, 4 and 5 with the same amount of fine fillers but of different types. The percentage of the submicron particles in those compositions are 7.8, 9.4 and 13.0 % for FM-2, 4 and 5, respectively.

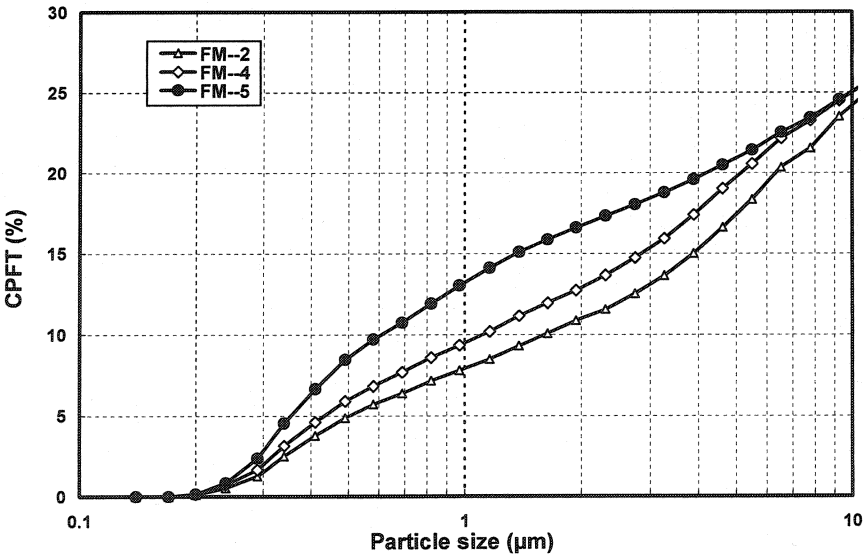


Figure 8.4 PSD of FM-2, 4 and 5 between 0.1 and 10 μm with different fine fillers.

8.4 Water Demand and Self-flowability

Self-flowability, measured for the five compositions as a function of water, is shown in Figure 8.5. Composition FM-4, which contains A3000FL alumina, exhibits in every case, at 6.0, 6.5 and 7.0 wt% addition of water, the best self-flow characteristic. Composition FM-5 containing ultra-fine A 1000SG alumina, is a sticky mix at 6.5 and 7.0 wt% water, most probably because of its use of particles with higher surface area and then faster coagulation. The compositions FM-1, FM-2 and FM-3 containing bauxite fines, have shown decreasing self-flowability with increasing Bauxite-3 content. This is due to the presence of excess fines in the matrix. FM-1 with 3 wt% bauxite-3 results in serious segregation. Though the self-flowability of FM-1 is higher compare to FM-2 and FM-3, composition FM-1 cannot be considered as a good mix due to this reason. Considering the minimum self-flowability as 100% for pumpable castable, the water amount for the present investigation has thus been fixed at 7 wt %.

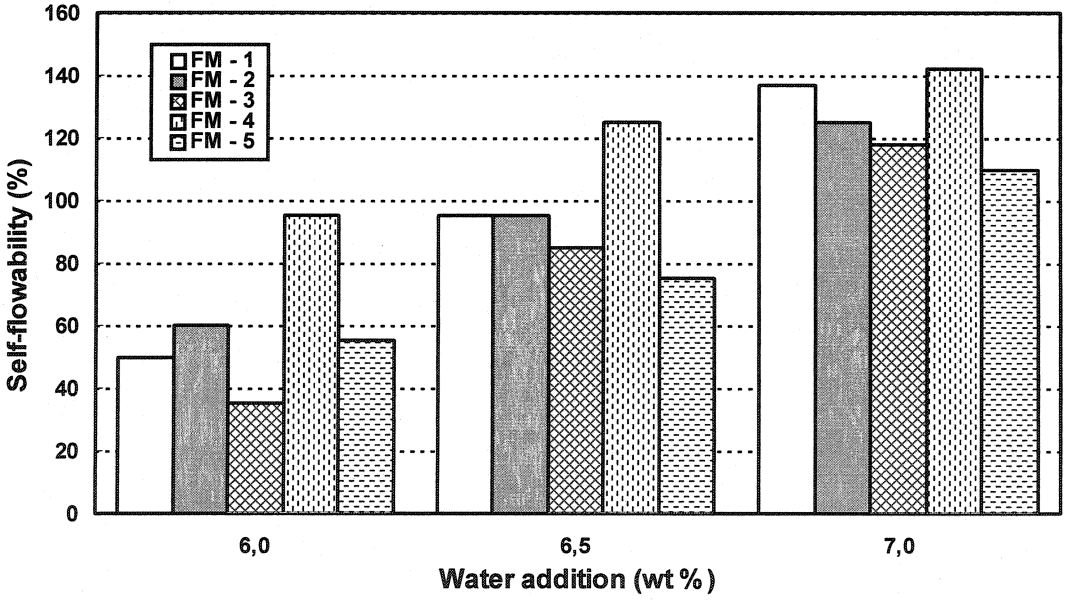


Figure 8.5 Self-flowability vs. water addition.

The self-flowability 0 min (immediately after mixing) and after 30 min of different compositions with 7.0 wt% water is compared in Figure 8.6. The self-flow values for all compositions are almost around 120% when measured at 0 min except for the composition FM-5. Good self-flowability is retained for all compositions after 30 min.

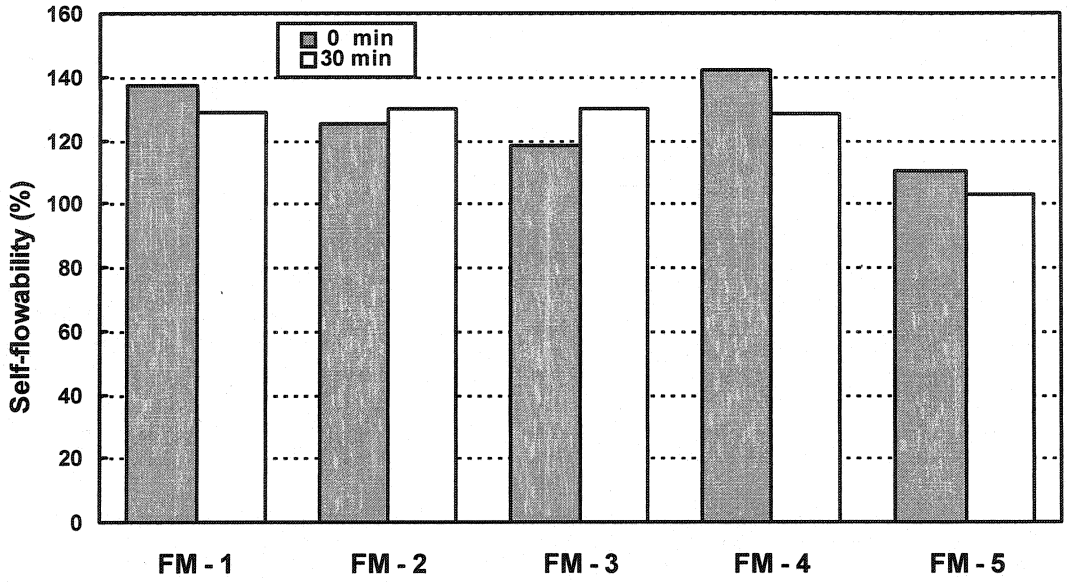


Figure 8.6 Comparison of self-flowability of the castables at different time.

8.5 Castable Rheology

8.5.1 Torque vs. Speed

The rheometer results for the compositions FM-1, 2, 3, 4 and 5 are shown in Figure 8.7, 8, 9, 10 and 11, respectively.

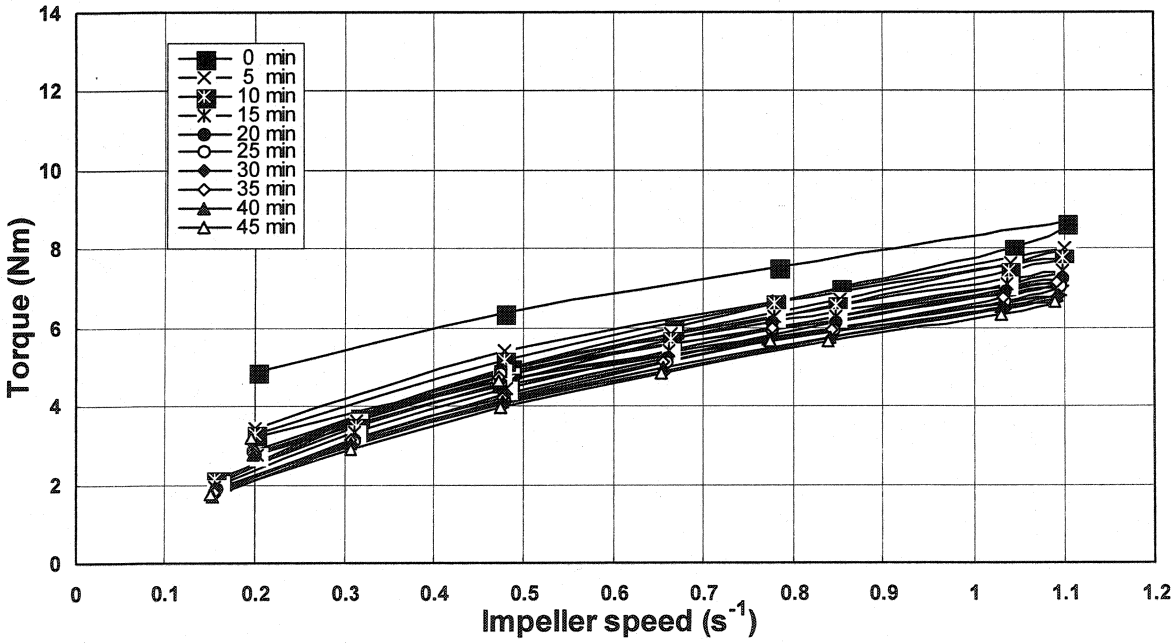


Figure 8.7 Torque vs. impeller speed for castable FM-1.

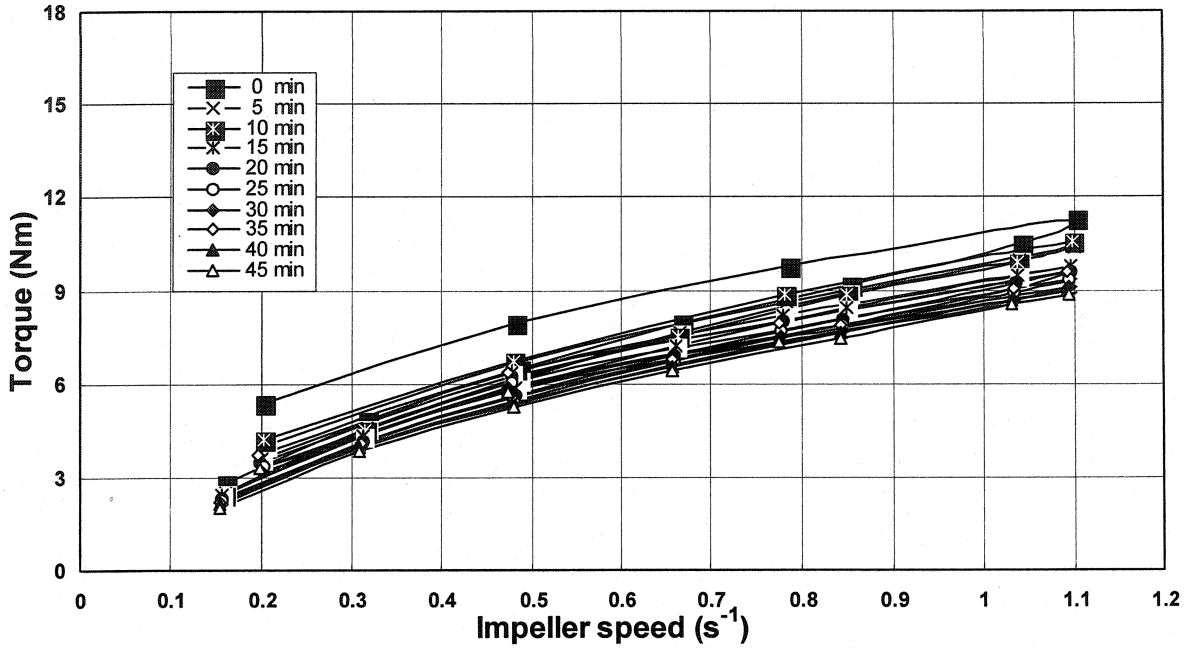


Figure 8.8 Torque vs. impeller speed for castable FM-2.

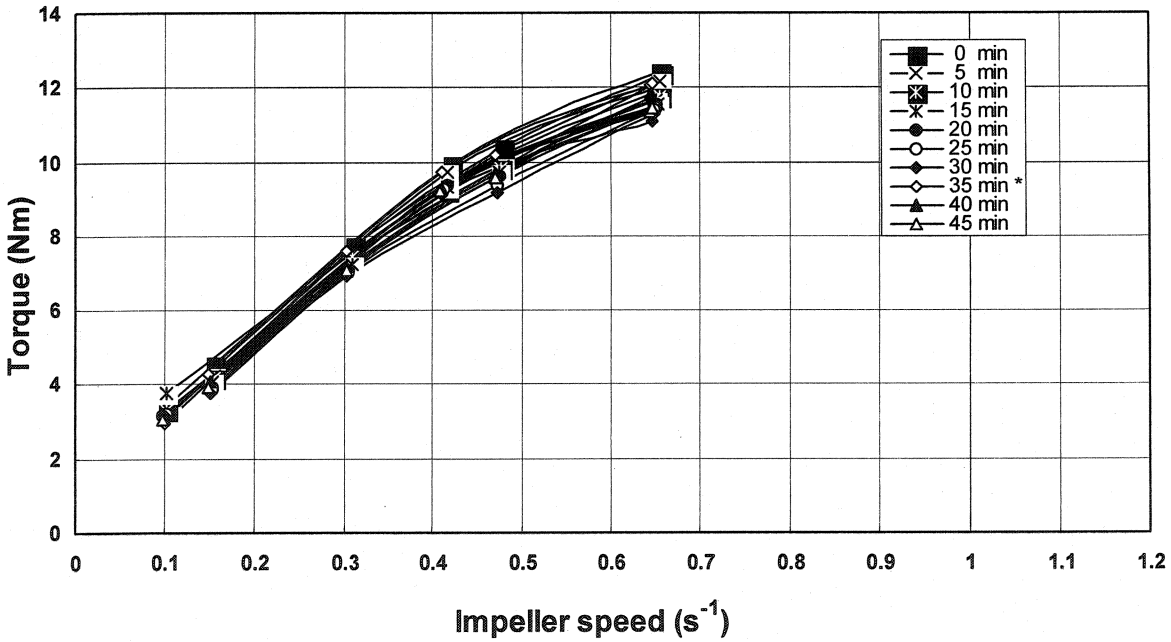


Figure 8.9 Torque vs. impeller speed for castable FM-3.

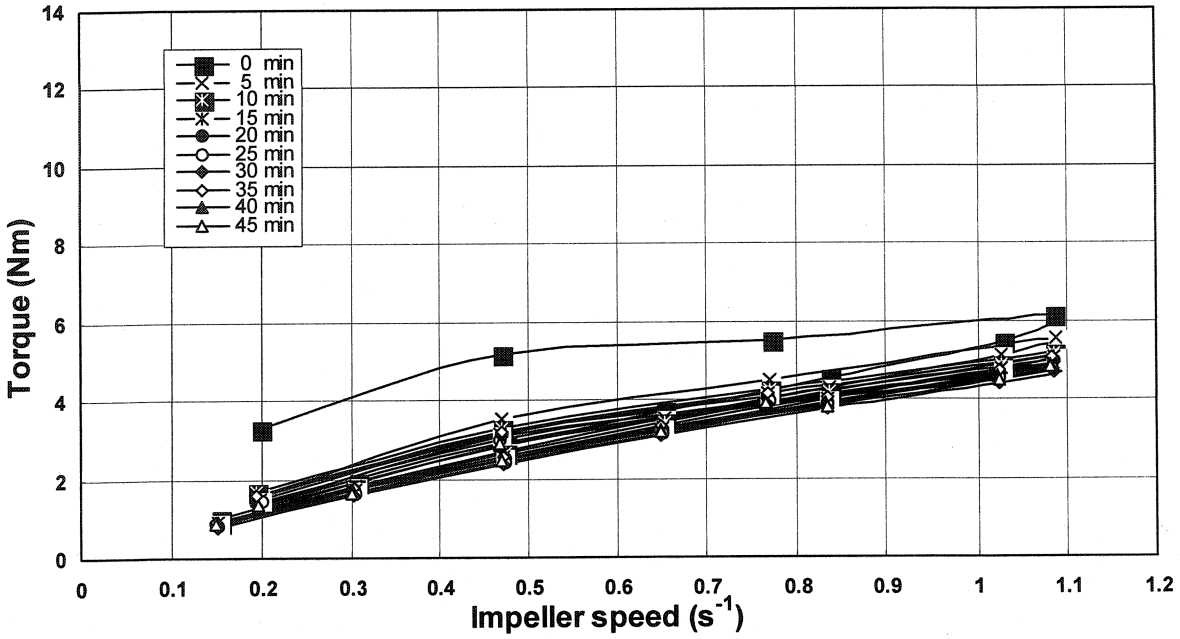


Figure 8.10 Torque vs. impeller speed for castable FM-4.

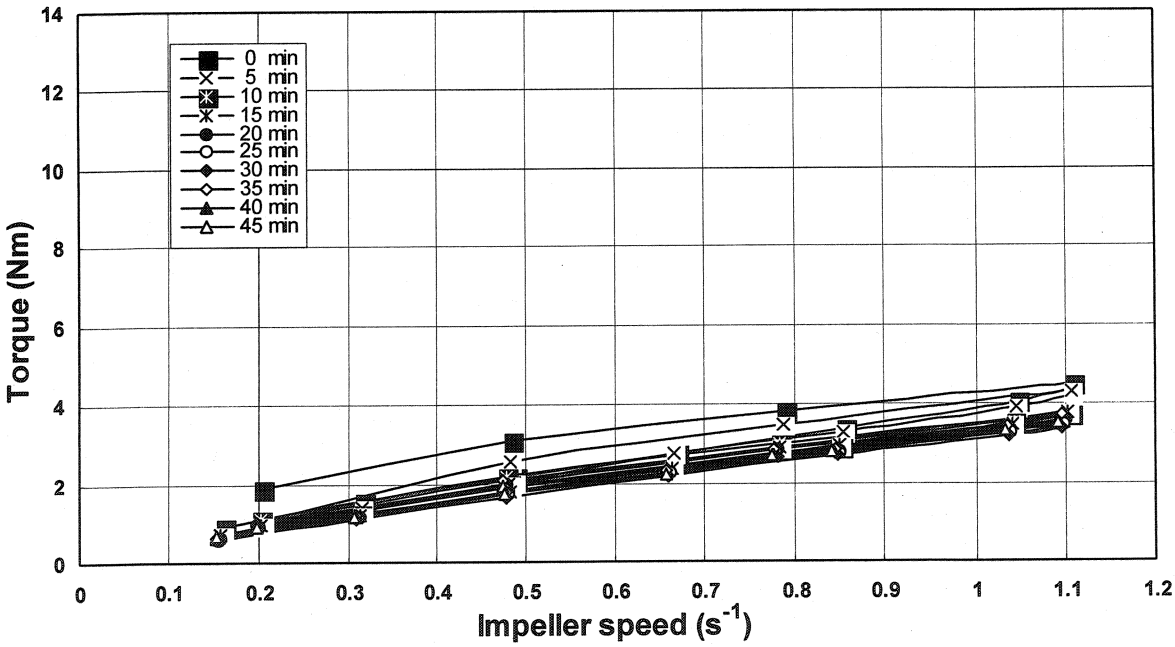


Figure 8.11 Torque vs. impeller speed for castable FM-5.

The similar trend of behaviour has been observed for the compositions FM-1, 2 and 3. The mixes FM-4 and FM-5 behave as Bingham fluid in both forward and reverse cycles.

The loops after 5min follow a similar path. The torques (T_{max}) for all the compositions FM-1 to FM-5 at the highest impeller speed of 1.10 s^{-1} at 0 min are given in Table 8.2. In the case of FM-1, 2 and 3, the T_{max} increases as the amount of ultrafine Bauxite-3 decreases. For FM-4 and FM -5, the T_{max} is lower than FM-2 with the same amount of the fine fillers of different source.

Table 8.2 T_{max} of the 5 compositions at the highest speed of 1.10 s^{-1} at 0 min

Composition	FM--1	FM--2	FM--3	FM--4	FM--5
T_{max} (Nm)	8.63	11.29	18.6	6.12	4.48

8.5.2 Equivalent Apparent Viscosity

The relationship between equivalent apparent viscosity (the specific torque values divided by the specific speed values) and impeller speed is shown in Figure 8.12 for FM-1. The behavior is similar to that of a Bingham fluid. FM-2 and FM-3 exhibit the same behavior and hence are not shown. The mixes FM-4 (not shown) and FM-5 (Figure 8.13) also perform like typical Bingham fluids.

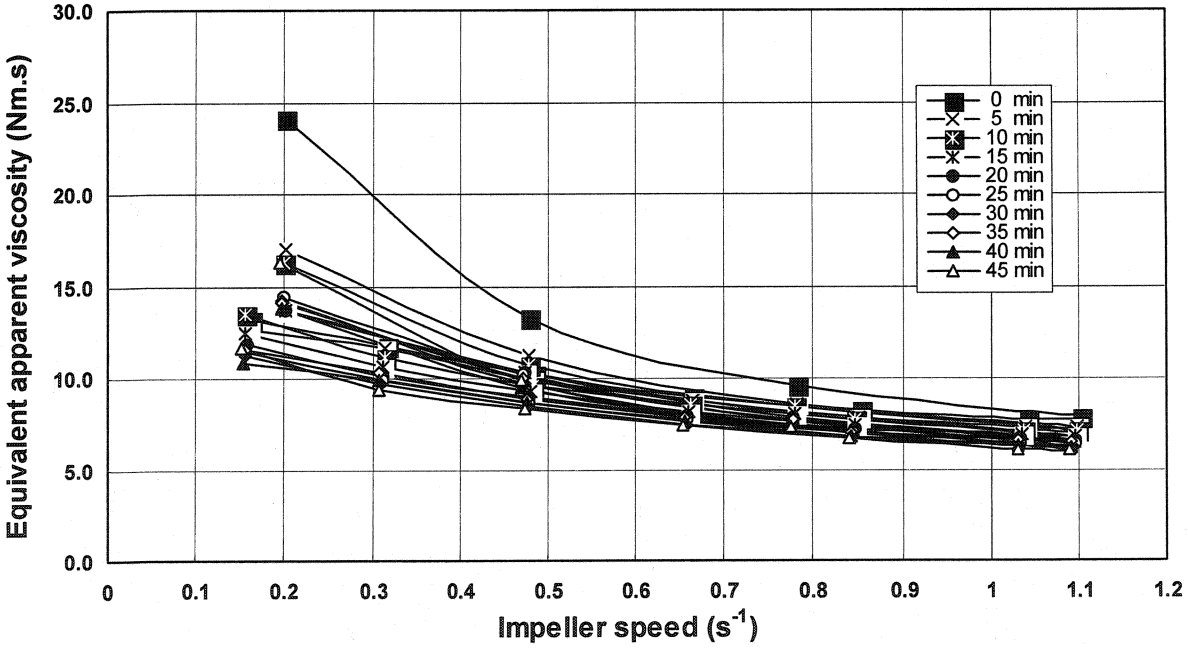


Figure 8.12 Equivalent apparent viscosity vs. impeller speed for castable FM-1.

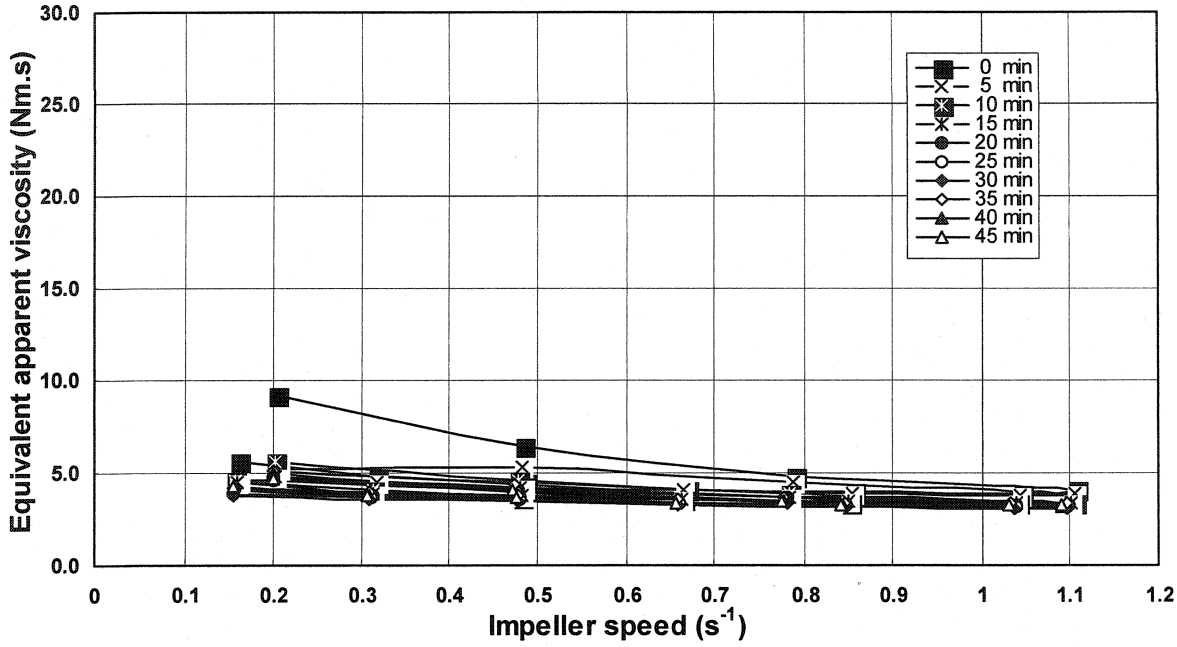


Figure 8.13 Equivalent apparent viscosity vs. impeller speed for castable FM-5.

8.5.3 Thixotropy

In all the mixes, as shown in Figure 8.14, the equivalent apparent viscosity values at the impeller speed of 1.10 s^{-1} decrease with time, and then stabilize at almost similar level...

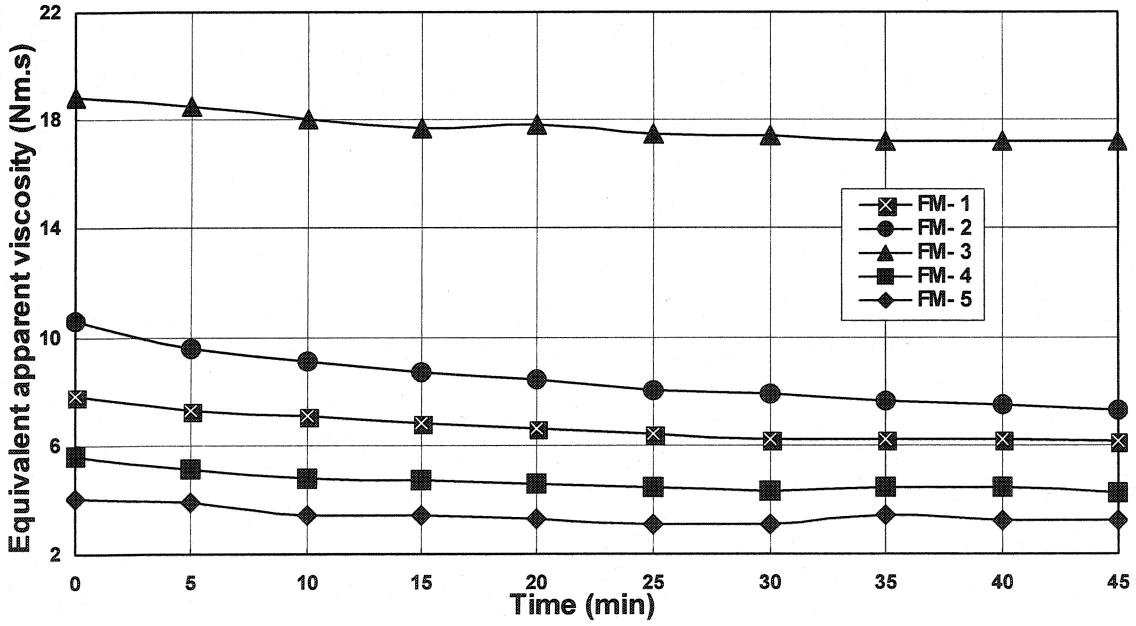


Figure 8.14 Equivalent apparent viscosity vs. time at the impeller speed of 1.10 s^{-1}.

Although the mixes FM-4 and FM-5 exhibit lower equivalent apparent viscosity values than those of the others, the rate of reduction in equivalent apparent viscosity is more pronounced. All the mixes are acting as Bingham fluids, but when analyzed as a function of time at constant impeller speed, thixotropic behavior is exhibited by all mixes (Figure 8.14). Mixes FM-4 and FM-5 are more thixotropic than the others

8.5.4 Flow Resistance and Torque Viscosity

The evaluation method for flow resistance (G) and torque viscosity (H) is shown in Figure 8.15 using the test results for mix FM-3 at 45min. Two test programs have been used: one using normal speed increment, and a large number of torque readings at each speed, and the other using fast speed increment as well as a fewer number of readings at each speed.

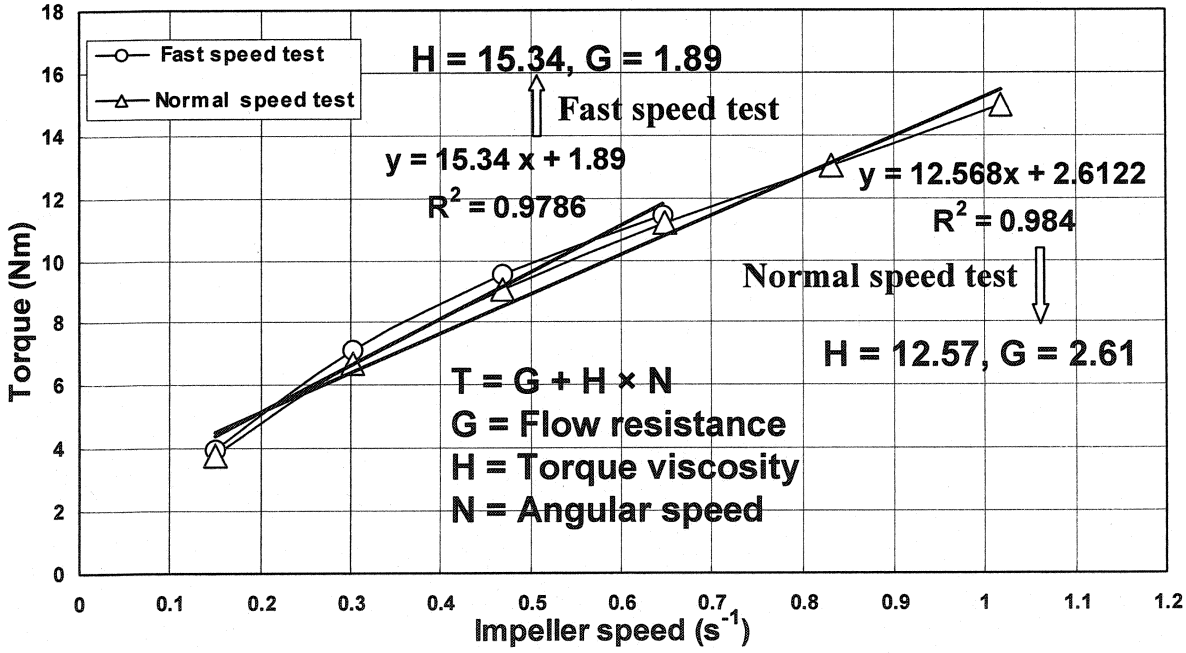


Figure 8.15 Comparison of the results obtained by the fast and normal speed tests.

The flow resistance (the intercept, G) and the torque viscosity (the slope, H) have been determined by a linear regression analysis using six and four points for the normal and fast speed test, respectively, in the reverse cycle (from high speed to low speed). In the first case (normal speed), H = 12.57 Nm and G = 2.61 Nm.s. In the second case (fast

speed), H = 15.34 Nm and G = 1.89 Nm.s. In the current study, all the mixes are tested with normal speed except for FM-3, which has to be tested with fast speed increment. The testing of FM-3 with normal speed increment is not possible due to its higher rigidity, meaning that more impeller force is required to overcome the yield stress of such a mix.

The flow resistance G and the torque viscosity H values of all compositions are given in Table 8.3. G and H values of compositions FM-1, FM-2 and FM-3 with the bauxite-based filler, increase as the amount of Bauxite-3 increase from 3 to 15 wt%. G and H values decrease with time after initial mixing and stabilize after 20 min. For compositions FM-4 and FM-5 with alumina-based fillers, the influence on both G and H values are drastic. Both properties are highly reduced for FM-4 and FM-5 when compared to FM-2 with equivalent weight percentage (9 wt%). Both ultra-fine aluminas act as good lubricant for the castable mix even if the self-flowability has not been modified extensively, as shown in Figures 5 and 6.

Table 8.3 G and H values for five compositions

Time (min)	Flow resistance G (Nm)					Torque viscosity H (Nm.s)				
	FM – 1	FM – 2	FM - 3	FM - 4	FM - 5	FM - 1	FM - 2	FM - 3	FM - 4	FM - 5
0	1.44	1.86	2.43	0.36	0.39	6.59	8.65	15.8	5.02	3.52
5	1.43	1.73	2.1	0.32	0.26	6.28	8.47	15.79	4.78	3.56
10	1.47	1.62	2.14	0.37	0.28	6.03	8.27	15.43	4.54	3.11
15	1.35	1.56	2.09	0.35	0.24	5.85	8.02	15.21	4.43	3.13
20	1.26	1.52	1.84	0.33	0.22	5.73	7.78	15.62	4.32	3.04
25	1.21	1.46	1.87	0.34	0.2	5.58	7.58	15.3	4.19	3.01
30	1.19	1.42	1.81	0.28	0.18	5.4	7.43	15.14	4.14	2.97
35	1.18	1.41	1.85	0.3	0.21	5.49	7.41	15.65	4.19	3.06
40	1.19	1.4	1.87	0.32	0.22	5.5	7.4	15.6	4.2	3.06
45	1.17	1.33	2.12	0.3	0.24	5.24	7.34	15.02	4.25	3.03

The influence of the type and amount of fine fillers on G and H values is given in Figure 8.16 and 17 respectively. Among FM-1, FM-2 and FM-3, with ultra-fine particle Bauxite-3 content increasing, the G and H values increase. The castable FM-3, with

15wt% Bauxite-3 possesses the highest G and H values, followed by castables FM-2 and FM-1 in order. Over time, the G values decrease till 20 min and then remain stable. The trend for H values is similar and only the reduction rate of H is lower than that of G.

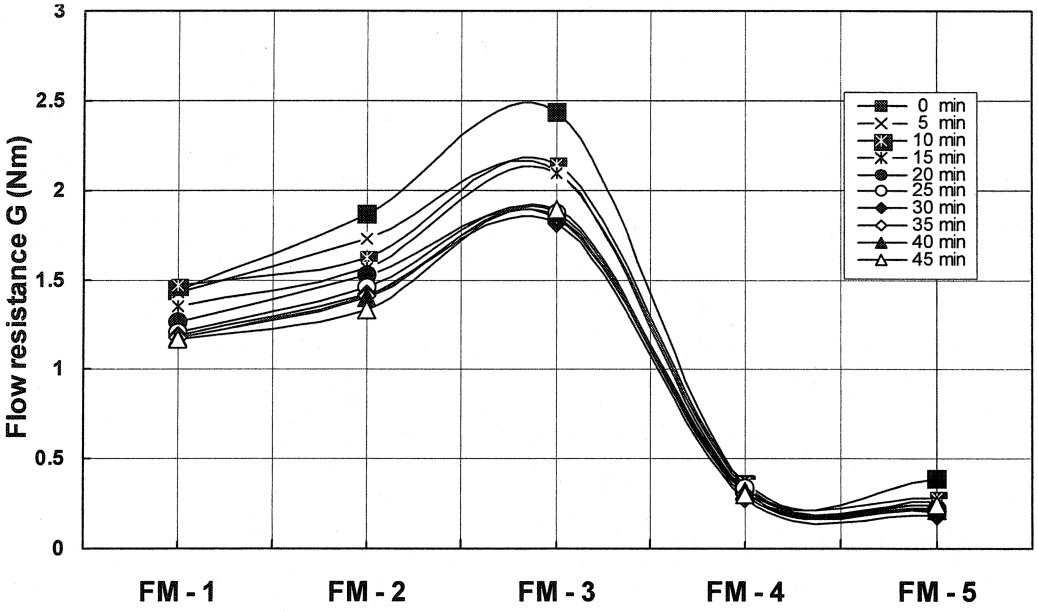


Figure 8.16 Flow resistance vs. fine fillers.

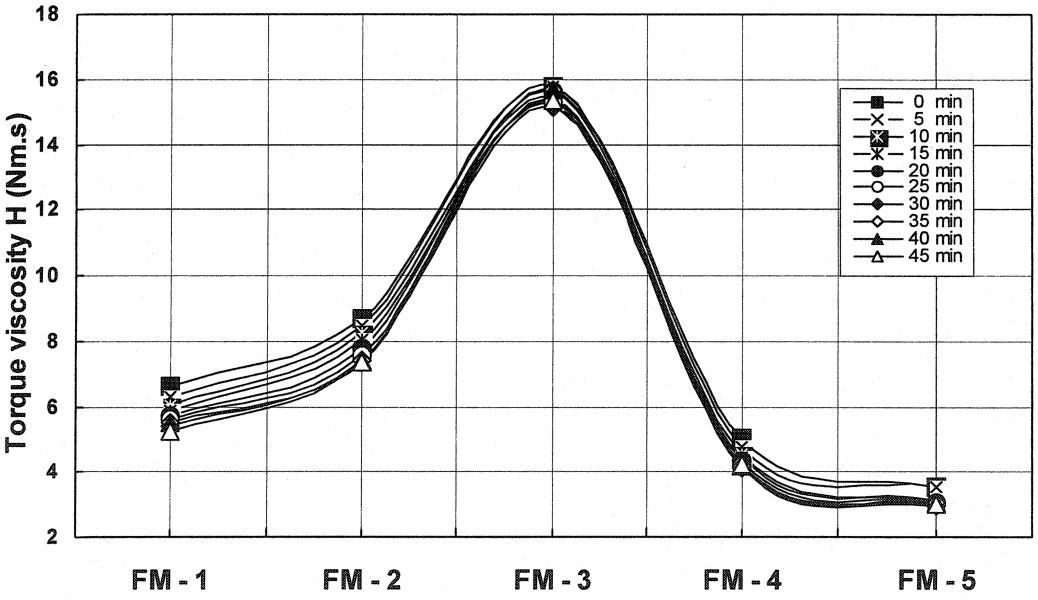


Figure 8.17 Torque viscosity vs. fine fillers.

With the same amount of alumina fillers, the G and H values of FM-4, with A 3000 FL are a bit higher than those of FM-5, with A 1000SG. Both of G and H maintain similar evolution with time. Comparing at the same level of 9 wt% addition, the 3 different fine aluminas contained in FM-2, FM-4 and FM-5, it is clear that the use of Bauxite-3 induces higher G and H values. In particular, G values are much higher.

8.6 Matrix Rheology

8.6.1 Shear Stress vs. Shear Rate

The shear stress as a function of shear rate of the matrix slurries of the 5 castables FM-1 to FM-5 is shown in Figure 8.18. In the case of the compositions FM-1, 2 and 3, with Bauxite-3 increasing, the loops shift upwards. The loops of FM-1, 4 and 5 look similar.

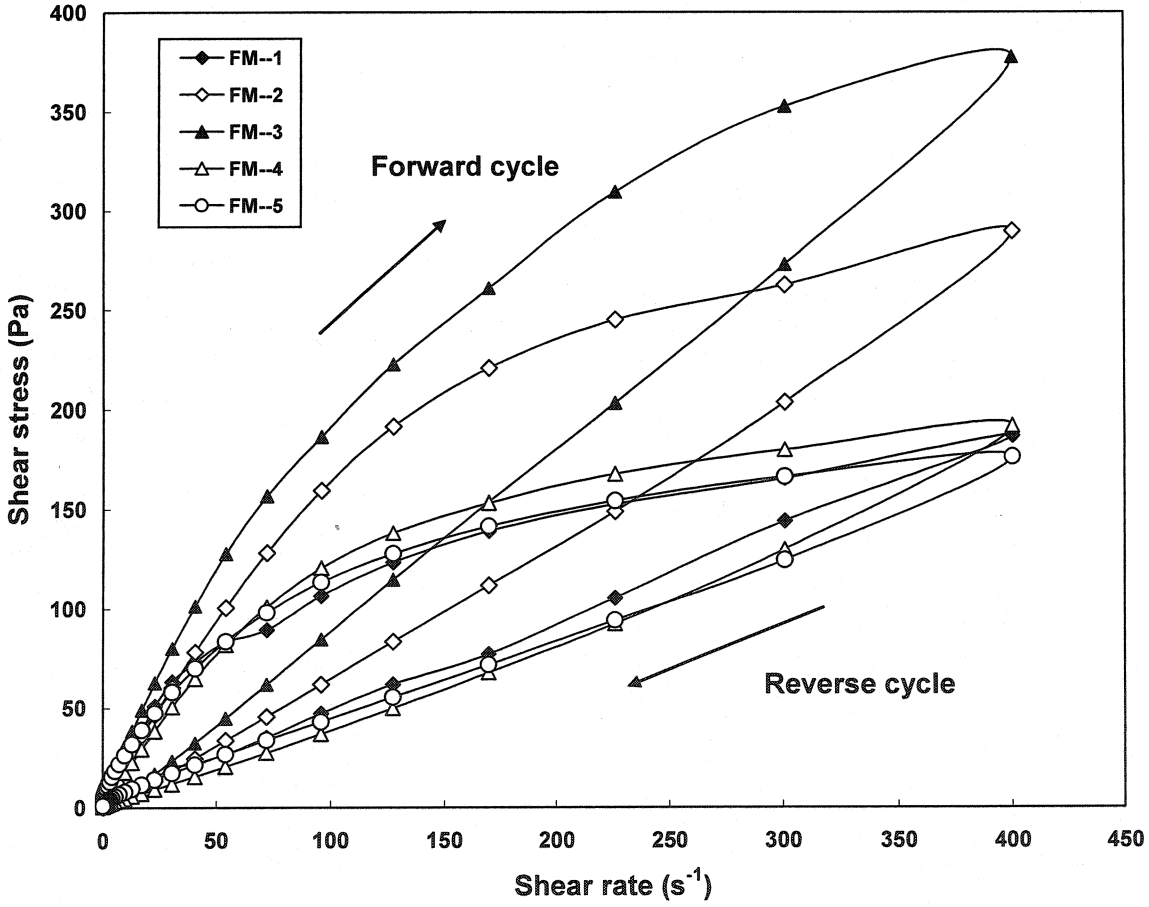


Figure 8.18 Shear stress vs. shear rate for all the matrix slurries.

The shear stress (τ_{max}) at the highest shear rate of 400 s^{-1}, for all the matrix slurries is given in Table 8.4. In the case of FM-1, 2 and 3, the τ_{max} increases with the amount of Bauxite-3 addition increasing. The τ_{max} of FM-1, 4 and 5 are similar, although the value of FM-4 is slightly higher than FM-5.

Table 8.4 τ_{max} of the 5 matrix slurries at the highest shear rate of 400 s^{-1}

Composition	FM--1	FM--2	FM--3	FM--4	FM--5
τ_{max} (Pa)	187	290	377	192	176

8.6.2 Apparent Viscosity vs. Shear Rate

The apparent viscosity as a function of shear rate of the matrix slurries of the 5 castables is shown in Figure 8.19.

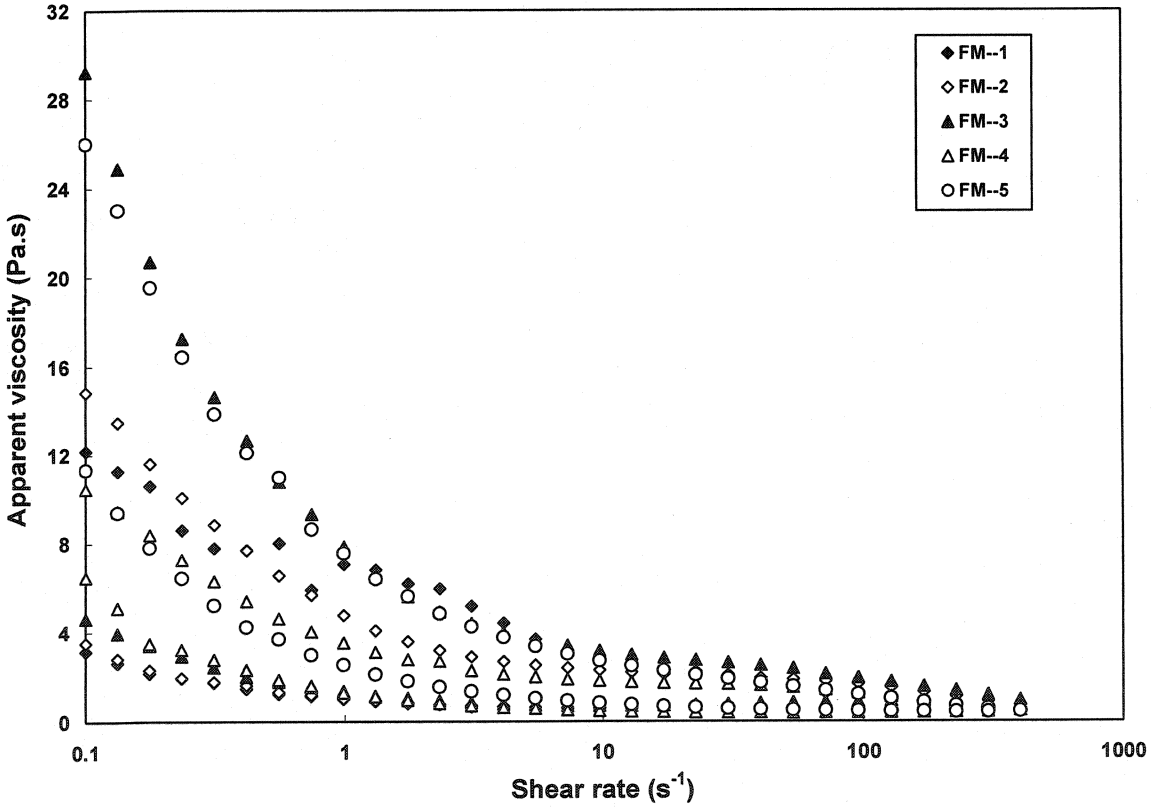


Figure 8.19 Apparent viscosity vs. shear rate for all the matrix slurries.

The apparent viscosity in the forward cycle (shear rate increasing) is higher than in the reverse cycle (shear rate decreasing). In the forward cycle, the apparent viscosity decrease sharply at the beginning and remains stable from 5.0 s^{-1} to 100 s^{-1} and finally

slightly decreases from 100 s^{-1} to 400 s^{-1}. The apparent viscosity of FM-3 and 5 are similar and ranked as first, followed by FM-2 and 4. In the case of FM-1, the apparent viscosity fluctuates from the beginning to 5.0 s^{-1} in the forward cycle. In the reverse cycle, the apparent viscosity of all the matrix slurries remains similar, except for FM-5. In the case of FM-5, the apparent viscosity is the highest among all slurries, because of its high content of submicron particles of reactive alumina, leading to gelation, especially at lower shear rates in both the forward and reverse cycle.

8.6.3 Thixotropy

The thixotropy degree and loop's area of the five matrix slurries are shown in Figure 8.20. The calculation method is as described in Section 4.6.3. The thixotropy degree increases as Bauxite-3 content increases. In the case of FM-4 and 5, with reactive alumina, the thixotropy degree is similar to that of FM-1. The loops' area values show the same trend as for the thixotropy degree.

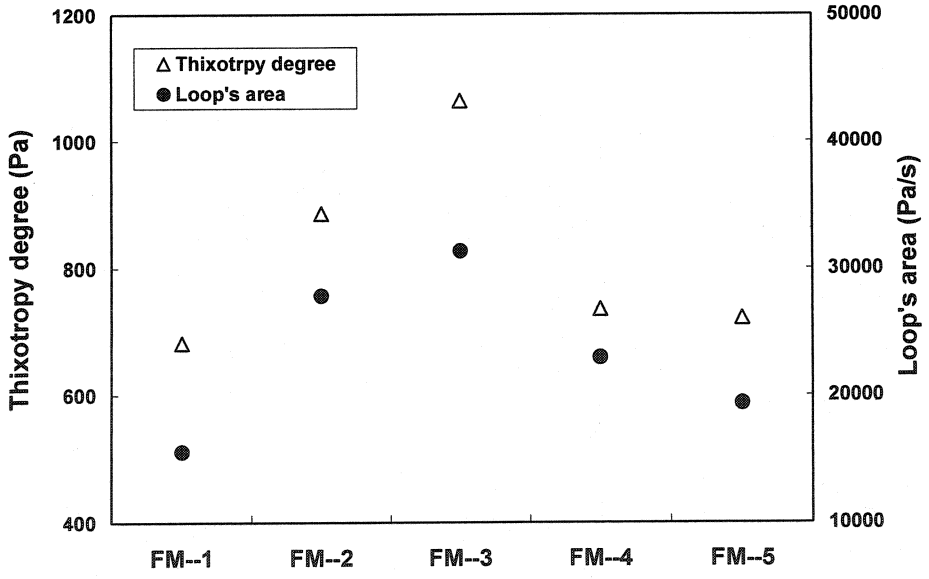


Figure 8.20 Thixotropy degree and loop's area for all the matrix slurries.

8.6.4 Plastic Yield Stress and Plastic Viscosity

The calculated values of plastic viscosity and yield stress of the 5 matrix slurries are given in Table 8.5. With the ultrafine particles Bauxite-3 increasing, the plastic viscosity increases, but the plastic yield stress decreases and then increases. In the case of FM-4

and 5, the plastic viscosity is the same as FM-1, but the plastic yield stress of FM-5 is much higher than FM-4.

Table 8.5 Plastic viscosity and yield stress of all the matrix slurries

Composition	FM--1	FM--2	FM--3	FM--4	FM--5
Plastic viscosity (Pa.s)	1.536	1.829	2.317	1.515	1.5
Plastic yield stress (Pa)	9.604	3.512	6.732	2.399	8.842

8.7 IPS of Matrix and MPT of Castables

The calculation methods of IPS of matrix and MPT of the castables have already been described as Equation 2.7 and 13. The IPS and MPT of MS-1, 2, 3 and 4 are given in Table 8.6. The IPS of the matrix slurries FM-1, 2 and 3 significantly decrease with Bauxite-3 increasing, which contains more submicron particles, but the MPT of the castables is the same. After added with reactive alumina A 3000FL and A 1000SG, the IPS significantly decrease for FM-4 and 5, respectively, although the MPT is the same, and slightly lower than FM-2.

Table 8.6 IPS of matrix and MPT of castables

Composition	FM--1	FM--2	FM--3	FM--4	FM--5
IPS (nm)	88.8	87.9	82.4	73.0	43.8
MPT (μm)	123.8	123.8	123.8	120.9	120.9

8.8 Mechanical and Physical Properties

The main purpose of addition of fine fillers is to fill voids and then decrease water addition and apparent porosity and increase density and strength. The mechanical properties CMOR and AP of all compositions are given in Table 8.7. At 0 min., the MOR of FM-4 is the highest, up to 10.9 MPa, followed by FM-5 and FM-3 is the lowest. At 45 min., the MOR of FM-5 is the highest, about 11.5 MPa and the others are the similar from 8.5 to 8.9 MPa. In case of AP, at 0 min., FM-5 is the highest up to 18.7 %, followed by FM-2, FM-3, FM-1 and FM-4 is the lowest about 17.1%. At 45 min., FM-2 decreases to 17.8 % and is the lowest, FM-1, FM-3 and FM-4 increase to the same level. The AP of FM-5 still remains the highest position although it does not change a lot. The apparent porosity has a close relationship with self-flowability and degasability of

castable as illustrated in Fig. 5 and 6. During mixing and testing, the impeller of mixer or rheometer moves through the mixture. Naturally, it entrains some air into the mixture. With a castable with good degas ability, the matrix paste fills the voids well and expels the air, some bubbles can then be seen on the top surface of samples. Otherwise, the matrix paste wraps air in the mixture and prevents it to migrate out of the castable mix. This results in an apparent porosity increase. For castable FM-5, with A 1000 SG, self-flowability and degas ability are not perfect and so the apparent porosity remains high, even after 45 min. This is because the matrix paste is too stick and keeps air inside the castable mix. For castable FM-4, with A 3000 FL, the fresh mixture self-flows and degases well, so that apparent porosity is rather low, but self-flowability decreases and apparent porosity increases a lot after 45 min. In reverse, the cold modulus of rupture of fresh castable is much higher than that of samples cast after 45 min as shown in Table 8.7.

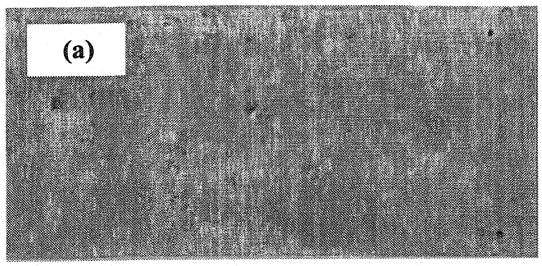
Table 8.7 CMOR and AP of all the compositions

Composition	CMOR (MPa)		AP (%)	
	0 min.	45 min.	0 min.	45 min.
FM - 1	9.1	8.5	17.7	18.5
FM - 2	9.3	8.7	18.2	17.8
FM - 3	8.3	8.8	17.9	18.2
FM - 4	10.9	8.9	17.1	18.2
FM - 5	9.8	11.5	18.7	18.6

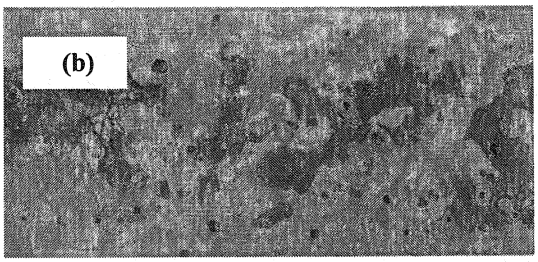
8.9 Appearance of Samples

Figure 8.21 shows the appearance of various samples, cast by self-flowing at different time. The appearance of all the fresh castables (0 min) is satisfactory. Some dark grey spots in the case of FM-4 and FM-5 are possibly due to floating of carbon present in the microsilica. This effect is not observed in the mixes without containing white-colour reactive aluminas, possibly due to lower contrast in colors and slight segregation. After 45min of testing, some bubbles due to degassing appeared on the surface of the castables FM-2 and FM-3, whereas surface segregation is observed in FM-1. Degassing indicates the release of air through the castable surface is normal for the cast structure of self-

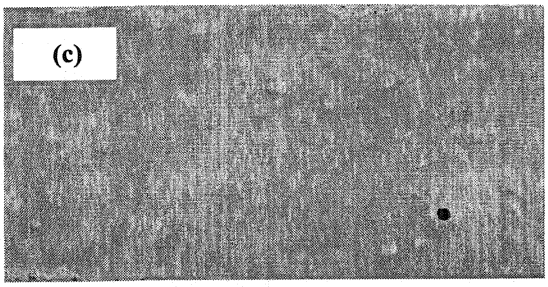
flowing castable. The appearance of castable surface is smooth in the case of FM-4 and FM-5 even after 45min of testing, although they exhibit slight segregation during self-flowability test where aggregates centralized in the castable patty, as also shown in Figure 8.22(h) and (j), with a lot of dark grey spots.



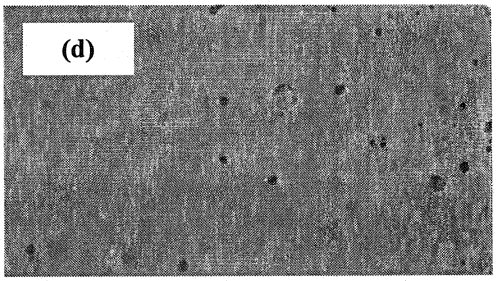
FM-1 (0 min)



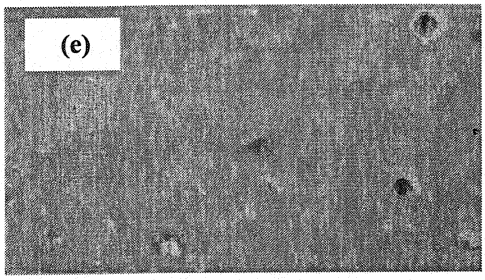
FM-1 (45 min)



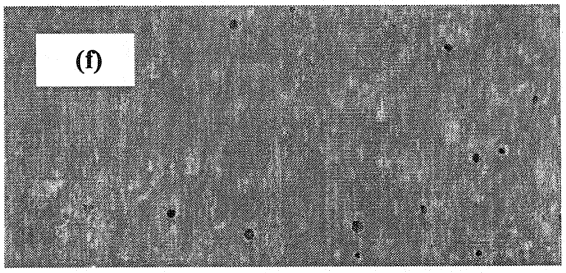
FM-2 (0 min)



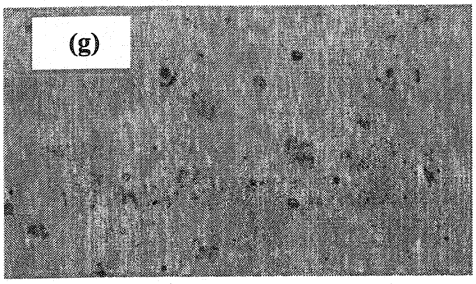
FM-2 (45 min)



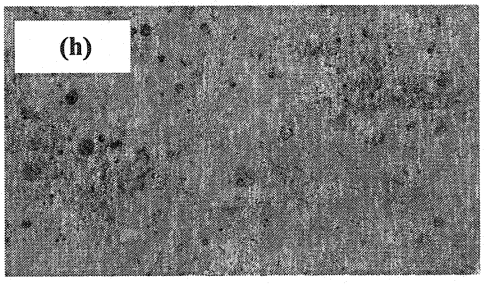
FM-3 (0 min)



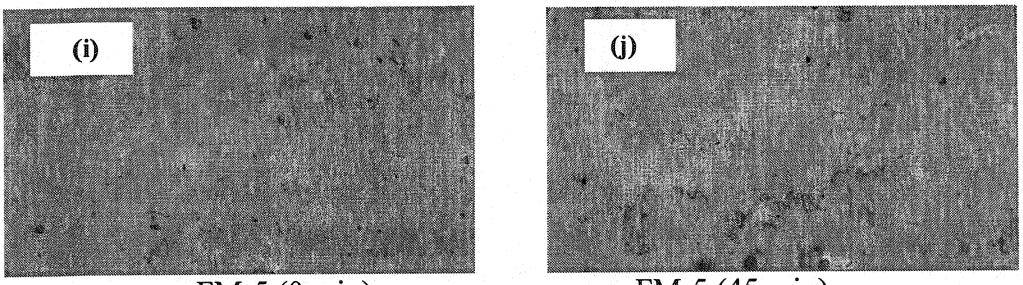
FM-3 (45 min)



FM-4 (0 min)



FM-4 (45 min)



FM-5 (0 min) FM-5 (45 min)

Figure 8.21 (a)-(j) Appearance of all the samples cast at different time.

8.10 Structure of Matrix and Castable

From rheometer results (Figure 8.7-11), it can be seen that the torque measurements in forward cycle differ from those obtained in reverse cycle. This indicates the occurrence of some structural breakdown or thixotropy in these castables. Castable structure can be considered as a suspension of large inert particles in a paste matrix and the paste matrix as a suspension of solid particles active in water. Several researchers reported on a complex rheological behaviour of matrixes [11, 76], and described the phenomenon of structural breakdown and thixotropy, but the knowledge of the rheology of the fine matrix only is not sufficient to predict the rheological behaviour of a castable. In the present work, the rheological behaviour of the paste matrix, consisted of CAC, microsilica, bauxite and/or reactive alumina fines, dispersant and water, is much different in the castables in comparison to its behaviour when used alone, without aggregates. The fine matrix particles tend to form flocs as their surfaces acquire opposite charges, as shown in Figure 8.22.

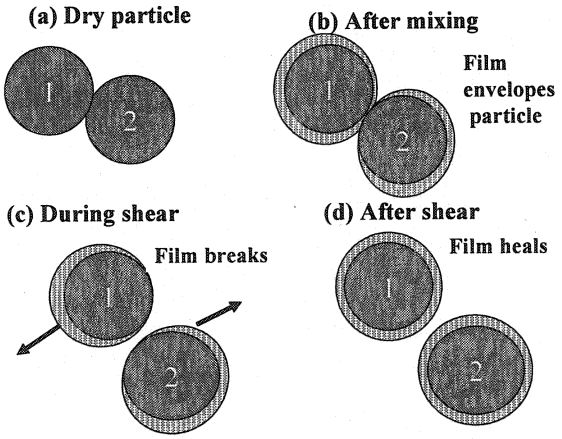


Figure 8.22 Flocs form and films envelope particles.

During and after mixing the castables, several physical and chemical reactions occur. Rapid reactions such as dissolution of dispersant, cement hydration, microsilica agglomeration, gelation around some hydrated minerals and other components of the mix, may take place during the first a few min after water is added. This is followed by a dormant period during which the paste matrix remains workable until setting takes place. After the initial contact between the matrix and water, the anhydrous $CaO.Al_2O_3$ (CA) grains of the cement slowly become covered by a layer of calcium-alumina-hydrates. These films form around the flocs, and they are responsible for the physical phenomenon known as structural breakdown, as Figure 8.23 [20, 76, 102].

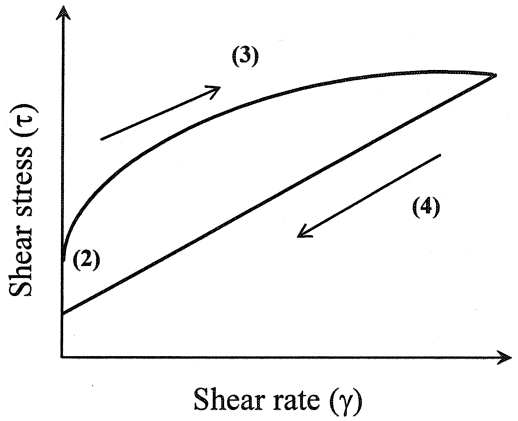


Figure 8.23 Flow curve and schematic model for structural breakdown.

As always shown in the previous chapters, the plot of the curve increasing the shear rate (arrow pointing up) is different from the curve of decreasing the shear rate (arrow pointing down). The "up-curve" is typical of a shear-thinning material, in which the apparent viscosity (the slope at any point on the curve) decreases when the shear rate increases. The destruction of the membrane surrounding the matrix floc explains the observed reduction in apparent viscosity. After the maximum shear is reached, the membranes around smaller flocs or individual matrix particles reform and the apparent viscosity remains almost constant (plastic viscosity) during the "down-curve". Figure 8.24 shows the steps at different points on the curves. This phenomenon is strongly dependent on the mixing method, time and temperature. Consequently, the rheological test at fast speed gives higher H and lower G than at normal speed. Also in the

rheological test, increasing or decreasing the shear rate will cause the equivalent apparent viscosity to change.

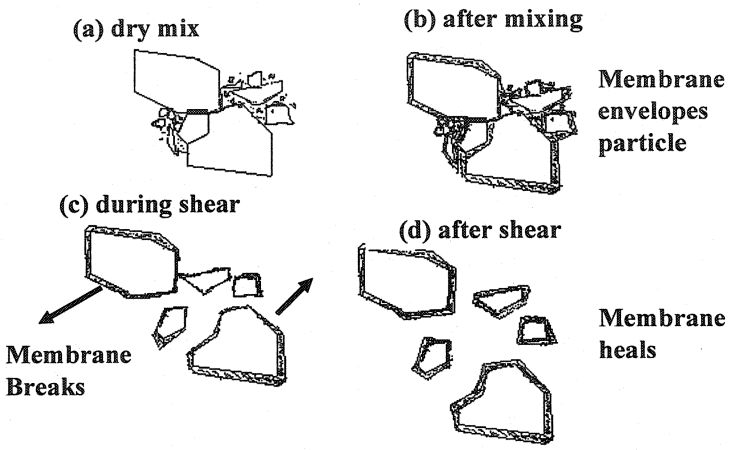


Figure 8.24 A matrix paste surrounding the aggregates.

Castables with different amounts of fine fillers would show different rheological behaviour depending on the thickness of the "layer" surrounding the aggregates. The differences observed in H and G values of the castables are highly related to the composition of the matrix, as PSD of the matrix affects the effective filling of the voids. In the case of castable FM-1, the fine fillers are insufficient to fill the voids. This results in too low viscosity of matrix paste to carry the aggregates to move together and tend to cause segregation during pumping. Furthermore, too thin paste layer surrounding the aggregate makes stronger and more frequent collisions of aggregates and friction. On the contrary, where there are excessive fine fillers in the castable, such as in FM-3, these excessive fine fillers have a tendency of agglomeration after voids-filling and then the matrix forms a paste layer with high viscosity and high rigidity around the aggregates. In the case of FM-4 and FM-5, there are sufficient fine fillers in the castables, but too fine fillers also cause some problems, since very fine particles have very high surface area, and are prone to agglomerate, attract and stick to each other. It is then important to distinguish matrix particles between above (>1μm) and below (<1μm) micron scale. The submicron-sized particles play a special role as they have much stronger tendency to flocculate and gelate. More the submicron particles are present, the more gelation is. The formed gel acts as a lubricant around the particles and reduces friction. As shown in

Figure 8.3 using the Bauxite-1, Bauxite-2 or bauxite-3 does not influence the cumulative volume distribution % of particles less than 1 micron, but as shown in Figure 8.4, the use of reactive alumina A 3000FL and A 1000SG, changes greatly the cumulative volume distribution % of submicron-sized particles to 7.8 and 13 %, respectively. So, the castables FM-1, FM-2 and FM-3 are expected to have higher H values than FM-4 and FM-5, as shown in Table 8.3, while the thixotropy and gelation increase for the later two castables, with higher equivalent apparent viscosity reduction rate with time, as shown in Figure 8.14.

8.11 Optimization of Castables

The relationship between G and H values is shown in Figure 8.25. Although all the castables in this study have shown good self-flowability at 7wt% water addition (Figure 8.5 and 6), only some of them are considered pumpable.

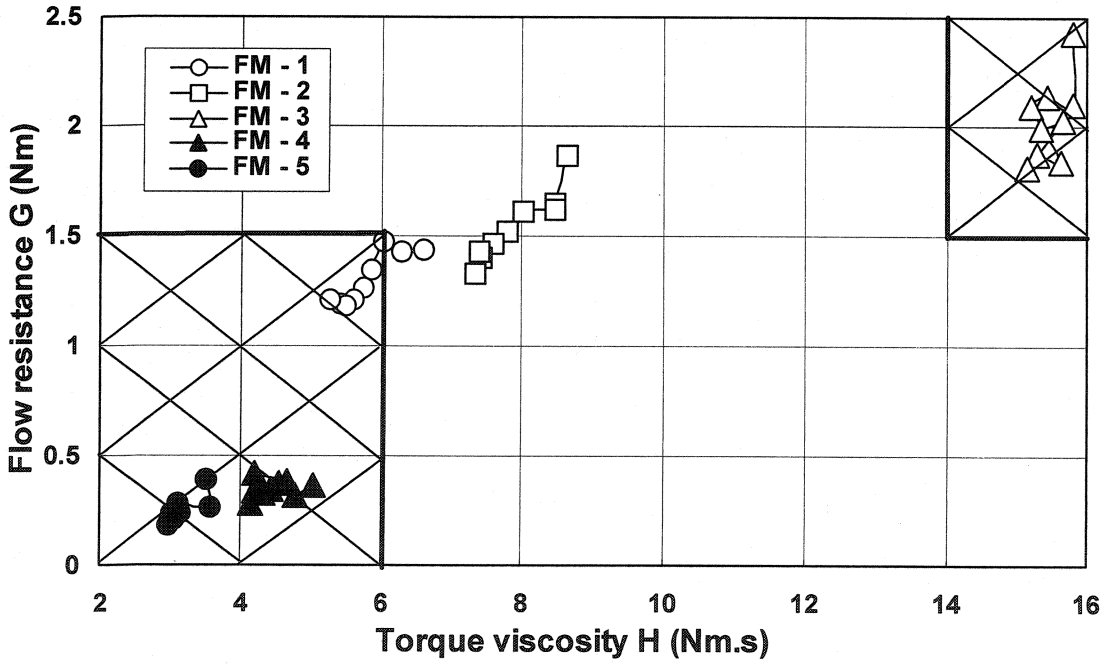


Figure 8.25 Flow resistance vs. torque viscosity.

The castable FM-1 exhibits moderate flow resistance, but unacceptably low stability due to insufficient amount of fine fillers to fill the voids in the castable. As a result, FM-1 exhibits serious segregation in Figure 8.22. The castable FM-3 has very high flow

resistance and torque viscosity with higher rigidity because of excessive fine fillers. Conversely, FM-4 and FM-5 exhibit very low flow resistance and torque viscosity because of too fine fillers, therefore slight segregation occurred during self-flowability tests. Moreover, the fresh mixes of FM-4 or FM-5 are too sticky and likely to cause casting and finishing problems. This indicates again that both flow resistance and torque viscosity should reach a certain critical value for a castable mix to remain stable without any segregation and to provide good mobility and stability.

8.12 Conclusions

The following conclusions can be drawn based on the results obtained by this investigation:

a) Appropriate selection of fine fillers is crucial to achieve a good pumpability for castables without obvious segregation. Insufficient fine fillers result in serious segregation, but excessive fine fillers cause high rigidity and viscosity. Too much submicronic fillers lead to high stickiness and also segregation.

b) Investigation and optimization of rheological parameters, in terms of flow resistance G and torque viscosity H values, leads to the finding that a castable composition with optimal G and H values can well avoid segregation and serious structural breakdown or strong thixotropy.

c) In the present study, castable composition FM-2 is considered to have the best pumpability due to its satisfactory combination of flow resistance and torque viscosity under the given conditions.

CHAPTER 9 - WATER ADDITION

Water addition has direct impact on castable placement; however it is more or less strictly controlled by installers. In this work, again, two basic rheological properties: flow resistance and torque viscosity have been measured against time, with different water addition in the same standard mix. The flow resistance indicates the mobility whereas the torque viscosity dictates the stability of a castable during installation. It has been observed that with 6.0 wt% water addition, such a mix possesses good vibration castable characteristics; with 6.5 wt%, it shows good self-flow castable characteristics; and with 7.0 wt%, it can be a good pumpable castable, in every case with comparable mechanical properties. While with 7.5 wt% water addition, the properties of such castable are definitively impaired

9.1 Introduction

As it is well known, water plays important roles in castables:

- To promote and take part in the formation of hydrates and/or of sol-gel as binders, which in turn influence strength after demoulding and initial drying out up to intermediate temperatures.
- To dissolve dispersants and additives, making them truly useful.
- To act as lubricant between solid particles, so as to insure good mixing and to favour good installation practices.

It is generally considered that the flowability could be improved with more water addition in a castable. Logically, the total amount of water needed is to be adjusted so that the free water amount can be kept to a minimum, but either too little or too much water is detrimental. The water amount has an impact on the homogenization of the mix and has direct influences on the flowability and workability, two major parameters influencing the installation methodology, and later on, on the open porosity after drying and the loss of strength after firing. Excessive water addition reduces the properties of the castables and results in segregation during mixing and contraction during curing and

firing. Once more, the amount of water in a castable must be controlled carefully. In the present work, the influence of water addition on the rheological behavior of bauxite-based low cement castable has been investigated.

9.2 Compositions

Based on the results in previous chapters, the same optimized composition has been used to test the influence of water addition. All compositions are the same, except for water addition. The water addition starts from 6.0 wt% to 7.5 wt% at interval of 0.5 wt% for each composition. The composition details for this step are given in Table 9.1.

Table 9.1 Details of castable mixes to study the effect of water additions

Castable		**WA-1**	**WA-2**	**WA-3**	**WA-4**
Aggregate (wt%)		59	59	59	59
Fine matrix (wt%)	Bauxite-1	11	11	11	11
	Bauxite-2	12	12	12	12
	Bauxite-3	9	9	9	9
	Cement CA-14	4	4	4	4
	Microsilica-1 (Elkem 971U)	5	5	5	5
Dispersant SHMP (wt%)		0.12	0.12	0.12	0.12
Water addition (wt%)		**6.0**	**6.5**	**7.0**	**7.5**

9.3 Self-flowability Vs. Water Addition

The self-flowability of the chosen composition as a function of water addition is shown in Figure 9.1. With 6.0 wt% water, the vibration flowability is around 130 % and the self-flowability is about 70 %. With 6.5, 7.0 and 7.5 wt% water, the self-flowability increases to 100, 125 and 138 % respectively. The flowability values measured after 30min (optimum working time) of rheological testing in comparison to those measured immediately after finishing mixing show the similar. Of course, flowability values measured with a flow cone, with or without vibration, are directly influenced by the amount of the added water.

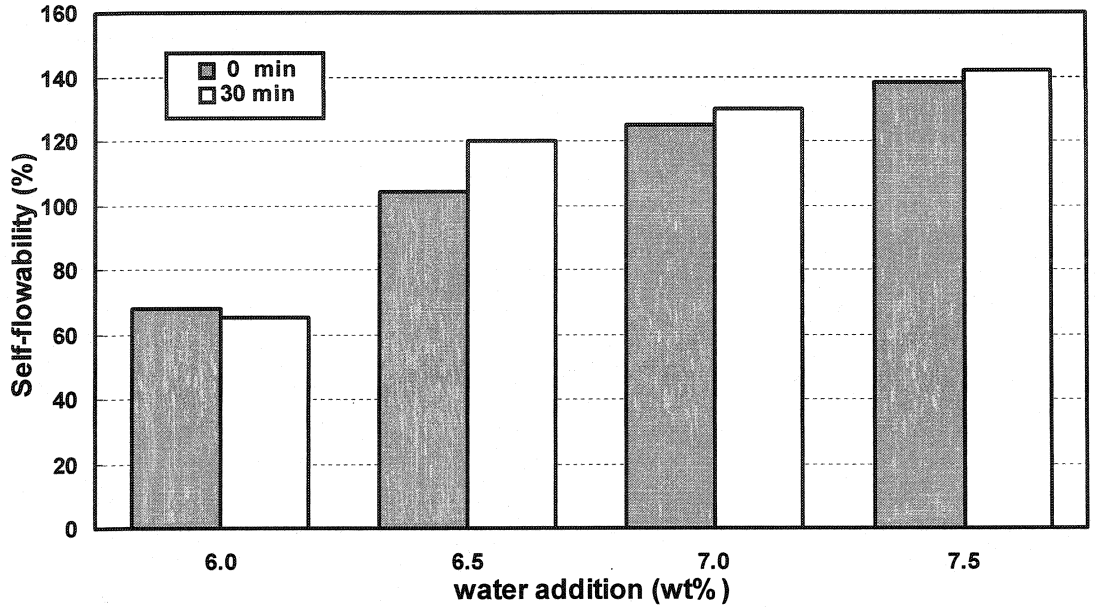


Figure 9.1 Self-flowability vs. water addition.

9.4 Castable Rheology

9.4.1 Torque vs. Speed

Typical rheometer results for composition WA-2, 3 and 4 are shown in Figure 9.2, 3 and 4, respectively. For WA-1with 6.0 wt% water, the mix may be considered as a good vibration castable with high enough vibration flowability, but its self-flowability is still quite limited. The mix is so stiff that the rheometer motor could hardly move the impeller. So the rheological properties of WA-1 have not been measured. In the case of WA-2 with 6.5 wt % water, the mix is much softer than WA-1, but the Fast test mode has to be used for the first two measurements (0 and 5 min). After that, the Normal test mode could be used and the tendency is similar to WA-3's. Otherwise, the impeller of the rheometer will be blocked and tests will abort. The difference between the two modes of testing is that with the Fast mode, the initial force imposed on the impeller is higher than when the Normal mode is used. This means the mix WA-2 needs more and higher shearing stress to break the agglomerates, to fill the voids and improve homogenization during the first two sequences. In the case of WA-4, with 7.5 wt% water, the trend of the rheological behavior is similar to WA-3's, but the cluster of all loops shift down (Figure 9.4).

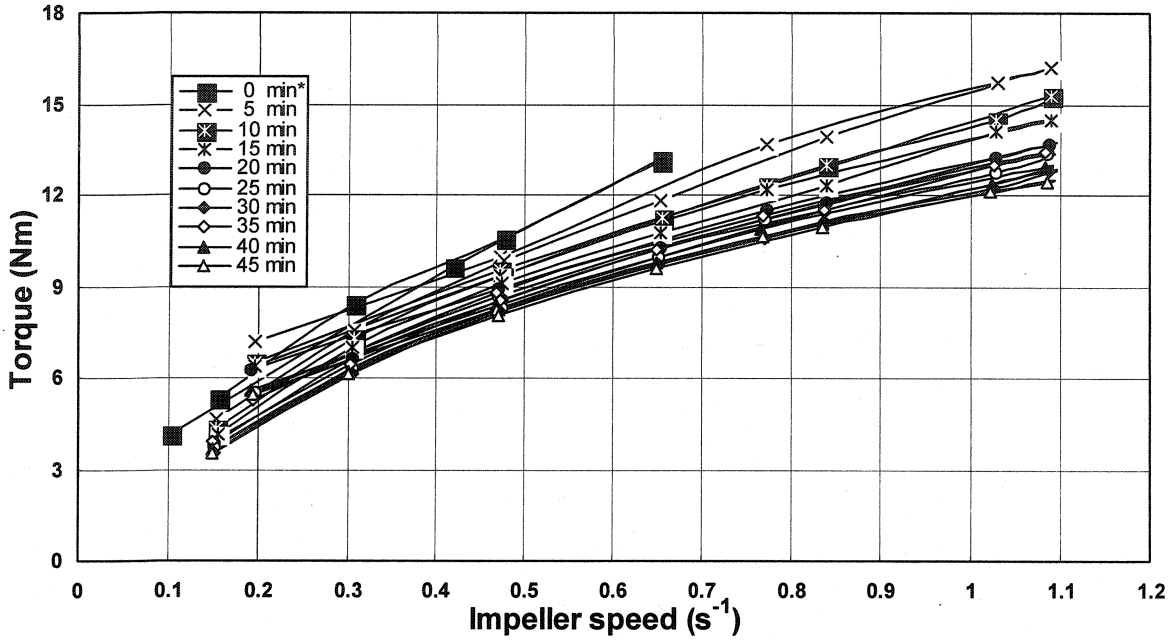


Figure 9.2 Torque vs. impeller speed for WA-2.

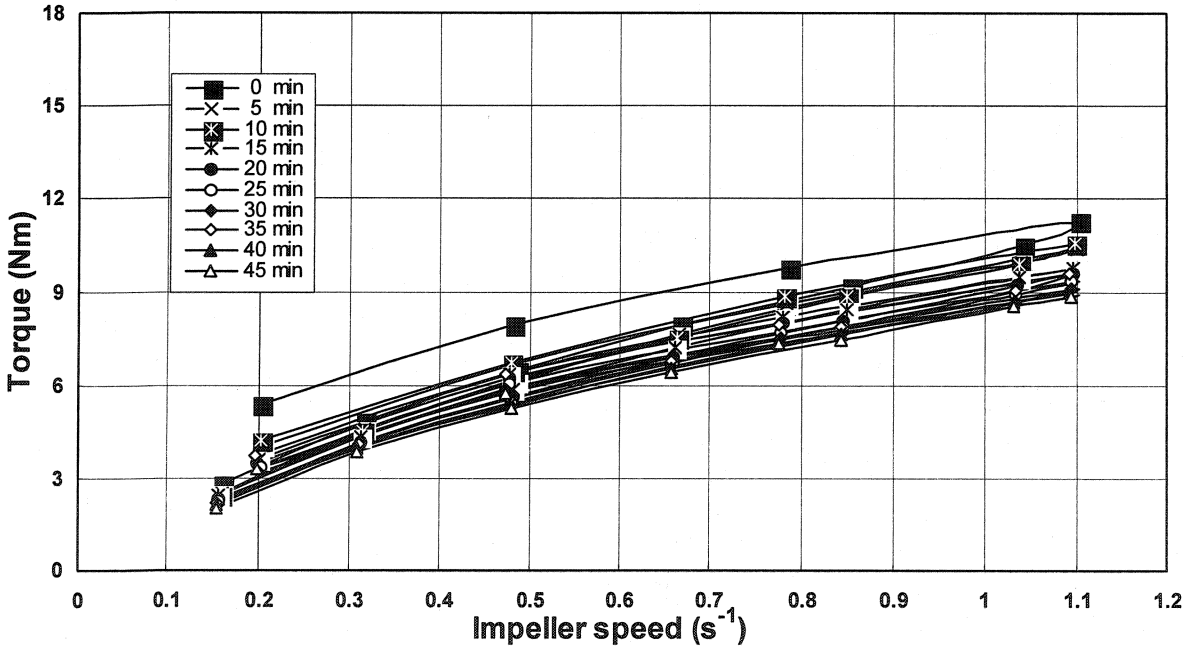


Figure 9.3 Torque vs. impeller speed for WA-3.

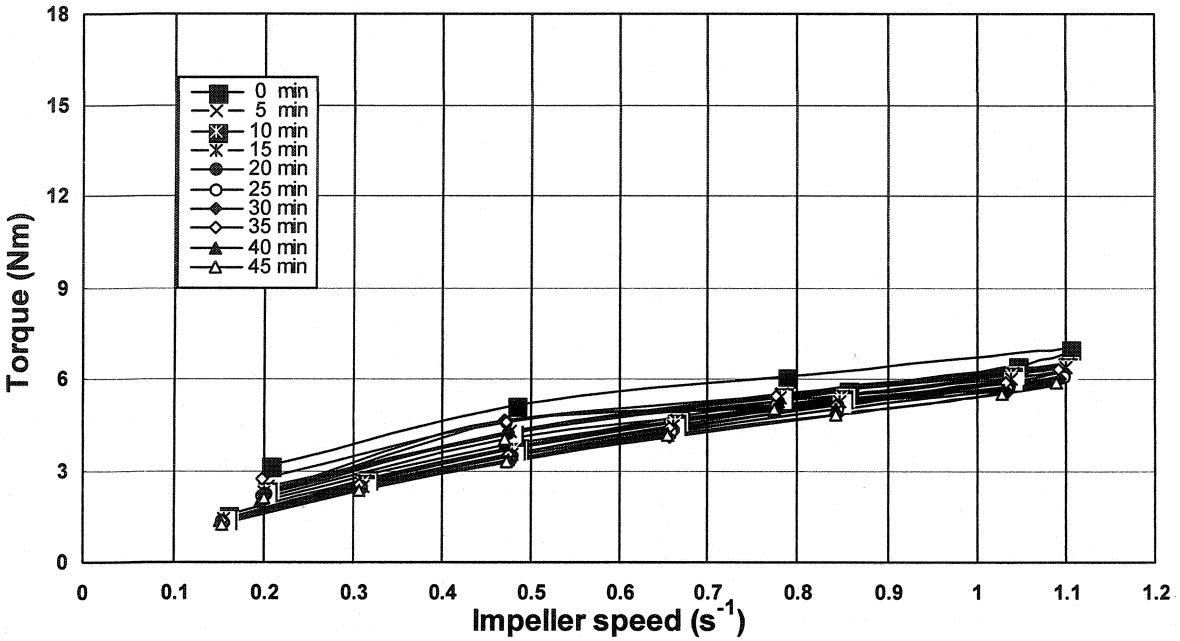


Figure 9.4 Torque vs. impeller speed for WA-4.

The torque (T_{max}) of compositions WA-2, 3 and 4 at the highest impeller speed of 1.1 s^{-1} at 0 min is given in Table 9.2. The T_{max} significantly decreases as the water addition increases.

Table 9.2 T_{max} of compositions WA-2 to WA-4 at the speed of 1.1 s^{-1} at 0 min

Composition	WA--2	WA--3	WA--4
T_{max} (Nm)	16.22	11.29	6.98

9.4.2 Equivalent Apparent Viscosity

The relationship between equivalent apparent viscosity and impeller speed of the composition WA-3 is shown in Figure 9.5, always closely typical to a Bingham fluid. The trends are similar for the other compositions and hence not shown.

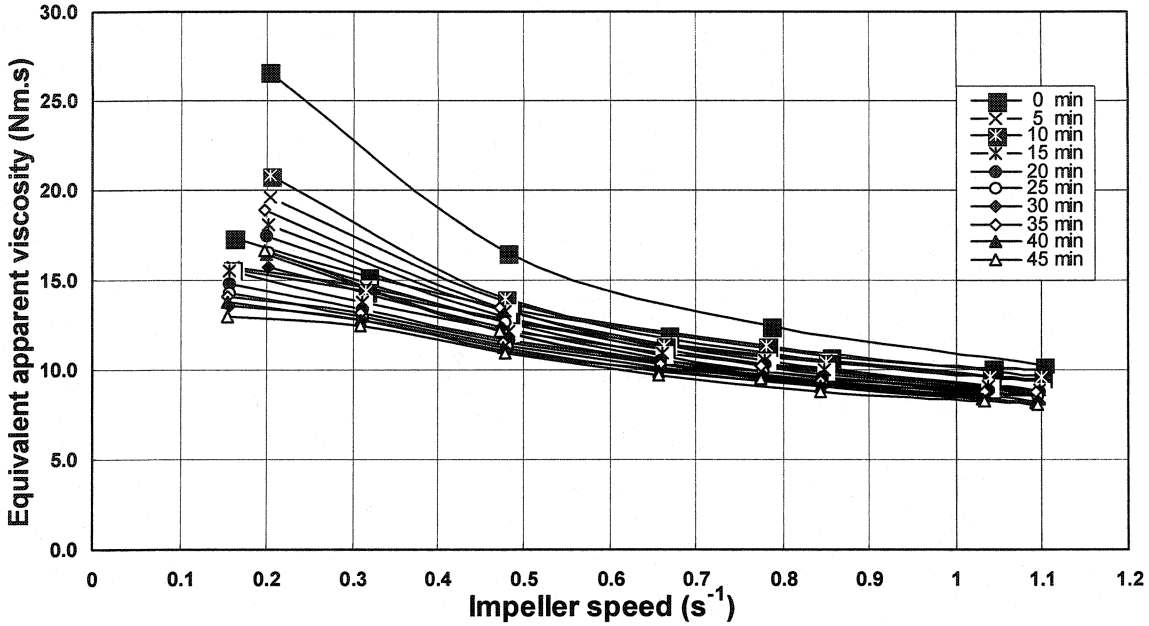


Figure 9.5 Equivalent apparent viscosity vs. impeller speed for WA-3.

9.4.3 Thixotropy

In Figure 9.6, WA-2 (a) and WA-2 (b) represents the equivalent apparent viscosity calculated for the higher (1.10 s^{-1}) and lower speed (0.48 s^{-1}) respectively (in the reverse cycle) in each five-minute cycle for the mix WA-2.

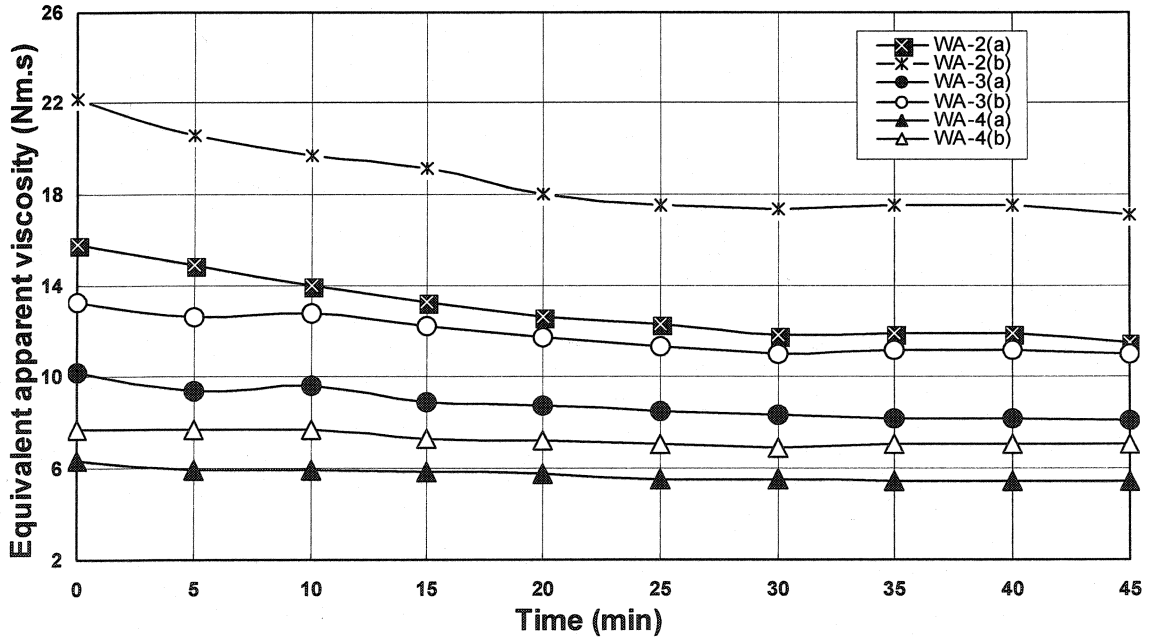


Figure 9.6 Equivalent apparent viscosity vs. time at high (a) and low (b) impeller speed.

The values of equivalent apparent viscosity for the constant speed 0.48 s^{-1} are higher than those at 1.10s^{-1}. At constant speed, the equivalent apparent viscosity is decreasing with testing time and stabilizes after 20 min of testing. The rate of reduction of equivalent apparent viscosity is less when the water addition is increased from 6.5 to 7.5 wt%, due to the influence of free water present in castable. The equivalent apparent viscosity is decreasing with the water addition, for WA-2 to WA-4, in a nearly parallel fashion.

To confirm the role of cement hydration, after cast, the castable samples of WA-1, 2, 3 and 4, are covered with a plastic film and cured at 20^{0}C for 24 hours, demoulded and dried for 24 hours at 110^{0}C, and fired at 1000^{0}C for 5 hrs. The bonding water remains unchanged at 1.1 wt % and the free water is proportional to water addition under the given experimental conditions (Figure 9.7), when the mixing water is changed from 6.0 to 7.5 wt%.

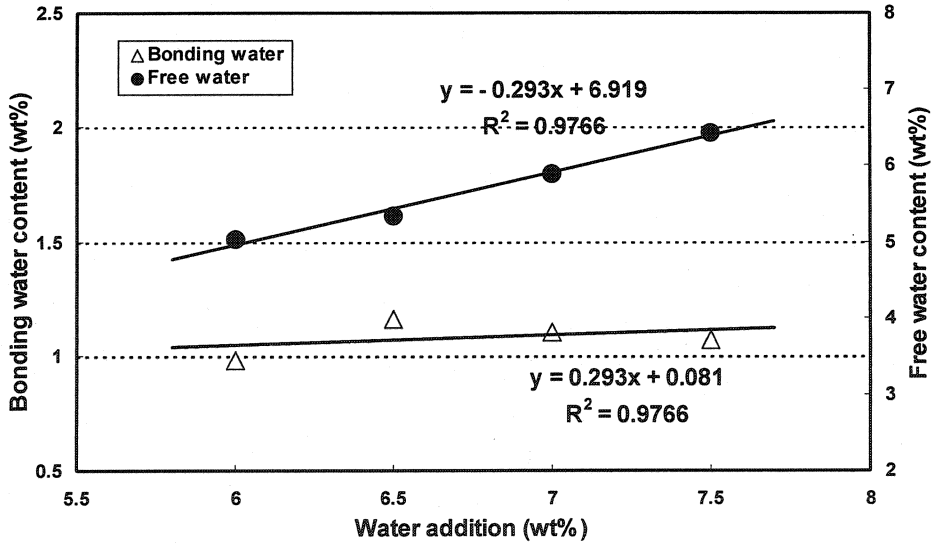


Figure 9.7 Bonding water and free water of castables WA-1, WA-2, WA-3 and WA-4.

9.4.4 Flow Resistance and Torque Viscosity

The method of evaluation of G and H values using the rheometer test results has been described in Chapter 4. The calculated values are shown in Table 9.3. The G values are

higher for WA-2, followed by WA-3 and WA-4 respectively. G values decrease for the initial 20min and remains constant further on for WA-2 and WA-3. For the mix WA-4, G values decline very slightly with time. Trends for H values are similar to the G values.

Table 9.3 G and H values for three compositions

Time (min)	Flow resistance G (Nm)			Torque viscosity H (Nm.s)		
	WA-2	WA-3	WA-4	WA-2	WA-3	WA-4
0	3.42	1.86	0.88	13.5	8.65	5.56
5	3.33	1.73	0.85	12.58	8.47	5.41
10	3.29	1.62	0.86	11.54	8.27	5.34
15	3.15	1.56	0.82	11.15	8.02	5.2
20	2.92	1.52	0.83	10.65	7.78	5.05
25	2.82	1.46	0.74	10.33	7.58	5.05
30	2.71	1.42	0.73	10.06	7.43	4.9
35	2.73	1.41	0.79	9.96	7.41	4.96
40	2.75	1.4	0.79	9.94	7.4	4.95
45	2.76	1.33	0.74	9.87	7.34	4.9

The relationships between water addition and G are shown in Figure 9.8. When the water addition is from 6.5 to 7.0 wt%, the G value decreases much more than from 7.0 to 7.5 wt%.

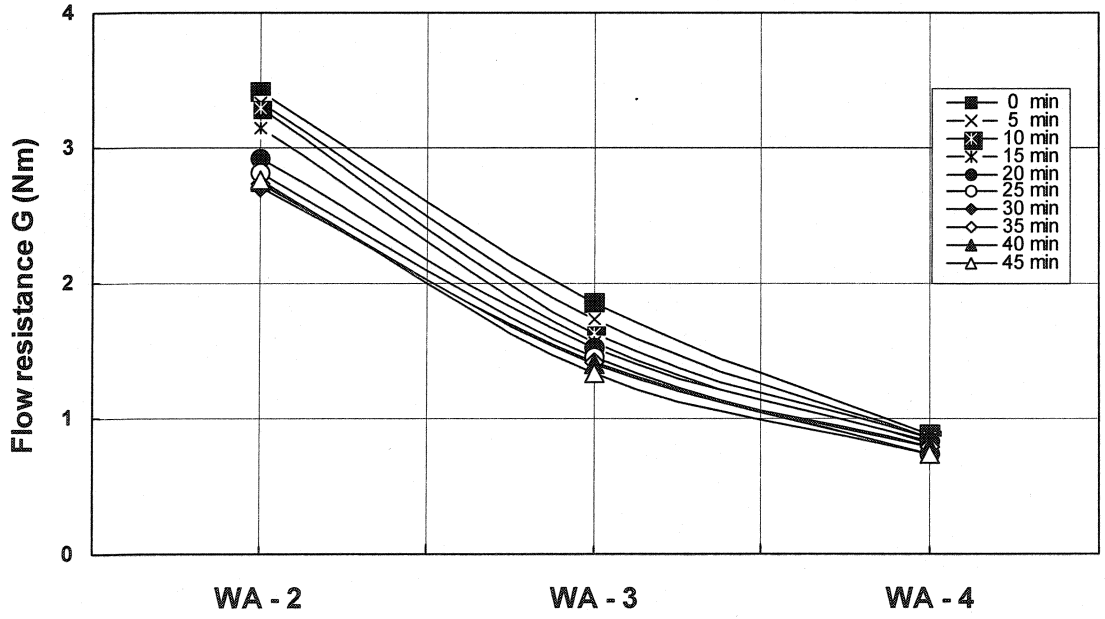


Figure 9.8 Flow resistance vs. water addition.

The relationships between water addition and H can be understood in Figure 9.9. The same trend has been observed for H, but the water addition has got more effects on G than H.

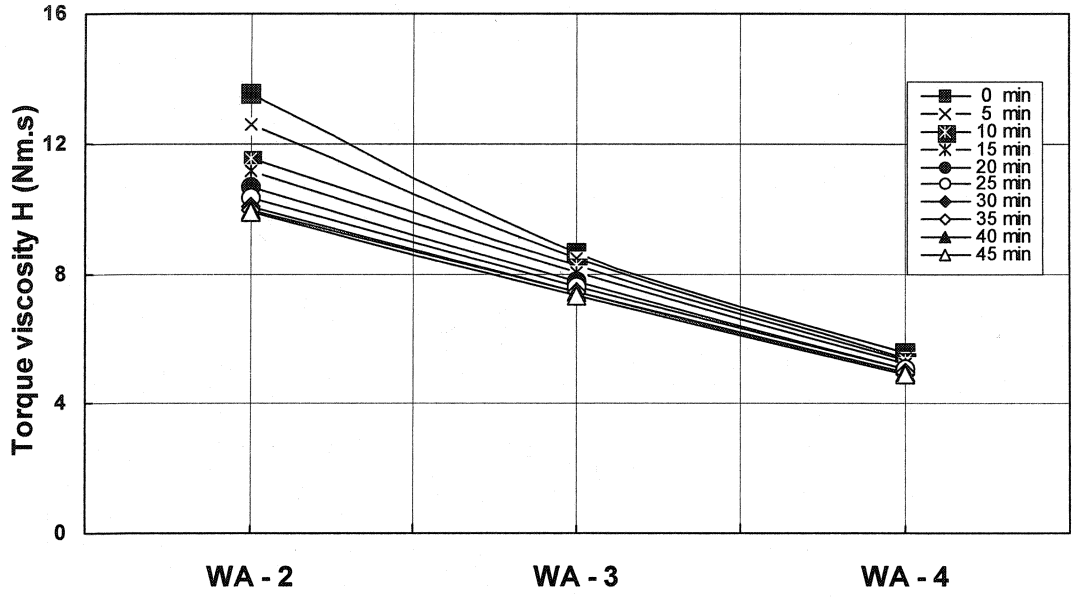


Figure 9.9 Torque viscosity vs. water addition.

9.5 Matrix Rheology

The Bohlin rheometer has been used instead of the IBB rheometer for the castable whole mix. The matrix slurry of castable WA-1 with 6.0 wt% water addition can be measured by Bohlin rheometer, but such whole castable mix could not be tested by IBB rheometer.

9.5.1 Shear Stress vs. Shear Rate

The shear stress as a function of shear rate of the matrix slurry of the four castables is shown in Figure 9.10. As for the castable mixes, the shear stress in the forward cycle (shear rate increasing) is higher than the rate in the reverse cycle (shear rate decreasing) and then forms a hysteresis loop. The forward cycle reveals the pseudoplastic nature of the slurry, and the reverse cycle Bingham behaviour. Added with more water, the loops shift downwards.

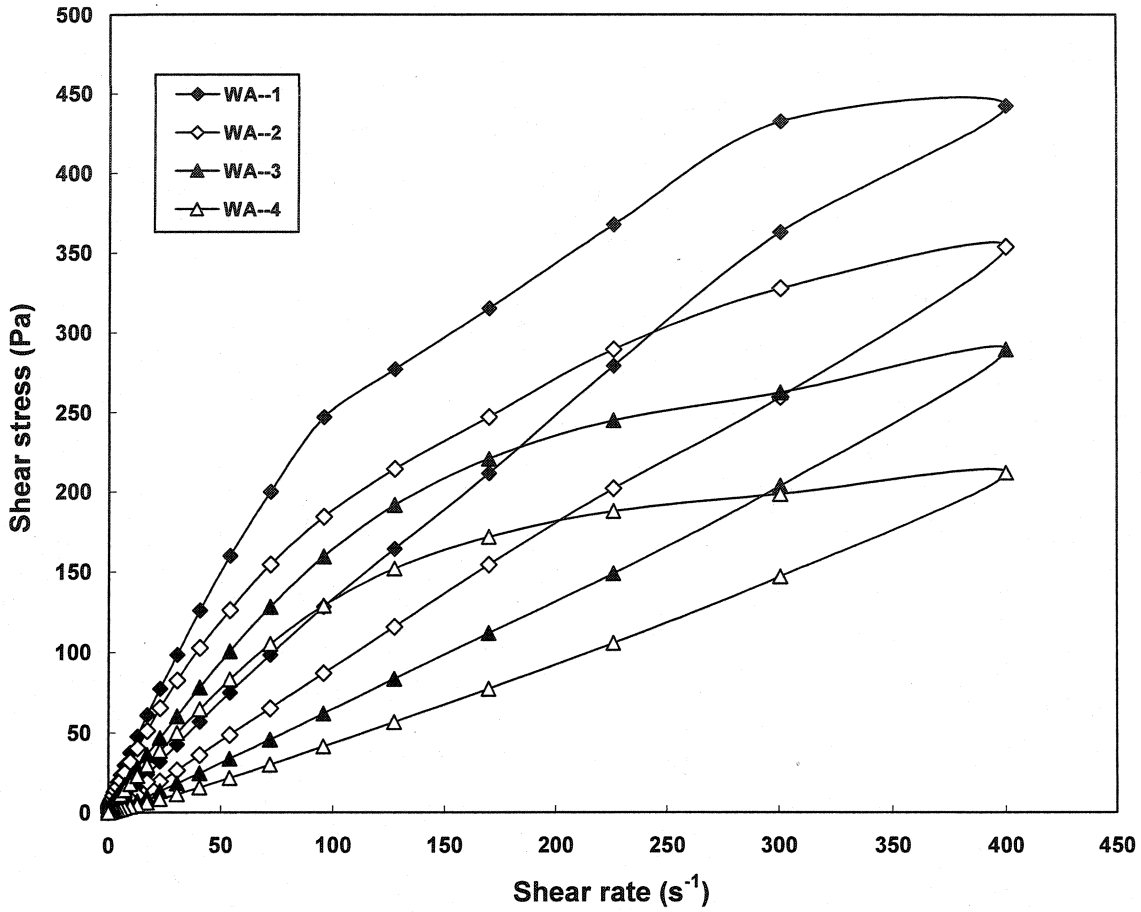


Figure 9.10 Shear stress vs. shear rate for all the matrix slurries.

The shear stress (τ_{max}) at the highest shear rate of 400 s^{-1}, of all slurries is given in Table 9.4. The τ_{max} decreases as water addition increases.

Table 9.4 The shear stress (τ_{max}) of the 4 slurries at the highest shear rate of 400 s^{-1}

Composition	WA--1	WA--2	WA--3	WA--4
τ_{max} (Pa)	442	354	290	212

9.5.2 Apparent Viscosity vs. Shear Rate

The apparent viscosity as a function of shear rate of the matrix slurries of castables WA-1 to WA-4 is shown in Figure 9.11. The apparent viscosity in the forward cycle is higher than rate in the reverse cycle. The apparent viscosity of WA-1 is ranked at the first place, followed by WA-2, 3 and 4. The lines are paralleling and WA-1 is close to WA-2 while WA-3 is close to WA-4. In the forward cycle, the apparent viscosity decrease

sharply from the beginning to 5.0 s^{-1} and remains stable between 5.0 s^{-1} and 100 s^{-1} and finally decreases slightly from 100 s^{-1} to 400 s^{-1}. In the reverse cycle, the apparent viscosity of all the slurries remains similar up to a shear rate of 1 s^{-1} and increase more clearly at very low shear rate 1.0 s^{-1} to 0.1 s^{-1}.

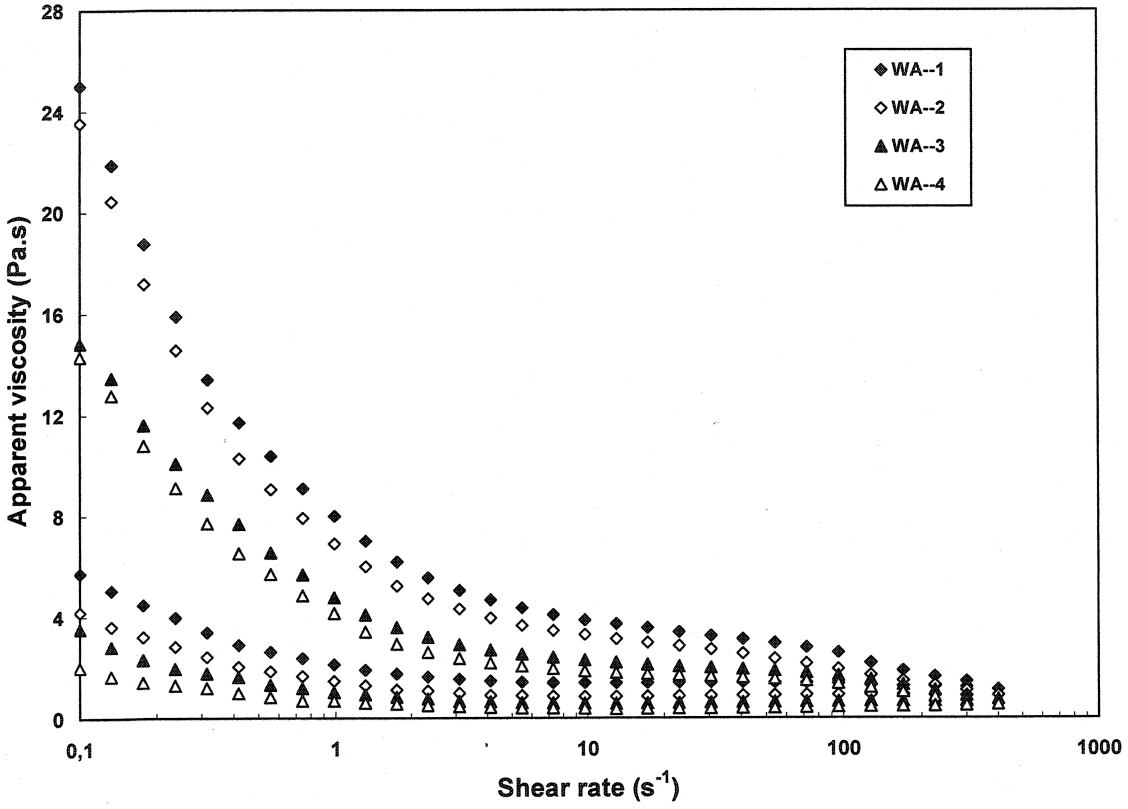


Figure 9.11 Apparent viscosity vs. shear rate for all the matrix slurries.

9.5.3 Thixotropy

The thixotropy degree and loop's area for the four matrix slurries are calculated in Figure 9.12, as defined in Chapter 4.6.3. The thixotropy degree decreases as the water addition increases. The loops' area also shows the same trend.

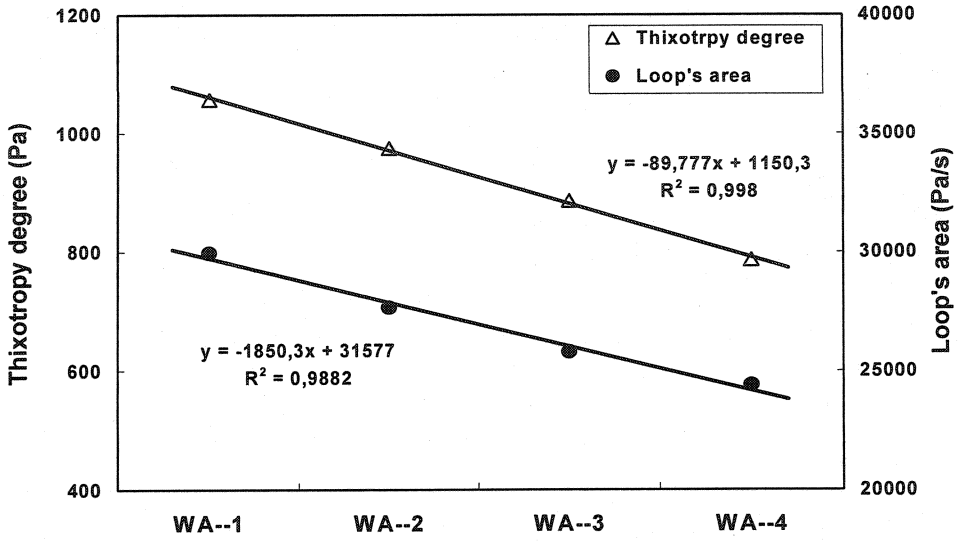


Figure 9.12 Thixotropy degree and loop's area for all the matrix slurries.

9.5.4 Plastic Yield Stress and Plastic Viscosity

The calculated values of plastic viscosity and yield stress of the matrix slurries are given in Table 9.5. Both the plastic viscosity and yield stress are decreasing as water addition increases.

Table 9.5 Plastic viscosity and yield stress of all the matrix slurries

Composition	WA--1	WA--2	WA--3	WA--4
Plastic viscosity (Pa.s)	2,92	2,34	1,829	1,51
Plastic yield stress (Pa)	7,000	6,803	3,512	2,817

9.6 IPS of Matrix and MPT of Castables

The calculation methods of IPS of matrix and MPT of the castables are described by Equation 2.7 and 13. The IPS and MPT of WA-1, 2, 3 and 4 are given in Table 9.6.

Table 9.6 IPS of matrix and MPT of castables

Composition	WA--1	WA--2	WA--3	WA--4
IPS (nm)	70.7	79.3	87.9	96.5
MPT (μm)	115.3	119.5	123.8	128.1

IPS is a major determinant of the rheology of a castable mix. Only when the water content is sufficient to separate the particles of more than 50 nm, the castable mix can be expected with reasonable fluidity. The IPS parameter is commonly used for the fine

fraction, since it considers water as the separation medium. In Figure 9.13, with the increase of water addition, the IPS values increase proportionally. The MPT parameter is used to estimate the average distance between aggregates (coarse particles). Actually, the MPT is derived from the IPS, as suggested by Dinger and Funk [10]. The MPT parameter is commonly used for the coarse fraction, since it considers water as the matrix part, instead of the separation medium. Higher MPT values, considering the castable discrete particle size distribution, are usually responsible for enhanced flowability. However, the MPT value must have an upper limit, otherwise some thermo-mechanical properties, such as the creep resistance at high temperature, could be seriously degraded. Since flow is a function of the MPT and of the matrix rheology, a combined analysis could be useful to predict the rheological behaviour of castables. Both IPS of all the matrix slurries and MPT of the castables proportionally increase as water addition increases.

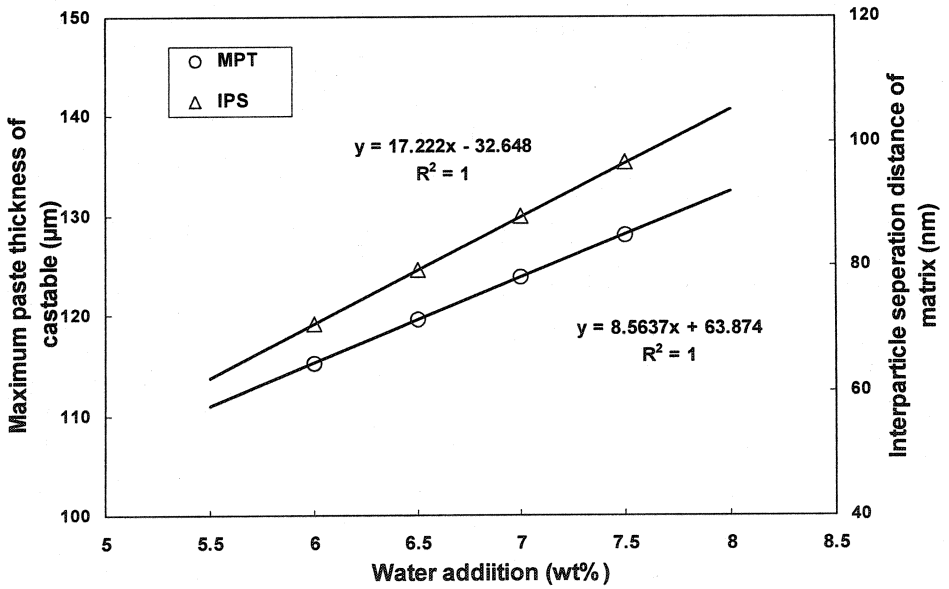


Figure 9.13 Relationship between water addition and IPS and MPT.

9.7 Discussions

9.7.1 Solid Content

The solid content of castable mix and matrix is shown in Figure 9.14. The solid content decreases proportionally as the water addition increases.

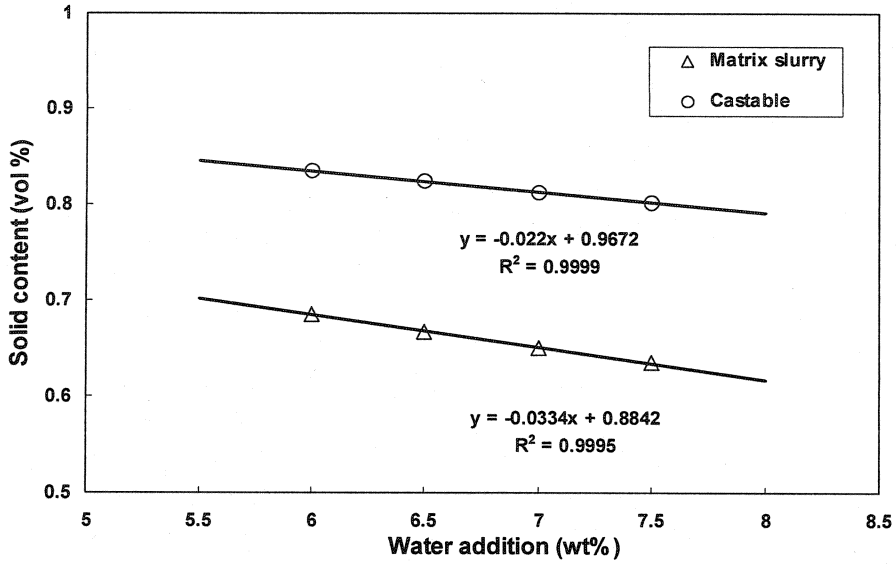


Figure 9.14 Solid content of the castables and matrix slurries.

9.7.2 Relationship between IPS and Rheology of the Matrix Slurries

The plastic yield stress and viscosity decrease as the IPS of the matrix slurries increases, as shown in Figure 9.15.

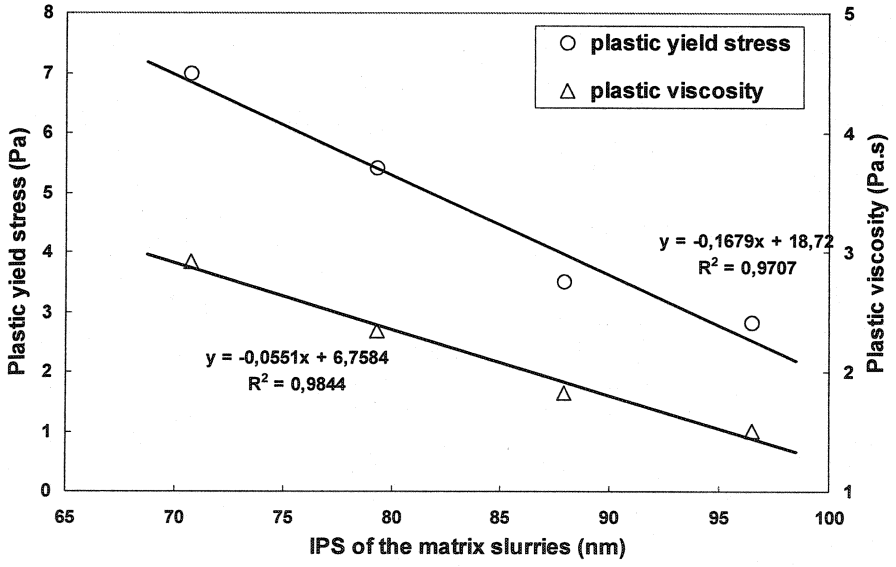


Figure 9.15 Relationship between IPS and plastic yield stress and viscosity.

9.7.3 Relationship between MPT and Rheology of the Castable Mixes

Both the flow resistance and torque viscosity decrease as the MPT of the castable mixes increases, as shown in Figure 9.16.

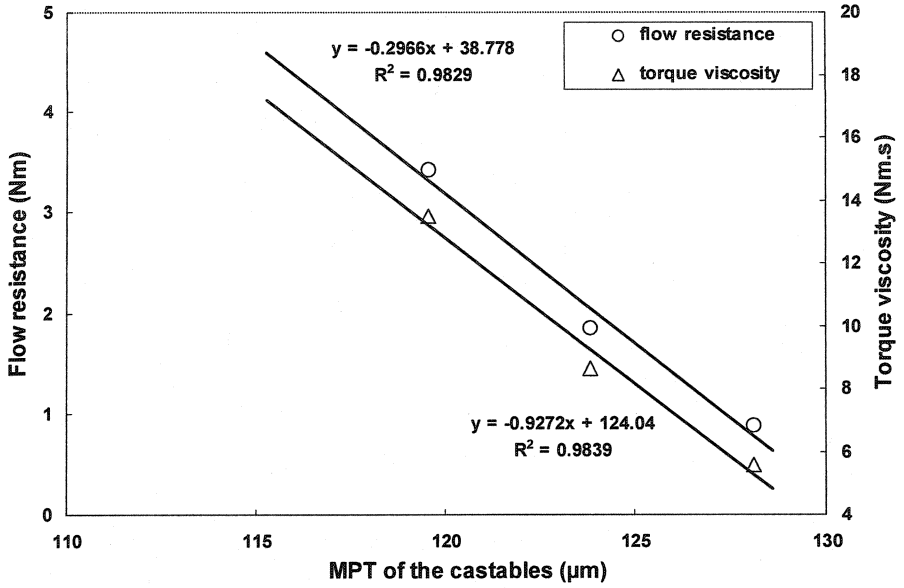


Figure 9.16 Relationship between MPT and flow resistance and torque viscosity.

9.7.4 Relationship between Castable and Matrix Rheology

The prime characteristics of flow resistance, G, of the castable is compared with plastic yield stress, τ_p, of the matrix slurry (Figure 9.17), showing a good correlation.

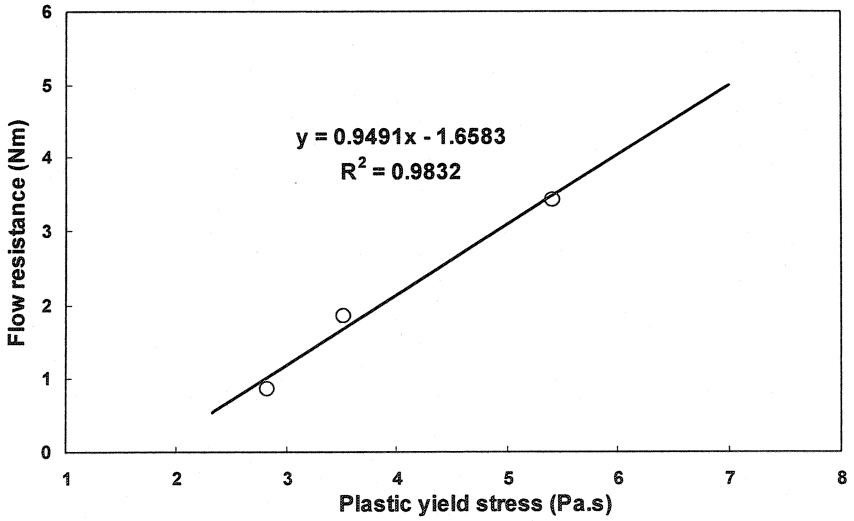


Figure 9.17 Relationship between flow resistance of the castables and plastic yield stress of the matrix slurries.

The parameter of torque viscosity, H, of the castable is compared with plastic viscosity, η_p, of the matrix slurry (Figure 9.18), also showing a good correlation.

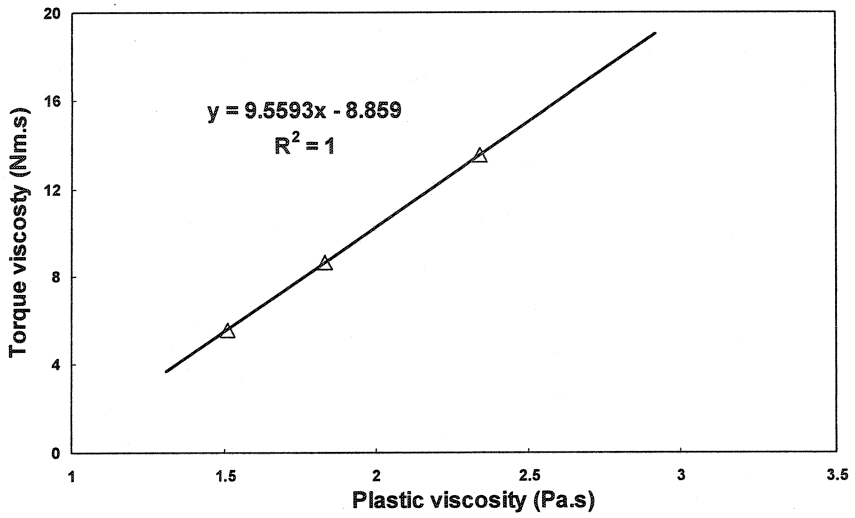


Figure 9.18 Relationship between torque viscosity of the castables and plastic viscosity of the matrix slurries.

9.7.5 Relationship between Self-flowability and Rheology

Self-flowability increases as the plastic yield stress and flow resistance decrease (Figure 9.19). The same trend is with plastic viscosity and torque viscosity (Figure 9.20).

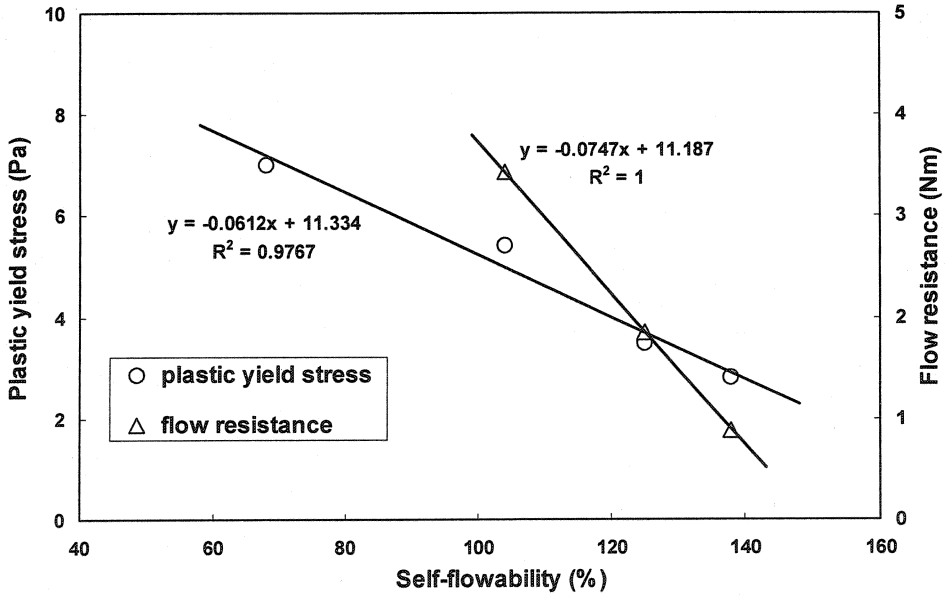


Figure 9.19 Relationship between self-flowability and flow resistance of the castables and plastic yield stress of the matrix slurries.

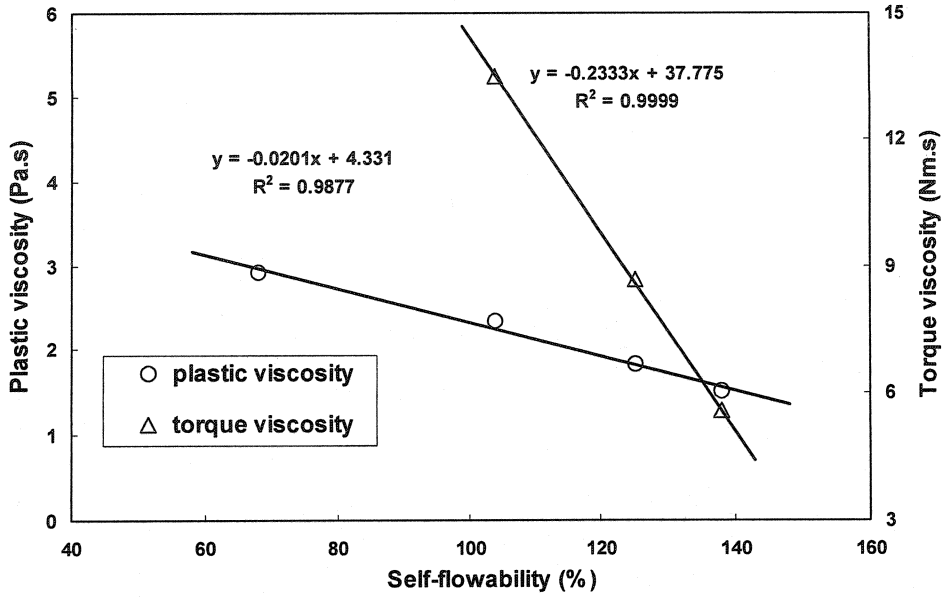


Figure 9.20 Relationship between self-flowability and torque viscosity of the castables and plastic viscosity of the matrix slurries.

9.7.6 Relationship between Self-flowability and IPS and MPT

Self-flowability increases when the IPS of the matrix slurries and MPT of the castable mixes increase (Figure 9.21).

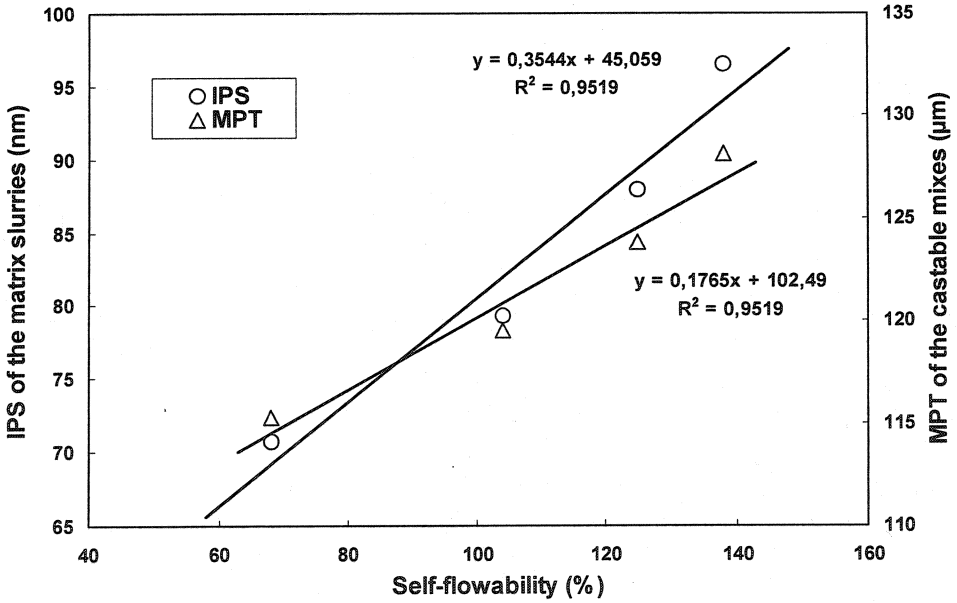


Figure 9.21 Relationship between self-flowability and IPS of the matrix slurries and MPT of the castables.

9.7.7 Summary

The rheological behaviours of the castable mixes are measured by IBB rheometer, with the highest impeller speed of 1.1 s^{-1}, while the matrix slurries are tested by Bohlin rheometer up to the shear rate of 400 s^{-1}. Although the shear rates are different, the rheological parameters of the castables: flow resistance and torque viscosity are related to plastic yield stress and viscosity of the matrix slurries, respectively. The water addition, solid content, IPS, MPT and self-flowability are all related to each other, through the rheological parameters.

9.8 Physical and Mechanical Properties

The mechanical properties of the castables are shown in Table 9.7. With water addition increasing, the CMOR values decrease and the AP values increase. In the case of WA-1, WA-2 and WA-3, the CMOR and AP values are beyond 8 MPa and below 18 % respectively. In the case of WA-4, the CMOR values are around 6 MPa and the AP values are beyond 19 %. Then over a certain amount, the excessive free water brings negative impacts on the mechanical properties of castable.

Table 9.7 CMOR and AP of all the compositions

Composition	CMOR (MPa)		AP (%)	
	0 min	45 min	0 min	45 min
WA--1	10.3	12.7	15.7	14.9
WA--2	9.9	10.2	17.6	17.6
WA--3	9.3	8.7	18.2	17.8
WA--4	6.7	6.3	19.3	19.6

9.9 Appearance of Samples

The appearance of the castables with different water additions at different time intervals is shown in Figure 9.22(a)-(h). In these figures, the samples of WA-1 are prepared by vibration and the others are made as self-flow castables. The appearance of the fresh (0min.) castables for WA-1, WA-2 and WA-3 look very good, whereas dewatering and bleeding have been observed for WA-4, with 7.5 wt% water addition. After 45min of

mixing, some degassed bubbles appear on the surface of WA-3, with 7.0 wt% water and major segregation is observed on WA-4, with 7.5 wt% water.

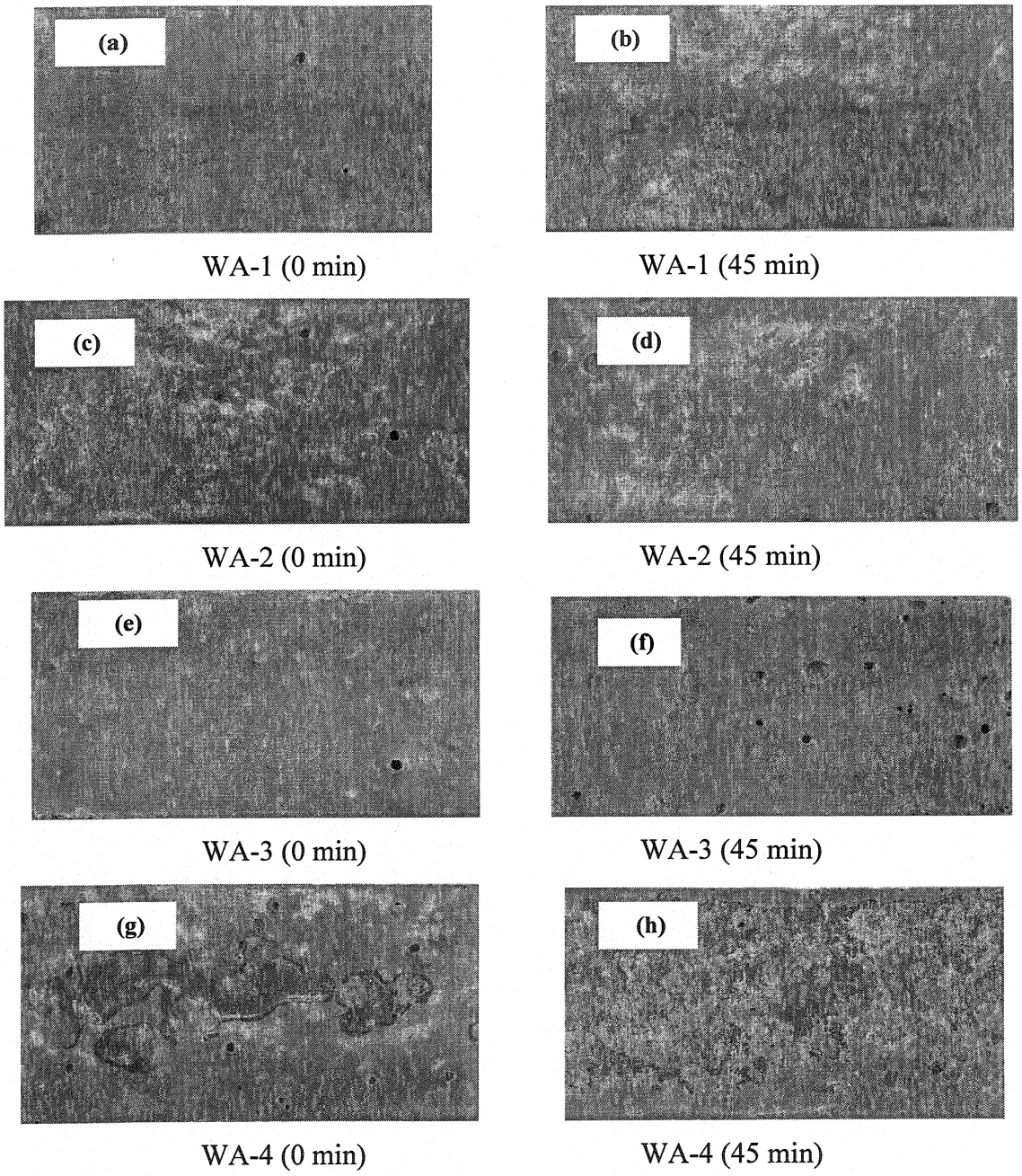


Figure 9.22(a)-(h) Appearance of samples WA-1, 2, 3 and 4 cast at different time.

9.10 Optimization of Castables

In this work, WA-2, WA-3 and WA-4 show a good self flowability (Figure 9.1); nevertheless they are not yet good pumpable castables. For good pumpability, a castable must possess optimum combination of torque viscosity and flow resistance in order to flow well and to avoid blockage and segregation. The relationship between G and H is shown in Figure 9.23. Furthermore, in practice, the type of pump and size of the pipe in which the castable is to be pumped are also very important parameters, not accounted for in this work.

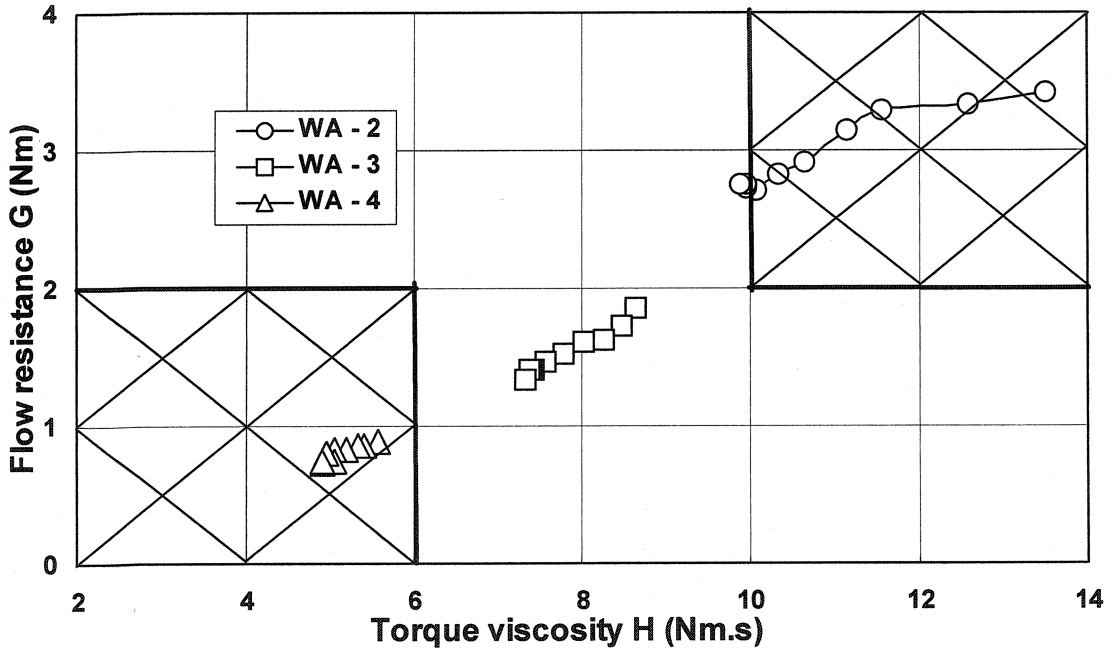


Figure 9.23 Flow resistance vs. torque viscosity.

The composition WA-2 is having good flow resistance (no segregation) but very high torque viscosity. In the case of WA-4, values of G and H are much lower, but as it has been shown in the previous sections, this mix with 7.5 wt% water is subjected to segregation (early separation of aggregates and matrix fines). Only composition WA-3 appears to have the optimum combination. Below 7.0 wt% water addition there is a drastic increase in flow resistance G, and above 7.0 wt%, however, there is a drastic reduction in torque viscosity H. This means that an optimum amount of water and

sufficient lubrication is required to avoid blockage inside pipes and sufficient viscosity is required to avoid segregation by maintaining flowability, coherence, integrity and stability of the castable mix. Only the measured rheological constants of WA-3 are found to be optimum, for the pumping and shotcreting trials. Experiences in the filed are now required to validate the data.

9.11 Conclusions

Based on this part of the investigation, the following conclusions can be drawn:

a) Water is a very important factor to define the placement of castable. In this work, the castable with 6.0 wt% water addition possesses good vibration castable characteristics; with 6.5 wt%, it shows a good self-flow castable characteristics; and with 7.0 wt%, it can be a good pumpable castable, in every case with satisfactory mechanical properties.

b) Rheological parameters G and H have direct correlation with the amount of water addition under the present set of conditions.

c) Only composition WA-3 with 7.0 wt% water has the optimum values of H and G to be both self-flowing and pumpable.

d) When the amount of water is beyond 7.0 wt% under the given conditions, the castable segregates and the mechanical properties do deteriorate drastically.

CHAPTER 10 - AGING TIME

In this chapter, the effect of aging time on the rheological behavior of an "optimum" bauxite-based low-cement self-flow castable has been studied in details. This "optimum" composition has been derived through the results obtained in the previous several chapters. The rheological parameters have been measured on the fine matrix portion as well as on the whole castable mix. Three stages have been distinguished from homogenization to saturation to setting effect state. The flow decreases during the homogenization state, remains stable during saturation state, and increases during setting effect state. The same is confirmed by conductivity and exothermic profile study on fine matrix also.

10.1 Introduction

There are many reports on the hydration process of calcium aluminate cement (CAC) and the setting mechanism of LCCs through which the hydration process of CAC in castable is by now clearly understood. The mechanism of hydration of calcium aluminate cement starts with the dissolution of the CA constituents then by various hydrates formation and is followed by the precipitation of the hydrates from solution. The hydration process is broken into three stages: (a) dissolution, (b) nucleation and (c) massive precipitation and crystallisation. The mechanism has been explained in details in the literature [40, 81, 82, 102, 103, 104].

Rheological characteristics can be expressed by the relationships between shear stress (τ) and shear rate (γ), apparent viscosity (η) and shear rate, and apparent viscosity and time under a constant shear rate. Commonly, flow behaviour of a fluid can be understood using flow curves (τ-γ or η-γ curves). As described in many references [10, 11], there are six flow patterns under a narrow range of shear rates: Newtonian, Bingham (or yield-Newtonian), Pesudoplastic, Yield-Pseudoplastic (plastic flow), Dilatant and Yield-Dilatant. Since dilatancy causes some problems during installation,

dilatant flow is an undesirable behaviour for castable. Castables commonly follow a Bingham or plastic flow behaviour [63], with a yield stress τ_y. At the applied stress $\tau \leq \tau_y$, no flow occurs; when $\tau \geq \tau_y$, plastic flow occurs. For self-flow castables, the gravity force of the castable overcomes τ_y and makes the castable self-level without any other external force. The rheological equation is followed by the Herschel-Bulkley model which incorporates the elements of Newtonian, Bingham and Power law (Ostwald model) models [67, 68, 105, 106].

$$\tau = \tau_y + (\eta_p \times \gamma^{n}) \qquad \textbf{(Equation 10.1)}$$

where, τ = shear stress,

τ_y = plastic yield stress,

η_p = plastic (or Bingham) viscosity,

γ = shear rate,

n = power law index of the material.

When n =1 and $\tau_y = 0$, the equation describes a Newtonian fluid; when n = 1, a Bingham fluid and when n < 1, a yield-pseudoplastic. Mathematically, Bingham rheology differs from yield-pseudoplastic, but in practice, they are quite similar. A yield-pseudoplastic rheology may really be Bingham, but the rheogram may not have been measured at sufficiently high shear rates to detect the constant, high shear, plastic viscosity. Such a flow pattern corresponds to a shear-thinning effect, which is desirable for casting by vibration. By and during the vibration, castables should easily flow to fill any cavity, during which the wrapped air should escape to avoid leaving big pores. This flowability comes from thixotropy, instead of too much water, otherwise the porosity of the placed body would be too high and segregation may happen. After casting, when the vibration stops, the internal structure should soon recover to avoid segregation of the coarse aggregates [63].

When CAC reacts with water to form a hydrate, the heat of hydration evolves. Most of the hydration reactions end in a short time, concentrating the heat of hydration to this period. Cement hydration process can be defined and quantified by some techniques, such as mixing energy, conductimetry and calorimetry [104, 107-109]. This hydration process does occur in the cement bonded castables but is more complicated since the matrix paste of a LCC is usually made by mixing CAC, micro-silica, fine fillers, dispersant and water. It is evident that no single technique is able to provide a complete understanding of the interactions that occur within castables during their placing. More predictive techniques are required for an efficient optimization of castable placing characteristics [104].

In practice, two important characteristics of castables are given more attention: the working time and setting time. Working time of self-flow castable is the time after mixing till the castable can still be well placed by vibration or self-flowing. The industrial condition needs at least 45 min of working time. There are ASTM standards to evaluate working time of both vibration and self-flow castable. Setting time is time after mixing where the cast part develops enough mechanical strength for demoulding. Usually, flow decay test is used to assess the working time of self-flow castable [77, 101, 110, 111]. Flow decay time is the time required to reach zero free-flow after wet mixing. For a castable, set time seems to be influenced not only by the individual characteristics of the raw materials, but to a large extent by synergistic effects from interactions between individual components. This makes it almost impossible to predict the behaviour without testing. It is relatively easy to measure flowability by flow table test using a cone described as ASTM test method [70]. In ASTM C 1446-99, working time of self-flowing castable is defined as the elapsed time from the first addition of water or liquid during mixing until the mix will only achieve 25% self-flow using the procedure described in this test method. Self-flowability of 25% has been selected as the minimum at which a mix can be poured into typical molds or forms in normal practice. In practice, flow decay is tested until zero self-flow, instead of 25 % flow. This test

method is not appropriate and sufficient for determining the pumpability of the castable refractories. As the attempts to predict the pumpability from self-flowability test alone are not always successful, the rheological properties of a castable with elapsing time must be considered for a good pumpable castable.

In castable research, it has been a long time practice to evaluate the rheological behaviour of fine matrix and to correlate the same with the behaviour of castable. It is an inadequate technique and further efforts are required to evaluate rheology of castable mixes also. It is well known that after the introduction of coarse grains into fine matrix, there are some changes in rheology due to effects such as absorption of a portion of water by grain pores or coarse grains size and shape etc. It has been clearly shown in the previous chapters than a more appropriate method is to evaluate the rheology of both fine matrix slurry and castable and correlate them. Since both working and setting time are a function of time, the rheology should also be evaluated with time. In this work, the influence of elapsing time on castable rheology is investigated in terms of the rheological parameters flow resistance (G) and torque viscosity (H) and matrix rheology with plastic yield stress (τ_y) and plastic viscosity (η_p). The correlations between these parameters are then analyzed and discussed.

10.2 Composition

The castable has, of course, the same q value of 0.26 and D_{max} of 5 mm as established in Chapter 4. The cement and microsilica contents are fixed at 4 and 5wt%, respectively, as such a formulation provided satisfactory results as shown in previous chapters. The amount of water is fixed at 7 wt% and Dispersant SHMP is taken as the dispersant with 0.12 wt% addition. All these characteristics are compiled in Table 10.1.

Table 10.1 Details of the mixes to study the effect of aging time

Aggregate (wt%)		59
Fine matrix (wt%)	Bauxite-1	11
	Bauxite-2	12
	Bauxite-3	9
	Cement CA-14	4
	Microsilica-1 (Elkem 971U)	5
	Dispersant SHMP (wt%)	0.12
Water addition (wt%)	7.0	
Rheology testing time for castable	**Total time (min)**	**185**
	Interval time (min)	**5**
Rheology testing time for matrix slurry	**Total time (h)**	**6**
	Interval time (h)	**1**

10.3 Flow Decay

The self-flowability as a function of time is shown in Figure 10.1. Self-flowability decreases with elapsing time. At 25 % self-flowability, the working time, according to ASTM C 1446-99 is 220 min. At 100 min, the self-flowability decreases to 100% and then reduces to 0% at around 275 min. 100 min is the working time as a self-flow castable and the time from 100 to 275 min is the interval where gelling is occurring progressively [107, 111].

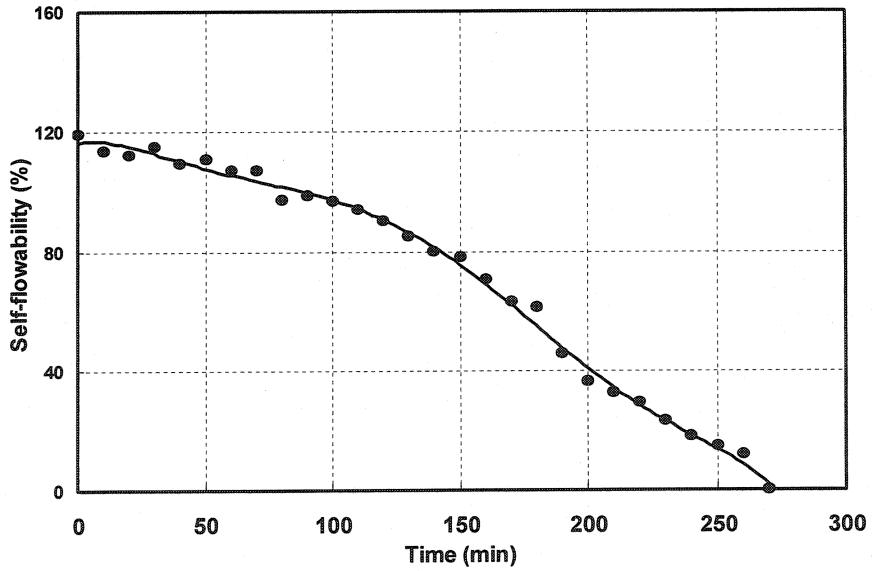


Figure 10.1 Flow decay.

10.4 Castable Rheology

10.4.1 Torque vs. Speed

Rheometer test on castable is carried out for 185 min, as shown in Figure 10.2. The rheograms are fragmented into 3 groups based on the changes in torque vs. speed relation. The group I of rheograms is formed with the rheometer results from 0 to 50 min, group II from 50 to 150 min and group III from 150 to 185 min.

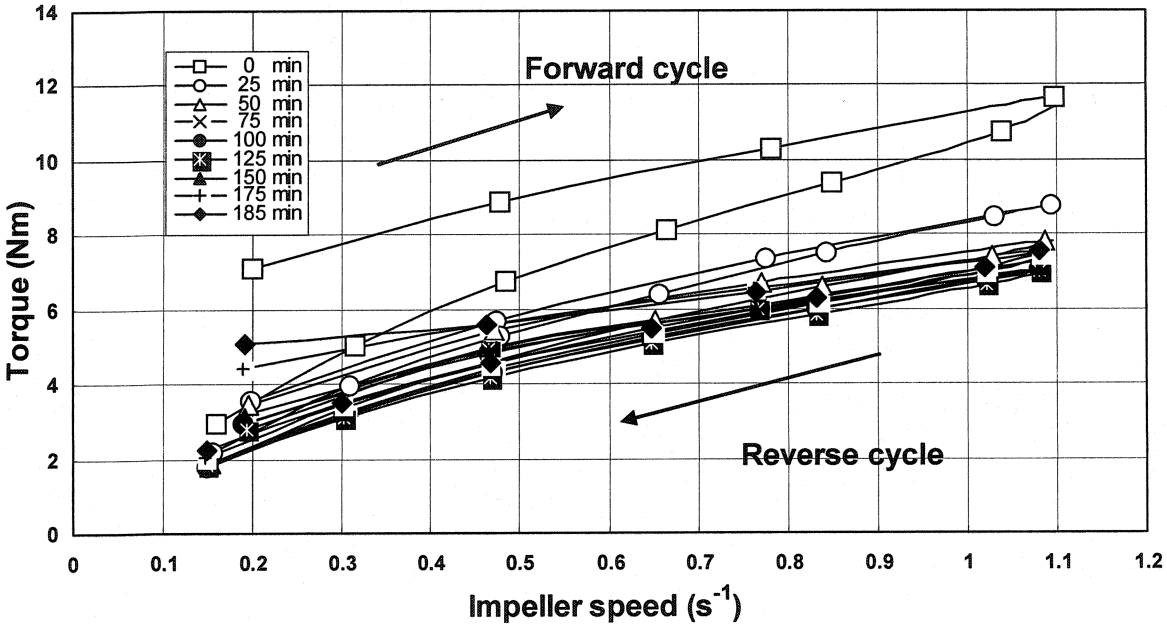


Figure 10.2 Torque vs. impeller speed for 0-185 min.

In Figure 10.2, at 0 min (the castable is tested immediately after poured in the bowl), the forward cycle reveals pseudoplastic nature, while in the reverse cycle the castable approaches a Bingham behaviour (Newtonian-type with yield).). In the forward cycle, the rate of torque increase is decreasing with testing speed and the mix is getting more homogenized. Once the maximum testing speed is reached, the homogeneous mix behaves almost linearly in the reverse cycle. In the same test, after 5min of mixing, there is a drastic reduction in the area of hysteresis loop, as compared to 0 min (the first testing) loop. The loop area remains almost the same after 10 to 50 min, but shifts downward. After 50 min, the loops follow the similar path till 150 min. After 155 min, the loops shift upward and the loop's area keeps on increasing till the end of the test.

These different rates of torque change with speed lead to different G and H values as shown later on. The important point to be noted here is that these changes could never be observed in flow decay test except gradual flow decay.

In the beginning of the test, the mix cannot be considered as completely mixed and gains in homogeneity with mixing speed. The shearing stress helps to the breaking of agglomerates, and to fill the voids and improve dispersion, due to the post mixing action of the impeller. Once the mix reaches the maximum speed, the mix is in a more homogeneous state and then shows Bingham behavior in the reverse cycle. Further on, in the testing cycle, the mix is more and more homogeneous and reaches after 50 min a state where further homogenization with mixing action is not possible. Since 50 min, the mix attains homogenous state and there is no change in rheograms. After 150 min, the rheograms start shifting upward due to strong cement reaction kinetics. These facts are explained well with the help of conductivity and exothermic profile studies later on.

The detailed rheometer results within the period of 185 min at 5-minute testing interval are shown in Figure 10.3, 4, 5 and 6, respectively. The hysteresis loops in these figures represent the relationship between torque and impeller speed for castable mix. The loops shift downward from 0 to 50 min as shown in Figure 10.3, and slowly then overlap in the time range between 50 and 100 min, as shown in Figure 10.4. The loops remain unchanged and merge in the period of 100-150 min and slightly rewind in the time interval of 150-185 min. The torque (T_{max}) at the highest impeller speed of 1.10 s^{-1}, at different testing time, is given in Table 10.2. The T_{max} decreases 33% in the first period of 50 min, slightly decreases from 50 to 100 min, remains the same from 100 to 150 min and increases from 150 to 185 min. The loops profiles change in much the same trend as T_{max} values versus time.

Table 10.2 T_{max} at the highest impeller speed of 1.10 s^{-1} at different testing time

Time (min)	0	25	50	75	100	125	150	175	185
T_{max} (Nm)	10.65	8.78	7.79	7.28	7.05	7.01	7.06	7.44	7.57

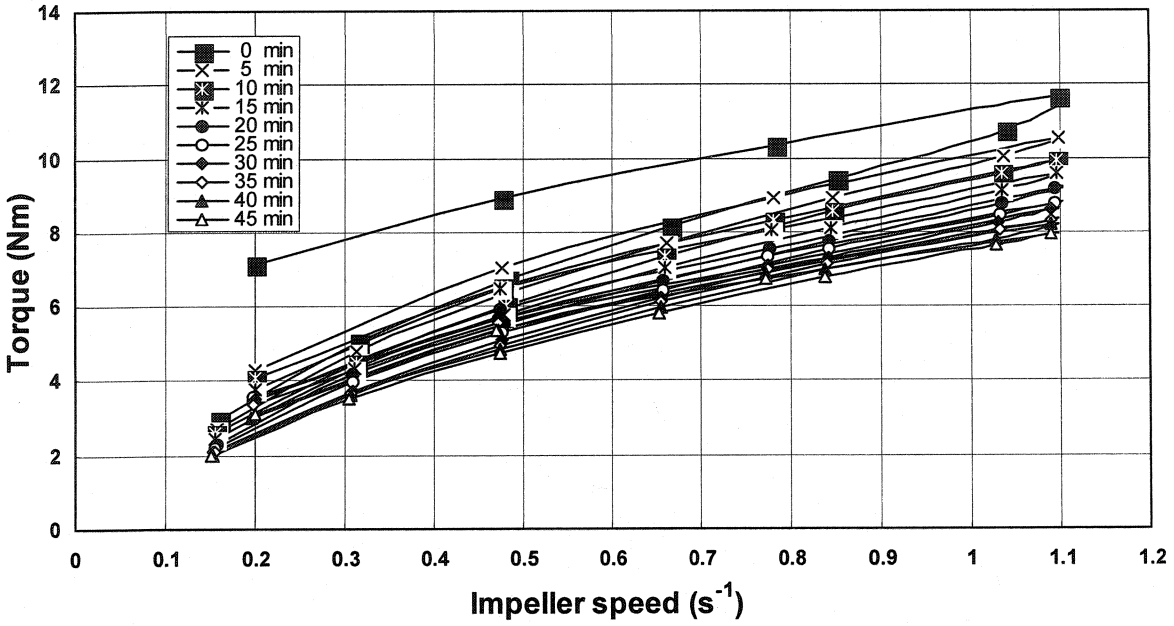


Figure 10.3 Torque vs. impeller speed for 0-45 min.

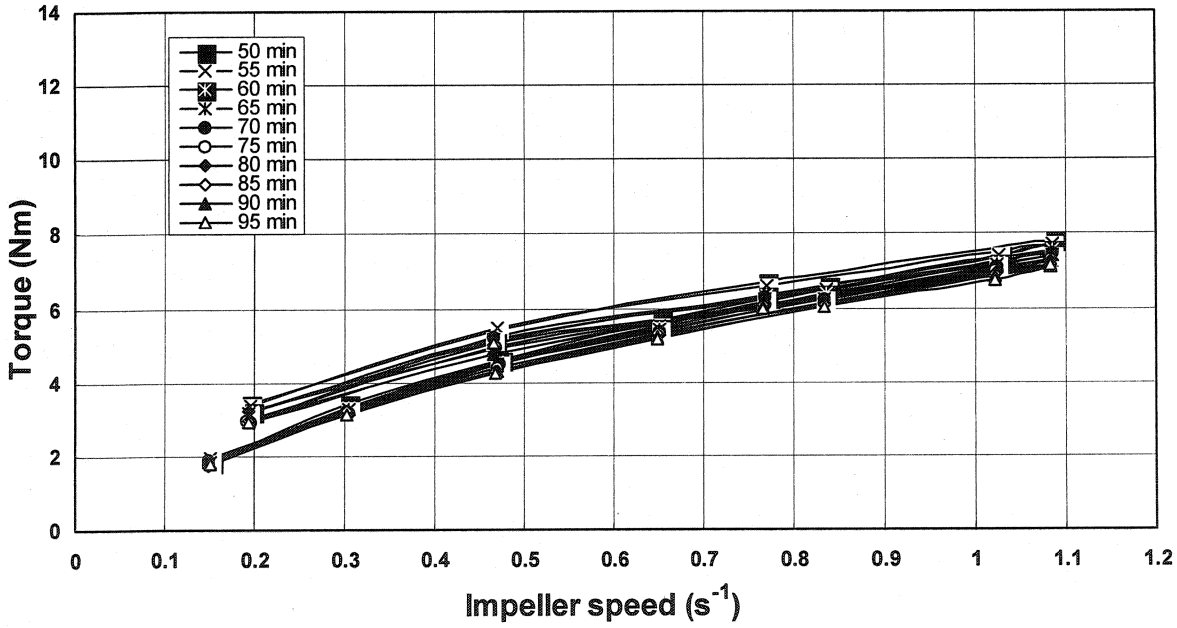


Figure 10.4 Torque vs. impeller speed for 50-95 min.

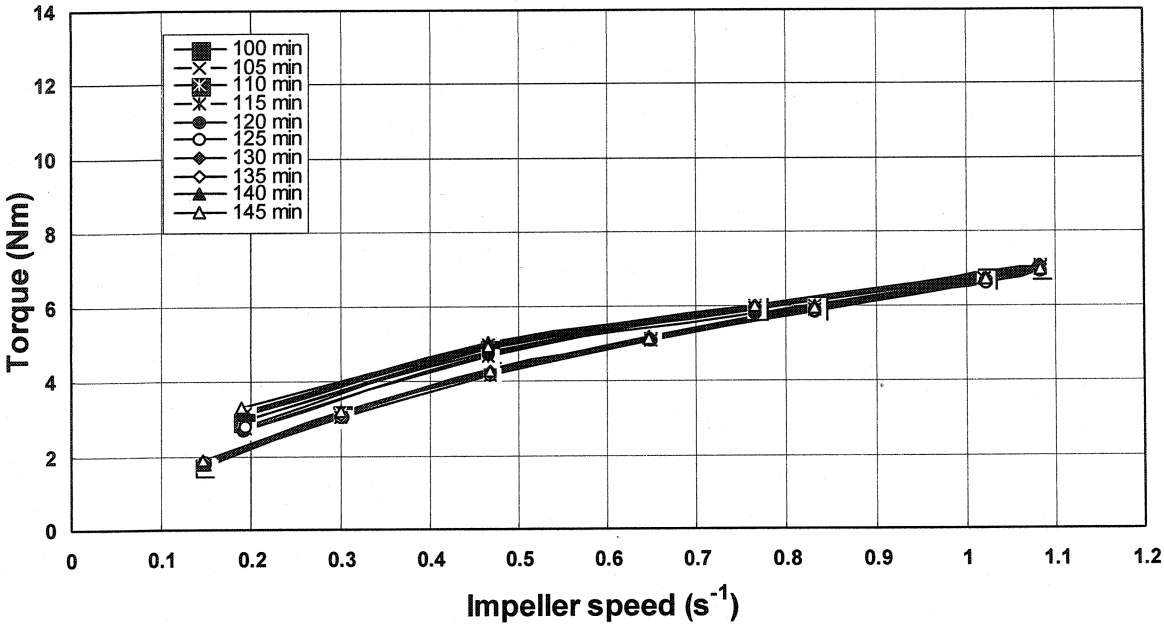


Figure 10.5 Torque vs. impeller speed for 100-145 min.

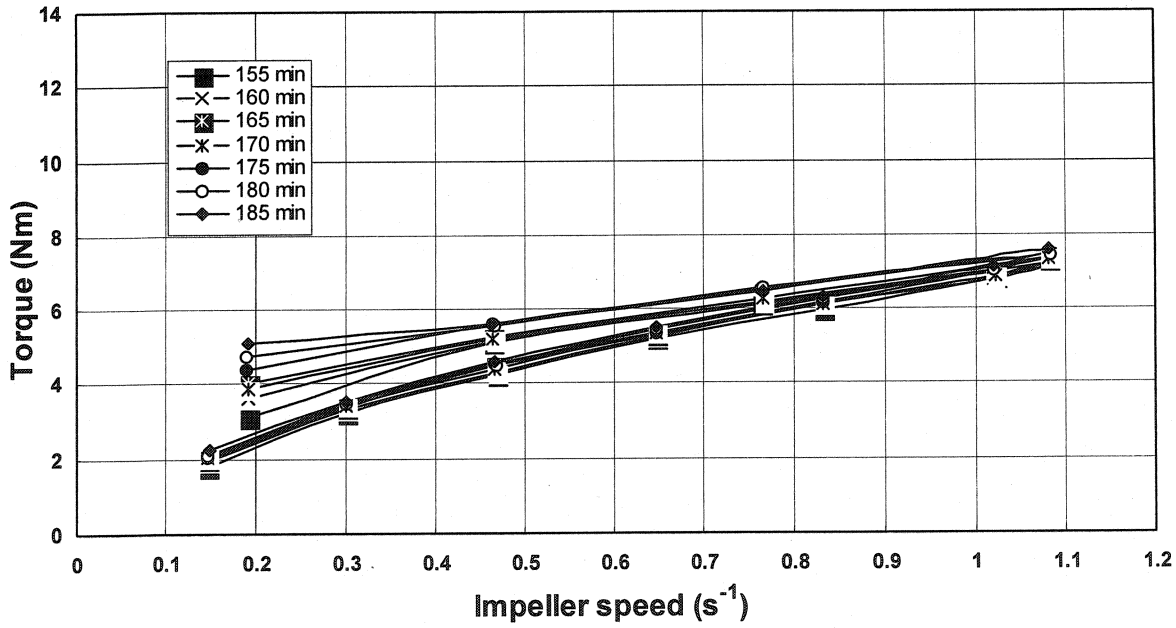


Figure 10.6 Torque vs. impeller speed for 150-185 min.

10.4.2 Equivalent Apparent Viscosity

The meaning of equivalent apparent viscosity has been described in Chapter 4.5.2. The relationship between equivalent apparent viscosity and impeller speed from 0 to 50 min of testing is shown in Figure 10.7. Typical Bingham behaviour is observed. The trends are the same with other different testing time and hence not shown.

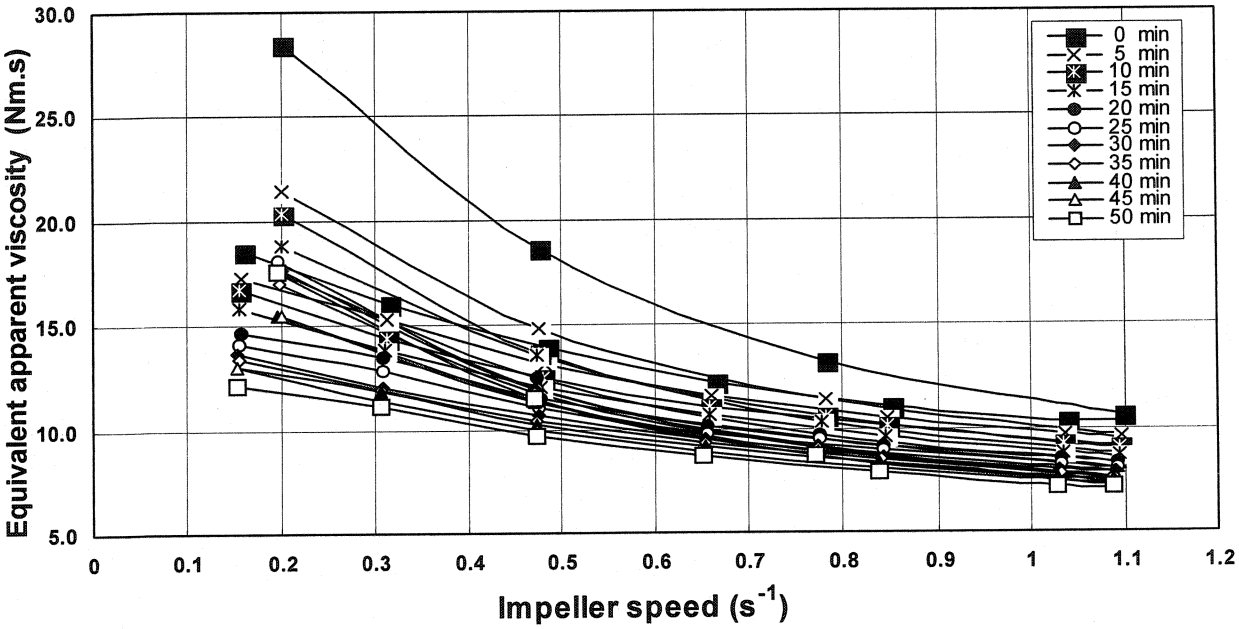


Figure 10.7 Equivalent apparent viscosity vs. impeller speed for 0-50 min.

10.4.3 Thixotropy

Figure 10.8 shows the equivalent apparent viscosity calculated for the higher (1.10 s^{-1}) and lower speed (0.48 s^{-1}) respectively (in the reverse cycle of the hysteresis loops) at each five-minute cycle. It is observed that the equivalent apparent viscosity at 1.10 s^{-1} is always lower than the value at 0.48 s^{-1}. At high speed, there is a reduction of about 9.4% after initial mixing at 0 min. It is around 26 % and 35 % for 30 min and 150 min, respectively. After 150 min, it increases by about 8%. The same trend has been observed at low speed. The change of equivalent apparent viscosity with testing time can be correlated with the hydration behaviour of mix discussed later on.

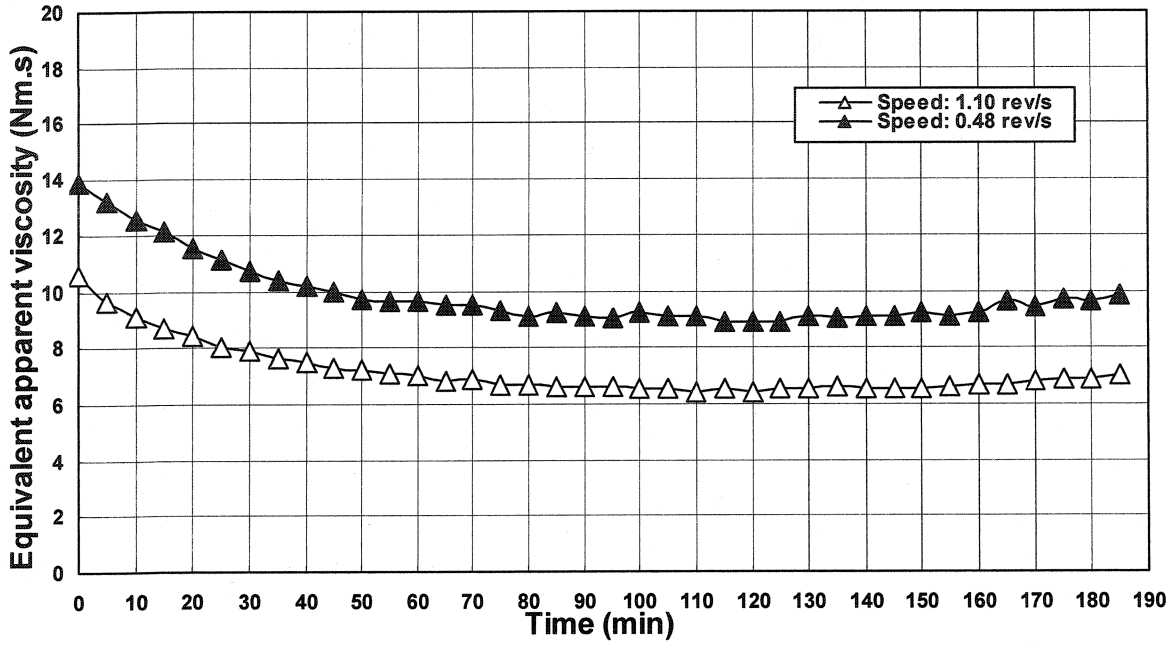


Figure 10.8 Equivalent apparent viscosity vs. time at high and low impeller speed.

10.4.4 Flow Resistance and Torque Viscosity

The method of evaluating G and H values, using the rheometer test results, has been described in Chapter 4.5.4. The calculated values of G and H are shown in Table 10.3.

Table 10.3 G and H values at different time from 0 to 185 min

Time (min)	H (Nm.s)	G (Nm)	Time (min)	H (Nm.s)	G (Nm)	Time (min)	H (Nm.s)	G (Nm)
0	8.76	2.04	65	6.04	1.28	130	5.61	1.3
5	8.28	1.92	70	5.96	1.3	135	5.61	1.28
10	7.92	1.82	75	5.93	1.26	140	5.63	1.33
15	7.56	1.74	80	5.92	1.2	145	5.52	1.4
20	7.3	1.62	85	5.83	1.27	150	5.62	1.36
25	7.12	1.52	90	5.72	1.29	155	5.67	1.32
30	6.98	1.41	95	5.71	1.26	160	5.54	1.45
35	6.81	1.4	100	5.7	1.27	165	5.56	1.52
40	6.65	1.37	105	5.7	1.26	170	5.49	1.58
45	6.45	1.36	110	5.61	1.28	175	5.6	1.58
50	6.35	1.27	115	5.63	1.24	180	5.62	1.6
55	6.25	1.29	120	5.6	1.25	185	5.56	1.7
60	6.15	1.28	125	5.48	1.32			

The G values changing with time as follows, as plotted in Figure 10.9: The values decrease by 38 % at 50 min of testing and remain almost constant from 50 to 150 min. There is an increase in values after 150 min until the end of test by about 29 %. These three periods correspond to: homogenization, saturation and setting effect. During the homogenization, the mix becomes more homogeneous with cumulative mixing energy and then flow resistance decreases sharply. After homogenization state, the rheological properties remain at constant level. This period corresponds to a saturation state. As the setting effect starts, the flow resistance goes up quickly. Similar changes are observed with H values measurements, although not synchronized in time.

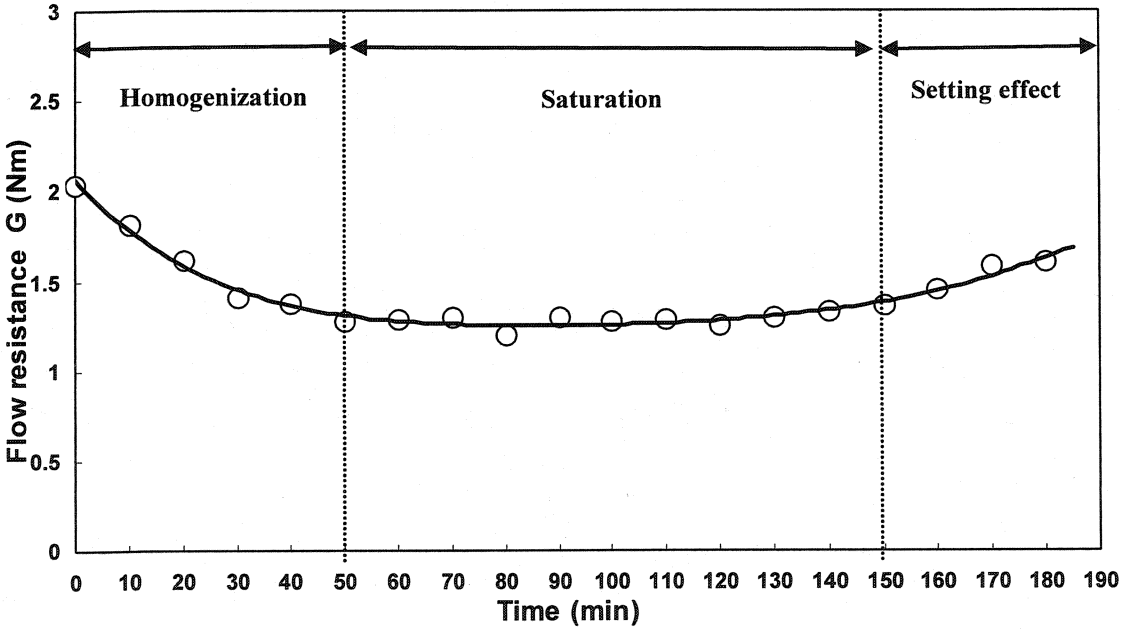


Figure 10.9 Flow resistance at different testing time.

10.5 Matrix Rheology

The Bohlin rheometer has been used instead of the IBB rheometer, and up to 360 min instead of 185 min for the castable whole mix. The shear rates are also much different in magnitude, being 400 times larger in this case, considering the matrix slurry only.

10.5.1 Shear Stress vs. Shear Rate

The relation between shear stress and shear rate is shown in Figure 10.10. The shear stress increases with increasing shear rate. The shear stress and apparent viscosity value

are higher during the forward cycle than the reverse cycle, leading to the formation of successive hysteresis loops.

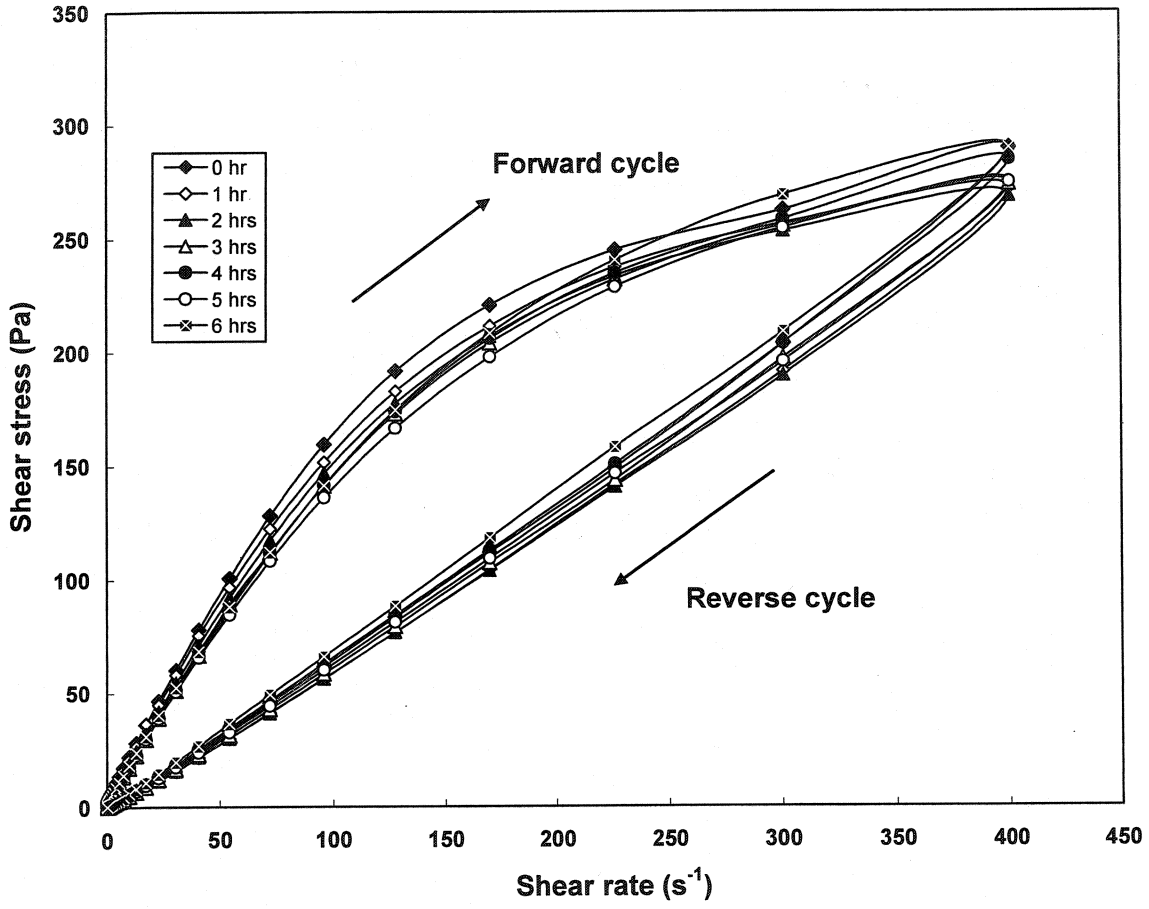


Figure 10.10 Shear stress vs. shear rate for the matrix slurry at different time.

The loops of matrix slurry slightly shift downwards from 0 hr to 3 hr and then rise up to 6 hr. The shear stress (τ_{max}) at the highest shear rate of 400 s^{-1}, at different time of testing, is given in Table 10.4. The τ_{max} decreases slightly and then rise up. The same trend has been found as the torque (T_{max}) at the highest impeller speed of 1.10 s^{-1} at different testing time, as given in Table 10.2. The forward cycle reveals pseudoplastic nature of the slurry, while the reverse cycle displays almost a Bingham behaviour.

Table 10.4 τ_{max} at the highest shear rate of 400 s^{-1} at different time

Time (hr)	0	1	2	3	4	5	6
τ_{max} (Pa)	290	272	268	274	285	275	290

10.5.2 Apparent Viscosity vs. Shear Rate

The apparent viscosity as a function of shear rate (on a log scale) of the matrix slurry at different time is shown in Figure 10.11. The apparent viscosity in the forward cycle (shear rate increasing) is higher than in the reverse cycle (shear rate decreasing). In the forward cycle, the apparent viscosity at different aging time decrease sharply from the beginning to 5.0 s^{-1} and remains similar till 100 s^{-1} and finally slightly decreases till 400 s^{-1}. The apparent viscosity at 0 hr is the highest, and decreases at 1 hr, 2 hrs and 3 hrs at shear rate below 5.0 s^{-1}. At shear rates higher than 5.0 s^{-1}, the apparent viscosity at different aging time stays almost constant. In the reverse cycle, the apparent viscosity remains similar from the shear rate of 400 s^{-1} to 1 $^{-1}$ and then increases at very low shear rate. At high shear rate, all values of apparent viscosity merge at one point of 0.7 Pa.s.

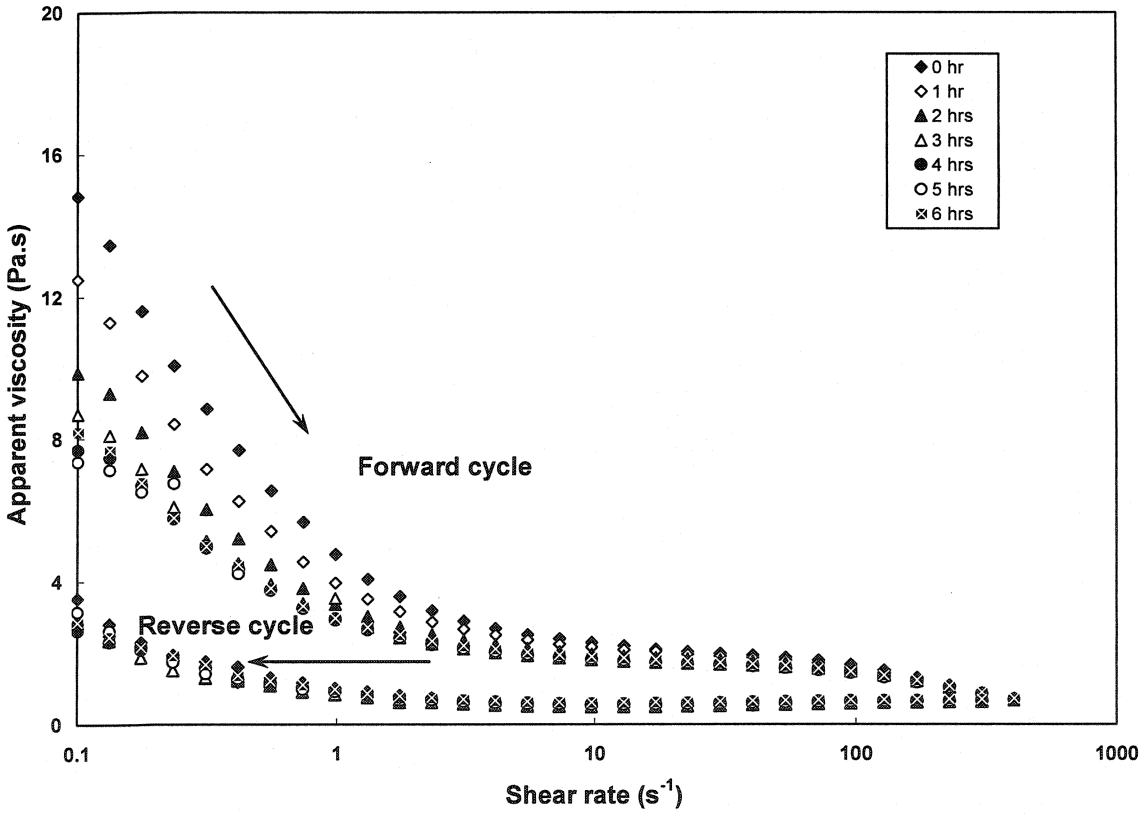


Figure 10.11 Apparent viscosity vs. shear rate of the matrix slurry at different time.

10.5.3 Shear-thinning and Thixotropy

If the viscosity decreases as the shear rate is increased, the material is said to be shear-thinning or Pseudoplastic. The opposite effect is known as shear-thickening. Often this thickening is associated with an increase in sample volume; which is called dilatancy. The relationship between apparent viscosity and time at constant shear rate is shown in Figure 10.12.

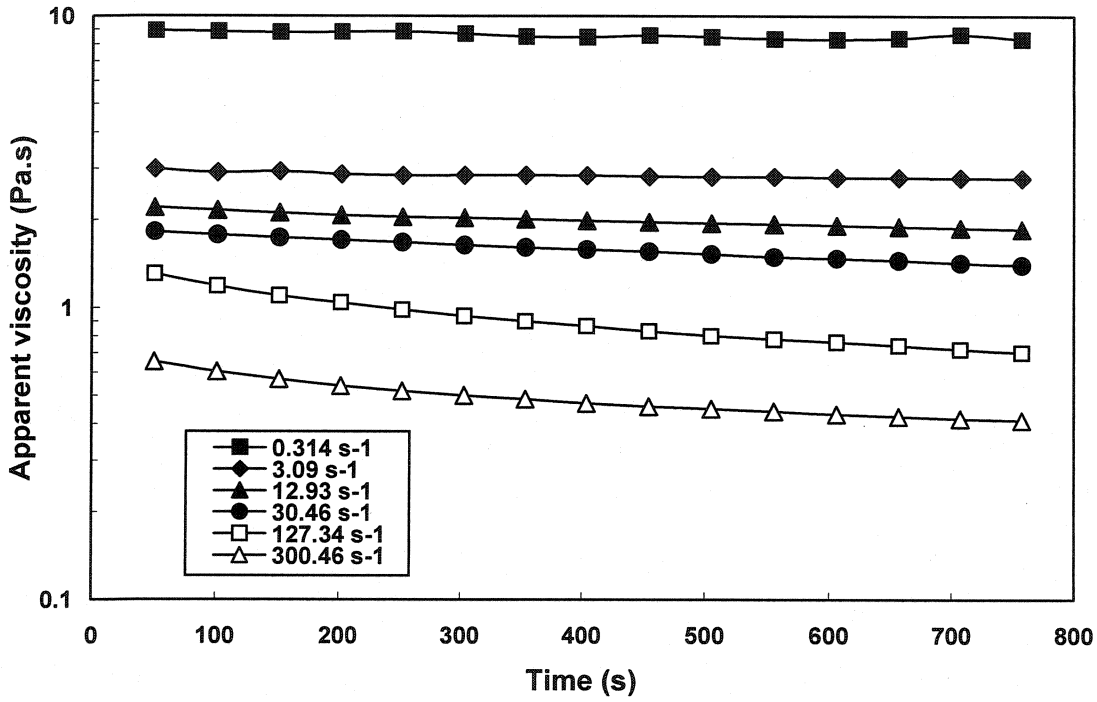


Figure 10.12 Apparent viscosity of the matrix slurry at different constant shear rates.

At the constant shear rate, the apparent viscosity decreases with time and then stabilizes and this effect is clearer at high shear rates. The apparent viscosity is higher at low shear rate than high shear rate. This confirms the thixotropic behavior of mix [10].

By the calculation method as described in Chapter 4.6.3, the degree of thixotropy decreases from the beginning to 4 hrs and then remains stable, as shown in Figure 10.13. There is no significant decrease in the first 1 hr. The loops' area shows the same trend.

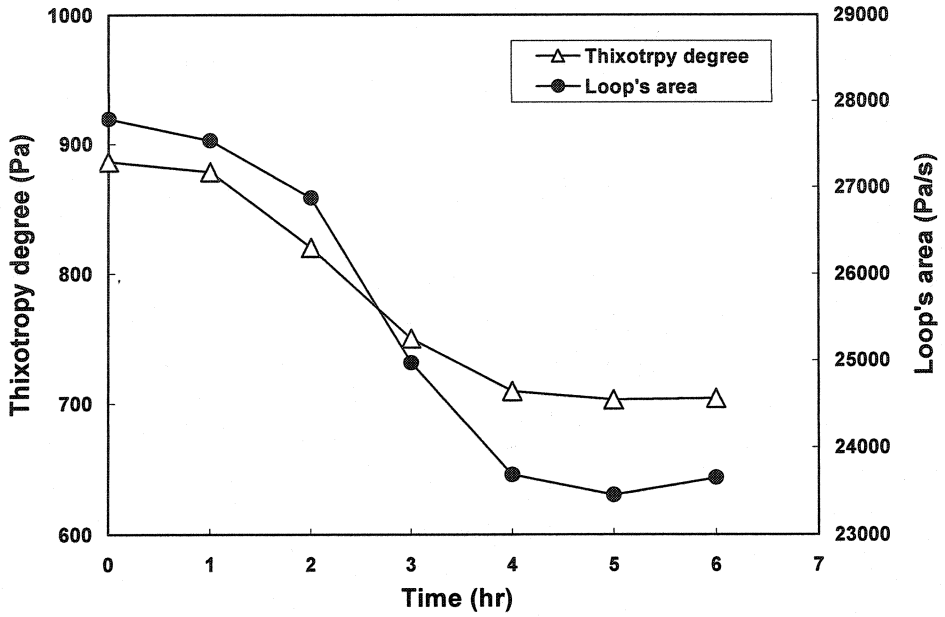


Figure 10.13 Thixotropy degree and loop's area for the matrix slurry at different time.

10.5.4 Plastic Yield Stress and Plastic Viscosity

The calculated values of plastic yield stress decrease with time and stabilize after 4 hrs. Plastic viscosity decreases with time till 4 hrs and then increases slightly, as given in Table 10.5. This is related to the hydration mechanism of CAC.

Table 10.5 Plastic viscosity and yield stress at different time

Time (hr)	0	1	2	3	4	5	6
Plastic viscosity (Pa.s)	1.829	1.776	1.691	1.62	1.593	1.565	1.626
Plastic yield stress (Pa)	3.512	2.982	2.123	1.513	1.669	1.879	1.925

10.6 Conductivity

To further confirm the observed results, the conductivity study on the fine matrix slurry is carried out and the results are shown in Figure 10.14. From 0 (Point A) to 10 min (Point B), the conductivity drastically increases due to quick dissolution of the dispersant SHMP present in the system. After this, from 10 (point B) to 150 min (point C), the conductivity increases very slowly because of the dissolution of the CAC. From 150 min (point C) to 345 min (point D), the conductivity increases sharply and reaches its peak due to the fast dissolution of CAC. At point D, nucleation starts, followed by massive precipitation at point E. At 415 min (point E), the massive precipitation occurs

and the conductivity decreases. After that, the conductivity increases to a given level and remain the same. This represents and equilibrium between anhydrous and hydrated phases in solution. In this experiment, the delayed dissolution of cement from Point B to C is due to the presence of fine fillers, which covers the cement grains. Moreover, the deposition of calcium phosphate precipitation also hinders dissolution of CAC grains. Microsilica also plays a key role to interact with the surface of the cement grain and a diffusion layer is created which controls the dissolution to delay the dissolution of CAC grains [104, 109].

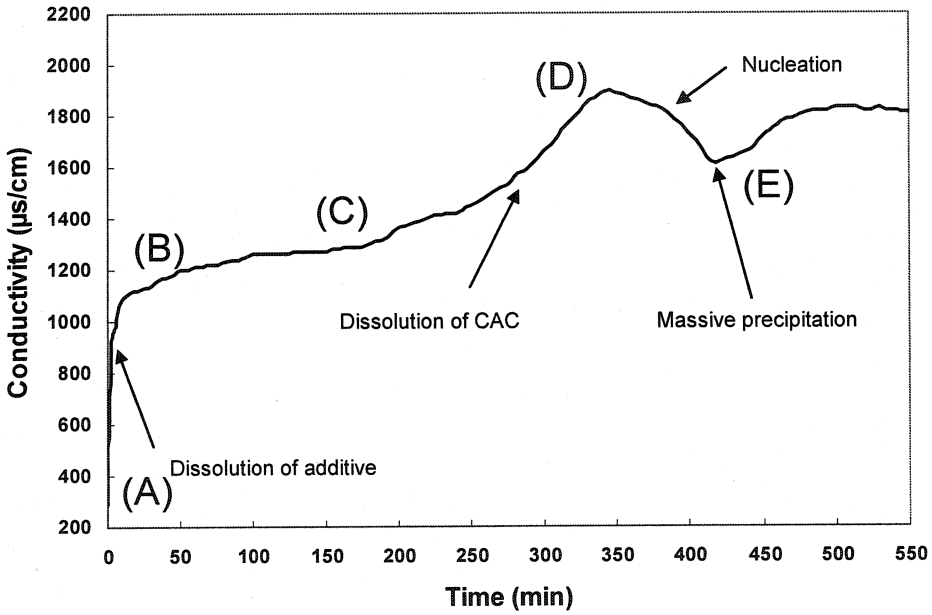


Figure 10.14 Conductivity curve of the matrix, with a water / solid ratio of 2.5 at 20 °C.

10.7 Exothermic Profile

The castable mix temperature and room temperature are measured as shown in Figure 10.15. The room temperature (the thin line) slightly fluctuates around 20 °C (point A). Two heat evolution peaks are observed for the castable mix. After the castable is wet-mixed for 4 min, the temperature (the thick line) reaches to 23 ^{0}C (point B) in a short time. The castable temperature remains stable for 6 hrs (point C) and then increases sharply to reach a first peak at 25.0 °C after 7 hrs (point D). Then, the castable mix temperature keeps increasing to a maximum of 29.3°C (the second peak) after 11 hrs

(point E). Further on, the castable temperature slowly decreases till the end (point F). The time measured from the start of mixing (zero) until the exothermic reaction shows a temperature increase of + 5.0 °C is recorded as EXO+5. For 70 % Al_2O_3 cement, CA-14, this point corresponds to the Vicat Final Setting Time. The time when the castable mix has reached its maximum temperature of the exothermic reactions is recorded as EXO max. This point corresponds to the time when there is sufficient green strength for demoulding [60]. In Figure 10.15, the EXO+5 is presented by point D at the time of 7hrs and the EXO max is presented by point E with the period of 11hrs. From point A to B, the temperature increases because of the dissolution of additives and mix energy brought inside the castable mix. From B to C, the temperature remains the same, during the slow dissolution of CAC. From C to D, the temperature increases to the first peak (point D) meaning that the final setting has started with hydrate products crystallization (nucleation of hydrates in matrix slurry as shown in Figure 10.14). From point D to E, the temperature keeps increasing to the maximum meaning development of sufficient green mechanical strength for demoulding. From point E to F, the castable temperature decreases as the hydrated products of CAC reach equilibrium and crystallize slowly.

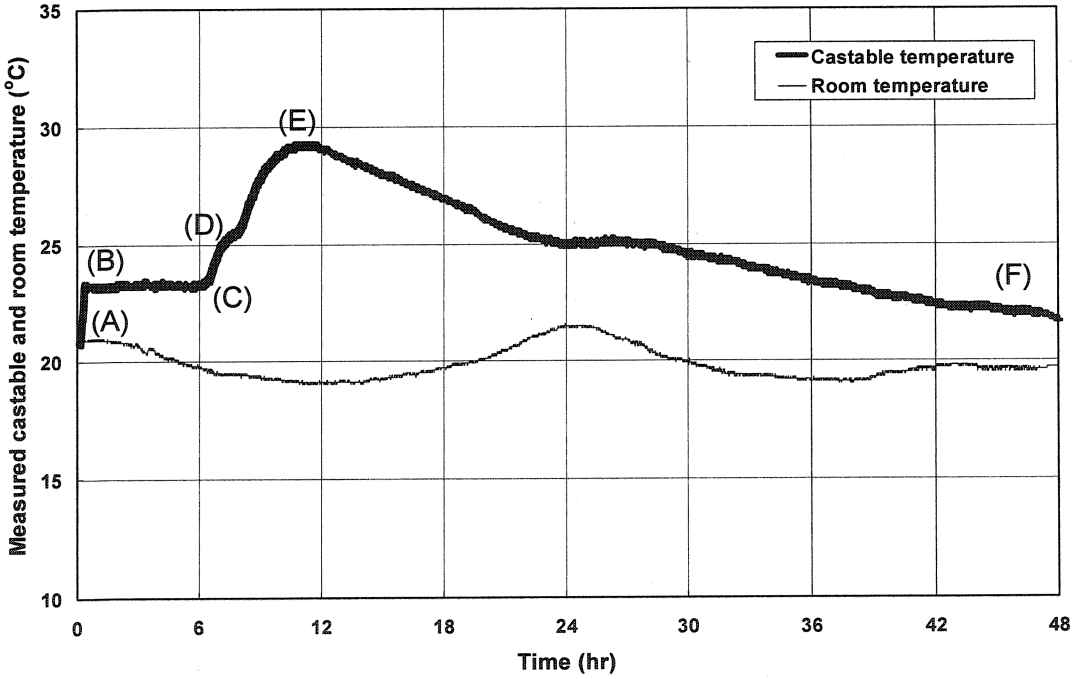


Figure 10.15 Exothermic profile of the castable at 20 °C.

10.8 Discussions

10.8.1 Relationship between Castable and Matrix Rheology

There are few practical difficulties is carrying out the rheological test of the matrix slurry and castable under similar conditions. The most important one is protection of water in castable from evaporation and heat input while testing. The rheological test on castable is carried out in open atmosphere without protecting water evaporation, while the fine matrix rheology is carried our under controlled atmosphere as described earlier. The variation of water to cement ratio is possible, when introducing coarse grain into the fine matrix as the porosity of grains absorbs water from fine matrix. The rheology of matrix and castable are to be compared keeping these variations in mind. The prime characteristics, flow resistance, G of a castable are compared with the plastic yield stress τ_p of the matrix slurry (Figure 10.16).

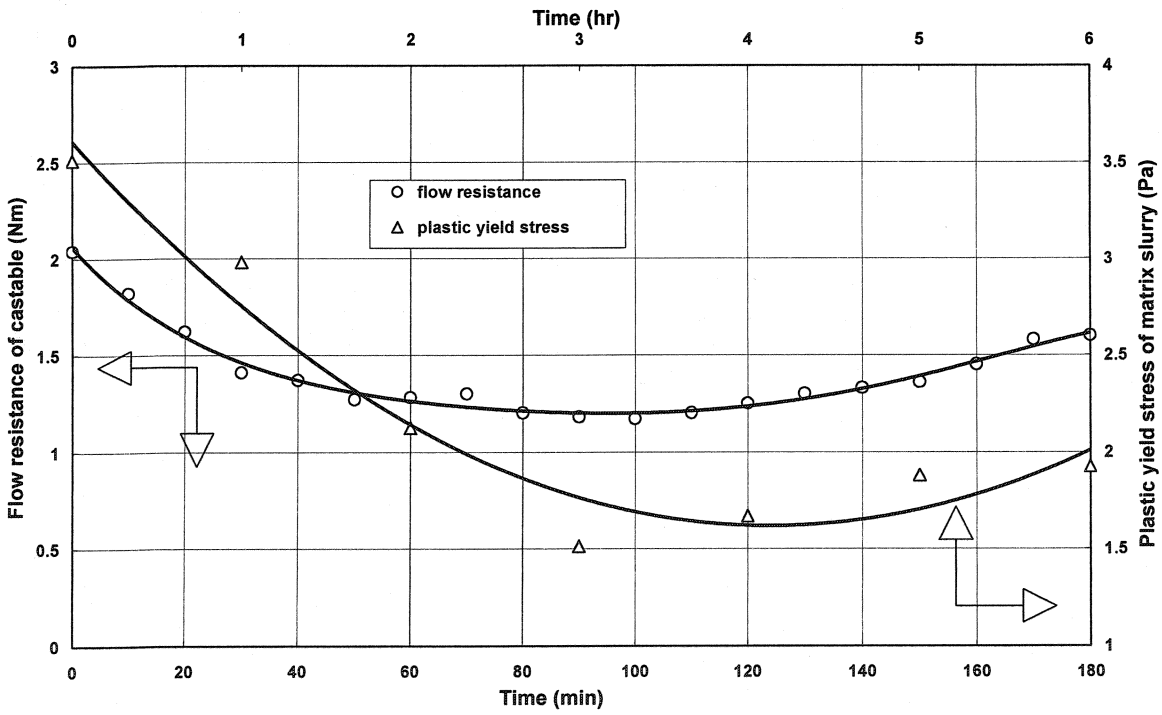


Figure 10.16 Flow resistance of the castable and plastic yield stress of the matrix slurry at different time.

Similarly, torque viscosity H is compared with plastic viscosity η_p in Figure 10.17. The curves show similar trends but at different time. This is so because the experiments are conducted under dissimilar conditions. The trend of comparison of Tmax (Table 10.2) and τ_{max} (Table 10.4) with aging time is similar, hence not shown.

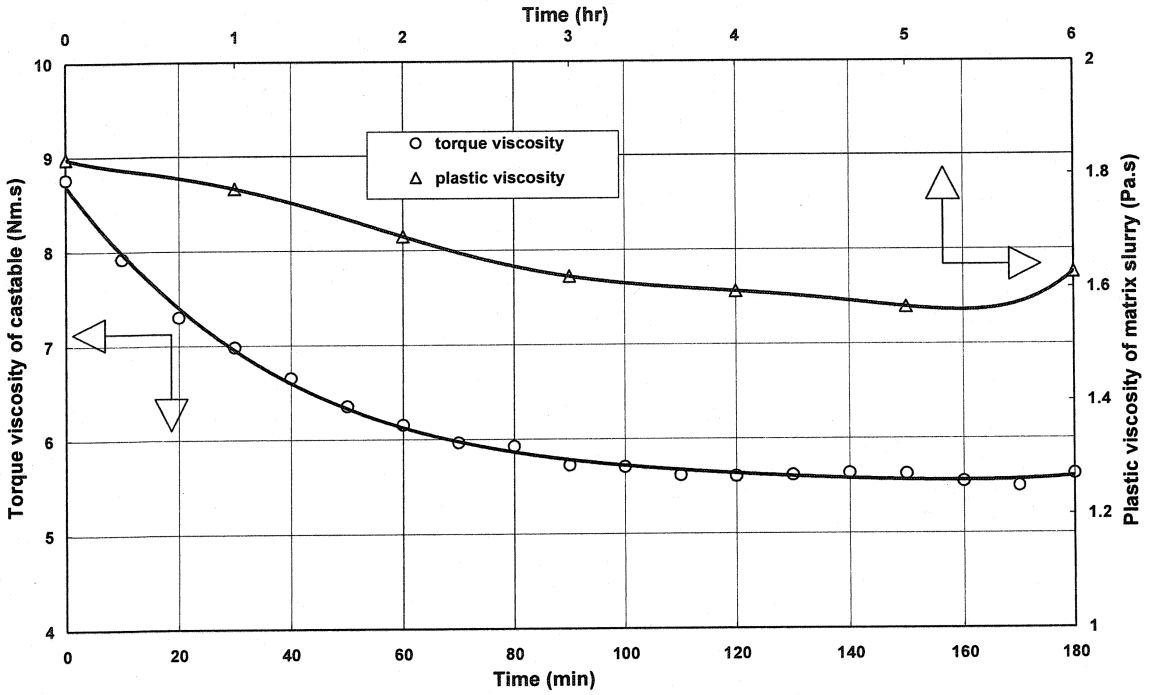


Figure 10.17 Torque viscosity of the castable and plastic viscosity of the matrix slurry at different aging time.

10.8.2 Relationship between Castable Rheology and Conductivity

This delay of bulk dissolution of CAC, observed initially in conductivity study (Figure 10.14), corresponds to the extension of the working time. This corresponds to the period in the castable rheology study, where flow resistance remains stable that is during the saturation state, from 50 to 150 min, as shown in Figure 10.9.

10.8.3 Relationship between Matrix Rheology and Exothermic Profile

The variation of the plastic viscosity and yield stress with time (Table 10.5) as well as the reduction in the degree of thixotropy for the matrix slurry (Figure 10.13) have been both slow in the first hour, and then decrease noticeably in the 1 to 5 hr. range. This is to

be correlated with the initial temperature inertia noticed in the exothermic profile curve, Figure 10.15, up to point C, followed by the fluctuations from Point C to E. The main difference is only in the time scale, the exothermic effect in the castable being much more sluggish.

10.9 Mechanical and Physical Properties

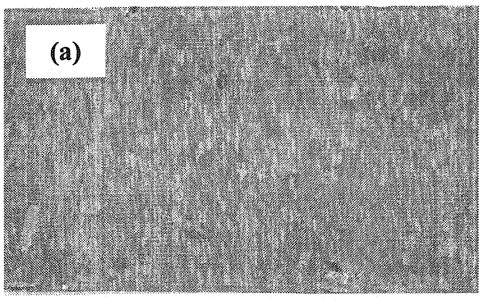
The CMOR and AP average values on 3 samples cast by self-flowing at different time are given in Table 10.6. The CMOR values are similar but the AP decreases at 45 min and then increases after 185 min of testing time. The later results maybe due to the positive effect of degassing before the beginning of setting takes place.

Table 10.6 CMOR and AP at different time.

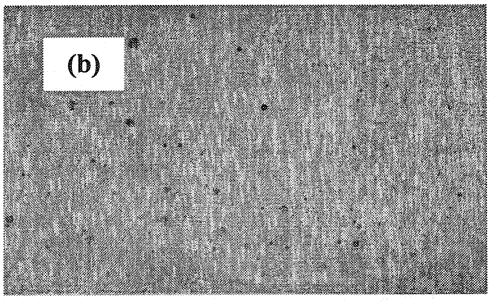
Time (min)	CMOR (MPa)	AP (%)
0	9.3	18.2
45	8.7	17.8
185	8.9	18.4

10.10 Appearance of Samples

Figures 10.18 (a)-(f) show the appearance of the castable samples as a function of time. Degassed bubbles are clearly observed on the surface of samples cast after 45 min but much less after 185 min. The bubbles observed on the side surface of the samples as also different at 01, 45 and 185 min, in terms of numbers, size ad position. It is however difficult to conclude from these observations which samples should have the lowest apparent porosity.



Surface (0 min)



Side surface (0 min)

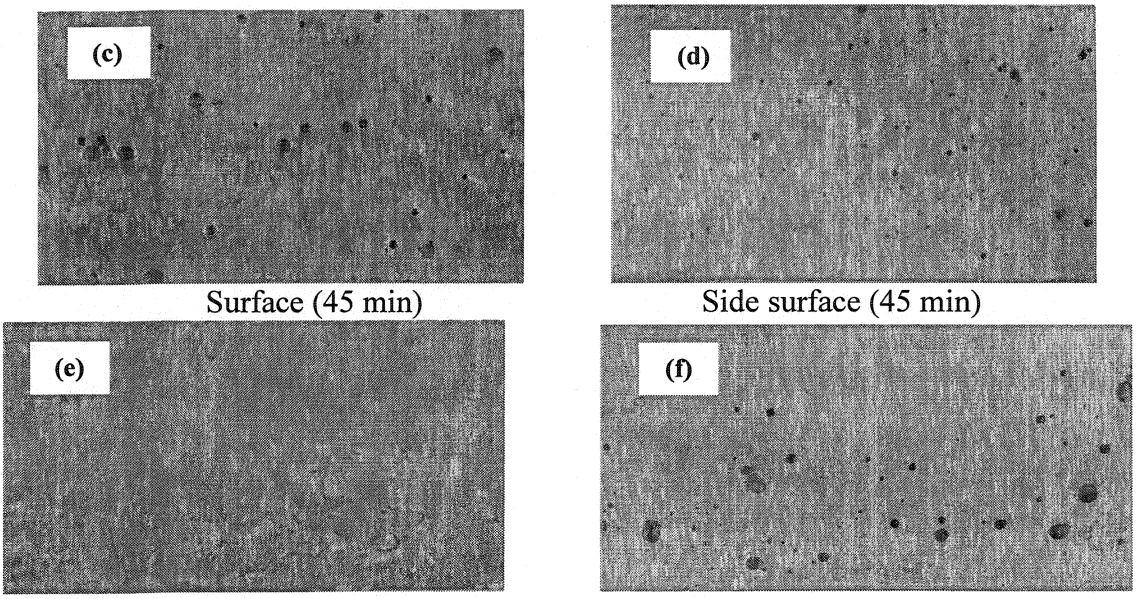


Figure 10.18 (a)-(f) Appearance of samples cast after 0, 45 and 185 min of testing.

10.11 Conclusions

The rheological behaviour of bauxite based low-cement castable and its fine matrix has been studied using different rheometers. The conclusions based on this investigation are:

a) The castable mix has shown Pseudoplastic and Bingham behaviours. The thixotropy has been observed when analysed with testing time at constant impeller speed. Similar behaviour has been observed be with τ_p and η_p of the matrix slurry of the same mix.

b) During aging, the rheological chrematistics change from a homogenous to saturation then to a setting effect controlled state.

c) Comparison of rheological results of the castable and matrix slurry between G-H and τ_p-η_p values shows similarity in trends but at different aging times. The castable and matrix rheology are correlated with conductivity and exothermic profile studies.

CHAPTER 11 – SHOTCRETING TRIAL

For the pumped and shotcreted samples, the chosen mixes were pumped and shotcreted by a shotcreting machine: Allentown RP-10 (Allentown Equipment, USA), as shown in Figure 11.1. It consists of 40 hp electric motor, 2 ½" hydraulic cylinders, accelerator pump, hopper, automatic lubrication of swing-tube and mounting rigs.



Figure 11.1 Photograph of the pumping and shotcreting equipment, Allentown Pump RP-10.

The castable were formulated by the same composition, which is considered from Chapter 9, WA-1, 2 and 3 with three levels of water addition, 6.0, 6.5 and 7.0 wt%, respectively. The castable were dry-mixed for 4 min in a large on-site mixer with a batch of 500 kg dry mixes once, and then wet-mixed for an additional 4 min with required water. 1000 kg, in two batches, mixed-fresh castables, were transported by a crane to the hopper of the pumping and shotcreting machine. The castable mixes were pumped and shotcreted by Allentown RP-10, under such operating parameters, as given in Table 11.1.

Table 11.1 Operating parameters of shotcreting machine

Pumping capacity (ton/h)	10-15
Pumping pressure (MPa)	14
Hose diameter (mm)	75
Hose length (m)	15
Nozzle tip (mm)	38
Air pressure (MPa)	0.7
Air flow (m^3/min)	6
Accelerator	0.12 % saturated $Al_2(SO_4)_3$ solution
Distance between nozzle tip and the shotcreted surface (m)	0.5-1
Ambient temperature in the workshop (°C)	25-28

The shoebox-like pumped blocks with a dimension of 230×160×140 mm and the shotcreted blocks with 900×700×150 mm (One is weld with anchors, the other is not), were properly cured and then subjected to 110°C treatment prior to being cut into 160×40×40 mm for different tests.

All the castable mixes with 6.0, 6.5, 7.0 wt% water could be pumped, but the flowability of the mix increases after pumping. Figure 11.2 shows the pumping of the castable with 7.0 wt% water addition. It has been found that the mix could be continuously pumped and self-flow well after pumping, but the castable mixes with 6.0 and 6.5 wt% could not self-low well after pumping.

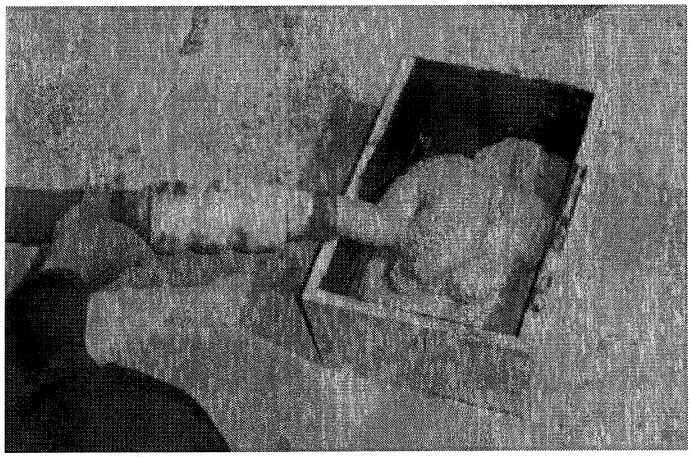


Figure 11.2 Pumping of the castable mix with 7.0 wt% water addition.

Figure 11.3 shows shoebox-like castable samples after pumped with different water addition. It is observed that the forming surface of the castable mix with 7.0 wt% is the best among the three mixes.

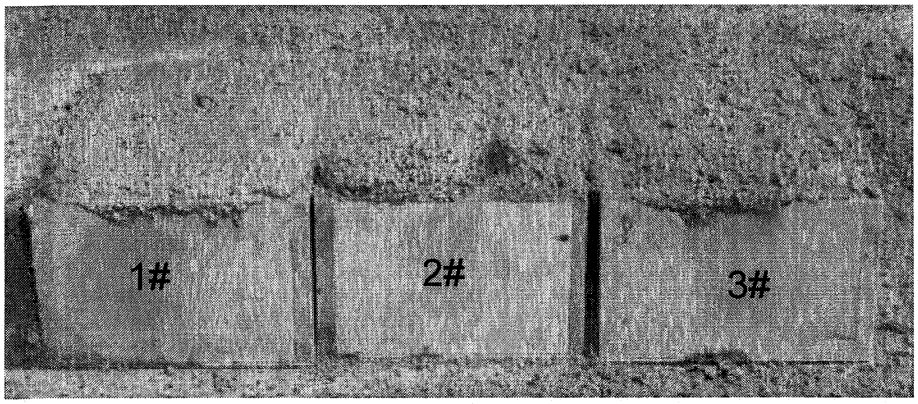


Figure 11.3 After pumping (1#: 7.0 wt%, 2#: 6.5 wt%, 3#:6.0 wt% water).

The shotcreted castable mixes with different water addition 6.0, 6.5, 7.0 wt% are shown in Figure 11.4, 5, 6, respectively. All the castable mixes could be shotcreted without dusting, but the rebound of the castable mix increases as the water addition decreases.

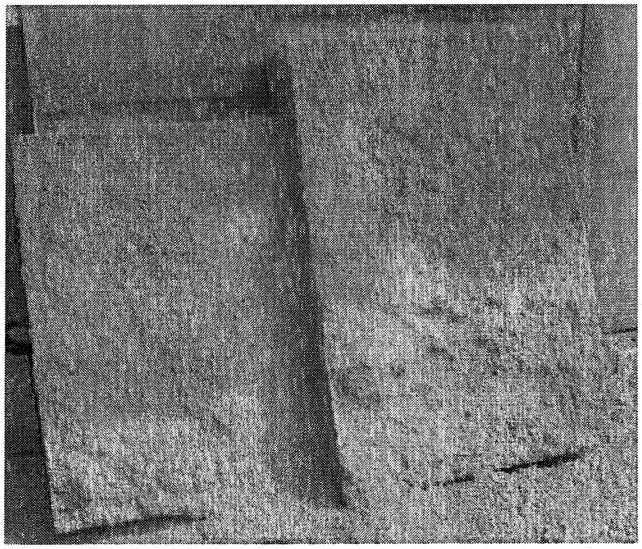


Figure 11.4 The castable mix with 6.0 wt% after shotcreting.

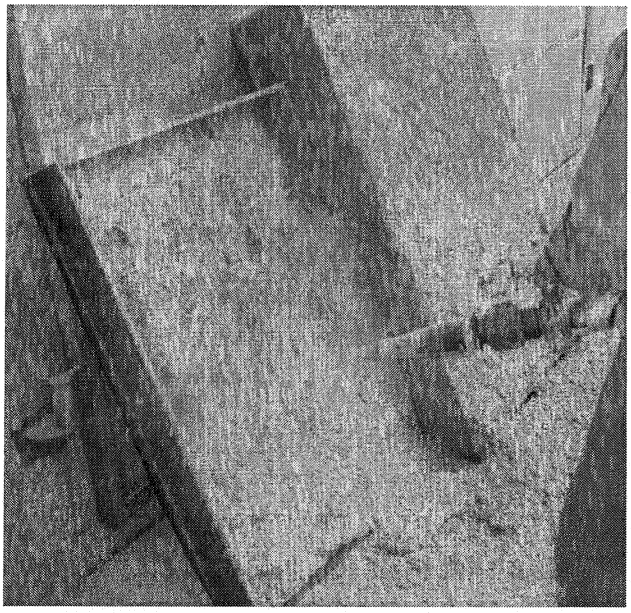


Figure 11.5 The castable mix with 6.5 wt% water is being shotcreted.

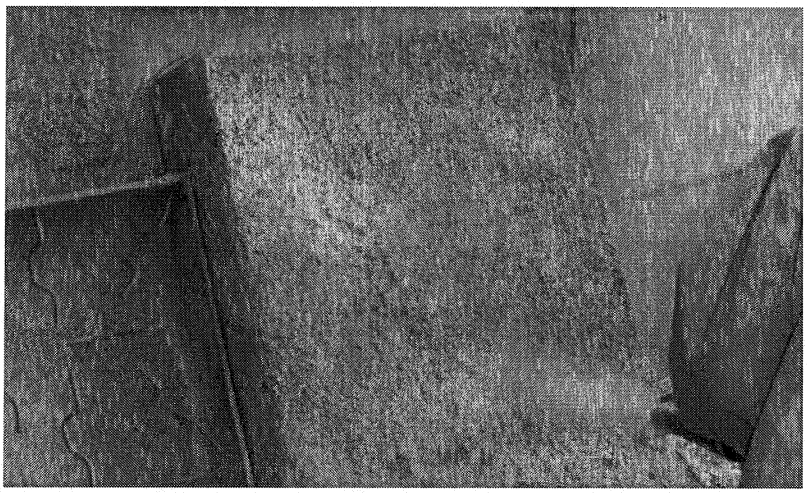


Figure 11.6 The castable mix with 7.0 wt% water is being shotcreted.

The physical, mechanical and other properties of the pumped and shotcreted castable with 7.0 wt% water addition, are given in Table 11.2.

Table 11.2 Physical and mechanical properties of the pumped and shotcreted castables

Composition		1	2	3
Installation method		Shotcreting	Pumping	Self-flowing
Bulk density (g/cm^3)	110°C×24h	2.78	2.81	2.84
	1000°C×3h	2.77	2.80	2.81
	1200°C×3h	2.79	2.82	2.83
	1400°C×3h	2.79	2.84	2.84
AP (%)	110°C×24h	20.8	19.4	18.3
	1000°C×3h	22.8	21.6	20.1
	1200°C×3h	23.2	22.2	--
	1400°C×3h	22.2	21.0	--
PLC (%)	110°C×24h	-0.02	-0.01	-0.02
	1000°C×3h	-0.20	-0.30	-0.16
	1200°C×3h	-0.20	-0.19	-0.16
	1400°C×3h	-0.16	-0.20	-0.62
CMOR (MPa)	110°C×24h	6.8	13.2	11.7
	1000°C×3h	8.2	16.9	22.7
	1200°C×3h	11.7	21.1	26.2
	1400°C×3h	12.9	21.5	24.8
CCS (MPa)	110°C×24h	25.6	36.9	30.3
	1000°C×3h	48.6	82.2	65.6
	1200°C×3h	55.2	83.1	110.3
	1400°C×3h	71.3	97.2	101.6

The self-flowability of the castable mix is 50, 80 and 120 % for 6.0, 6.5 and 7.0 wt% water, respectively, which is the same as the laboratory results. Although the physical and mechanical properties of the shotcreted castable with 7.0 wt% water are slighter lower than pumping and self-flowing castables, it still shows satisfactory results. This proves the chosen composition with 7.0 wt% water addition possesses superior and optimal rheological properties among all compositions in previous chapters.

CHAPTER 12 – COMPREHENSIVE DISCUSSIONS, CONCLUSIONS AND RECOMMENDATIONS

This work has paved a new way to design a self-flowing, pumping and shotcreting castable, using a rheological approach.

As discussed in the introduction of Chapter 8, some castables may be self-flowing but not necessarily pumpable. Some difficulties are to be expected during placement. A general problem encountered during pumping a castable is the blockage in the hose due to quick setting and/or segregation of the castable. Quick setting of a castable during placing may be caused by an increase of temperature in the hose due to excessive castable-wall friction, warm working environment or inappropriate selection of additives Segregation is a phenomenon causing separation of matrix paste from aggregates, and it can be avoided by choosing proper aggregate-to-matrix and water-to-matrix ratios.

Therefore, a pumpable castable should have adequate pumpability and workability. The pumpability of a castable refers to its mobility and stability under pressure within an enclosed hose. Mobility and stability are related to rheological properties of a castable but may act differently. The degree of mobility of a castable can be referred to self-flowability, which indicates the degree of self-levelling of the castable under its own weight after mixing with water. It is relatively easy to measure mobility by flow table test using a cone described as ASTM test methods [70, 100]. However, the stability of a castable, which can be defined as the capacity to maintain its initial homogeneity during transporting, handling and placing, is a complex parameter to measure, for which no standard test has yet been defined. As the attempts to predict the pumpability from self-flowability test alone are not always successful, both mobility and stability must be considered and kept in balance for a good pumpable castable.

In this work, the IBB rheometer is used to measure rheology of castables through two important parameters: flow resistance and torque viscosity, to represent mobility and stability, respectively. These parameters should be controlled together to obtain good pumpability. Based on the overall results in this work, some border lines of maximum and minimum flow resistance and torque viscosity values have been found, as shown in Figure 12.1. If the castable exhibits moderate flow resistance G ($1 < G < 2.5$ Nm), but unacceptably low torque viscosity H (< 6 Nm.s), due to insufficient amount of fine fillers to fill the voids, will be susceptible to segregation. If the castable exhibits moderate torque viscosity H ($6< H < 10$ Nm.s), but too low flow resistance G (< 1 Nm), some segregation will also appear. Conversely, if the castable shows too high flow resistance G (> 2.5 Nm) and/or torque viscosity H (>10 Nm.s) because of excessive fine fillers, blockage will occur during pumping or shotcreting.

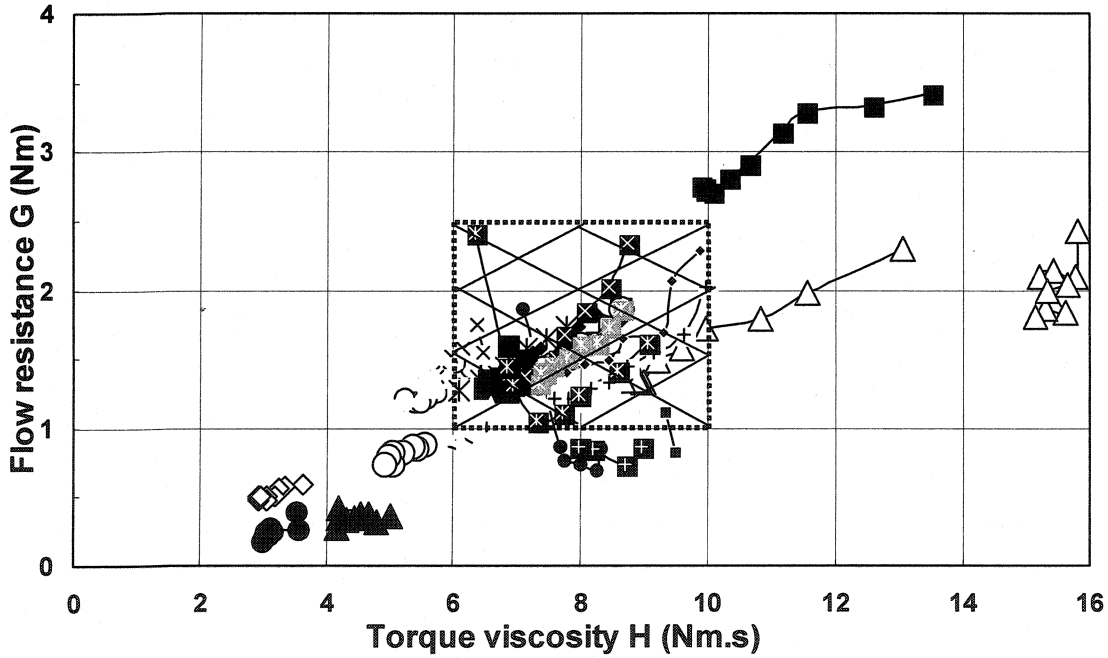


Figure 12.1 Flow resistance vs. torque viscosity of all the castables.

From our results, it has been possible to define experimentally those limits of flow resistance and torque viscosity, for a castable mix to remain stable without any segregation and to provide good mobility and stability. It is concluded that flow

resistance values must lie between 1.0 to 2.5 Nm and torque viscosity values between 6.0 to 10.0 Nm.s in order to avoid segregation and to achieve adequate pumpability. So, a "PUMPING BOX" has been defined which predicts the minimum and maximum values of G (1 ~ 2.5 Nm) and H (6 ~10 Nm.s) for trouble-free pumping of castable, as shown in figure 12.2.

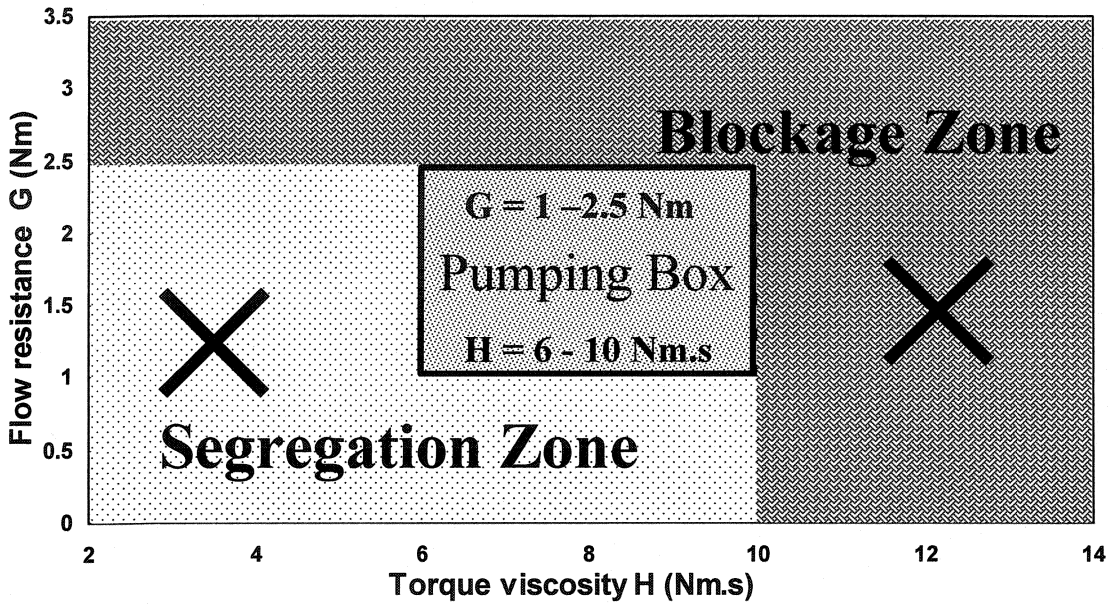


Figure 12.2 "PUMPING BOX" for predicting the pumping of all the castables.

In order to obtain an adequate pumpability, the castable composition must be optimized to reach a proper combination of flow resistance and torque viscosity, which provides good flowability and avoids blockage and/or segregation. The castable should be designed with appropriate PSD, dispersants, cement bonding agent, microsilica, other fine fillers and additives so that well-dispersed fine particles will efficiently fill the voids between aggregates and the matrix slurry will possess the sufficient viscosity to support the yield stress needed to carry away the big aggregates, without sedimentation or segregation. These parameters directly influence the viscosity and flow of the castable. In this work, one composition is optimized with such following parameters in Table 12.1. This castable composition appears to possess optimum combination of G and H among the studied mixes. The rheological behaviour of this castable indicates it has the best workability and pumpability characteristics.

Table 12.1 Optimized composition with different parameters

Aggregate (wt%)	Bauxite, 5-3 mm	13
	Bauxite, 3-1 mm	23
	Bauxite, 1-0.21 mm	23
Fine matrix (wt%)	Bauxite-1	11
	Bauxite-2	12
	Bauxite-3	9
	Cement CA-14	4
	Microsilica (Elkem 971U)	5
Dispersant (wt%)	SHMP	0.12
Andreasen modulus (q value)		0.26
D_{max} (mm)		5
Working time (min)		100

Based on all results achieved from this work, the following general conclusions are drawn:

1) The IBB rheometer is an effective tool to measure the rheology of castable mix directly. Two important properties torque viscosity (H) and flow resistance (G) can be evaluated using this rheometer. The mixes are all following a Bingham behavior and thixotropy has been observed when analyzed against time at constant impeller speed.

2) Though self-flowability is found to be same for all compositions at water amount of 7 wt%, they have shown different flow resistance and torque viscosity. This confirms that only flow measurement is not sufficient to define the castable behavior.

3) Self-flow castables also follows a Bingham behavior and are thixotropic and shear-thinning in nature. Similar behaviour has been observed with τ_p and η_p on the matrix slurry.

4) PSD is one of the most important parameters for castable design. Too much fines cause blockage and too much coarse aggregates lead to segregation. G and H have got direct correlation with Andreasen modulus Based on Andreasen's equation, the continuous distribution of particles with the q value of 0.26 and D_{max} of 5 mm shows appropriate rheological behavior and pumpability.

5) The type and amount of dispersant also affect considerably the flowability of mixes. When SHMP (sodium hexametaphosphate) is used, the self-flowability remains the same at all levels of addition. With the dispersant Darvan 811D, the mixes exhibit flash setting. As the amount of Darvan 811D is increased, the setting time becomes shorter.

6) G is influenced by the type and amount of dispersant under the present set of conditions. The optimum amount of 0.08-0.16 wt% SHMP has been found for achieving good G and H values. Darvan 811D accelerate the setting of castable, the flow decay of castable with 0.05 wt% Darvan 811D is 35 min. With 0.16 wt% Darvan 811D, the working time is shortened to 5 min.

7) The G values are not strongly influenced by the type and amount of CAC which is also proven by similarity of self-flowability for all compositions. The H values have shown strong dependency on the amount of CAC due to cement hydration leading to different free water left in the mix. To increase cement, the rheological behavior does not change a lot with the same kind of cement. The castable with 4 wt% cement CA-25R has the shortest working time.

8) Increasing cement addition with increasing bonding water content leads to higher cold strengths. The CMOR and AP values show an increase of around 1.5 MPa and a decrease of 0.25 % respectively with each 1 wt% CA-14 cement addition.

Under the same condition, at the same amount of cement, 4 wt%, CA-14 samples have shown higher CMOR and lower AP than that of CA-25R samples.

9) Type and amount of microsilica play a major role in the flowability of castables. In this study, microsilica 971 U shows better performance with respect to flowability. Increasing microsilica content does not mean better rheology. It is observed that the castable with 5 wt% microsilica is rheologically more favourable than the mix with 7 wt% microsilica. The chemistry of microsilica (presence of silica, soda and carbon) influences the rheological properties of mixes.

10) Appropriate selection of fine fillers is crucial to achieve a good pumpability for castables without obvious segregation. Insufficient fine fillers result in serious segregation, but excessive fine fillers cause high rigidity and viscosity. Too much submicron fine fillers lead to high stickiness and also segregation. With an increase of the fine fillers, flow resistance and torque viscosity increase. Insufficient fine fillers cause segregation and excessive fine fillers cause blockages. Use of excessive submicron fillers decrease flow resistance and torque viscosity.

11) Water is a very important factor to define the placement of castable. In this work, the castable with 6.0 wt% water addition possesses good vibration castable characteristics; with 6.5 wt%, it shows a good self-flow castable characteristics; and with 7.0 wt%, it can be a good pumpable castable, in every case with satisfactory mechanical properties.

12) Rheological parameters G and H have direct correlation with the amount of water addition under the present set of conditions. The maximum amount of water should not exceed 7.0 wt% for achieving favourable G and H values.

When the amount of water is beyond 7.0 wt% under the given conditions, the castable segregates and the mechanical properties are being deteriorated drastically.

13) Under aging conditions, the rheological characteristics change from homogenous to saturation to setting effect controlled state. Comparison of rheological measurements on castable (full mix) and matrix slurry (partial mix) shows similarity in trends at different aging time. The steps in castable rheology are in line with the conductivity and exothermic profile studies.

14) After optimizing all parameters, the castable with q value of 0.26 and D_{max} of 5 mm, 0.12 wt% dispersant SHMP, 4 wt% cement CA-14, 5 wt% microsilica 971 U, 9 wt % Bauxite-3 and 7 wt% water shows overall desirable rheological properties. The castable is considered to have the best pumpability due to satisfactory combination of flow resistance and torque viscosity under the given conditions.

15) Investigation and optimization in the rheological parameters in terms of flow resistance G and torque viscosity H values leads to the finding that a castable composition with G =1-2.5 Nm and H =6-10 Nm.s can well avoid segregation and serious structural breakdown or strong thixotropy. To consider all variables, a "PUMPING BOX" has been designed which predicts the minimum and maximum values of flow resistance G (1 ~ 2.5 Nm) and torque viscosity H (6 ~10 Nm.s) for trouble-free pumping of castable.

16) The shotcreting trials prove that the prediction of pumpability is valid and that the test method is meaningful.

This work is to be taken as the initial stage of a long-term endeavour. Some recommendations and suggestions for further improvements and studies are as follows:

1) The work is only based on bauxite-based low-cement castables with 4 wt% cement and 5 wt% microsilica. More systems with different parameters should be studied. The utility for the pumping box would then be confirmed with more results.

2) This work is concentrated on rheology of castable at room temperature, which is only one of part of overall properties of castable. The other properties after firing at high temperatures are needed for further clarification.

3) For shotcreting castables, the effect of retarder and accelerator on self-flowability and rheology would require extra-investigation. The mechanism of dispersant with different inorganic chemicals or organic compounds is to be further confirmed.

4) The field trials are done with a big amount of raw material and high cost. Some small-scale pumping system should be designed for cost-saving purpose.

5) Applications of shotcreting castables should be monitored for torpedo cars or tundishes in iron & steel-making plants.

REFERENCES

1. R. G. Pilieggi, Y. M. Marques, D. Vasques Filho, A. R. Studart and V. C. Pandolfelli, Wet-shotcrete for Refractory Castables, *Am. Ceram. Soc. Bull.*, Vol. 81, No. 10, **2002**, pp. 51-56.

2. A. M. Hundere, B. Myhre, C. Ødegård and B. Sandberg, Wet Shotcreting Refractory Castables with Varying Cement Content, *Proceedings of XII Conference on Refractory Castables*, The Czech Republic, **1998**, pp. 135-142.

3. R. C. Moore, Shotcreting Monolithic Steel Ladle Safety Linings at Dofasco, *Proceedings of UNITECR'01*, Vol. 3, **2001**, pp. 1733-1745.

4. S. Odanaka, K. Nakashima, M. Toh and H. Nagata, Effect of Alumina Fine Powder and Silica Flour Addition on Fluidity of Castable Refractories, *Taikabutsu Overseas*, Vol. 10, No. 1, **1990**, pp. 35-37.

5. Z. Li, S. Zhang, N. Zhou and G. Ye, Difference in Dispersing Effect Between Organic and Inorganic Deflocculants in Castable, *Proceedings of UNITECR'97*, Vol. 3, **1997**, pp. 1355-1361.

6. G. Opera, T. Troczynski and F. Esanu, Rheology Studies on Binding Systems for Self-flow Refractory Castable, *Proceedings of UNITECR'97*, Vol. 2, **1997**, pp. 613-624.

7. N. Fukami and M. Ishikawa, Effect of Viscosity and yield Stress of a Particle-Water Suspension on the Fluidity of Monolithic Refractories, *Journal of the Technical Association of Refractories*, Japan, Vol. 22, No. 3, **2002**, pp. 193-197.

8. N. S. Zhou, Some Fundamentals of Rheology and Their Relevance to Monolithic Refractories, *Internal Report at CIREP*, **1998**, pp. 1-33.

9. H. A. Barnes, J. F. Hutton, and K. Walters, *An Introduction to Rheology*, Elsevier Science Publishers B. V., **1989**.

10. J. E. Funk and D. R. Dinger, *Predictive Process Control of Crowded Particulate Suspensions: Applied to Ceramic Manufacturing*, Kluwer Academic Publishers, USA, **1994**.

11. K. Watanabe, M. Ishikawa and M. Wakamatsu, Rheology of Castable Refractories, *Taikabutsu Overseas*, Vol. 9, No.1, **1989**, pp. 41-53.

12. J. MEWIS, Thixotropy – a General Review, *J. Non-Newtonian Fluid Mechanics*, Vol. 6, **1979**, pp. 1-20.

13. H. A. Barnes, Thixotropy – A Review, *J. Non-Newtonian Fluid Mechanics*, Vol. 70, **1997**, pp. 1-33.

14. F. S. Ortega, R. G. Pileggi, A. R. Studart and V. C. Pandofelli, IPS, a Viscosity – Predictive Parameter, *American Ceramic society Bulletin*, Vol. 81, No. 1, **2002**, pp. 44-52.

15. A. Einstein, Berichtigung zu meiner Arbeit: Eine neue Bestimmung der Molekuldimension, *Ann. Physik*, Vol. 34, **1911**, pp. 591-592.

16. M. Mooney, The Viscosity of Concentrated Suspensions of Spherical Particles, *J. Coll. Sci.*, Vol. 3, **1951**, pp. 162-195.

17. R. M. German, *Particle Packing Characteristics, Metal Powder Industries federation*, Princeton, NJ, **1989**.

18. C. W. Macosko, *Rheology principles, Measurements, and Applications*, VHC Publications, New York, NY, **1994**.

19. R. J. Hunter, *Introduction to Modern Colloid Science*, Oxford University Press, Oxford, UK, **1993**.

20. R. M. German, Particle Size Distribution as a Predictor of Suspension Flow behaviour, *Ceramic Transactions, Vol. 125: Fundamentals of Refractory Technology*, The American Ceramic Society, **2001**, pp. 3-28.

21. P. Bonadia, A. R. Studart, R. G. Pileggi and V. C. Pandolfelli, Applying MPT Principle to High-Alumina Castables, *American Ceramic society Bulletin*, Vol. 78, No. 3, **1999**, pp. 57-60.

22. F. LArrard and T. Sedran, Optimization of Ultra-High-Performance Concrete by the Use of a Packing Model, *Cement and Concrete Research*, Vol. 24, No. 6, **1994**, pp. 997-1009.

23. M. Ishikawa, Refractory Concrete, *Taikabutsu Overseas*, Japan, Vol. 19, No. 3, **1999**, pp. 7-12.

24. J. S. Reed, *Introduction to Principles of Ceramic Processing*, John Wiley & Sons Publications, 1**986**.

25. D. Beaupré, Rheology of High Performance Shotcrete, *Ph. D. Thesis*, the University of British Columbia, Canada, **1994**.

26. R. E. Fisher, Installation of Monolithic Refractories: Critical Issues for Successful Performance, *Proceedings of 32nd Annual Symposium St. Louis Section American Ceramic Society*, St. Louis, USA, **1996**.

27. ASTM C143-90a: Slump of Hydraulic Cement Concrete, *Annual Book of ASTM Standards*, Vol. 04.02, **1994**, pp. 85-87.

28. ASTM C1445-99: Standard Test Method for Measuring Consistency of Castable Refractory Using a Flow Table, *Annual Book of ASTM Standards*, Vol.15.01, **2004**, pp. 687-689.

29. N. Fukami, N. Takahashi and M. Ishikawa, Effect of Additives on the Pumpability of Low Cement Castables, *Proceedings of UNITECR'01*, Cancun, Mexico, **2001**, pp. 1142-1158.

30. H. Sumimura, R. Nakamura and T. Kaneshige, Installation Method of New Wet Type High Density Gunning Castable, *Journal of the Technical Association of Refractories, Japan*, Vol. 20, No. 3, **2000**, 168-172.

31. R. Moreno, The Role of Slip Additives in the Tape Casting Technology, Part-I Solvents and Dispersants, *Ceram. Bull*, Vol. 71, No. 10, **1992**, pp. 1521-1531.

32. T. Mizunuma and F. Yamato, Role of Surfactants in Concrete Fields, *Taikabutsu Overseas*, Vol. 11, No. 2, **1991**, pp. 38-43.

33. S. Fujimoto, S. Kiwaki and M. Mishima, Rheological Approaches to Monolithic Refractories (2), *Taikabutsu Overseas*, Vol. 2, No.2, **1982**, pp. 55-60.

34. S. Fujimoto, T. Yoshimura and M. Ezaki, Fundamental Approach to Workability of Monolithic Refractories, *Taikabutsu*, Vol. 30, No.12, **1978**, pp. 678-682.

35. G. Landman, B. Piscael, J. Radal, The Rehabilitation of Gunning Refractories, *Proceedings of 2nd International Conference on Refractories (Refractories' 87)*, Tokyo, Japan, **1987**, pp. 746-753.

36. G. A. William, Advanced Equipment Systems for Refractory Placement, *Proceedings of UNITECR'97*, New Orleans, USA, Vol. 2, **1997**, pp. 523-530.

37. Y. Eguchi, N. Takahashi, M. Ishikawa and K. Watanabe, Development of Accelerators for Refractory Gunning Mix, *Proceedings of UNITECR'99*, Berlin, Germany, **1999**, pp. 102-104.

38. T. Richter and D. Mclntyre, Novel Form Free Installation Method for Refractory Castables, *Proceedings of XXIX CONGRESS of ALAFAR 2000*, Pucon, Chile, **2000**, pp. 437-446.

39. D. Peters, Current Practice and Future Trends in the Monolithic Refractory Industry in the United States, *Proceedings of 39th Annual Symposium St. Louis Section American Ceramic Society*, St. Louis, USA, **2003**, pp. 21-34.

40. A. Nishikawa, Editor, *Technology of Monolithic Refractories*, Pub. Plibrico Japan Company limited, Japan, **1984**, 598 Pages.

41. N. Cassens, Jr., R. A. Steinke and R. B. Videtto, Shotcreting Self-flow Refractory Castables, *Proceedings of UNITECR'97*, New Orleans, USA, Vol. 2, **1997**, pp. 531-544.

42. M. Koga, I. Takita, M. Kataoka and K. Kawasaki, New Wet Spray Method for Castables, *Taikabutsu Overseas*, Japan, Vol. 19, No. 3, **1999**, pp. 14-20,.

43. G. D. Yoggy, The history of Shotcrete, Part I of a Three-part Series, *Shotcrete Magazine*, Fall, **2000**, pp. 28-29,.

44. G. D. Yoggy, The history of Shotcrete, Part II of a Three-part Series, *Shotcrete Magazine*, Spring, **2001**, pp. 22-23.

45. G. D. Yoggy, The history of Shotcrete, Part III of a Three-part Series, *Shotcrete Magazine*, Winter, **2003**, pp. 20-23.

46. Y. Ono, S. Sakamoto and E. Kudou, Development of Spray Operation Method for Self-flow Castables, *Proceedings of UNITECR'97*, New Orleans, USA, Vol. 2, **1997**, pp. 545-552.

47. S. Banerjee, H. Harbin and E. Reno, Spray-gunning Refractories, *Proceedings of UNITECR'97*, New Orleans, USA, Vol. 2, **1997**, pp. 553-562.

48. Y. Tsuji, Y. Ohtsubo, M. Koga and Y. Suekawa, Wet-sprayed Monolithic Refractory Lining for Steel Ladles, *Proceedings of UNITECR'99*, Berlin, Germany, **1999**, pp. 288-291.

49. J. P. Sutton, M. Kataoka, K. Kawasaki, M. Koga and Y. Tsuji, Development and Installation of Low and Ultra-low Cement Wet spray Mixes, *Proceedings of UNITECR'97*, New Orleans, USA, Vol. 2,**1997**, pp. 593-602.

50. K. Matsumura, R. Nakamura, T. Kaneshige and H. Sasaki, Thermal Properties of Shotcreting Material for Steel Ladles, *Taikabutsu Overseas*, Japan, Vol. 20, No.3, **2000**, pp. 204.

51. N. Shirama, K. Murakami and I. Shimizu, Development of Low Silica Wet Gunning material for Steel Ladles, *Journal of the Technical Association of Refractories, Japan*, Vol. 22, No. 2, **2002**, pp. 161-163.

52. W. G. Allen, Current Developments in Equipment for Refractory Placement, *Proceedings of 32nd Annual Symposium St. Louis Section American Ceramic Society*, St. Louis, USA, **1996**.

53. M. Rigaud and N. S. Zhou, Major Trends in Refractories Industry at the Beginning of the 21st Century, *China's Refractories*, Vol. 11, No. 2, **2002**, pp. 3-8.

54. K. Nonaka, Gunning Refractory Technology – Development and Future Trends, *Journal of the Technical Association of Refractories*, Japan, Vol. 20, No. 4, **2000**, pp. 283-291.

55. A. E. C. Peres, C. P. Neto and V. C. Pandolfelli, A Rheological Approach on Selection of Additives for Wet Gunning Castables, *Canadian Metallurgical Quartly*, Vol. 42, No. 3, **2003**, pp. 327-332.

56. N. Shirama, K. Yamada and I. Shimizu, Influence of Particle Size Distribution on Workability of Material for Wet Gunning, *Taikabutsu Overseas*, Japan, Vol. 18, No. 4, **1998**, pp. 66.

57. ASTM C33-03, Standard Specification for Concrete Aggregates, *Annual Book of ASTM Standards*, Vol. 04.02, **2003**.

58. B. Myhre and K. Sunde: Alumina Based Castables with Very Low Contents of Hydraulic Compound, Part I: The effect of Binder and Particle Size Distribution on Flow and Set, *Proceedings of UNITECR'95*, Kyoto, Japan, Vol.1, **1995**, pp.309-316.

59. S. Banerjee, *Monolithic Refractories: A Comprehensive handbook*, World Scientific Publishing Co. Pte. Ltd., **1998**, 401 Pages.

60. Alcoa Industrial Chemicals (ALMATIS), *Product Data: Calcium Aluminate Cements* (GP/005/R00/1001/MSDS 993), **1999**.

61. Alcoa Industrial Chemicals (ALMATIS), *Product Data: High Performance Refractory Grade Aluminas for Castables* (USA/0075-R01/0997), **1997**.

62. Alcan Chemicals, *Product Data: Aluminas*, **1996**,

63. N. S. Zhou, Elaboration of Al_2O_3-based Graphite Containing Castables, *PhD Thesis*, University of Montreal, Canada, **2000**.

64. SKW Polymers GMBH, *Preliminary Technical Data Sheet: CASTAMENT® FS-20*, **2003**.

65. Anachemia Canada, *Material safety Data Sheet: Sodium Hexametaphosphate*, **2003**.

66. R. T. Vanderbilt Company, Inc., *Material Safety Data Sheet and Specification: Darvan 811D*, **2002**.

67. C. F. Ferraris, Measurement of the Rheological Properties of High Performance Concrete: State of the Art Report, *Journal of Research of the National Institute of Standard and Technology*, Vol. 104, No. 5, **1999**, pp. 461-478.

68. C. F. Ferraris, F. de Larrard and N. Martys, Fresh Concrete Rheology : Recent Developments, *Materials Science of Concrete VI*, Sidney Mindess and Jan Skalny, eds., The American Ceramic Society, **2001**, pp. 215-241.

69. Bohlin Instruments UK, *User Manual for Bohlin Rheometers*, **1999**.

70. ASTM C1446-99, Standard Test Method for Measuring Consistency and Working Time of Self-flowing Castable Refractories, *Annual Book of ASTM Standards*, Vol. 15.01, **2004**, pp. 690-693.

71. ASTM C830-00, Test methods for Apparent Porosity, Liquid Absorption, Apparent Specific Gravity, and Bulk Density of Refractory Shapes by Vacuum Pressure, *Annual Book of ASTM Standards*, Vol. 15.01, **2004**, pp. 133-137.

72. ASTM C1407-98, Practice for Calculating Areas, Volume and Linear Change of Refractory Shapes, *Annual Book of ASTM Standards*, Vol. 15.01, **2004**, pp. 625-626.

73. ASTM C133-97 (2003), Test Methods for Cold Crushing Strength and Modulus of Rupture of Refractories, *Annual Book of ASTM Standards*, Vol. 15.01, **2004**, pp. 27-32.

74. C. Ødegård, B. Myhre, A. Hundere and B. Sandberg, Mullite-bonded Castable with Andalusite as Aggregate, *Proceedings of 41st International colloquium on Refractories*, Aachen, Germany, **1998**, pp. 119-122.

75. M. D. M. Innocentini, A. R. Studart, R. G. Pileggi and V. C. Pandolfelli, How PSD Affects Permeability of Castables, *American Ceramic society Bulletin*, Vol. 780, No. 5, **2001**, pp. 31-36.

76. A. Q. Ma, M. S. Liu, M. X. Jiang, et al, Factors Influencing the Thixotropy of High Alumina Castable Slurry, *Refractories* (In Chinese), Vol. 37, No. 2, **2002**, pp. 89-91.

77. V. Jones, Flow Control of Low-cement Self-flow Castable, *Proceedings of UNITECR'97*, New Orleans, USA, Vol. 2, **1997**, pp. 635-644.

78. A. R. Studart and V. C. Pandolfelli, Dispersants for High-Alumina Castables, *American Ceramic society Bulletin*, Vol. 81, No. 4, **2002**, pp. 36-44.

79. C. J. Brinker and G. W. Schere, *Sol-Gel Science: the Physics and Chemistry of Sol-gel Processing*, Academic Press, Inc., New York, **1990**, pp. 239-250.

80. N. Bunt, C. Revais and M. Vialle, Additives in Calcium Aluminate Containing Castables, *Proceedings of UNITECR'97*, New Orleans, USA, Vol. 3, **1997**, pp. 1347-1354.

81. Y. Sasagawa, M. Sato and K. Nozawa, Role of Alumina Cement in Castable Refractories, *Proceedings of UNITECR'95*, Kyoto, Japan, Vol. 2, **1995**, pp. 301-308.

82. C. Parr, R. Roseky and C. Wöhrmeyer, Calcium Aluminate Cements for Unshaped Refractories, *CN Refractories Special Issues*, No. 5, **2001**, pp. 6-12.

83. B. Clavaud, J. P. Kiehl and R. D. Schmidt-Whitely, Fifteen Years of Low-cement Castables in Steelmaking. *Proceedings of 1st Internat. Conf. on Refractories*, Tokyo, Japan, **1983**, pp. 589–606.

84. www.refractories.elkem.com

85. L. R. Roberts, Microsilica in Concrete, *Materials Science of Concrete*, The American ceramic Society, Vol. 1, **1989**, pp. 197–221.

86. P. White, N. C. Fletcher and T. D. Reeves, Use of Fume Silica and Other Ultrafine Particles in Low Cement Castables. *Proceedings of UNITECR'91*, Aachen, Germany, **1991**, pp. 181–185

87. A. Hundere, B. Myhre, N. S. Zhou, et al, Magnesium-silicate-hydrate Bonded MgO-Al_2O_3 Castables, *Proceedings of the International Symposium on Advances in Refractories for the Metallurgical Industries III*, Canada, **1999**, pp. 135-150.

88. B. Monsen, A. Seltveit, B. Sandberg, and S. Bentsen, Effect of Microsilica on Physical Properties and Mineralogical Composition of Refectory Concretes, *Advances in Ceramics, Vol. 13, Proceedings of an International Symposium on New Developments in Monolithic Refractories at the 86th Annual Meeting of the American Ceramic Society*, The Am. Cer. Soc. Inc, **1985**, pp. 201-210.

89. A. M. Hundere and B. Myhre, Substitution of Refractive Alumina with Microsilica in Low Cement and Ultra Low Cement Castables, P art II: the Effect of Temperature on Hot Properties *Proceedings of UNITECR'97*, New Orleans, USA, Vol. 1, **1997**, pp. 91-100.

90. N. Li, Y. W. Wei, B. Myhre and C. Odegard, Properties of MgO Castables and Effect of Reaction in Microsilica-MgO Bond System, *Proceedings of UNITECR'99*, Berlin, Germany, **1999**, pp. 97-101.

91. Y.- C. Ko, Influence of Microsilica Addition on the Properties of Alumina-spinel Castables. *Proceedings of UNITECR'99*, Berlin, Germany, **1999**, pp. 22-25.

92. R. Corrêa da Silveira, et al, Silica Fume CCM – Production and Application, *Proceedings of UNITECR'93*, Sao Paulo, Brazil, **1993**, pp. 717-727.

93. X. M. Li, Q. S. Wu, Study on Varied Types of Ultra-fine Powder Used in Refractory, *China's Refractories*, Vol. 6, No. 3, **1997**, pp. 17-26.

94. C. Ødegård, H. Feldborg and B. Myhre, Magnesia-silica-hydrate bonded MgO castables, *Proceedings of UNITECR'01*, Cancun, Mexico, Vol. 1, **2001**, pp. 220-235.

95. D. A. Fumo and A. M. Segadães, Effect Silica Fume Additions on the Hydration Behaviour of Calcium aluminates, *Proceedings of UNITECR'97*, New Orleans, USA, Vol. 3, **1997**, pp. 1325-1333.

96. S. Savarmand, P. J. Carreau, et. al. Rheological Properties of Concentrated aqueous silica Suspensions: Effects of ρH and Ions Content, *Journal of Rheology*, Vol. 47, No. 5, **2003**, pp.1133-1149.

97. X. X. Zhou, M. Rigaud, N. S. Zhou and S. Q. Zhang, Multipurpose Bauxite-based Low Cement castables, *Proceedings of UNITECR'03*, Osaka, Japan, **2003**, pp.81-84.

98. B. Myhre, The Effect of Microsilica Addition on Flow and Strength of alumina Castables, *Proceedings of the 95th Annual Meeting and Exposition of the American ceramic Society*, Cincinnati, **1993**.

99. X. X. Zhou, K. Sankaranarayanane and M. Rigaud, "Design of Bauxite-based Low-cement Pumpable Castable: A Rheological Approach", *Ceramics International*, Vol.30, No. 1, **2004**, pp. 47-55.

100. ASTM C230/C230M-03, "Standard Specification for Flow Table for Use in Tests of Hydraulic Cement," *Annual Book of ASTM Standards*, Vol. 04.01, **2003**.

101. Z. Q. Chen, B. Myhre and B. Sandberg, Flow and Flow Decay of Refractory Castables, *China's Refractories*, Vol. 12, No. 4, **2003**, pp. 16-19.

102. K. Fujii, W. Kondo and H. Ueno, "Kinetics of Hydration of Monocalcium Aluminate", *J. Am. Ceram. Soc*, Vol. 69, No. 4, **1986**, pp. 361-364.

103. W. W. Wright, The Effect of High Temperature Phases on Low and Ultra Low Cement Castables Hot Properties, *Ph. D Thesis*, Monash University, Australia, **2000**, pp. 6-16.

104. C. D. Parr, C Revais and H. Fryda, The Nature of Chemical Reactions That Occur During castable Installation and Analytical Techniques Used to Follow These Reactions, *Fundamentals of Refractory Technology, Ceramic Transactions*, Ed. James P. Bennett and Jeffery D. Smith, The American Ceramic Society, Vol. 125, **2001**, pp. 53-71.

105. T. Hemphill, W. Campos and A. Pilehvari, Yield-Power Law Model More Accurately Predicts Mud Rheology, *Oil & Gas Journal*, Vol. 91, No. 34, **1993**, pp. 45-50.

106. V. A. Hackley and C. F. Ferraris, National Institute of Standard and Technology Special Publication 946, *Guide to Rheological Nomenclature: Measurements in Ceramic Particulate Systems*, **2001**, 31 pages.

107. C. Parr, C. Wöhrmeyer, B. Valdelièvre and A. Namba, Effect of Formulation Parameters upon the Strength Development of Calcium Aluminate Cement Containing Castables, *Journal of the Technical Association of Refractories*, Japan, Vol. 23, No. 4, **2003**, pp. 231-238.

108. R. Funakoshi, T. Mastue, N. Takahashi and M. Ishikawa, A Study of the Setting Mechanisms of Low-cement Castables by Exothermic Profile, *Journal of the Technical Association of Refractories, Japan,* Vol. 23, No. 4, **2003**, pp. 286-289.

109. C. Alt, C. Parr and C. Revais, The Effect of environmental Temperature Conditions on the Rheology of Deflocculated Refractory Castable, *Refractories Application and News,* Vol. 7, No. 1, **2002**, pp. 9-15.

110. C. Parr, B. Valdelièvre and C. Wöhrmeyer, Application of Calcium Aluminate Cement to Desense Low Water Demand Refractory Castables, *Refractories Application and News,* Vol. 7[3] **2002**, 17-23.

111. P. C. Evangelista, C. Parr and C. Revais, Control of Formulation and Optimization of Self-flow Castables Based on Pure Calcium Aluminates, *Refractories Application and News,* Vol. 7[2] **2002**, 14-18.